Université Joseph Fourier - Grenoble 1
Ecole Doctorale Chimie et Sciences du Vivant

Thèse presentée par

Ricardo Simão Vieira Pires

pour obtenir le titre de:

Docteur de l'Université Joseph Fourier - Grenoble 1

discipline:

Biologie Structurale et Nanobiologie

Etudes structurales et fonctionnelles de la protéine ALIX

Soutenance publique le 22 Septembre 2008

devant le jury composé de:

Président:	Prof. Rémy Sadoul
Rapporteurs:	Dr. Denis Gerlier
	Prof. Juan Martin-Serrano
Examinateurs:	Dr. Carlo Petosa
	Dr. Laurence Aubry
	Prof. Masatoshi Maki
Directeur de thèse:	Prof. Winfried Weissenhorn

Thèse préparée au sein de:

EMBL Grenoble (Laboratoire Européen de Biologie Moléculaire)
UVHCI (Biologie structurale des interactions entre virus et cellule-hôte)
UMR 5233 UJF-EMBL-CNRS

Etudes structurales et fonctionnelles de la protéine ALIX

Structural and functional studies of ALIX

Ricardo Simão Vieira Pires

Université Joseph Fourier - Grenoble 1
Ecole Doctorale Chimie et Sciences du Vivant
2008

To the memory of my beloved grandmother Mariazinha.

Acknowledgements

A special thanks to my PhD supervisor, Prof. Winfried Weissenhorn, for the quality of his scientific guidance throughout these four years of work, for every opportunity to learn and to be involved in such interesting scientific projects.

I would like to thank the two members of my thesis advisory committee, Dr. Christoph Müller and Dr. Michael Knop for all the discussions, suggestions and advice during the PhD work.

I would like to thank Prof. Rémy Sadoul, for his collaboration in this work, for his help as a thesis advisory committee member and especially for his enthusiastic discussions, suggestions and criticisms. Thanks also to his group, in particular to Béatrice Blot and Christine Chatellard-Causse for their help and kindness.

I am very grateful to the European Molecular Biology Laboratory for all the scientific opportunities and in particular to Dr. Stephen Cusack and Prof. Rob Ruigrok, leading the new "unité mixte" Unit of Virus Host Cell Interactions (UVHCI) where I performed the second half of my PhD work.

I am also grateful to all those who contributed to the present work, in particular Dr. Guy Schoehn for all the electron microscopy work, Dr. Eric Forest and Dr. Luca Signor for the mass spec analysis, Dr. Dmitri Svergun and Dr. Manfred Roessle for the collaboration in SAXS experiments, Dr. Marc Jamin for the MALLS analysis, Prof. Heinrich Göttlinger for testing the Alix dimerization mutants, Dr. Carlo Petosa, Dr. Andrew McCarthy and Dr. Charles Sabin for crystallographic advice, Dr. Juan Sanchez-Weatherby and Dr. Monika Budayova-Spano for the work and advice in optimization of crystals and Dr. Véronique Boyer for the immunofluorescence analysis. I would also like to thank all scientific and non-scientific UVHCI staff for their help and kindness.

A special thanks to all my friends and colleagues, who have supported me during this difficult but nevertheless creative period. A special word to Carlos Fernández Tornero for his help and inspiration and to Thibault Crepin for the careful reading of the thesis.

Last, but not least, special thanks to my family for their continuous encouragements and full-time support:
to my father Euclides, who has been my inspiration throughout life and the person who best understands my fears and my dreams,
to my mother Regina, with whom I learnt to be persistent and perfectionist and whose love and support is specially important each and every day,
to my brother Alexandre, always silent, but always there,
to Milene, for reminding me what life is about!

Abbreviations ..... **i**
Abstract ..... **iii**
Résumé ..... **v**

Chapter I - INTRODUCTION **1**

The Endosomal Sorting Pathway **3**
Biogenesis of multivesicular bodies: the ESCRT machinery 4
Overall mechanism of the ESCRT machinery 5
Structure and function of the ESCRT complexes 7
ESCRT-0 7
ESCRT-I 8
ESCRT-II 10
ESCRT-III 12
Deubiquitylation in the ESCRT pathway 15
Membrane disassembly of the ESCRT machinery 17
Reasons for exploring the ESCRT machinery 19
Alix, a multifunctional protein **22**
Modular organization of Alix 22
Alix homologues in *Saccharomyces cerevisiae* 25
Interactions between Alix and the ESCRT machinery 26
Functional links between Alix and MVB trafficking 27
Mammalian homologs of Alix 30
Alix cooperates with ALG-2 to promote apoptosis 32
Alix supports budding of some enveloped viruses 34
Dictyostelium reveals a role for Alix in developmental signaling 35
Alix in the recycling endocytic pathway 36
Structure of mammalian Alix **38**
Structural details of Alix-CHMP4 interaction 41
Structural basis of Alix interaction with YPX_nL late domain 43

Aims of the present work **47**
Objectifs **49**

Chapter II - RESULTS 51

Mapping and preliminary characterization of Alix major domains 53
Oligomerization of Alix 60
Alix forms monomers and dimers in solution 60
Mapping Alix dimerization interface 63
Global kinetics of H/D exchange 63
Local kinetics of H/D exchange 64
Alix-V mutants impair dimerization and adopt elongated conformations 71
Solution structure of Alix by small angle X-ray scattering (SAXS) 74
Alix-ΔPRD folds into a crescent-shaped dimer 74
Alix-V mutant adopts an extended conformation 75
Crystallization and preliminary X-ray crystallographic analysis of Alix 82
Crystallization of Alix-V dimer 82
Crystallization of Alix-V mutant 84
Alix interaction with lipid bilayers 88
Monomeric and dimeric Alix interact with liposomes 88
Alix-ΔPRD and Alix-V dimerize upon lipid bilayer binding 91
Alix-ΔPRD liposome interaction does not depend on the vesicle curvature 92
Alix-ΔPRD deforms lipid membranes *in vitro* 93
Alix distribution on the lipid bilayer 97
Binding of monomeric and dimeric Alix-V to EIAV late domain 101
Characterization of Alix-CHMP4B interaction 102
Alix binds a C-terminal region of CHMP4B 102
CHMP4B forms ring-like polymers *in vitro* 102
Localization of endogenous Alix in mammalian cells 107
Alix dimerization is involved in HIV-1 release 110

Chapter III - DISCUSSION 113

Chapter IV - CONCLUSIONS AND PERSPECTIVES 135

Chapter V - MATERIALS AND METHODS 145

Expression and purification of Alix-ΔPRD 147
Cloning Alix-Bro1 and Alix-V 148
Expression and purification of Alix-Bro1 and Alix-V 148
Mutagenesis of Alix-V 149
Expression and purification of Alix-V mutants 150
Cloning CHMP4B deletions mutants 150
Expression and purification of CHMP4B forms 151
Limited proteolysis 151
Chemical cross-linking 152
Size exclusion chromatography and multi-angle laser light scattering 153
Small angle X-ray scattering data collection and analysis 154
Ab initio shape modeling of Alix-ΔPRD and Alix-V 155
Hydrogen/deuterium (H/D) exchange mass spectrometry (MS) 156
Isothermal titration calorimetry (ITC) 157
Liposome preparation 158
Liposome binding, floatation and co-sedimentation experiments 159
Characterization of Alix associated with liposomes 159
Electron microscopy 160
Microscopy of fluorescence labeled Alix-ΔPRD and liposomes 161
Saturation of liposomes surface 161
Nanogold-labeling of Alix-ΔPRD 162
Cloning and purification of Alix-ΔPRD and Alix-V new constructs used for crystallization 162
Alix-V dimer and Alix-V_{Mut1} crystallization and data collection 163
Selenomethionine labelling 164
Alix antibodies 165
Immunofluorescence studies 165
Mammalian expression constructs and viral release assays 166

Supplementary figures 167
References 171

Abbreviations

Alix/AIP1	ALG-2-interacting protein X (or 1)
ALG-2	Apoptosis-linked gene 2
CHMP	Charged multivesicular body protein
ESCRT	Endosomal sorting complex required for transport
FYVE	Fab1, YOTB, Vac1 and EEA1 (domain)
HRS	Hepatocyte growth factor (HGF)-regulated Tyr-kinase substrate
MIR	MIT interacting region
MIT	Microtubule interacting and trafficking domain
STAM	Signal transducing adaptor molecule
UEV	Ubiquitin E2 variant domain
UIM	Ubiquitin interacting motif
VHS	Vps27, HRS and STAM domain
WH	Winged helix (protein)

Abstract

Alix is an adaptor protein involved in several cellular processes including apoptosis, endocytic membrane trafficking, budding of retroviruses (e.g. HIV-1, EIAV) and cytokinesis. Alix is organized in three major domains: an N-terminal BRO domain, a V-shaped domain in the middle (Alix-V) and a C-terminal proline rich domain (PRD). We have shown that a C-terminal truncated form lacking the PRD (Alix-ΔPRD) forms monomers and dimers in solution and that the V-shaped domain is sufficient to mediate dimerization. Small angle X-ray scattering analyses revealed that Alix-ΔPRD folds into an elongated curved structure that resembles membrane bending BAR domains. Although we determined that Alix interacts efficiently with membranes *in vitro* its potential deformation capability has yet to be confirmed. We further determined by isothermal titration calorimetry measurements that both monomeric and dimeric Alix-V interact with a peptide derived from EIAV Gag p9 with micromolar affinities. We obtained crystals of dimeric Alix-V which, however, diffracted X-rays no better than 10Å. We further crystallized a mutant of Alix-V (Mut1) that no longer dimerizes and folds into an open elongated monomeric structure as determined by small angle X-ray scattering. The crystals diffracted X-rays to 3Å resolution and structure determination is underway. Moreover, we showed that the deficient release of virus-like particles (VLP) upon overexpression of a human Alix-ΔBro form (residues 358-868), was rescued by generating a Mut1 version of this form, thus suggesting a role for dimerization in viral release. Dimeric Alix-V was also used to produce an Alix antiserum, which showed that endogenous Alix co-localizes with recycling endosomes. Finally, we showed that CHMP4B forms polymeric ring-like structures that are able to bind Alix. Together our data give insight into the conformational flexibility of Alix and its potential implications in concert with CHMP4 ring-like polymers in membrane budding processes. Our work also

provides the framework for further functional analyses on the physiological relevance of dimeric Alix namely in HIV-1 infected cells.

Key words: Alix, ESCRT, endocytic trafficking, viral budding.

Résumé

Alix est une protéine adaptatrice impliquée dans plusieurs processus intracellulaires, dont l'apoptose, l'endocytose et le trafic membranaire, le bourgeonnement de certains rétrovirus (ex. HIV-1, EIAV) à travers la membrane plasmique ou encore la cytokinèse. Alix est constituée de trois domaines majeurs: un domaine BRO N-terminal, un domaine spécifique « en V » central (Alix-V) et un domaine C-terminal riche en prolines (PRD). Nous avons montré que la forme tronquée en C-terminal au niveau du domaine PRD (Alix-ΔPRD) formait des monomères et des dimères en solution, et que le domaine Alix-V était suffisant pour permettre cette dimérisation. La diffraction de rayons X aux petits angles (SAXS) a montré que Alix-ΔPRD se structurait en une forme incurvée et allongée qui rappelle les domaines BAR impliqués dans les phénomènes d'incurvation de membrane. Bien que l'interaction d'Alix avec la membrane ait été mise en évidence *in vitro,* sa capacité à déformer la membrane doit encore être confirmée. En outre, nous avons déterminé lors d'expériences de microcalorimétrie que les formes monomériques et dimériques de Alix-V interagissent avec un peptide dérivé de la protéine p9 EIAV Gag avec une affinité de l'ordre du micromolaire. Des cristaux de la forme dimérique de Alix-V ont été obtenus. Ces cristaux présentaient un faible pouvoir de diffraction (10Å). En revanche, des cristaux diffractant à 3Å ont été obtenus à partir d'une forme mutante de Alix-V (Mut1) incapable de dimériser et qui se structure en une forme monomérique ouverte et allongée ; la résolution de cette structure est en cours. De plus, nous avons montré que l'absence de relarguage des particules virales (VLP) après surexpression de la forme humaine de Alix-ΔBro (résidus 358-868) pouvait être rétablie à partir de la version Mut1 de cette forme, ce qui suggère donc un rôle de cette dimérisation dans le relarguage des VLP. La protéine Alix-V dimérique a également été utilisée pour produire un antisérum Alix, qui a montré que la protéine endogène Alix

pouvait être co-localiser avec les endosomes de recyclage. Enfin, nous avons montré que CHMP4B formant des structures polymériques en anneaux, pouvait interagir avec Alix. L'ensemble de ces résultats donne de nouvelles informations sur la flexibilité conformationnelle d'Alix et, associée avec CHMP4, sur son implication dans les processus de bourgeonnement membranaire. Ce travail définit également le cadre des futures analyses fonctionnelles visant à définir le rôle de la protéine dimérique Alix dans les cellules infectées par le virus HIV-1.

Mots clés : Alix, ESCRT, trafic endocytaire, bourgeonnement viral.

Chapter I

INTRODUCTION

The Endosomal Sorting Pathway

The composition of cellular plasma membranes is tightly controlled by complex internal trafficking pathways (Figure 1). Transmembrane proteins such as receptors are removed from the plasma membrane by incorporation into endocytic vesicles that are internalized and fuse with early endosomes also named sorting endosomes. These compartments of tubulovesicular morphology sort cargos either for degradation or for recycling back to the plasma membrane. Ubiquitin serves as the main targeting signal that directs transmembrane cargo to be incorporated into intralumenal vesicles (ILVs) of morphologically distinctive endosomes that are known as multivesicular bodies (MVBs).

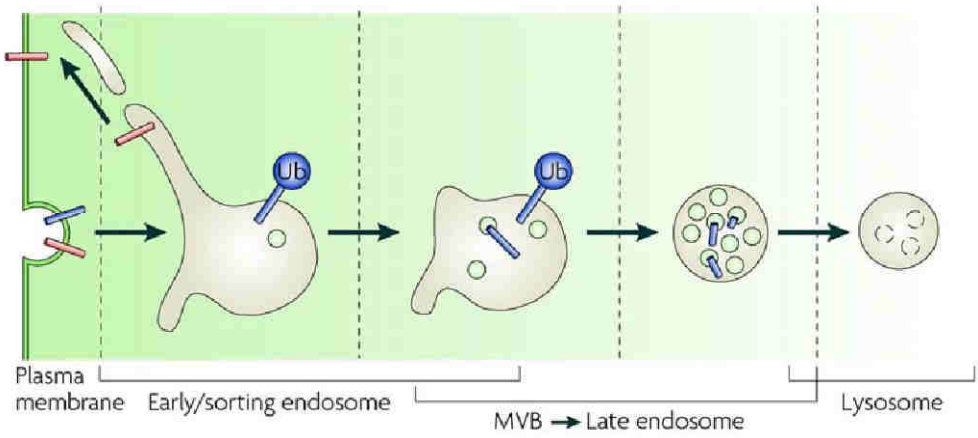

Figure 1. Overview of the endocytic pathway. Membrane proteins such as receptors are internalized into endocytic vesicles that fuse with an early/sorting endocytic compartment. At this stage cargoes can either be recycled back to the plasma membrane or follow the degradative branch of the pathway. Ubiquitin (Ub) is the main signal directing cargo for incorporation into intralumenal vesicles (ILV) to form multivesicular bodies (MVBs). The latter ultimately fuse with late endosomes and finally with lysosomes where the ILV and their cargo are delivered for degradation by lysosomal hydrolases. *Adapted from (Williams and Urbe 2007)*

Ultimately, mature MVBs (late endosomes) fuse with lysosomes delivering their ILVs and respective cargo for degradation by lysosomal hydrolases (proteases and lipases). The sorting of transmembrane proteins into intraluminal vesicles plays also other important functions besides promoting cargo degradation; it may serve as storage of transmembrane proteins destined to control release from the cell or even promote the shutting down of signaling processes due to a segregation of signaling receptors away from the cytoplasm. MVBs have indeed different functions in different types of cells. They can be precursors for lytic granules in T-lymphocytes (Persechini, Liu *et al.* 1989), MHC class II compartments and exosomes in antigen presenting cells (Denzer, Kleijmeer *et al.* 2000; Kleijmeer, Ramm *et al.* 2001), melanosomes in melanocytes (Katzmann 2006) and lysosomes in most nucleated cells (Raiborg, Rusten *et al.* 2003).

Biogenesis of multivesicular bodies: the ESCRT machinery

The endosomal sorting complex required for transport (ESCRT) machinery is an intricate cellular machinery that acts primarily on the endosome and is critical for monoubiquitin-dependent protein cargo recognition, protein sorting and formation of multivesicular bodies. Its components were initially identified in yeast (*Saccharomyces cerevisae*) as so called class E Vps (vacuolar protein sorting) mutants. Indeed, deletion of each class E *VPS* gene in yeast results in mislocalization of MVB cargoes to the vacuole (yeast equivalent of the lysosome) and accumulation of endosomal cargoes in large aberrant prevacuolar structures, called “class E compartments” (Raymond, Howald-Stevenson *et al.* 1992; Vida, Huyer *et al.* 1993). The ESCRT machinery is highly conserved and its components have been found in all six major subgroups of eukaryotes (Metazoa, Fungi, Amoebozoa, Plantae, Chromalveolate and Excavata) (Williams and Urbe 2007) and some in Archaea (Obita, Saksena *et al.* 2007) suggesting a crucial importance of this trafficking apparatus.

Overall mechanism of the ESCRT machinery

A set of four distinct cytosolic complexes, known as ESCRT-0, -I, -II and –III (Table 1; see also Figure 5) are recruited to the endosomal membrane through both protein and lipid interactions. Monoubiquitylation of target proteins is a critical signal for recognition by ESCRT-0, I and II (harbouring ubiquitin-interacting modules) and subsequent cargo retention and concentration on the endosomal membrane (Katzmann, Babst *et al.* 2001; Reggiori and Pelham 2001; Urbanowski and Piper 2001). The ESCRT-III complex acts later in the pathway and unlike the other ESCRTs is composed of several subcomplexes that assemble into a lattice as a result of heteromeric interactions and a direct interaction with the membrane (Babst, Katzmann *et al.* 2002; Whitley, Reaves *et al.* 2003; Muziol, Pineda-Molina *et al.* 2006). ESCRT-III has no ubiquitin-interacting module, but instead interacts with de-ubiquitylating enzymes (DUBs) that remove the ubiquitin from the cargo before incorporation into ILVs (Amerik and Hochstrasser 2004). In addition ESCRT-III is targeted by the ATPase VPS4 (Babst, Wendland *et al.* 1998; Lin, Kimpler *et al.* 2005; Obita, Saksena *et al.* 2007) which disassembles the ESCRT complexes from membranes, recycling them back to the cytosol for further sorting cycles (Babst, Katzmann *et al.* 2002).

Table 1. Components of the ESCRT machinery. *Adapted from (Saksena, Sun et al. 2007)*

	S. cerevisae	Mammalian	Domains/motifs	Proposed function
ESCRT-0	Vps27	HRS	UIM, FYVE, VHS	Cargo and PI3P interaction
	Hse1	STAM1, STAM2	UIM, VHS, SH3	Interaction with Hua1 and Rsp5
ESCRT-I	Vps23	TSG101	UEV, coiled-coil, S box	Cargo and Vps27 interaction
	Vps28	VPS28	-	Assembly with ESCRT-II (Vps36)
	Vps37	VPS37A,B,C,D	-	-
	Mvb12	MVB12A,B	-	-
ESCRT-II	Vps22	EAP30, SNF8	Coiled-coil, WH	Assembly with ESCRT-III (Vps20);
	Vps25	EAP20	PPXY, WH	cargo and PI3P interaction; assembly
	Vps36	EAP45	GLUE, NZF, WH	with ESCRT-I (Vps28)
ESCRT-III	Vps20	CHMP6	Charged, coiled-coil, MIR	Assembly with ESCRT-II (Vps25);
	Vps32/Snf7	CHMP4A, B, C	Charged, coiled-coil, MIR	membrane deformation; vesicle invagination
	Vps2	CHMP2A, B	Charged, coiled-coil, MIR	
	Vps24	CHMP3	Charged, coiled-coil, MIR	
	Did2	CHMP1A, B	Charged, coiled-coil	
	Vps60/Mos10	CHMP5	Charged, coiled-coil	
	-	CHMP7	Charged, coiled-coil	
Vps4 complex	Vps4	VPS4A, B (SKD1)	AAA+ ATPase, MIT	ESCRT disassembly and recycling
	Vta	LIP5	-	Positive regulator of Vps4
Modulator/adaptor	Vps31/Bro1	ALIX/AIP1	Bro1	Doa4 recruitment, ESCRT-III interaction
Ubiquitin ligase	Rsp5	Nedd4	C2, WW, HECT	Cargo ubiquitination
Deubiquitinating enzymes	Doa4	UBPY/USP8	Rhod, UBP	Cargo deubiquitination
	Ubp7	AMSH	MIT, JAMM	Cargo deubiquitination

Structure and function of the ESCRT complexes

ESCRT-0

The first component of the endosomal sorting pathway recruited to the endosomal membrane is ESCRT-0, a complex made up by two subunits interacting constitutively with each other: HRS (Vps27 in yeast) and STAM (Hse1 in yeast). The association with endosomal membranes is mediated by the N-terminal FYVE domain of HRS, that is a double zinc-finger domain (Mao, Nickitenko *et al.* 2000) able to specifically recognize a highly abundant phosphoinositide in these membranes - phosphatidylinositol-3-phosphate (PtdIns3P) (Raiborg, Bremnes *et al.* 2001). HRS also binds ubiquitin through its ubiquitin-interacting motif (UIM) and this is critical for initiating the sorting of ubiquitylated membrane proteins (Urbe, Sachse *et al.* 2003). Both HRS and STAM harbour VHS domains that are common N-terminal elements found in several proteins involved in intracellular trafficking and are thought to participate in cargo binding. Moreover endosome-associated HRS recruits clathrin, a protein that forms a double layered coat thought to sequester and concentrate ubiquitylated cargo (Raiborg, Bache *et al.* 2001). Endosomes with a HRS-clathrin coat present typically a low number of internal vesicles and are referred as early-endosomes. The interaction of ESCRT-0 with the downstream ESCRT-I, is mediated via the Pro-(Ser/Thr)-X-Pro (X being any aminoacid) motif of HRS that binds directly to ubiquitin E2 variant (UEV) domain of tumor susceptibility gene-101 (TSG101, Vps23 in yeast) (Lu, Hope *et al.* 2003). Interestingly, studies in yeast suggest that this interaction only occurs on membranes and therefore activation of ESCRT-I requires endosomal membrane association (Katzmann, Stefan *et al.* 2003).

ESCRT-I

ESCRT-I complex consists of four subunits: TSG101 (Vps23), VPS28, VPS37 and MVB12. The structure of a core heterotetrameric ESCRT-I from yeast revealed an overall organization consisting of a globular headpiece attached to an extended rigid stalk (Figure 2) with a subunit stoichiometry of 1:1:1:1 (Kostelansky, Schluter *et al.* 2007). As previously reported (Kostelansky, Sun *et al.* 2006; Teo, Gill *et al.* 2006) the core of the headpiece assembles into a six helical bundle structure, with Vps23 (TSG101 in mammals), Vps28 and Vps37, each contributing with one helical hairpin. In addition, extended helical segments of both Vps23 and Vps37 assemble a triple-stranded coiled coil together with Mvb12 forming a cylindric stalk of ~20 Å x130 Å. Mvb12 contains a short N-terminal helix that interacts with the globular headpiece. The Vps23 UEV domain and the Vps28 C-terminal domain are important ESCRT-I adaptor domains that interact with ubiquitin (Sundquist, Schubert *et al.* 2004; Teo, Veprintsev *et al.* 2004), ESCRT-II Vps36 NZF domain (Teo, Gill *et al.* 2006; Gill, Teo *et al.* 2007) and ESCRT-III Vps20 (Pineda-Molina, Belrhali *et al.* 2006). They are linked at the opposite ends (180 Å apart from each other) of the central core of ESCRT-I via flexible thethers.

The Mvb12 subunit was only recently described as a fourth component of yeast ESCRT-I complex (Chu, Sun *et al.* 2006). Its knockout phenotype in yeast is not as severe as that of the other ESCRT-I components. Nevertheless, Mvb12 clearly contributes to stabilize the long stalk of ESCRT-I, since no stalk structure is obtained in the absence of Mvb12. Currently, several roles for Mvb12 are debated. It has been proposed that Mvb12 drives a cytosolic oligomeric state of ESCRT-I that is inactive for ESCRT-II binding, therefore restricting the assembly of the ESCRT-I/II supercomplex to the endosome (Chu, Sun *et al.* 2006).

Two forms of the mammalian counterpart of yeast Mvb12, MVB12A and B, seem to exist and participate in the formation of mammalian ESCRT-I complex (Morita, Sandrin

et al. 2007). Together with existence of different paralogs for VPS37 (Table 1), mammalian ESCRT-I may assemble up to eight different complexes that could extend the scenario of sorting activities in mammalian cells.

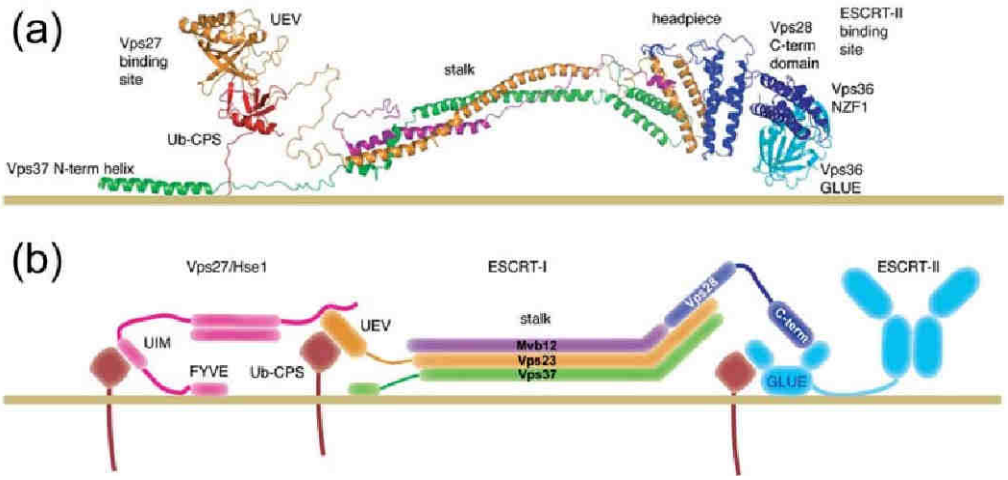

Figure 2. Membrane-docked model for the yeast ESCRT-I. (a) The structure of the heterotetrameric yeast ESCRT-I complex (PDB code 2P22) (Kostelansky, Schluter *et al.* 2007) is used to model the docking to an endosomal membrane. The GLUE domain (PDB code 2CAY) (Teo, Gill *et al.* 2006) and the NZF1 domain of ESCRT-II (PDB code 2J9U) (Gill, Teo *et al.* 2007) are cyan, ubiquitinated Cps1 is red, and ESCRT-I subunits are colored as in (b). **(b)** Schematic diagram of the docked model, incorporating simplified models of the interacting Vps27/Hse1 and ESCRT-II complexes. *Adapted from (Kostelansky, Schluter et al. 2007)*.

ESCRT-I is transiently recruited to the endosomal membranes via the Vps23 UEV ubiquitin-cargo interaction. The Mvb12 subunit may play simultaneously a structural role (stabilizing the stalk) and a regulatory one, suggested for instance by the fact that mammalian cells depleted of MVB12 still contain a functional ESCRT-I for viral release, though only able to produce amorphous virions (Morita, Sandrin *et al.* 2007). Ultimately, through the C-terminal domain of Vps28, ESCRT-I can engage the downstream ESCRT-II complex as well as ESCRT-III complex (Bowers, Lottridge *et al.* 2004; Pineda-Molina, Belrhali *et al.* 2006).

ESCRT-II

Yeast ESCRT-II consists of three subunits: Vps36, Vps22 and Vps25 that assemble a trilobal Y-shaped heterotetramer, with two subunits of Vps25 forming two lobes, while tightly packed Vps22 and Vps36 form the third one (Hierro, Sun *et al.* 2004; Teo, Perisic *et al.* 2004). Each subunit of the complex is composed of two winged helix (WH) domains, that are compact domains which fold into an helical part followed by a twisted antiparallel beta-sheet and two large loops (wings) (Hierro, Sun *et al.* 2004; Teo, Perisic *et al.* 2004; Wernimont and Weissenhorn 2004). The two Vps25 subunits do not contact each other but interact with Vps22 and Vps36 separately. Vps25 binds the downstream Vps20 component of ESCRT-III (Teo, Perisic *et al.* 2004; Yorikawa, Shibata *et al.* 2005) using a conserved C-terminal patch. The N-terminal region of Vps36 contains a phosphoinositide-binding GLUE domain (Slagsvold, Aasland *et al.* 2005; Teo, Gill *et al.* 2006) that in the yeast homologue harbors two additional NZF domain (NZF-N and NZF-C; see also Figure 5). Only the NZF-C possesses ubiquitin binding activity and recognizes monouibiquitylated proteins. NZF-N, on the other hand, binds to the C-terminus of Vps28 (ESCRT-I) (Gill, Teo *et al.* 2007). The GLUE domain found in human VPS36 lacks the NZF domains but is still able to bind both ubiquitin and PI3P. In fact, the crystal structure of human ESCRT-II was recently solved (Im and Hurley 2008) (Figure 3a) and brought new information about the arrangement of the N-terminal predicted helical regions of both Vps22 and Vps36 (between the GLUE and the core). It was shown that most of the N-terminal predicted helix (H0) of the core of each subunit is flexibly attached to the core of the assembly and that the VPS22-H0 participates in direct membrane binding, while the VPS36-H0 interacts with the human VPS28 C-terminal domain (Figure 3b,c). Of note, portions of VPS-22 and VPS-36 assemble a helical domain that appears to serve as a structural platform for the GLUE domain. This might therefore bind to the core assembly, stabilizing a compact ESCRT-II complex.

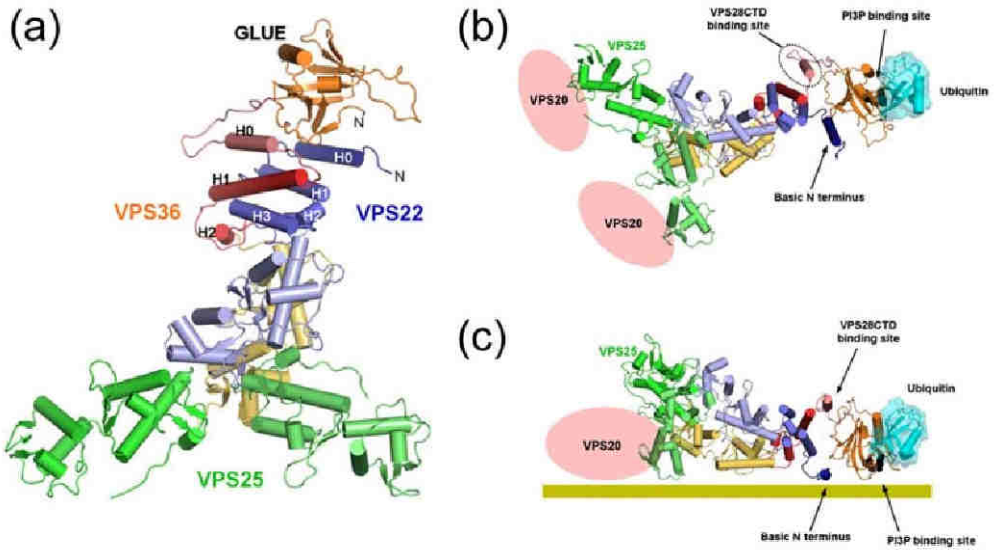

Figure 3. Structure of the human ESCRT-II complex. (a) The overall structure of the intact human ESCRT-II complex depicted here is a solution conformation derived by fitting structural coordinates to hydrodynamic data from four different ESCRT-II complexes (Im and Hurley 2008). The GLUE domain structure (Alam, Langelier *et al.* 2006; Hirano, Suzuki *et al.* 2006) has been positioned packing against the HD domain of the crystallized ESCRT-II (PDB codes 3CUQ and 2ZME) (Im and Hurley 2008). **(b)** Overall schematic representation of full-length ESCRT-II structure showing the binding site for VPS28-CTD and the VPS22-H0 (basic N terminus) as well as the previously described binding sites for PI3P (Teo, Gill *et al.* 2006), ubiquitin (Alam, Langelier *et al.* 2006; Hirano, Suzuki *et al.* 2006) and VPS20 (Langelier, von Schwedler *et al.* 2006). **(c)** Model for combinatorial targeting by specific and nonspecific interactions with membrane (solid horizontal bar) lipids. *Adapted from (Im and Hurley 2008)*.

The recruitment of ESCRT-II to the endosomal membrane is independent of ESCRT-I, since the loss of ESCRT-I can be rescued by the overexpression of ESCRT-II subunits (Babst, Katzmann *et al.* 2002). Nevertheless, ESCRT-II seems to be functionally activated by ESCRT-I, a process still unclear which might involve major conformational changes in both complexes (Im and Hurley 2008). Additionally, the stability and function of membrane-bound ESCRT-II are heavily dependent on the binding partners, such as PI3P, ubiquitin, ESCRT-I and/or other charged lipids, since MVB sorting defects are triggered when such interactions are compromised.

ESCRT-III

Unlike the ESCRT-I and -II complexes, which target the endosomal membrane as preformed complexes (from the cytosol), ESCRT-III proteins exist as monomers in the cytosol and are recruited to the membrane where they are thought to assemble a heteroligomeric protein complex (protein lattice) of indeterminate stoichiometry (Saksena, Sun *et al.* 2007; Williams and Urbe 2007).

Yeast expresses six ESCRT-III-like proteins (Babst, Katzmann *et al.* 2002) while mammalian cells express ten, known as *CH*arged *M*ultivesicular Body *P*roteins (CHMPs) 1 to 6 (von Schwedler, Stuchell *et al.* 2003). Some mammalian ESCRT-III subunits present multiple isoforms whose functional role is not yet clear (Table 1).

All ESCRT-III-like proteins have a similar organization, consisting of an N-terminal basic and a C-terminal acidic region (Figure 4a). The crystal structure of C-terminally truncated human VPS24/CHMP3 (Muziol, Pineda-Molina *et al.* 2006) reveals an organization that is thought to be common to all the ESCRT-III-related proteins (Figure 4b). The core of this protein assembles an asymmetrical antiparallel four-helix bundle with the first two N-terminal helices forming a 70 Å long helical hairpin. The C-terminal region of VPS24/CHMP3, like for all the other ESCRT-III subunits, constitutes the autoinhibitory region that comprises the helix α-5 (seen in the crystal structure) and the C-terminal microtubule-interacting and transport (MIT)-interacting region (MIR) not present in the crystal structure. The autoinhibitory C-terminal blocks homo- or heterodimerization of ESCRT-III components by forming a competing electrostatic interaction with the core (negative C-terminal back folds to interact with the positive N-terminal, Figure 4b). In fact, VPS24/CHMP3 exists in the cytosol in an autoinhibited monomeric form (Zamborlini, Usami *et al.* 2006; Lata, Roessle *et al.* 2008), but the truncated form crystallized lacks a main portion of the autoinhibitory C-terminal and mimics the activated form of the protein. It was indeed observed that VPS24/CHMP3

crystal lattice was formed by linear arrays of homodimers that might represent the typical arrangement of ESCRT-III subunits on the putative protein lattice assembled on the endosomal membrane (Muziol, Pineda-Molina *et al.* 2006). Two dimer interfaces were observed: one mediated by the antiparallel packing of the long N-terminal helix α-2 and a second one occurring through the tips of the α1-α2 helical hairpin (Figure 4c). Both dimerization interfaces were shown to be essential for membrane targeting as well as HIV-1 budding. Dimerization mutants no longer localized predominately to the plasma membrane, since they disrupt an extended basic surface observed on the crystalline lattice that most likely mediates a strong interaction with negatively charged membranes. The current data suggest that activation of CHMP proteins entails displacement of the C-terminal region from the N-terminal core, inducing membrane targeting and polymerization (Lin, Kimpler *et al.* 2005; Muziol, Pineda-Molina *et al.* 2006).

The actual trigger for the formation of an ESCRT-III lattice on the endosomal membranes might involve Vps20/CHMP6 which contains a myristoylation tag that could allow spontaneous membrane association and topologically orient Vps20/CHMP6 for stable interaction shown to occur with Vps25 (ESCRT-II) (Yorikawa, Shibata *et al.* 2005). Such interaction could induce the displacement of the autoinhibitory MIR domain, thus activating Vps20/CHMP6 for heterodimerization. In yeast it has been suggested that Vps20/CHMP6 can form a subcomplex with Snf7/CHMP4 (Babst, Katzmann *et al.* 2002). This means that activated Vps20/CHMP6 on the membranes could recruit Snf7/CHMP4 and initiate a cascade of heterodimerization events involving recruitment and activation of other ESCRT-III subunits to assemble the protein lattice.

Several studies pointed out the importance of the ESCRT-III membrane polymerization in the processes of membrane deformation and completion of budding.

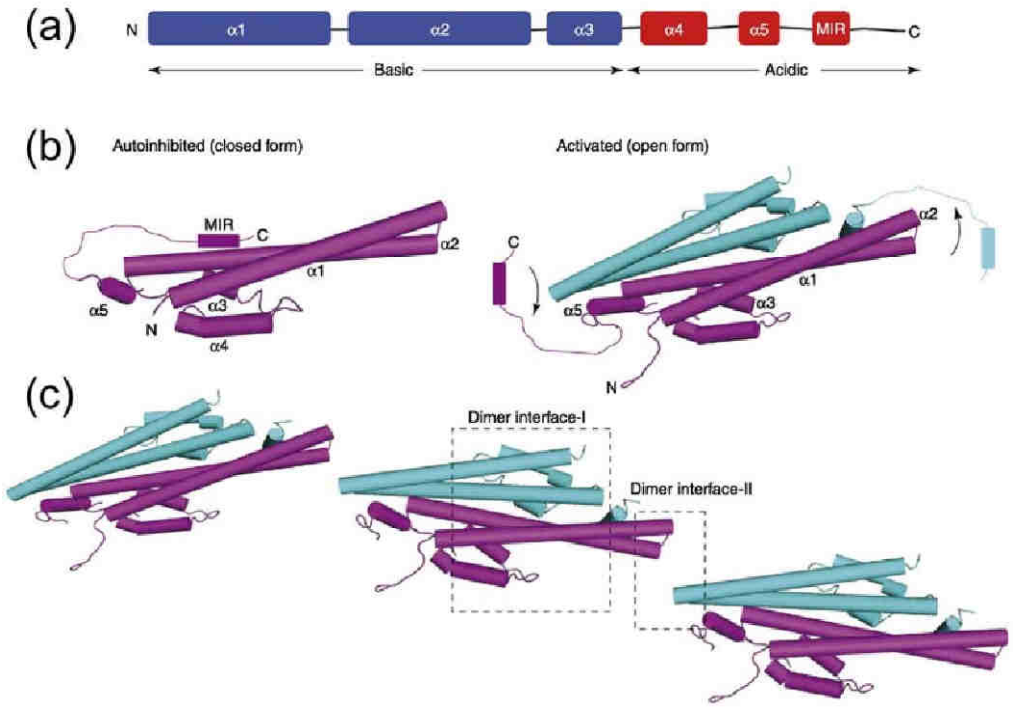

Figure 4. The ESCRT-III complex. (a) ESCRT-III subunits have a related sequence with prominent bipolar character and probably similar helical organizations like the one depicted here (hVps24/CHMP3). **(b)** The structure of hVps24/CHMP3 (PDB code 2GD5) (Muziol, Pineda-Molina *et al.* 2006) is shown in both putative conformations: autoinhibited (left panel), corresponding to a closed conformation with the MIR domain forming a competing interaction with the ESCRT-III core; activated (right panel) where the MIR is displaced (indicated by black arrows) allowing ESCRT-III dimerization. Of note, neither the MIR domain nor the loop connecting it to helix α5 were see in the crystal structure and have been added here to complete the model. For this reason the hVps24/CHMP3 homodimer observed in the crystal structure reflects the activated (open) form of the molecule. **(c)** A linear array of hVps24/CHMP3 dimers as packed in the crystal is depicted. The dimer interfaces as observed in the crystal are highlighted by dashed-black boxes. *Adapted from (Saksena, Sun et al. 2007)*.

The first evidences for the role of ESCRT-III in final stages of budding, was revealed by the dominant negative effect of ESCRT-III mutants that led to an arrest of retrovirus budding, characterized by viral particle buds that fail to pinch off and remain associated with the cell membrane (Strack, Calistri *et al.* 2003; von Schwedler, Stuchell *et al.* 2003). Further evidence was provided by overexpression of CHMP4 in mammalian cells which

polymerize into circular filaments that induce tubules protruding from the cell surface in the presence of catalytically inactive VPS4B (Hanson, Roth *et al.* 2008). In addition it was demonstrated that CHMP2A and CHMP3, produced as C-terminal truncations in their proposed activated forms, assemble helical tubular structures *in vitro* with a diameter of ~40-70 nm. VPS4 was shown to bind on the inside and disassemble the tubules upon ATP hydrolysis and membrane binding surface of the tubules was shown to be exposed on the outside (Lata, Schoehn *et al.* 2008). These polymeric CHMP structures suggest a model where helical structures of ESCRT-III CHMP2A-CHMP3 assemble on the inside of a membrane bud that recruits VPS4 and their concerted action lead to membrane constriction and fission.

Deubiquitylation in the ESCRT pathway

Deubiquitylation of cargo precedes its incorporation into ILVs and serves to recycle and maintain cytoplasmic levels of free ubiquitin. Deubiquitylating enzymes (DUBs) are an integral part of the MVB machinery and are thought to act earlier in the endocytic pathway where they provide a proofreading mechanism important for disengagement of cargo from the ESCRT machinery. In addition, since many proteins of the endocytic pathway are ubiquitylated, DUBs might directly regulate certain activities of different ESCRT components (Amerik and Hochstrasser 2004; Luhtala and Odorizzi 2004).

Out of the 16 DUBs found in yeast, only Doa4 (degradation of α-4) has been implicated in the MVB pathway (Reggiori and Pelham 2001; Amerik and Hochstrasser 2004). Efficient deubiquitylation by Doa4 requires Bro1, which has an important role in recruiting Doa4 to endosomes (Luhtala and Odorizzi 2004; Kim, Sitaraman *et al.* 2005) although a direct interaction between Doa4 and Snf7 has also been reported (Bowers, Lottridge *et al.* 2004). Enzymatic activation of Doa4 occurs through binding of a conserved proline-based sequence near the C-terminus of Bro1 to an YPXL motif in

Doa4. Thus Bro1 coordinates both function and specificity of Doa4 (Richter, West *et al.* 2007).

In mammalian cells two endosomal DUBs are recruited by STAM: UBPY/USP8 and AMSH (associated molecule with the SH3 domain of STAM). UBPY is most likely the Doa4 ortholog in mammalian cells. It interacts with SH3-domain of the ESCRT-0 component STAM via two non-canonical binding motifs (Kato, Miyazawa *et al.* 2000; Kaneko, Kumasaka *et al.* 2003). UBPY-depleted cells fail to degrade multiple activated receptor Tyr kinases, which accumulate on endosomes in their ubiquitylated form. HD-PTP is the mammalian homolog of Bro1p, but to date it is unclear if it is able to recruit and activate deubiquitynating enzymes (such as UBPY).

The other mammalian DUB, AMSH, is activated upon association with STAM and also conserves one of binding motifs present in UBPY (Kato, Miyazawa *et al.* 2000; McCullough, Row *et al.* 2006). In addition AMSH binds to clathrin, and contains an N-terminal MIT-like domain that binds multiple CHMPs, including CHMP3 (Agromayor and Martin-Serrano 2006; McCullough, Row *et al.* 2006; Tsang, Connell *et al.* 2006; Zamborlini, Usami *et al.* 2006; Kyuuma, Kikuchi *et al.* 2007; Lata, Roessle *et al.* 2008). AMSH binds with high affinity to both close (inactive) and open (active) conformations of CHMP3 indicating that, in addition to the C-terminal MIR domain, other regions of CHMP3 contribute for this interaction (Lata, Roessle *et al.* 2008). Expression of an AMSH mutant unable to bind CHMP3 caused the formation of aberrant endosomes with accumulations of ubiquitylated cargo. Depletion of AMSH or expression of a catalytic inactive AMSH also promoted accumulation of ubiquitylated cargo on endosomes (McCullough, Clague *et al.* 2004; Kyuuma, Kikuchi *et al.* 2007). This indicated that both CHMP3-binding ability and the DUB activity of AMSH are required to clear ubiquitylated cargo from endosomes.

Membrane disassembly of the ESCRT machinery

The different ESCRT components are recycled back to the cytosol by the activity of Vps4, an enzyme belonging to the family of AAA+ ATPases that catalyzes the disassembly of membrane-bound ESCRT-III subunits upon ATP hydrolysis. Such activity seems critical for sorting into MVB vesicles, since in both yeast and mammalian cells the loss of Vps4 function results in accumulation of ESCRT components on membranes, impairment of cargo sorting and a class E phenotype (Babst, Wendland *et al.* 1998; Fujita, Yamanaka *et al.* 2003; Sachse, Strous *et al.* 2004).

In humans there are two isoforms of VPS4 (A and B) that are 80% identical. The crystal structure of VPSB has been determined in a monomeric, ATP-free form (Scott, Chung *et al.* 2005). In the presence of ATP, VPS4 assembles into a complex of 10-12 subunits, thought to be organized in two hexameric rings stacked on each other, forming a hydrophobic pore in the center (Scott, Chung *et al.* 2005). It has been suggested that ESCRT-III subunits might be drawn into the central cavity of VPS4 and due to the narrow diameter of the pore, partial unfolding of ESCRT-III substrate might be required.

The recruitment of VPS4 to endosomal membranes occurs through an interaction between its N-terminal three-helical bundle MIT domain and the C-terminal segment of ESCRT-III proteins (Babst, Katzmann *et al.* 2002; Lin, Kimpler *et al.* 2005; Scott, Gaspar *et al.* 2005; Tsang, Connell *et al.* 2006). Conserved C-terminal helical peptide motifs (MIMs; MIT domain interacting motif) present in yeast Vps2 and Did2 proteins as well as in human CHMP1 and 2 bind directly to Vps4 MIT domain (Obita, Saksena *et al.* 2007; Stuchell-Brereton, Skalicky *et al.* 2007). In contrast CHMP4 to 6, lack the C-terminal MIM consensus sequence and contain a second MIM that mediates their interaction with VPS4 MIT domain (Kieffer, Skalicky *et al.* 2008). As mention above, ATP binding leads to VPS4 oligomerization. However the association of the protein LIP5 (Vta1 in yeast) has been shown to increase the rate of ATP hydrolysis and therefore accelerate VPS4

activity (Yeo, Xu *et al.* 2003; Scott, Chung *et al.* 2005; Azmi, Davies *et al.* 2006). LIP5 also interacts with CHMP5 (Ward, Vaughn *et al.* 2005; Azmi, Davies *et al.* 2006) and this interaction does not compete with VPS4 (Azmi, Davies *et al.* 2006). In yeast, deletion of VPS60 (CHMP5 ortholog) causes prolonged retention of Vta1 in class E compartments, suggesting that Vps60 migh have a role in recycling Vta1 (Shiflett, Ward *et al.* 2004; Azmi, Davies *et al.* 2006).

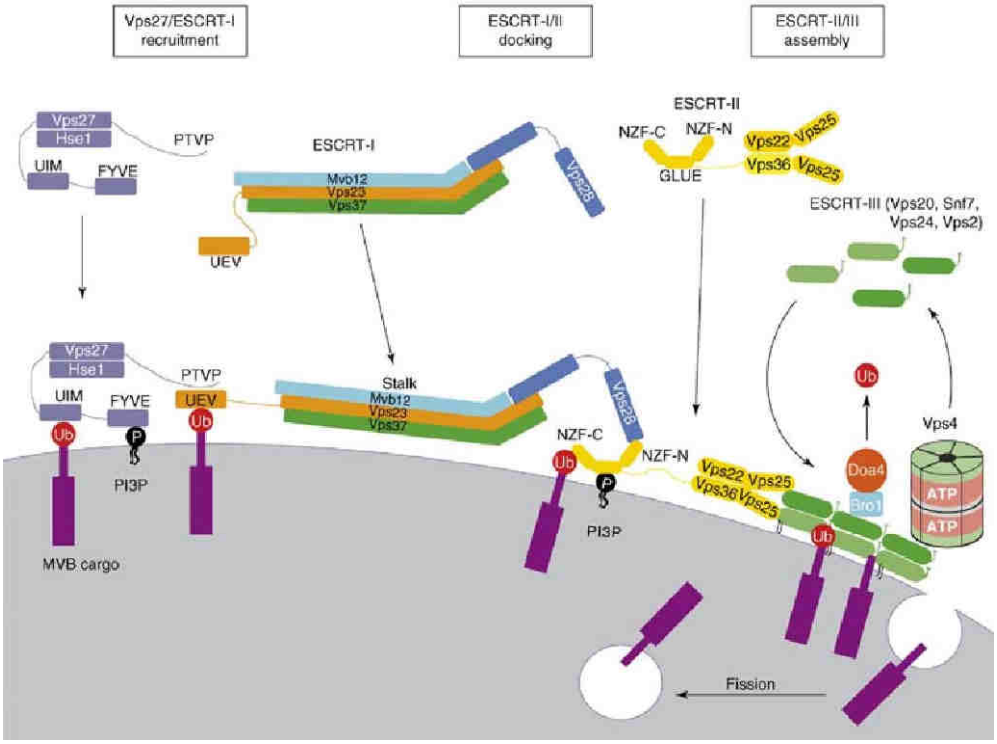

Figure 5. Membrane-docked model for the yeast ESCRT complexes. The recruitment of Vps27/ESCRT-I to the endosomal membranes is mediated Vps27 FYVE domain, that directly binds to PIP3. The UIM domains of Vps27 and Hse1 recognize and bind ubiquitylated cargo for sorting into MVB vesicles. Vps27-Hse1 complex recruits the ESCRT-I complex to the membrane via interactions with the UEV domain of Vps23. Membrane bound ESCRT-I binds ubiquitylated cargo via the UEV domain of Vps23 and recruits ESCRT-II to the membrane via interactions between the Vps28 C-terminus and the NZF-N domain of Vps36 (ESCRT-II). The GLUE domain of Vps36 binds endosomal PI3P, while the NZF-C domain binds ubiquitylated cargo. Membrane ESCRT-II recruits the downstream ESCRT-III complex via interactions between Vps25 and Vps20. The ESCRT-III lattice assembled on the endosomal membrane is disassembled following cargo sorting into MVB vesicles via interactions between the C-terminal MIR region of ESCRT-III subunit at the leading edge of the lattice and the MIT domain Vps4. The majority of the features depicted in this model are conserved in the mammalian pathway. *Adapted from (Saksena, Sun et al. 2007)*.

Reasons for exploring the ESCRT machinery

Several pathophysiological disorders have been associated with misregulation of ESCRT and/or ESCRT-associated components. Misregulation of protein trafficking can have serious implications in the control of cell growth. High levels of epidermal growth factor receptor (EGFR) are associated with tumor growth and metastasis in several types of cancer. Deletion of components of ESCRT-0 (Hrs) (Bache, Brech *et al.* 2003) and ESCRT-I (Tsg101) (Babst, Odorizzi *et al.* 2000) have been shown to impair EGFR degradation and consistent with this, mutations of human TSG101 have been linked to many different types of cancers such as cervical, breast, prostate and gastrointestinal cancers. In *Drosophila melanogaster* similar defects in cell proliferation were also observed due to misregulation of surface receptors (e.g. Notch and EGFR) upon inactivation of Tsg101 or Vps25 (ESCRT-II) (Moberg, Schelble *et al.* 2005; Thompson, Mathieu *et al.* 2005). In addition the absence of Vps28 (ESCRT-I) and mutations on Shrub (equivalent of yeast Snf7, ESCRT-III) resulted respectively in dysfunctional actin cytoskeleton and loss of epithelial organization due to abnormal branching of neuronal cells (Sevrioukov, Moghrabi *et al.* 2005; Sweeney, Brenman *et al.* 2006). ESCRT is also required for the proper turnover of autophagosomes, since the depletion of ESCRT subunits results in the inhibition of autophagic clearance of cytosolic protein and organelles and accumulation of protein aggregates (Filimonenko, Stuffers *et al.* 2007; Rusten, Vaccari *et al.* 2007; Lee and Gao 2008). This relates to neurodegenerative diseases, as for instance frontotemporal dementia linked to chromosome 3 (FTD3), found to result from dysfunction of an ESCRT-III component (VPS2B/CHMP2B) that leads to autophagosome accumulation and dendritric retraction before neurodegeneration in cultured mature cortical neurons (Skibinski, Parkinson *et al.* 2005; Lee, Beigneux *et al.* 2007; Lee and Gao 2008).

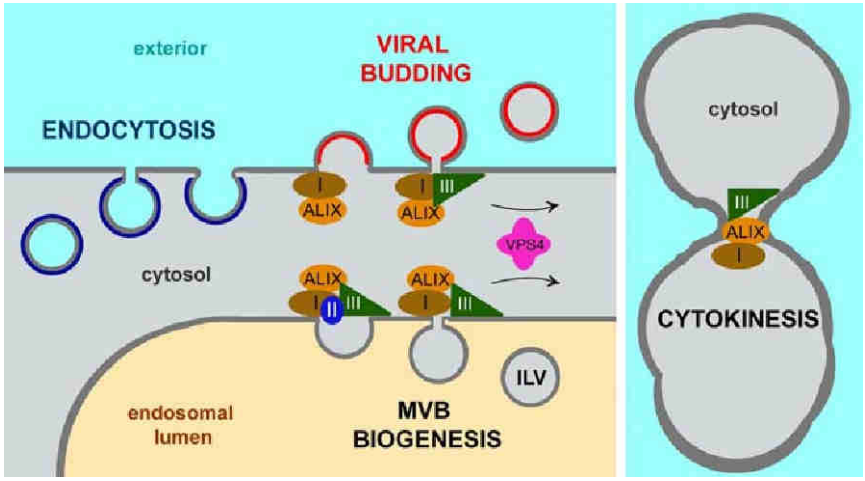

Figure 6. Cellular processes involving vesicle formation and budding. During *endocytosis* the plasma membrane suffers an inward vesiculation and budding normally supported by a clathrin coat and other effector proteins (*e.g* endophylins, dynamins). In the multivesicular body (*MVB*) pathway the endosomal membrane undergoes an outward deformation to form intralumenal vesicles (ILV). A topological similar process occurs at the plasma membrane during release of new viral particles (*viral budding*). In *cytokinesis* (cell division) the plasma membrane rearrangements in the cleavage furrow resemble the process of outward budding. Both MVB biogenesis, viral budding and cytokinesis engage a set of cellular components responsible for membrane constriction and fission (*e.g.* ESCRT-I, –III and Alix).

Apart from all the pathophysiological disorders much of the impetus for the studying of the ESCRT machinery relates to the fact that some enveloped viruses can efficiently hijack this cellular apparatus to escape from the host cell. Indeed, the non-lytic production of virions that bud from the plasma membrane is topollogically equivalent to the budding of vesicles into the MVB (Figure 6). In both cases, an outward vesiculation of the limiting membrane is observed, different from inward vesiculation as seen in endocytosis (Figure 6). Structural proteins of retroviruses such as HIV-1 Gag^{p6} contain sequence motifs termed “late domains” that bind directly to different components of the ESCRT machinery (Alix, TSG101 and Nedd4) (Morita and Sundquist 2004) and allow their recruitment and subsequent activity in viral budding zones. Late domains are discussed in more detail later in the text.

Recent reports have extended the importance of the ESCRT machinery to the process of cell division (Carlton and Martin-Serrano 2007; Morita, Sandrin *et al.* 2007) (Figure 6). Cytokinesis involves constriction of the cell membrane by actin and myosin forming a cleavage furrow which further develops into a protein-rich membranous midbody structure. The final step of abscission requires the cleavage of this midbody structure and separates two new daughter cells. It was shown that the centrosomal protein Cep55, was able to directly interact with TSG101 and Alix and mediate their recruitment to the midbody. In addition RNAi-mediated depletion of TSG101 and Alix resulted in multinucleated cells indicating cytokinesis defects.

Overall, it seems that the ESCRT and ESCRT-associated components are recruited to different biological processes that involve a terminal membrane fission event. Indeed in both endosomal intraluminal vesicle formation, HIV budding and cytokinesis a membrane tubule needs to be constricited and ultimately cleaved by a cellular machinery acting from the inside.

Alix, a multifunctional protein

Alix/AIP1 is a cytosolic protein in mammalian cells that was initially described as an interacting partner of ALG-2 (apoptosis-linked gene 2), a Ca^{2+}-binding protein implicated in apoptotic signaling (Missotten, Nichols *et al.* 1999; Vito, Pellegrini *et al.* 1999). Both nomenclatures derive in fact from this original discovery: Alix/AIP1, ALG-2 interacting protein X or 1.

Several studies showed that besides apoptosis, Alix participates in a large spectrum of activities including endocytic membrane trafficking (Saksena, Sun *et al.* 2007), cytoskeleton remodeling (Cabezas, Bache *et al.* 2005), retrovirus budding (von Schwedler, Stuchell *et al.* 2003) and cytokinesis (Carlton and Martin-Serrano 2007; Morita, Sandrin *et al.* 2007), expanding the functions of Alix to numerous apparently unrelated cellular processes (Table 2). The challenge has been to understand the role of Alix in each of these processes and potentially reveal new functional links between some of them. Even in the presence of the structural details for yeast and human Alix orthologs obtained by X-ray crystallography (Kim, Sitaraman *et al.* 2005; Fisher, Chung *et al.* 2007; Lee, Joshi *et al.* 2007), the specific molecular functions of the protein in the distinct cellular processes have been difficult to infer. Thus Alix remains as an attractive multifunctional protein to study.

Modular organization of Alix

The ability of Alix to participate in distinct cellular activities relates with its domain architecture (Figure 7a). Mammalian Alix contains approximately 868 residues (human ortholog) and is organized in three major domains that can be considered distinct functional modules.

The N-terminal Bro1-domain is ~ 360 residues long and mediates the binding to CHMP4 (Katoh, Shibata *et al.* 2003) and subsequent localization of Alix to endosomes. The middle domain (~ residues 360-702) harbors an important binding site for YPX_nL motifs present in Gag proteins of different retroviruses, that use this interaction to usurp Alix activities to facilitate their budding from the plasma membrane (Martin-Serrano, Yarovoy *et al.* 2003; Strack, Calistri *et al.* 2003). Finally the C-terminal (PRD) domain of ~ 150 residues is rich in proline (32%), tyrosine and glutamine and harbors the majority of the binding motifs that connect Alix to different cellular processes: i) it contains several SH3 (Src Homology 3) domain binding motifs (like PXXP, Pro-X_{aa}-X_{aa}-Pro), that bind at least Src kinase (Schmidt, Dikic *et al.* 2005), endophilins (Chatellard-Causse, Blot *et al.* 2002) and the adaptor protein SETA (Chen, Borinstein *et al.* 2000); ii) two WW-binding domains (PPXY); iii) binds to ALG-2 through a PXY-containing sequence (Shibata, Yamada *et al.* 2004; Trioulier, Torch *et al.* 2004); iv) binds to TSG101 (ESCRT-I) through a P(T/S)AP motif (Martin-Serrano, Yarovoy *et al.* 2003; Strack, Calistri *et al.* 2003; von Schwedler, Stuchell *et al.* 2003).

Table 2. Summary of Alix protein-protein interactions. *Adapted from (Odorizzi 2006)*

Alix-binding protein	Alix-binding motif	Binding site in Alix	Cellular activity
TSG101 (ESCRT-I)	UEV domain	P717SAP720	MVB sorting and viral budding
CHMP4 (ESCRT-III)	M/L/IxxLxxW *	Bro1 domain, Patch 1	MVB sorting and viral budding
Gag †	YPx_nL‡	V domain	Viral budding
SETA	SH3 domain	P_{740}TPAPR$_{745}$ (PRD)	Growth factor receptor endocytosis; focal adhesion remodeling
Endophilin	SH3 domain	P_{755}ARPPPP$_{761}$ (PRD)	Growth factor receptor endocytosis
Src	SH3 domain	Phospho-Y_{319} (Bro1)	Growth factor receptor endocytosis; focal adhesion remodeling
Src	SH3 domain	P_{752}QPPAR$_{757}$ (PRD)	Growth factor receptor endocytosis; focal adhesion remodeling
ALG-2	Unknown	PGY repeats (aa 802-813)	Apoptosis
RabGAPLP	Unknown	N-term (aa 1-423)	Cell adhesion and signal transducing pathways
Actin	Unknown	Bro1 and PRD domain	Cytoskeleton remodeling

* x unspecified amino acid. † Gag proteins encoded by EIAV, HIV-1, and murine leukemia virus. ‡ x_n indicates 1 to 3 unspecified amino acids.

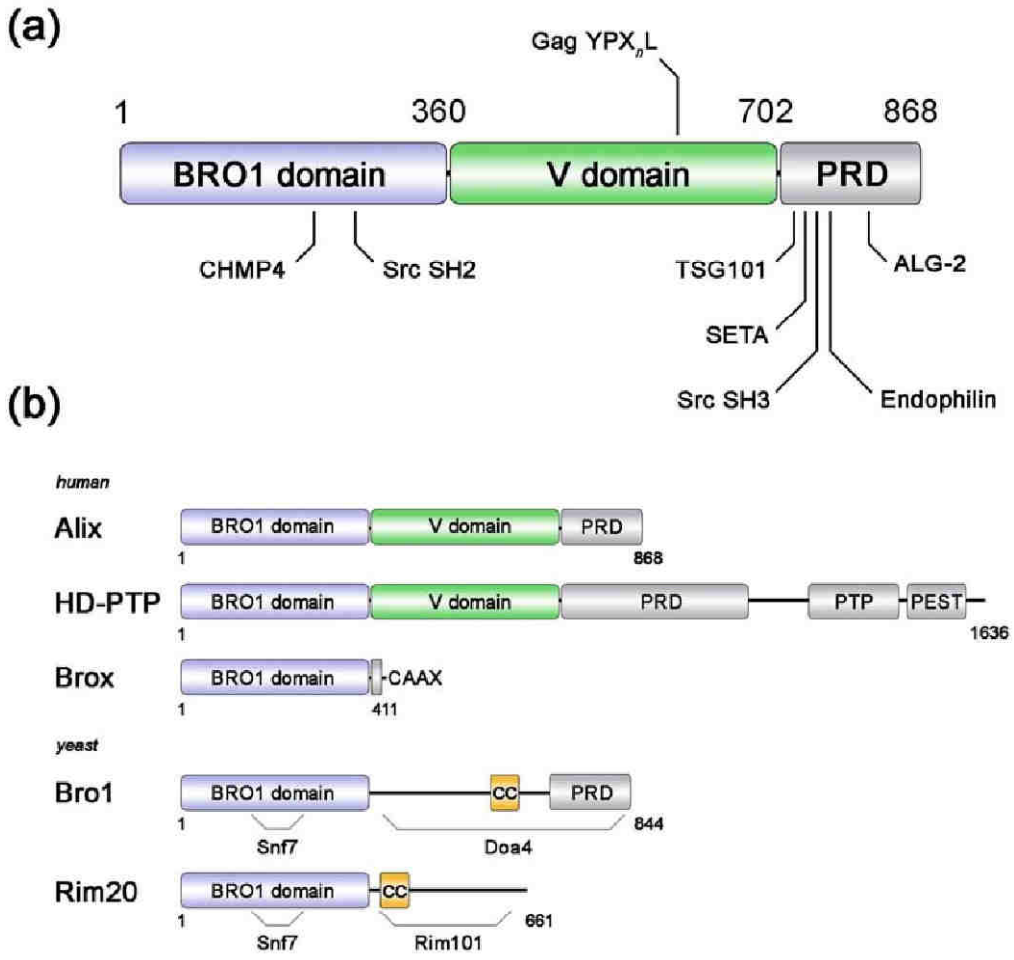

Figure 7. Domain architecture of Alix and related Bro1 domain-containing proteins. (a) Schematic representation of the domains of Alix. In addition to the binding sites for CHMP4 and Gag YPX$_n$L motifs, Alix harbors interaction sites for TSG101, SETA, Src and endophilins in its PRD. **(b)** Comparison of the domain organization between Alix and its family members in human and yeast. HD-PTP contains in addition to the PRD a protein tyrosine phosphatase domain (PTP) and a PEST motif (Pro-Glu-Ser-Thr; putative signal peptide for protein degradation). Brox contains a thioester-linkage site of isoprenoid lipid (CAAX motif; C, Cys; A aliphatic residue; X any residue). Yeast Bro1 is similar in length to Alix and its PRD is contained within the region for interaction with Doa4 (Kim, Sitaraman *et al.* 2005). The C-terminal of Rim20 binds the Rim101 transcription factor (Xu and Mitchell 2001). See also supplementary Figure S1.

Alix homologues in *Saccharomyces cerevisiae*

Much of the advances in the understanding of Alix functions result form the characterization of the endocytic membrane trafficking in yeast. The role for Alix in this process was initially suggested by the fact that the loss of Bro1 function (Alix ortholog, Figure 7b) in yeast impairs the down regulation of cell-surface proteins that normally undergo endocytosis and delivery to the vacuole (equivalent to lysosome in higher eukaryotes) (Forsberg, Hammar *et al.* 2001; Springael, Nikko *et al.* 2002). Subsequent characterization of Bro1 allowed to integrate it on the class E Vps family (Nikko, Marini *et al.* 2003; Odorizzi, Katzmann *et al.* 2003).

Bro1 binds to Snf7/Vps32, which is part of the ESCRT-III (Odorizzi, Katzmann *et al.* 2003) and is therefore recruited to the endosomes. Once on the endosomal surface, Bro1 recruits and stimulates the catalytic activity of the ubiquitin thiolesterase Doa4 (Luhtala and Odorizzi 2004; Richter, West *et al.* 2007) that de-ubiquitinates endosomal cargo, which is subsequently sorted in the membranes of ILV and ultimately end up in the vacuole. Moreover the PRD region of Bro1 mediates an association with the ubiquitin ligase Rsp5 which also regulates sorting of cargoes through MVBs (Springael, Nikko *et al.* 2002; Katzmann, Sarkar *et al.* 2004; Nikko and Andre 2007). Thus Bro1 contributes simultaneously to associating ubiquitinating and deubiquitinating enzymes with the MVB sorting machinery.

In addition to Bro1, *Saccharomyces cerevisiae* has another Alix homolog named Rim20 (Figure 7b). This protein also contains a Bro1-domain but lacks the PRD region found in Bro1 and Alix. Rim20 was first described in *Aspergillus nidulans* as PalA, which is a component of a signalling pathway for changes in pH that is conserved throughout fungi (Arst and Penalva 2003). Indeed the association of Rim20/PalA with Snf7 at the endosomes does not serve any protein sorting activity (Odorizzi, Katzmann *et al.* 2003); instead it results in the recruitment of the protease Rim13/PalB, as well as the

transcription factor Rim101/PacC. The present model is that Rim20/PalA forms a scaffold together with Snf7, bringing the protease Rim13/PalB into close proximity with its substrate Rim101/PacC (Xu and Mitchell 2001). Rim101/PacC activation is required for cells to grow normally in an alkaline environment.

The Bro1-domain seems to be a common element in several proteins that localize to endosomes due to interaction with Snf7 but have not necessarily a function in protein sorting.

Interactions between Alix and the ESCRT machinery

The characterization of mammalian homologues of ESCRT proteins and their mutual interactions revealed a link between Alix and the ESCRT machinery.

Alix was shown to use a P(T/S)AP motif in its C-terminal region to bind the UEV domain in the TSG101 subunit of ESCRT-I (Martin-Serrano, Yarovoy *et al.* 2003; Strack, Calistri *et al.* 2003; von Schwedler, Stuchell *et al.* 2003). Since Bro1 lacks a P(T/S)AP motif and does not directly interact with Vps23, the yeast ortholog of TSG101 (Bowers, Lottridge *et al.* 2004) and the same occurs for the *Dictyostelium* ortholog of Alix (Mattei, Klein *et al.* 2006), the importance of such Alix-TSG101 interaction is still not clear.

ESCRT-III CHMP4 interacts directly with Alix, three isoforms of which exist in mammalian cells (CHMP4A, B and C). Alix is able to bind each CHMP4 isoform (Katoh, Shibata *et al.* 2003; Martin-Serrano, Yarovoy *et al.* 2003; Strack, Calistri *et al.* 2003; von Schwedler, Stuchell *et al.* 2003; Katoh, Shibata *et al.* 2004; Peck, Bowden *et al.* 2004), but CHMP4B is considered as its major interaction partner (Katoh, Shibata *et al.* 2004). The structural details of Alix-CHMP4 interaction are described later on in the text. Similarly as described for Bro1, the interaction of Alix with CHMP4 mediates the recruitment of Alix to endosomes. This is supported by immunoflurescence studies showing that the overexpression of CHMP4B causes the accumulation at the

endosomes of both full-length Alix and a truncated form containing the Bro1 domain (Katoh, Shibata *et al.* 2003).

Functional links between Alix and MVB trafficking

In mammalian cells lysobisphosphatidic acid (LBPA), an isomer of phosphatidylglycerol, is enriched in late endosomal membranes (Kobayashi, Stang *et al.* 1998; Kobayashi, Beuchat *et al.* 2002). LBPA plays a role in trafficking through late endosomes, as first suggested by the fact that endocytosed anti-LBPA antibodies cause lumenal vesicles to adopt a disorganized appearance (Kobayashi, Stang *et al.* 1998). The hypothesis that the content of LBPA in membrane bilayers influences the dynamics of MVBs, was indeed confirmed by Matsuo et al. (Matsuo, Chevallier *et al.* 2004) who observed that synthetic liposomes prepared with LBPA spontaneously accumulated ILVs in their lumen, provided a pH difference between the inside of the liposomes (pH= 5.0) and the exterior (pH= 7.0). The incubation of LBPA-liposomes with cytosol allowed to identify Alix (together with 4 other proteins) that is selectively recruited to such lipid structures. Remarkably, the incubation of LBPA-liposomes with recombinant Alix blocked the formation of multivesicular liposomes, whereas depletion of Alix from the cytosol favoured the accumulation of vesicles.

The specific mechanism by which LBPA induces membrane curvature and/or fission of membrane bilayers is not yet clear. Curiously, LBPA also stimulates fusion between liposomes *in vitro* (Kobayashi, Beuchat *et al.* 2002). Therefore, the current scenario is that LBPA is able to destabilize endosomal membranes, promoting both budding of MVB vesicles and their back-fusion with limiting endosomal membranes and that Alix might fulfill a specific regulatory role by serving as a sequestration factor to limit the availability of LBPA. Since LBPA has not been detected in yeast, this Alix-LBPA relationship appears to be unique to higher eukaryotic organisms.

In addition, Alix has been proposed to regulate vesiculation of the MVBs through a cooperative interaction with endophilins. The Alix PRD region binds the SH3 domains of several endophilins (A1,A2 and A3) through a PXRPPPP consensus sequence also found within other endophilin interactors (Chatellard-Causse, Blot *et al.* 2002).

Endophilins (type A) are enriched in synapses and were initially shown to be essential for the formation of synaptic vesicles from the plasma membrane (Gad, Ringstad *et al.* 2000). Currently they are known as major accessory proteins acting in the process of endocytosis in concert with other adaptor and effector proteins (*e.g.* dynamin, amphiphysin, synaptojanin) leading to an increase of membrane curvature, membrane invagination and the formation of a clathrin-coated vesicle (Fotin, Cheng *et al.* 2004). Endophilins contain BAR domains that sense and/or induce membrane curvature (Farsad, Ringstad *et al.* 2001; Zimmerberg and McLaughlin 2004), a fact consistent with their recruitment in a number of processes that involve membrane vesiculation, including virus budding (Wang, Kim *et al.* 2003), maintenance of mitochondrial morphology (Karbowski, Jeong *et al.* 2004) and inhibition of receptor-mediated endocytosis (Sugiura, Iwata *et al.* 2004).

Still concerning vesiculation activities, it was suggested that Alix itself may be responsible for membrane deformation. The expression of several deletion mutants of Alix, in particular Alix-CT form (lacking the N-terminal half of the protein) resulted in the accumulation of small abnormal tubulo-vesicular structures in the cytoplasm of HEK293 cells (Chatellard-Causse, Blot *et al.* 2002; Strack, Calistri *et al.* 2003). Such vacuolization was not induced by over-expression of endophilin A1 alone, but was actually enhanced upon co-expression of endophilin A1 and Alix-CT.

Upstream of any MBV activities, Alix has been shown to antagonize epidermal growth factor receptor (EGFR) endocytosis compromising related signaling cascades (Schmidt, Hoeller *et al.* 2004). The E3 ubiquitin ligase Cbl binds to phosphotyrosine

residues of the cytosolic domain of EGFR and is activated upon phosphorylation by the receptor. On its turn, Cbl mono-ubiquitylates the EGFR and triggers its endocytosis. Activated Cbl also recruits the adaptor protein SETA (also named CIN85 or Ruk) that constitutively interacts with endophilins, a fact that is thought to promote endocytosis (Soubeyran, Kowanetz *et al.* 2002).

The PRD region of Alix also interacts with an SH3 motif in SETA (Chen, Borinstein *et al.* 2000) and overexpression of Alix is thought to sequester the SETA-endophilin complex preventing it from binding to Cbl and causing subsequent reduction of EGFR internalization (Schmidt, Hoeller *et al.* 2004). In addition, Alix also seems to facilitate deubiquitylation of both EGFR, Cbl and SETA that seems to contribute to inhibit receptor endocytosis (Schmidt, Hoeller *et al.* 2004). In this context, phosphorylation of Alix by Src (a protein kinase activated in response to stimulation of EGFR and other receptor tyrosine kinases) prevents Alix from binding SETA and appears as a critical regulatory step in the whole process.

Since Alix interacts with the main regulators of endocytosis (SETA and endophilins) and with the ESCRT proteins (TSG101 and CHMP4), this suggested that Alix could accompany and regulate endocytosed tyrosine kinase receptors from endosomes to lysosomes. Indeed Alix appears to have a role in negative regulation of EGF endocytosis at the plasma membrane. However, the effect seems only limited to internalization (Schmidt, Hoeller *et al.* 2004) and the ability of Alix to participate in the downstream ESCRT-mediated protein sorting at endosomes still lacks a definite prove.

Although Alix is structurally related to yeast Bro1 (Fisher, Chung *et al.* 2007), localizes to endosomes (Welsch, Habermann *et al.* 2006) and binds ESCRT proteins *in vitro* (Strack, Calistri *et al.* 2003; von Schwedler, Stuchell *et al.* 2003), recent studies brought the first evidence that Alix is most likely not the mammalian counterpart of yeast

Bro1 and another Alix-related protein, HD-PTP, acts in concert with the ESCRT machinery in receptor sorting (Doyotte, Mironov *et al.* 2008).

Mammalian homologs of Alix

In mammalian cells there are three genes encoding proteins related to *S.cerevisiae* Bro1p: Alix, HD-PTP and Brox (Figure 7b; see also supplementary Figure S1). As mentioned above, because of its pattern of molecular interactions and ability to support virus budding, Alix was the most likely candidate in mammalian cells to be the Bro1p counterpart thus supporting MVB sorting.

HD-PTP (His domain phosphotyrosine phosphatase; also known as PTPN23, type N23 protein tyrosine phosphatase) (Toyooka, Ouchida *et al.* 2000) appears to be a functional paralog of Alix; it possesses a Bro1 domain that has been shown to bind CHMP4B and a central proline-rich region that binds TSG101, endophilin A1 and ALG-2 (Ichioka, Takaya *et al.* 2007). In addition the predicted secondary structure of HD-PTP suggests that the V-domain of Alix, which could bind HIV p6, is also conserved.

Doyotte *et al.* investigated the involvement of Alix recruitment in MVB sorting (Doyotte, Mironov *et al.* 2008). Using a transferrin receptor with a HIV p6 segment fused to the cytoplasmic domain (p6-TfR) that presented a continued trafficking to MVB, no altered behaviour could be observed for p6-TfR upon Alix depletion. This suggested that a different factor is responsible for the Bro1-related activity or at least to compensate such loss of Alix. Indeed, upon silencing of HD-PTP, p6-TfR relocalized in clusters associated with EEA1 (early endosome marker) indicating that its forward trafficking had been impaired.

Additional observations reinforced the hypothesis that HD-PTP is a key regulator of endocytic trafficking. Loss of HD-PTP resulted in: i) reduction of degradation and subsequent intracellular retention of EGFR; ii) defects in the structural organization of

endosomes, affecting translocation of cargo and fluid phase markers; iii) accumulation of aberrant endosomes containing ubiquitinated proteins, like observed for ESCRT-I depletion. Moreover, the C-terminal PRD and PTP domains seemed dispensible for the sorting activity of HD-PTP and the Bro1-V domain appeared as the minimal fuctional unit of the protein able to rescue the activity of the full-length protein. Finally, ESCRT-III binding turned out to be important but not strictly essential for HD-PTP endocytic trafficking activity, implying another essential function for such interaction.

A second Alix homolog in mammalian cells is Brox (Figure 7b), a 411 residues protein first identified in the pool of protein present in exosomes in human urine (Pisitkun, Shen *et al.* 2004). Brox lacks the V-domain and the proline-rich region and diverges in sequence from Alix and HD-PTP and is even more distantly related to yeast Bro1.

A recent work by Ichioka *et al.* investigated the ability of Brox to interact with CHMP4s and the importance of a post translational lipid modification in Brox subcellular distribution (Ichioka, Kobayashi *et al.* 2008). Indeed, a unique feature of Brox is that it harbours a C-terminal tetrapeptide motif CAAX (C being cysteine, A an aliphatic residue and X any residue) which is a site for post-translation modification with isoprenoids (prenylation) (Clarke 1992). Brox gets farnesylated through this motif and such modification was shown to facilitate the interaction with CHMP4 by restricting its subcellular localization. However, farnesylation did not significantly affect Brox intracellular distribution or its extracellular release, implying an indirect binding of Brox to membranes mediated by other proteins. Indeed, like other Bro1 domains proteins, Brox bound specifically to all CHMP4 proteins independently of its farnesylation state.

Further studies are needed in order to understand the physiological relevance of Brox in mammalian cells. Curiously, the study mentioned above also showed that neither Brox nor HD-PTP were able to bind RabGAPLP (Ichioka, Kobayashi *et al.* 2008),

indicating that such ability might be specific for the N-terminal domain of Alix (Ichioka, Horii *et al.* 2005).

Alix cooperates with ALG-2 to promote apoptosis

ALG-2 (apoptosis linked gene-2) is a cytosolic 28kDa protein, belonging to the penta-EF-hand family of Ca^{2+}-binding proteins (Maki, Kitaura *et al.* 2002), that is required for induction of apoptosis by a variety of stimuli (Vito, Lacana *et al.* 1996). ALG-2 has been linked to both intrinsic and extrinsic apoptotic signaling pathways (Hwang, Jung *et al.* 2002; Rao, Poksay *et al.* 2004; Chen and Sytkowski 2005).

Alix was first described as an interacting partner of ALG-2 (Missotten, Nichols *et al.* 1999; Vito, Pellegrini *et al.* 1999). ALG-2 forms dimers and binds Ca^{2+} on EF1, EF3 and EF5; Ca^{2+} binding induces conformational changes in ALG-2 which are required for its interaction with Alix (Jia, Tarabykina *et al.* 2001). A 12 residues long PXY repeat in the PRD region of Alix mediates the interaction with ALG-2 (Trioulier, Torch *et al.* 2004) and each tyrosine residue of the motif seems to be critical for regulation of the binding, since their phosphorilation by kinases alters the binding behaviour to ALG-2 (Schmidt, Dikic *et al.* 2005; Sadoul 2006).

Several observations suggested the cooperative effect between Alix and ALG-2 to promote apoptosis. Up-regulation of endogenous Alix expression *in vivo* was seen to correlate with cell death (Blum, Hemming *et al.* 2004; Hemming, Fraboulet *et al.* 2004) and overexpression of Alix triggered caspase activation and apoptosis in the absence of pro-apoptotic signals (Trioulier, Torch *et al.* 2004; Mahul-Mellier, Hemming *et al.* 2006). On the other hand, expression of truncated Alix, lacking the Bro1 domain (Alix-CT) produced a dominant negative effect, protecting cells against apoptosis (Vito, Pellegrini *et al.* 1999; Trioulier, Torch *et al.* 2004; Mahul-Mellier, Hemming *et al.* 2006). Both the pro-apoptotic effect of full-length Alix and the anti-apoptotic ability of Alix-CT were shown

to be strictly dependent on ALG-2 binding (Shibata, Yamada *et al.* 2004; Trioulier, Torch *et al.* 2004), since deletion of the PXY repeat on Alix, rendered the full-length Alix unable to induce apoptosis and abolished the protective ability of Alix-CT (Trioulier, Torch *et al.* 2004; Mahul-Mellier, Hemming *et al.* 2006).

In cerebellar granule cell cultures, neuronal death induced by lowering extracellular potassium concentrations could not be prevented by caspase inhibition (Trioulier, Torch *et al.* 2004). On the other hand Alix-CT blocked caspase activation and in addition allowed neuronal survival. Taken together, these results suggested that the Alix-ALG2 complex was able to control a signalling or execution step common to both caspase dependent and caspase independent programs of neuronal death. Because of the involvement of Alix in MVB trafficking, it was suggested that Alix over-expression could perturb normal endosomal trafficking leading to cell death. In this line, the overexpression of Alix-CT, defective for CHMP4 binding (since it lacks the Bro1 domain) but that still binds TSG101, produced abnormal cytoplasmic vacuolization (Chatellard-Causse, Blot *et al.* 2002), indicating that the ESCRT proteins could participate in cell death. This hypothesis was further supported by the fact that the protective role of Alix-CT was abolished when its ability to bind TSG101 was compromised (Mahul-Mellier, Hemming *et al.* 2006).

Another potential explanation for the pro-apoptotic ability of Alix, could be its involvement in a caspase execution programme controlled by calcium. Since Alix-ALG2 interaction is tightly controlled by Ca^{2+}, it has been suggested that this complex, once formed, could serve as a scaffold for proteolytic activation of caspases that promote cell death pathways (Sadoul 2006).

The current hypothesis presents a dual function for Alix in cell death, both regulating caspase activation and controlling the endosomal machinery (Sadoul 2006).

Alix supports budding of some enveloped viruses

Cellular components involved in MVB biogenesis support late events during retroviral budding. Their recruitment occurs via conserved short peptide sequences known as late domains (L domains) present in viral Gag or matrix proteins, structural proteins that attach to the cytosolic face of the membranes and support viral particle formation (Morita and Sundquist 2004).

Different motifs engage different components of the MVB machinery to support late phases of budding. The PT/SAP motif binds TSG101 and is found for instance in HIV-1, -2, FIV (feline immunodeficiency virus) and HTLV-I, -II (human T-cell leukemia virus); the YPX_nL motif binds to Alix and is found in HIV-I and EIAV (equine infectious anaemia virus); the PPXY motif binds to Nedd4 (a HECT domain-containing E3 ligase important for internalization of membrane proteins) and is found in HTLV-I, -II and BLV (bovine leukaemia virus). These interactions permit access to the whole or part of the ESCRT machinery.

Interestingly, it seems that most lentiviruses engage Alix in some way, although only those that do not interact with TSG101 harbor optimal Alix-binding sites. This is the case of EIAV that harbours an YPDL motif that binds Alix, but does not contain a binding motif for TSG101. The overexpression of truncated Alix fragments or the silencing of Alix expression with RNAi results in significant inhibition of EIAV viral release (Martin-Serrano, Yarovoy *et al.* 2003; Strack, Calistri *et al.* 2003) indicating that this process is strictly dependent on the presence of Alix. In the case of HIV-I, Alix binds a related motif (YPLTSL) in the p6 domain of Gag, however the disruption of Alix function causes only a moderate effect on HIV-I budding. In fact, HIV-I p6 harbours another motif for binding TSG101 and this is sufficient to promote viral release (Garrus, von Schwedler *et al.* 2001). The C protein encoded by Sendai virus is a viral accessory protein that does not have the ability to form VLPs (virus-like particles) and does not contain YPX_nL motif

(Sakaguchi, Kato *et al.* 2005), but recruits Alix to enhance the efficiency of viral release (Sakaguchi, Kato *et al.* 2005; Irie, Nagata *et al.* 2008).

Alix itself contains a PSAP motif that binds TSG101 and two PPXY motifs that potentially bind Nedd4 (Martin-Serrano, Yarovoy *et al.* 2003; Strack, Calistri *et al.* 2003; von Schwedler, Stuchell *et al.* 2003). In *S.cerevisiae* and *A.nidulans* two YPXL/I motifs of Rim101/PacC are recognized by Rim20/PalA (Vincent, Rainbow *et al.* 2003). Also in *C.elegans*, RME1 (a regulatory protein in recycling endosomes) uses a YPSL sequence to bind ALX-1, the ortholog of Alix (Shi, Pant *et al.* 2007).

Dictyostelium reveals a role for Alix in developmental signaling

The knockout (*alx* null phenotype) of the Alix ortholog in *Dictyostelium*, Dd-Alix, was shown to lead to major defects in differentiation and morphogenesis, suggesting that Dd-Alix is an important signalling molecule during these processes (Mattei, Ryves *et al.* 2005). In order to identify which function(s) of Alix is responsible for such developmental defects in *Dictyostelium*, several cellular processes have been investigated.

In what concerns cell death signalling, two ALG-2 homologues have been identified and shown to interact with Dd-Alix in a Ca^{2+}-dependent manner, even though unlike in mammalian cells such interaction was not mediated by a PXY-containing sequence that is absent in Dd-Alix (Aubry, Mattei *et al.* 2002). Alix knockout defects were shown to be independent of extracellular Ca^{2+} (Aubry, Mattei *et al.* 2002; Mattei, Ryves *et al.* 2005) and overexpression of a mutant Dd-Alix unable to bind ALG-2, could fully complement these defects, demonstrating that ALG-2 has no essential role in the Dd-Alix pathway. In contrast Ohkouchi *et al.* showed that abnormal development of another *alx* null mutant only occurred in the presence of lower extracelular Ca^{2+} concentrations (Ohkouchi, El-Halawany *et al.* 2004; Ohkouchi, Saito *et al.* 2005). Moreover, the death program of *Dictyostelium* stalk cells did not require a functional Dd-Alix (Mattei, Ryves *et al.* 2005).

Since in other organisms Alix might control the repertoire of cell surface proteins, the conservation of certain critical interactions was also analyzed. Both the Bro1 domain and the middle V region, but not the PRD region, were needed for the Dd-Alix developmental function (Mattei, Ryves *et al.* 2005). Dd-Alix co-localized to enlarged Vps32(CHMP4) positive vesicles containing ubiquitinated protein, suggesting the conservation of the Bro1-domain-Vps32 interaction (Mattei, Klein *et al.* 2006). As seen for Bro1p, Dd-Alix lacked a PT/SAP motif to bind TSG101. In fact the *alx* null phenotype was much stronger than the *tsg101* null phenotype (Mattei, Klein *et al.* 2006), a fact that can be explain by the different fate of internalized receptors in the different null strains.

Based on the current knowledge of Alix activities in different organisms, several models for the function of Alix in *Dictyostelium* development have been suggested: i) Dd-Alix might control downregulation of cell surface proteins/receptors acting together with the ESCRT machinery and therefore activate/inactivate developmental signalling; ii) Dd-Alix could act at the plasma membrane negatively regulating the internalization of surface receptors responsible for differentiation; iii) Dd-Alix might regulate the processing of a transcription factor and subsequent expression of essential genes for development.

Alix in the recycling endocytic pathway

In *C. elegans* the only apparent Alix/Bro1p family protein, ALX-1, was shown to have a dual function, acting in both recycling and degradative endocytic pathways.

ALX-1 functions in the endocytic recycling pathway in association with the recycling endosome regulator RME-1 (Shi, Pant *et al.* 2007). The central region of ALX-1 (residues 365-752) interacts with the YPSL motif located at the C-terminus of RME-1; a second interaction, less critical for ALX-1-RME-1 association, occurs between the NPF (asparagine-proline-phenylalanine) tripeptide motif at the C-terminus of ALX-1 and the EH-domain of RME-1. The involvement of Alix family proteins in the endocytic recycling

pathway seems to be phylogenetically conserved, since the expression of truncated human Alix in Hela cells disrupted MHC (major histocompatibility complex) class I recycling (Shi, Pant *et al.* 2007), known to be dependent on mammalian RME-1 (Edh1) function. In addition endogenous Alix is enriched in tubular vesicular structures (recycling platforms) in human T cells and macrophages (Welsch, Habermann *et al.* 2006).

ALX-1 is also required for degradation of membrane proteins in *C. elegans*, likely functioning with the ESCRT machinery in the multivesicular endosome (MVE) as suggested for the yeast ortholog (Odorizzi, Katzmann *et al.* 2003). No previous mechanistic links were ever reported between the degradative and recycling branches of the endocytic pathway, but a coordination of both transports seems advantageous for cells to control cargo type, overall cargo load and cellular local environment.

Curiously ALX-1 seems specifically required to recycle clathrin-independent cargo (like MHC class I) (Shi, Pant *et al.* 2007). Efficient transport of such cargo from recycling endosomes to the plasma membrane involves local actin dynamics, as described for the membrane-associated actin regulator Arf6 (Radhakrishna and Donaldson 1997; Brown, Rozelle *et al.* 2001). Indeed, Alix has been shown to copurify with cytoskeleton components and to perturb intracellular actin distribution (Schmidt, Chen *et al.* 2003; Cabezas, Bache *et al.* 2005; Pan, Wang *et al.* 2006) suggesting a potential functional link between Alix family proteins and membrane-associated actin dynamics. Moreover, Alix may promote recycling through sydapins that facilitate the recruitment of N-WASP and subsequent activation of Arp2/3-directed actin branching and polymerization (Qualmann and Kelly 2000; Kessels and Qualmann 2004).

Structure of mammalian Alix

The crystal structure of a truncated form of human Alix lacking the proline-rich region (Alix-ΔPRD) has been solved by Fisher et al (Fisher, Chung *et al.* 2007) and revealed a protein with an extended conformation, where the Bro1 and V domains form discrete modules (Figure 8b). The molecule spans ~ 150 Å between its distal ends, due to the fact that the Bro1 and V domains connect to each other with their major axis aligned in parallel. In addition, because both modules are structurally different, the overall shape of the molecule presents no major symmetry.

An interesting feature revealed by the crystal structure involves the V-shaped fold of the V-domain. As a consequence of this peculiar shape, the Bro1-domain and the PRD (not present in the structure), which are at opposite ends of the primary sequence, may actually end up in close proximity in the native molecule (Figure 8b), consistent with the fact that Src kinase can simultaneously dock to the Bro1 domain and phosphorylate Tyr residues in the Alix C-terminal PRD tail (Schmidt, Dikic *et al.* 2005).

The Bro1 domain of human Alix generally resembles its yeast counterpart (Kim, Sitaraman *et al.* 2005). The core of the domain is a tetratricopeptide repeat (TPR) composed of three helical hairpins of ~ 50 residues long that form a right-handed solenoid with a rotation of ~ 20° between each helical pair. The core is flanked on one side by a helical segment (α-10) and on the other side by both a small β sheet (β1, β2) and a three-helix bundle (α1-3). Both N and C termini adopt extended conformations that traverse opposite sides of the domain. The first 17 residues extend along the convex surface and the final 43 residues extend across the concave surface. Like its yeast analog, the domain presents two exposed hydrophobic patches (Figure 8b); a first one centered about Tyr319, that forms a docking site for Src kinase (when Tyr 319 is

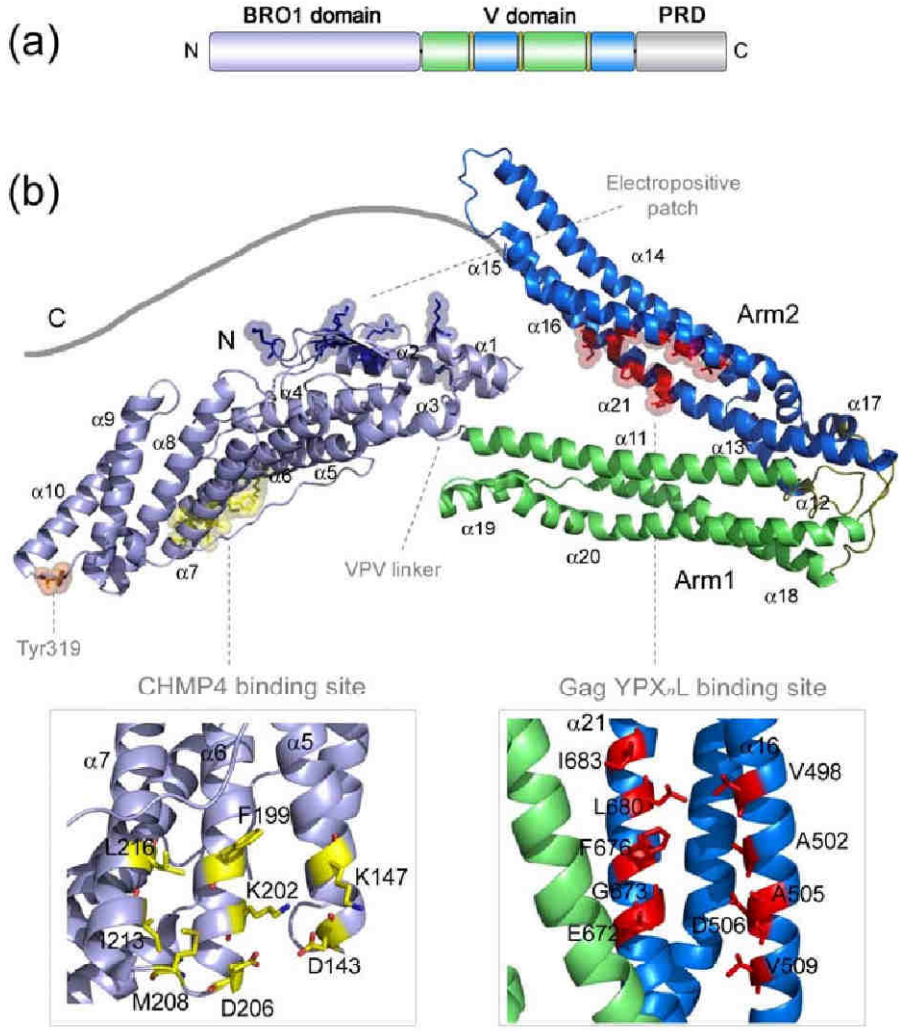

Figure 8. Structure of human Alix. (a) Domain organization of Alix colored as the in (b). **(b)** Crystal structure of human Alix (residues 1-702 ; PDB code 2OEV) (Fisher, Chung *et al.* 2007). The PRD absent in the structure has been added as a C-terminal solid grey line. The electropositive patch in Bro1 domain as well as the $_{359}$VPV$_{361}$ linker between the Bro1 and V domains are shown. The Tyr319 localizes in a conserved hydrophobic region that has not been highlighted here. The panels below are close-up views of the binding sites of CHMP4 (in the concave side of the Bro1 domain) and YPX$_n$L (in arm 2 facing the arm1). Critical residues composing each site are shown explicitly as well as the helices they belong to.

phosphorilated) (Schmidt, Dikic *et al.* 2005) and a second one forming the bindingsite for the CHMP4B subunit of the ESCRT-III complex (Kim, Sitaraman *et al.* 2005). An additional electropositive patch present in yeast Bro1, seems also partially conserved in the human protein (Figure 8b).

The Bro1 domain is connected to the V-domain by a single tripeptide linker ($_{359}$VPV$_{361}$; Figure 8b) that makes only limited noncovalent contacts. This feature is thought to provide flexibility to the molecule, since the two domains may adopt different relative positions upon external stimuli.

The Alix V-domain is composed of two extended arms that fold back on themselves at an angle of ~ 30°. The first arm (arm1) that connects to Bro1 domain is 77 Å in length and the second (arm2), connecting to the PRD, is 90 Å long. Of note, the polypeptide chain of the V domain crosses three times the arm1/arm2 “loop” region to assemble the 2 three-helix bundles. This indicates that the fold of the V domain is highly dependent on the primary polypeptide sequence; hence the domain might represent a single functional entity.

Each of the V domain arms is stabilized mainly by hydrophobic side-chain-packing interactions that are based on heptad repeats and that adopt canonical “knobs into holes” side-chain packing. In contrast, the three loops in the region connecting the two arms are stabilized almost exclusively by hydrophilic interactions, most of which are mediated by the backbone. This region also encloses a hydrophilic interior cavity and the water molecules buried inside also contribute for local structure stability.

The position the two arms of the V relative to each other was moderately variable in different crystal forms with observed displacements reaching up to 10 Å. This revealed an intrinsic conformational flexibility of the V domain, consistent with a molecular hinge function. The differences in the crystal forms seem to result from cumulative changes in the interhelical packing interactions along both arms, rather than major structural

reorganization on the loop region or elsewhere. To date, the biological significance of such flexibility remains to be elucidated.

A notable feature of the V-domain is the presence of a highly conserved hydrophobic pocket on arm2 (Figure 8b) that turned out to be crucial both for binding YPX_nL-type late domains and for the function of Alix in virus budding (Fisher, Chung *et al.* 2007; Lee, Joshi *et al.* 2007).

Overall, due to its structural organization, Alix is likely to be a versatile scaffold molecule whose domains are able to reorient in response to ligand binding.

Structural details of Alix-CHMP4 interaction

The crystal structures of Alix in complex with human CHMP4 C-terminal peptides revealed that all three CHMP4 (A/B/C) isoforms contain short amphipathic helices that bind across the conserved concave surface of Alix Bro1 domain (McCullough, Fisher *et al.* 2008). The amphipathic helix of each CHMP4 contacts helices 5-7 of the Bro1 domain as well as the extended C-terminal strand that traverses the domain (Figure 8b and Figure 9b). Several sidechains of the Alix binding site suffer minor shifts to accommodate the CHMP4 helix, with the largest adjustment being made by the Alix Phe199 ring (shifted ~ 1.5 Å).

The C-terminal CHMP4 recognition helices display a conserved pattern (M/L/IxxLxxW), consisting of three hydrophobic residues located on three successive turns of the helices, that mediate critical interactions with Alix. The C-terminal Leu and Trp residues are invariant in metazoan CHMP4 proteins (Figure 9a) and this is consistent with the fact that both bind well defined pockets of Alix (Figure 9b), whereas the first hydrophobic residue can vary between Met, Leu, Ile and Phe and therefore binds against a flat hydrophobic surface that tolerates greater side chain variability (Figure 9b). Of note, the longer length of CHMP4B recognition helix (Figure 9a)

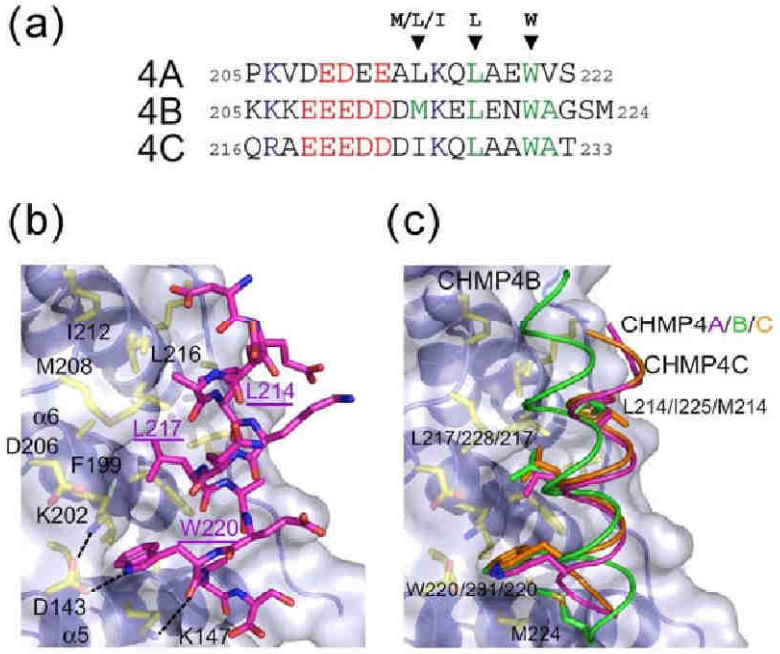

Figure 9. Molecular recognition and structural details of Alix-CHMP4 complexes. (a) Sequences of the C termini of the three human CHMP4 proteins revealing the conserved recognition pattern M/L/IxxLxxW. **(b)** Close-up view of Alix-CHMP4A interface. Alix is represented as a blue ribbon and surface with residues in the binding site shown explicitly (yellow sticks, black labeling). The CHMP4 helix is oriented N to C from top to bottom; dashed lines indicate hydrogen bonds or salt bridges and key hydrophobic residues are underlined. The Trp220 binds in a hydrophobic pocket located between Alix helices 5 and 6; Leu217 binds in an adjacent hydrophobic pocket located between helices 6 and 7; Leu214 binds on a more open hydrophobic surface of Alix helix 6. **(c)** Overlay of the bound CHMP4 A/B/C helices. The orientation is the same as in (b) and the three key hydrophobic CHMP4 residues are shown in sticks. Note that CHMP4A (purple) and CHMP4C (orange) helices overlay well, whereas the CHMP4B helix (green) is rotated ~20°. The CHMP4B Ser223 hydroxyl caps the helix and hydrogen bonds with Alix Lys147 side chain; the terminal CHMP4 Met224 contacts a hydrophobic patch between Alix helices 5 and 6. *Adapted from (McCullough, Fisher et al. 2008).*

conserves the same three hydrophobic side chains in analogous binding sites. However both N and C termini get displaced allowing additional interactions with Alix which appear to reorient the CHMP4B helix (Figure 9c).

Previous studies showed that mutations of Alix residues Phe199, Ile212 and Leu216 impaired enveloped virus budding and release (Fisher, Chung *et al.* 2007; Usami, Popov *et al.* 2008), consistent with the Alix-CHMP4 interface.

The CHMP4 binding appears to be a conserved function of Bro1 domains, because three other Bro1 domain-containing proteins Rim20p, HD-PTP and Brox also bind CHMP4 proteins (Xu, Smith *et al.* 2004; Ichioka, Kobayashi *et al.* 2008). As expected, a sequence alignment of these Bro1 domains with those from metazoan Alix proteins, revealed strong, although not absolute conservation of CHMP4 contact residues, indicating a similar fashion of CHMP4 binding (McCullough, Fisher *et al.* 2008).

Structural basis of Alix interaction with YPX$_n$L late domain

A conserved hydrophobic groove on arm2 of the Alix V-domain recognizes viral YPX$_n$L motifs (Fisher, Chung *et al.* 2007; Lee, Joshi *et al.* 2007) and mediates binding to other endogenous cellular partners (Vincent, Rainbow *et al.* 2003; Geminard, De Gassart *et al.* 2004). The site is exposed to solvent but is located near the base of the V where the two arms are separated by only 5-10 Å (Figure 8b). The main residues composing the groove are: Ala502, Ala505, Asp506, Val509, Glu672, Gly673, Phe676 and Tyr677 (Figure 10b,c). Mutational analyses confirmed that most of them are required for binding to HIV p6^{Gag} and EIAV p9^{Gag} (Fisher, Chung *et al.* 2007; Lee, Joshi *et al.* 2007).

The crystal structures of Alix in complex with the YPX$_n$L late domains from HIV and EIAV (Figure 10b,c) revealed the structural basis of this interaction (Zhai, Fisher *et al.* 2008). The most prominent feature of the interaction was the burial of the late-domain tyrosine side chain deep into the hydrophobic pocket and the formation of a hydrogen bond between the hydroxyl group of the tyrosine and Alix Asp506 (Figure 10b,c). The conserved leucine and proline residues that flank this tyrosine residue of the late domain make equivalent hydrophobic interactions with Alix. Of note, the terminal leucine residues within the YPX$_n$L late domains of HIV-1 and EIAV also make equivalent Alix

interactions, despite spacing differences (HIV-1, n=3; EIAV, n=1, Figure 10a); this is made possible by alternative helical (HIV) or extended (EIAV) main chain conformations.

In contrast to the equivalent affinities found for the isolated late domain peptides of HIV $p6^{Gag}$ and EIAV $p9^{Gag}$ (respectively 15 and 13 residues in length), full-length late domains (HIV, 52 residues; EIAV, 51 residues) showed significantly different affinities (Lee, Joshi *et al.* 2007; Munshi, Kim *et al.* 2007), with EIAV $p9^{Gag}$ binding Alix 60-fold more tightly than HIV $p6^{Gag}$. This reflectes a fine tuning of binding affinities towards Alix most likely due to context-dependent effects.

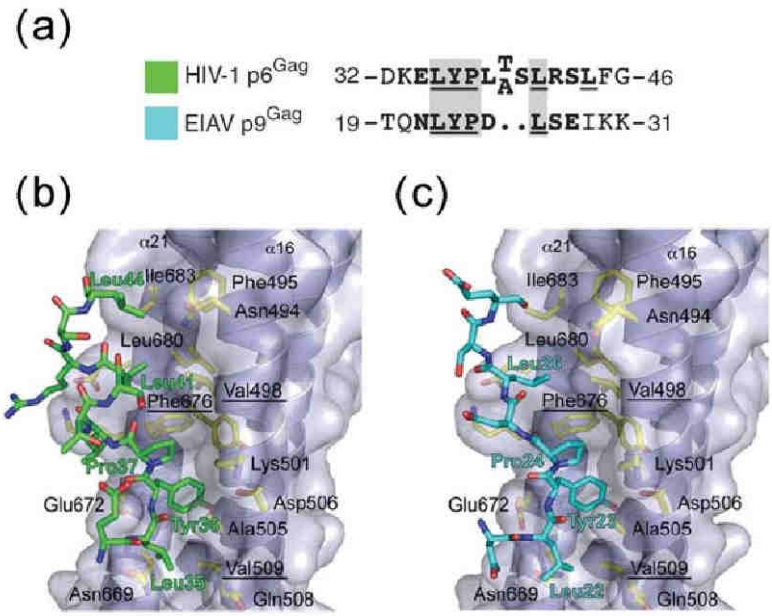

Figure 10. Molecular recognition and structural details of Alix-YPX$_n$L complexes. (a) HIV $p6^{Gag}$T and $p6^{Gag}$A and EIAV $p9^{Gag}$ YPX$_n$L late domain peptide sequences used for crystallography aligned on the basis of the crystal structures. Residues modeled in the crystal structures are in boldface and residues that lack electron density are in normal font. Structurally equivalent residues are on a gray background and residues that contact the protein are underlined. **(b,c)** Close-up views of YPX$_n$L late domain (sticks) for HIV-1 $p6^{Gag}$T (green) and EIAV $p9^{Gag}$ (light blue). Alix is represented as a blue ribbon and surface with residues in the binding site highlighted as yellow sticks. Alix residues previously shown by mutagenesis to be important for $p6^{Gag}$ and $p9^{Gag}$ binding and Alix function in viral budding are underlined (Fisher, Chung *et al.* 2007; Lee, Joshi *et al.* 2007). *Adapted from (Zhai, Fisher et al. 2008)*.

Finally, the fact that the hydrophobic conserved surface of Alix extends ~10 Å (toward the base of the V domain) beyond the region used for binding the viral late domain suggests that the extra conserved residues might have a function in binding other Alix cellular partners.

Aims of the present work

The main goal of this work is to contribute to the understanding of the structure and function of Alix. We use biochemical and biophysical approaches to characterize the structure of recombinant Alix and to demonstrate its conformational flexibility *in vitro* and *in vivo*.

The following specific aims have been proposed at different stages during the work.

- Identification of the major structural domains of Alix.
- Characterization and structural analysis of the dimerization properties of Alix and its role in HIV-1 budding.
- Mapping of the dimerization interface of Alix and analysis of dimerization mutants.
- Evaluation of the relevance of Alix dimerization in HIV-1 infected cells, focused on the step of viral release.
- Characterization of the interaction between Alix and CHMP4B.
- Characterization of Alix interaction with model membranes (liposomes) *in vitro*.
- Evaluation of endogenous Alix distribution in mammalian cells.

Objectifs

Le travail réalisé au cours de cette thèse a pour objectif de contribuer à la compréhension des mécanismes structuraux et fonctionnels associés à la protéine Alix. Des approches biochimiques et biophysiques ont été utilisées pour caractériser la structure de la protéine Alix recombinante mais également pour démontrer, *in vitro* et *in vivo*, sa flexibilité conformationnelle.

Les points suivants ont été proposés à différentes étapes durant ce travail.

- Identification des domaines structuraux majeurs de la protéine Alix.

- Caractérisation et analyse structurale des propriétés de dimérisation de la protéine Alix et son rôle dans le processus de bourgeonnement de HIV-1.

- Analyse de l'interface de dimérisation de la protéine Alix et des mutants de dimérisation générés.

- Etude de l'implication du processus de dimérisation sur des cellules infectées par HIV-1, notamment lors de l'étape de libération du virus.

- Caractérisation de l'interaction entre les protéines Alix et CHMP4B.

- Caractérisation *in vitro* de l'interaction entre la protéine Alix et des modèles membranaires (liposomes).

- Evaluation de la distribution endogène de la protéine Alix dans des cellules de mammifères.

Chapter II

RESULTS

Mapping and preliminary characterization of Alix major domains

In order to characterize mouse Alix protein, a recombinant truncated form lacking a C-terminal proline rich region (Alix-ΔPRD, Figure 11) was cloned and expressed in a bacterial system. Since the proline rich region does not contain any predicted secondary structure it was deleted for structural studies. Unstructured regions (like PRDs) are generally excluded since they tend to compromise crystallogenesis. In fact, several attempts to produce full-length Alix protein in *E.coli* also failed. Apparently the expression of the full-length protein is compromised by the long proline-rich region, leading to truncated expression products in bacterial systems (B. Blott, personal communication).

Alix-ΔPRD was well expressed in *E.coli* as a soluble 100KDa GST-fusion protein and was purified on a Glutathione sepharose column (Figure 12a). After GST-tag cleavage the untagged protein (Alix-ΔPRD, 80KDa) was isolated on an anionic exchange column. Using an initial buffer salt concentration of 80mM the protein elutes in the flow-through free of any major contaminants while GST is retained on the column (Figure 12b). The protein elutes as two distinct peaks from size exclusion chromatography column (Figure 12c), a minor one at 11.3ml corresponding to the dimeric form and another at 13.5ml corresponding to the monomeric form (see section on the characterization of the oligomeric states).

Limited proteolysis experiments were performed on monomeric Alix-ΔPRD in order to map putative stable domains. These revealed a fragment of ~37KDa that accumulates in the course of the reaction and is particularly stable after 60min of trypsin digestion (Figure a). Several attempts to scale-up the production of this fragment by trypsination, revealed a persisting problem due to trypsin residual activity even in the presence of

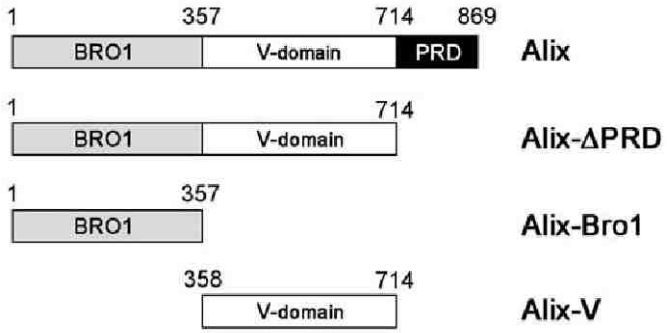

Figure 11. Domain organization of Alix and deletion mutants created. Mammalian Alix is organized in three main domains: Bro1, V-domain and Proline-Rich-Domain (PRD). Alix-ΔPRD is well expressed in bacterial systems in contrast to the full length protein. Alix-Bro1 and Alix-V represent deletion mutants designed after limited proteolysis domain mapping on Alix-ΔPRD. Current structural knowledge defines a shorter V-domain (up to the residue 702). However, for simplification, the domains are represented as studied in the present work.

protease inhibitors. The result was the production of an additional proteolytic band of about ~20KDa on a purified sample of the 37KDa fragment (Figure b).

Incubation of monomeric Alix-ΔPRD at 4ºC is particularly stable for periods of weeks (the same is true for the dimeric form). Depending on the preparation, smaller proteolytic products are also observed. This was indeed the case for an Alix-ΔPRD sample resulting in the production of another fragment of ~37KDa, running however slightly lower than the one obtain by trypsination (Figure b).

The described fragments (bands A, B and C, Figure b) were analyzed by N-terminal sequencing and two distinct domains were identified on Alix-ΔPRD. Band A was identified as the N-terminal half fragment of Alix-ΔPRD, a result further supported by band B, determined to constitute an internal digestion product within the same region. Interestingly, band C was identified as a different domain, comprising in fact the C-terminal region of Alix-ΔPRD, a domain apparently non resistant to trypsination. Based

on these results two new truncated forms of Alix were design and cloned (Figure 11): Alix-Bro1 (residues 1-357) and Alix-V (residues 358-714).

Both constructs were expressed is bacteria as His_6GST-fusion proteins and a first purification step performed on a Nickel column revealed significant protein yields (Figure 14a, Figure 15a). Alix-Bro1 fusion protein ran on a SDS-PAGE as a 75KDa band, however tag cleavage turned out to be highly inefficient even upon extension of the cleavage time to 48h. On a size exclusion chromatography column, a significant amount of fusion protein could be further purified (12.25ml peak), but a major peak came off in the column void volume (8.02ml peak) indicating a tendency for aggregation (Figure 14b). This behavior was also observed for a His-tagged version of Alix-Bro1 that revealed a similar tendency to aggregate upon overnight incubation at 4ºC. For this reason the characterization of Alix-Bro1 was limited. In contrast, the tag was efficiently cleaved from the Alix-V fusion protein upon overnight digestion at 4ºC with PreScission protease and the untagged protein recovered in the flow-through of a second Nickel column purification step (Figure 15b). On a size exclusion chromatography column Alix-V presented to distinct soluble peaks (Figure 15c), one at 12.16ml corresponding to the dimeric form and the other at 14.04ml corresponding to the monomeric form. Of note, this profile resembles the one observed for Alix-ΔPRD, presenting though a more significant amount of protein in the dimer peak.

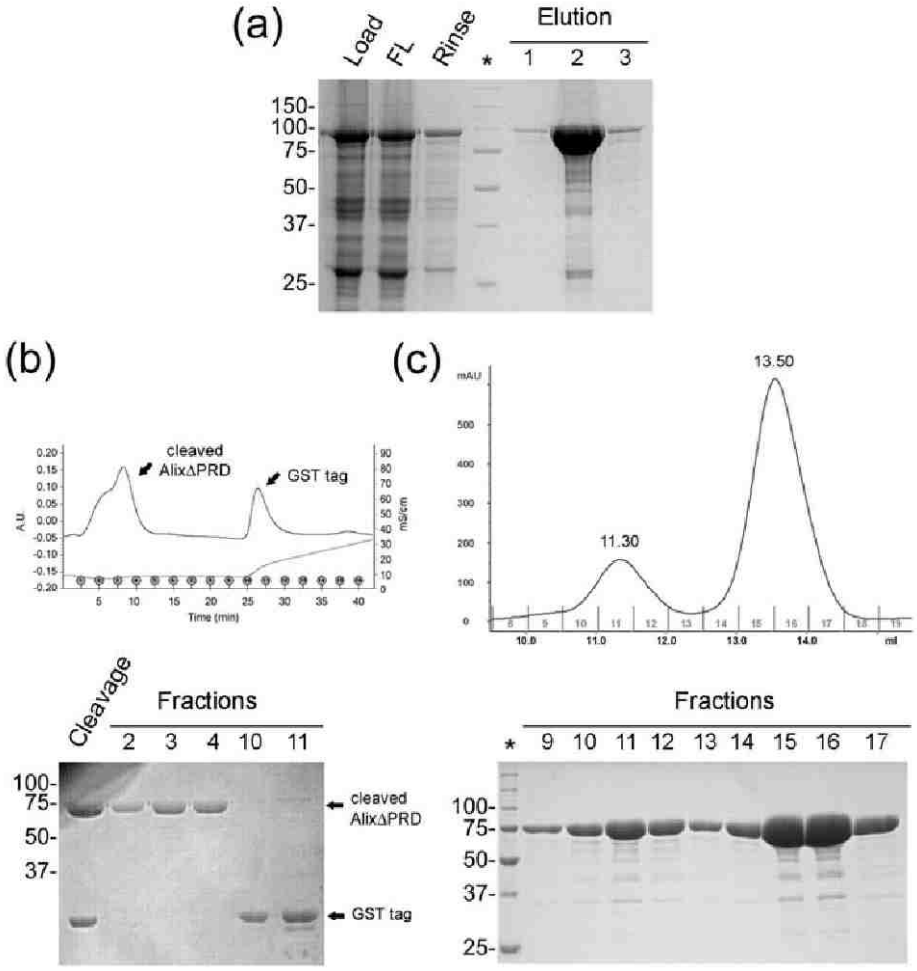

Figure 12. Purification of recombinant Alix-ΔPRD. (a) The fusion protein is first purified on a Glutathione sepharose affinity column (LOAD, cleared starting cell lysate; FT, flow-through; RINSE, washing step; ELUTION, GST-fusion protein elution,* Molecular weight marker). **(b)** Anionic exchange chromatography profile and respective SDS-PAGE of the peak fractions (below); (Cleavage, PreScission protease digestion performed to Fraction 2 eluted in the previous step; Fraction 2-4, flow-through containing the cleaved protein; Fraction 10-11, GST-tag elution with a 0.1-1M NaCl gradient). **(c)** Size exclusion chromatography profile obtained for the cleaved protein and respective SDS-PAGE of the peak fractions (below). Alix-ΔPRD is purified in two distinct forms: a dimer eluting at 11.30ml and as a monomer eluting at 13.50ml.

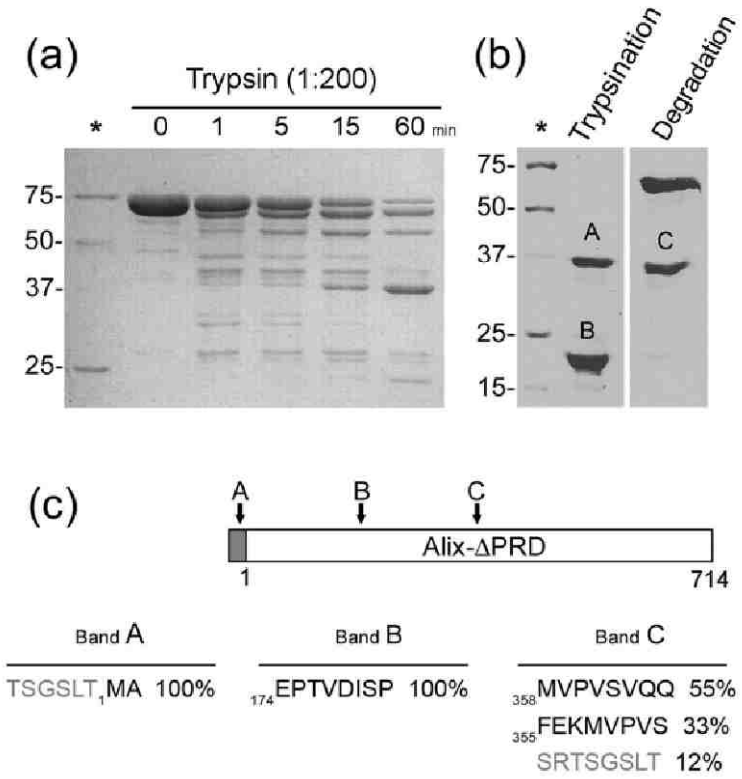

Figure 13. Limited proteolysis of Alix-ΔPRD. (a) Proteolytic profiles on SDS-PAGE obtained for Alix-ΔPRD at different reaction time points (0, 1, 5, 15, and 60 min) using trypsin at an enzyme/protein ratio of 1:200 (w/w). * Molecular weight marker. **(b)** Proteolytic fragments selected for N-terminal sequencing analysis: Trypsination sample contains a 37KDa fragment (band A) purified after 1h of trypsin digestion to Alix-ΔPRD. As result of trypsin residual activity further digestion occurs on the sample producing a second fragment (band B). Degradation sample contains a different fragment (band C) obtained by unusual degradation of Alix-ΔPRD incubated at 4ºC for several days. **(c)** N-terminal sequencing results obtained for the different fragments (bands A, B and C). The schematic representation indicates the position of each identified N-terminal within Alix-ΔPRD. Below, the sequence details and relative amounts of each fragment are specified. The region and sequences depicted in grey correspond to extra sequence that remains after GST-tag cleavage.

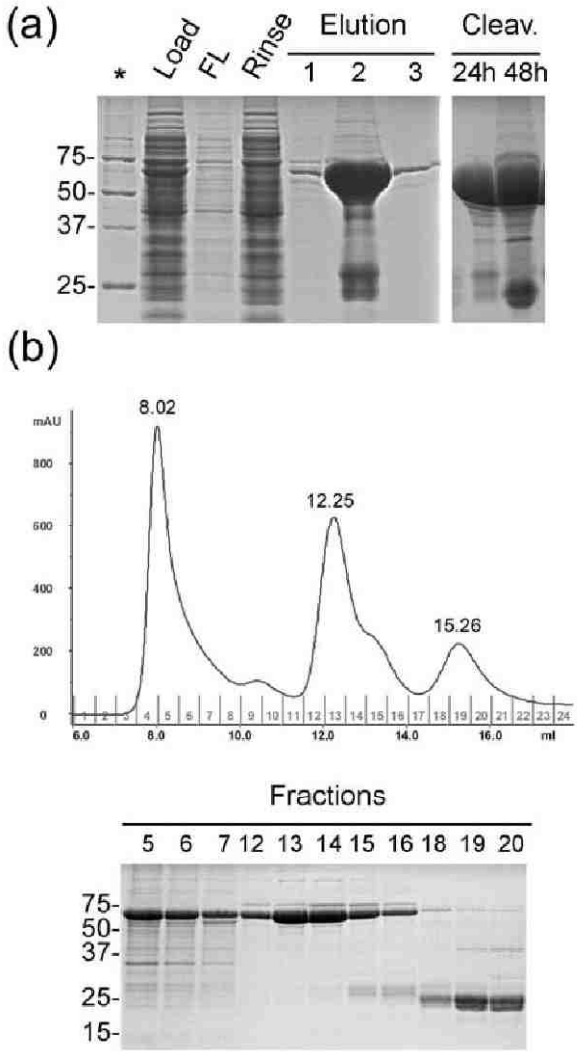

Figure 14. Purification of Alix-Bro1 deletion mutant. (a) The fusion protein is purified on a Nickel Chelating Sepharose affinity column (* Molecular weight marker; LOAD, cleared starting cell lysate; FT, flow-through; RINSE, washing step; ELUTION, His_6GST-fusion protein elution). Tag cleavage using TEV protease is highly inefficient even for extended cleavage periods (Cleav., TEV protease digestion performed to Fraction 2 for a period of 24h and 48h). **(b)** Size exclusion chromatography to the 48h-cleaved sample presents a major peak on the column void volume (8.02ml) indicative of protein aggregation. A significant peak of relatively pure fusion protein elutes at 12.25ml and a last one most likely corresponding to His6GST-tag elutes at 15.26ml. **(c)** SDS-PAGE analysis of size exclusion chromatography fractions. The SDS-PAGE analysis of the size exclusion chromatography fractions is shown below.

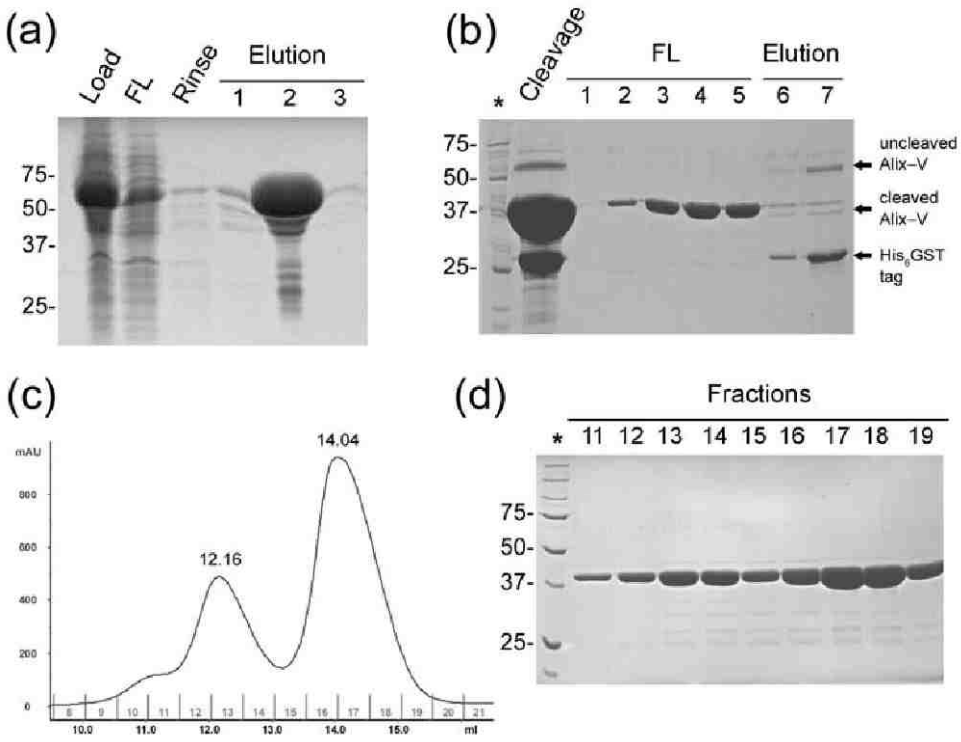

Figure 15. Purification of Alix-V deletion mutant. (a) The fusion protein is purified on a Nickel Chelating Sepharose affinity column (LOAD, cleared starting cell lysate; FT, flow-through; RINSE, washing step; ELUTION, His_6GST-fusion protein elution). **(b)** Fraction 2 eluted from the Nickel column is digested with TEV protease for tag cleavage (Cleavage). The sample is then reloaded on a Nickel column and the cleaved protein recovered in the flow-through (FL, Fractions 1-5). * Molecular weight marker; ELUTION, His_6GST-tag elution (Fractions 6-7). **(c)** Size exclusion chromatography profile of the cleaved sample on a Superdex S-200 allows the separation of two distinct soluble forms of Alix-V: a dimer form eluting at 12.16ml and a monomer form eluting at 14.04ml. **(d)** SDS-PAGE analysis of size exclusion chromatography fractions.

Oligomerization of Alix

Alix forms monomers and dimers in solution

As described in the previous section, Alix-ΔPRD and Alix-V presented a similar profile on size exclusion chromatography (Figure 16a). For each deletion mutant an early peak corresponding to a high molecular weight form preceded the major peak of the monomer. A native gel analysis confirmed the presence of distinct species, either running as single (Alix-ΔPRD 11.30ml peak) or multiple (Alix-V 12.16ml peak) bands above the monomer control (Figure 16b). Chemical cross-linking showed that the Alix-ΔPRD peak 1 (Figure 16a) can be cross linked to a second species that migrates as a broad band at ~250 kDa on SDS-PAGE (Figure 17a), hence revealing a new oligomeric state for Alix-ΔPRD. Upon cross-linking of the second peak no defined higher molecular weight band was obtained, suggesting it corresponds to the monomeric fraction. The compactness of the band may be affected by the cross linker, that promotes intramolecular cross-linking reactions compromising the monomer conformation.

Similarly, chemical cross-linking of the peak 1 of Alix-V (Figure 16a) indicated an oligomeric form since it also produced a second broad band on SDS-PAGE migrating below 100 kDa, clearly different from the monomeric form migrating at 37 kDa (Figure 17a). The second peak corresponding to Alix-V remained monomeric upon cross linking.

To determine the oligomeric state of the Alix-ΔPRD and Alix-V oligomers, both samples were separated on a HPLC size exclusion chromatography column and the eluates were analyzed by multi-angle laser light scattering and refractive index measurements. This revealed average molecular weights of 158 ± 3 kDa for oligomeric Alix-ΔPRD and 76 ± 3 kDa for oligomeric Alix-V, indicating that both form monodisperse dimers in solution (Figure 17b). The fact that cross-linked dimers run on SDS-PAGE with an apparent molecular weight higher than expected might reflect an elongated shape of

the dimer. Noteworthy for both Alix-ΔPRD and Alix-V, monomers and dimers are not in a concentration dependent equilibrium, since contents of both peaks will either remain monomeric or dimeric as analyzed by size exclusion chromatography and SAXS. In addition, dilution of Alix-ΔPRD and Alix-V dimers does not produce monomers, as observed on a size exclusion chromatography and native gel. This indicates that both monomers and dimers fold into stable entities when expressed in *E. coli*.

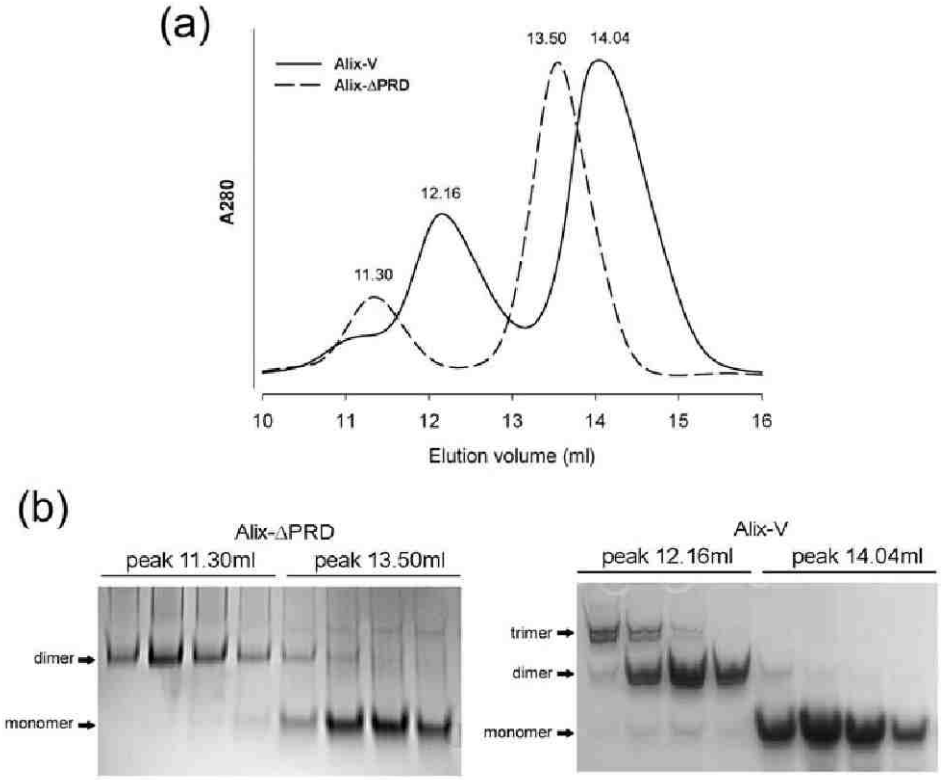

Figure 16. Oligomerization of Alix-ΔPRD and Alix-V. (a) Superposition of the size exclusion chromatography profiles for Alix-ΔPRD (dashed line) and Alix-V (solid line) on a Superdex 200 column. The early peaks (11.30ml and 12.16ml) observed for each deletion mutant correspond to soluble oligomers. Elution volumes are indicated above the elution peak. **(b)** Native gel analysis (10% native gels ran at 4ºC for 4h) to four consecutive elution fractions within each different peak present in (a). The arrows indicate the oligomeric states as determined by multi-angle laser light scattering performed to each peak.

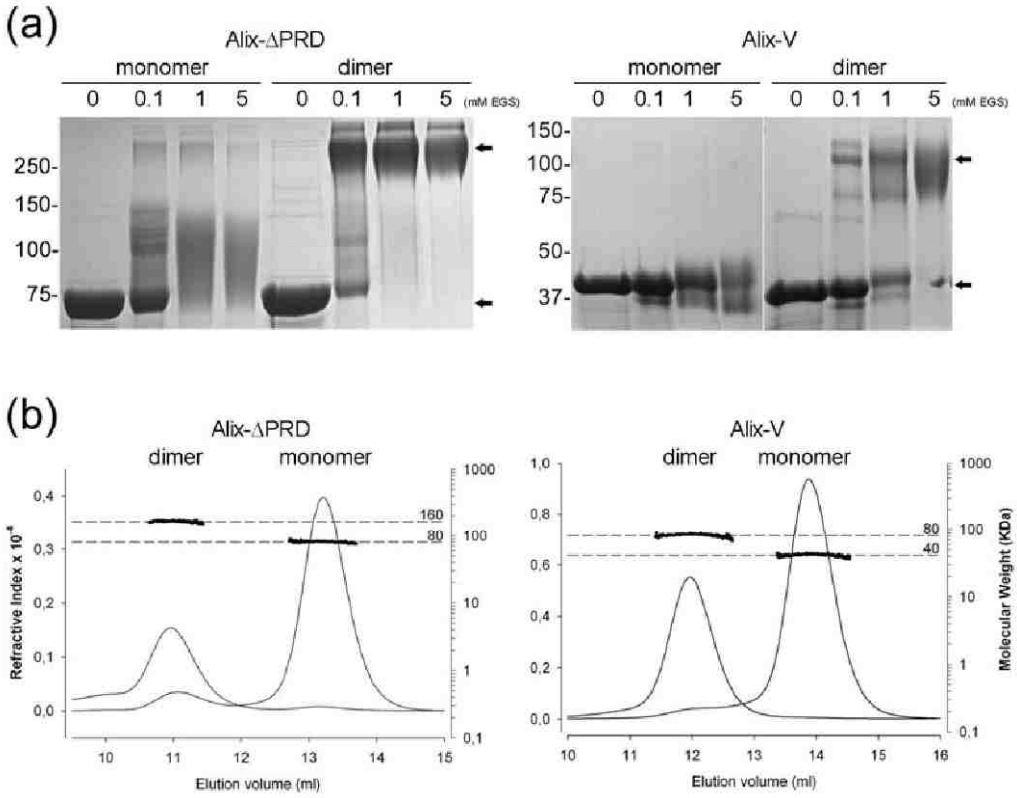

Figure 17. Soluble monomers and dimers of Alix-ΔPRD and Alix-V. (a) Chemical cross-linking to both elution peaks of Alix-ΔPRD and Alix-V, using increasing concentrations of EGS. Alix-ΔPRD early peak cross-links to a new band migrating at ~250kDa on SDS-PAGE. Alix-V early peak also produces a second band migrating close to ~100kDa upon cross-linking. Monomeric peaks do not cross-link to form higher molecular weight species. For simplification both peaks are labeled according to the oligomerization state determined by multi-angle laser light scattering (monomer or dimer). Black arrows indicate monomer and dimer migrations on the SDS-PAGE upon cross-linking. **(b)** Molecular weight determination of monomers and oligomers. Each elution peak was reinjected on a HPLC size exclusion column and analyzed by multi-angle laser light scattering and by a refractometer. The continuous line shows the change of refractive index (the measured signal is converted into the refractive index change after multiplication with a calibration constant α= 9.6×10^{-5} V^{-1}) and the data points represent the molecular weight calculated from the scattered intensity and the refractive index change. This analysis revealed a monodisperse molecular weight of 158 ± 3 kDa for oligomeric Alix-ΔPRD and 76 ± 3 kDa for oligomeric Alix-V. Monomeric molecular weights were confirmed in parallel. Dashed lines indicate the averaged molecular weights.

Mapping Alix dimerization interface

Hydrogen/deuterium (H/D) exchange experiments were coupled with mass spectrometry (MS) to target potential dimerization interfaces on Alix-ΔPRD. The method is based on the hypothesis that part of the protein's surface involved in the dimer interface is protected from the solvent upon dimerization. Therefore, the approach consisted in identifying protein regions presenting different levels of deuterium incorporation, hence different accessibility to the amide backbone hydrogens when comparing Alix-ΔPRD monomer and dimer. A first analysis was performed with the intact proteins (monomer and dimer) for monitoring the global kinetics of H/D exchange. However, a detailed mapping of the dimer interface was obtained by monitoring local kinetics, analyzing the deuteration level of peptide fragments obtained after protein digestion.

Global kinetics of H/D exchange

In order to monitor the overall kinetics of deuterium incorporation, Alix-ΔPRD monomers and dimers were incubated in a deuterated buffer for different time periods ranging from 10 seconds to 4 hours and the mass differences analyzed by LC ESI-TOF-MS. After 10sec. of exchange an average mass difference of ~14Da was already clear between monomer and dimer. As the exchange period increases the average mass differences tend to decrease, this is particularly clear when the results are plotted in a logarithmic time scale (Figure 18). However, after 4h the average masses for monomer and dimer still differ ~6 Da. Overall, the data showed an average difference in deuterium incorporation of about 10 Da, with the Alix-ΔPRD monomer presenting a higher level of deuteration than the dimer. The slower kinetics of H/D exchange observed for the dimer was a first indication that in the dimeric state Alix-ΔPRD presents a significant number of amides protected against deuteration that might belong to the dimer interface region.

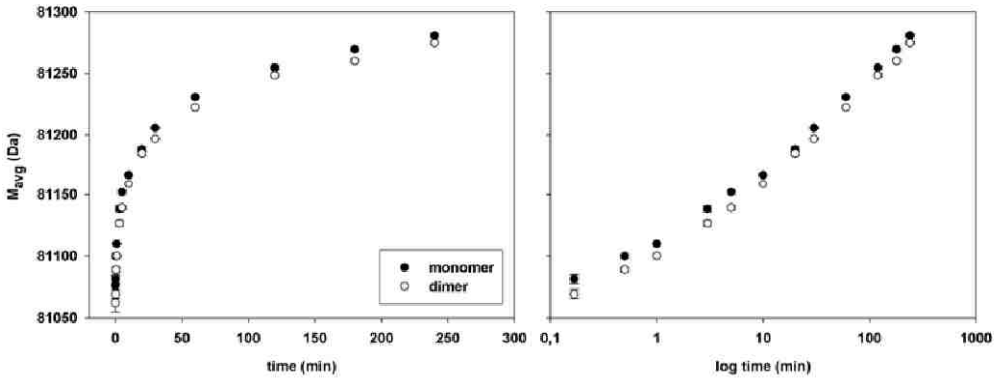

Figure 18. Kinetics of global H/D exchange monitored for Alix-ΔPRD monomer and dimer. Deuteration was carried out by 20-fold dilution of the protein in deuterated buffer (final protein concentration of 0.4μM) followed by incubation at ice-bath temperature for different time intervals (from 10sec. to 4h). Global deuterium incorporation was monitored by LC ESI-TOF-MS. In the left panel the kinetics is plotted on a normal time scale and in right panel on a logarithmic time scale. Each point is the average of a duplicate analysis for monomer (●) or dimer (○) and error bars indicate the range of standard deviation.

Local kinetics of H/D exchange

For detailed mapping of the dimerization interface, local kinetics studies were performed on individual regions of Alix-ΔPRD monomer and dimer. Following deuteration for different time periods as described for the global kinetics experiments, the proteins were digested with pepsin and the peptides produced analysed by MS. The same mapping method was used to generate a peptide map of the native protein for comparison.

The MS analysis was performed with monomeric Alix-ΔPRD, digested with pepsin. This identified 110 peptides that covered ~85% of the protein sequence, corresponding to about 610 residues out of 714 residues (Figure 19). Local kinetics experiments performed with a final protein concentration of 1μM allowed monitoring of 32 peptides well dispersed throughout the protein and covering ~57% of its sequence (Figure 21). The majority of these peptides presented no obvious mass differences between

monomer and dimer (<0.2 Da) indicating a similar accessibility in both protein states. Only 8 peptides showed a significant mass difference (0.2-0.5 Da), most of them having higher masses for the dimer than for the monomer, reflecting a gain of accessibility to this regions upon dimerization. Interestingly the opposite was observed for the peptide 637-SKMKQSNNEANL-648, being the only one identified (within the current sequence coverage) that seemed to be more protected against deuterium exchange in the dimer.

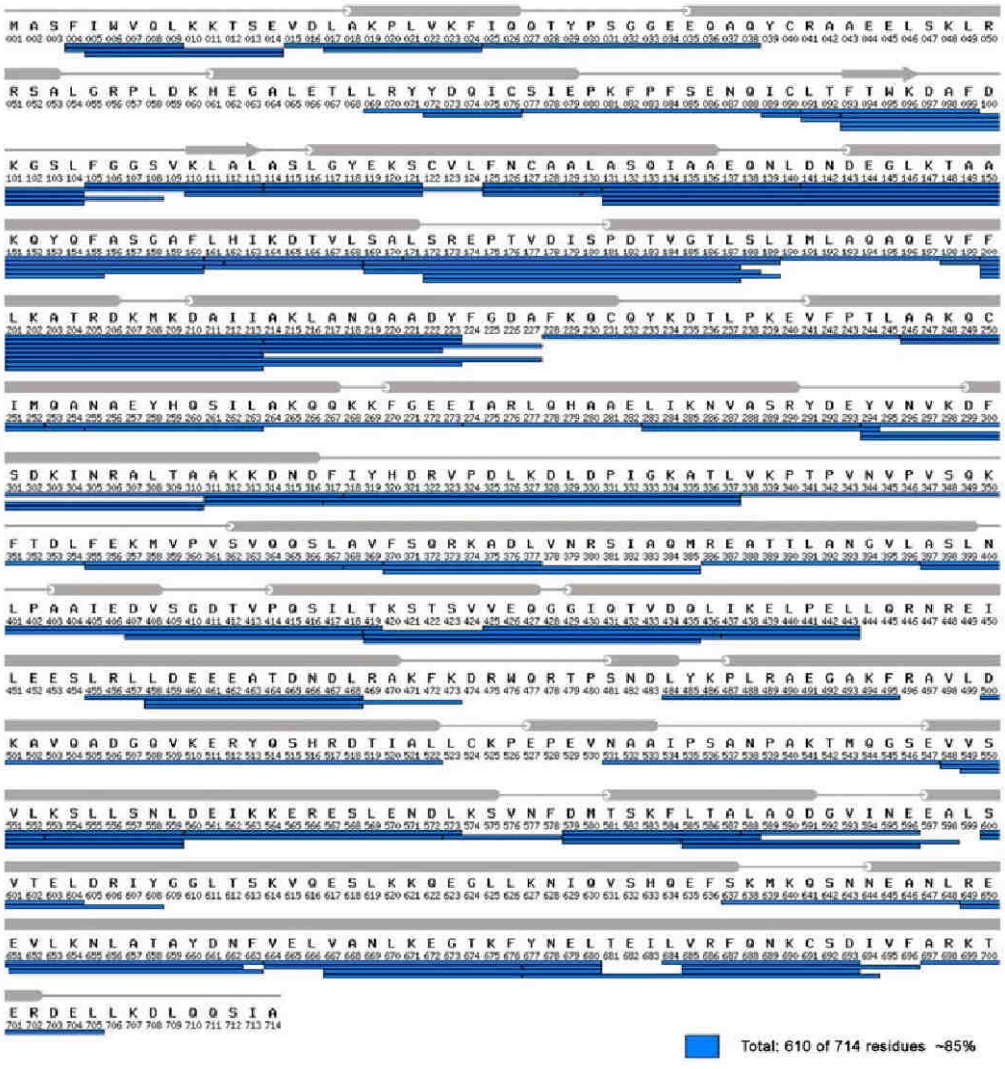

Figure 19. Peptide map of Alix-ΔPRD. Peptide fragments obtained by pepsin digestion of Alix-ΔPRD (residues 1-714) and identified by LC MS/MS are depicted in blue. One hundred and ten peptides were identified covering about 85% of the protein sequence. Secondary structure elements based on the crystal structure of the human Alix ortholog (Protein Data Bank code 2OEV) (Fisher, Chung *et al.* 2007) are indicated above the sequence; cylinders represent α-helices, large arrows are β-strands and straight lines unstructured regions.

Indeed, the local kinetics observed for this peptide reflects a slower H/D exchange for the dimer when compared to the monomer (Figure 20), indicating a loss of accessibility upon dimerization and therefore a potential dimer interface. This peptide maps to a loop connecting the two arms of the V-domain (Figure 22).

As mentioned above, several peptides derived from the dimer displayed a higher deuteration rate as compared to those derived from the monomer. This suggests that dimerization might trigger small conformational changes which expose regions in the dimeric state that are occlused in the monomer. The following regions covered by the peptides 15-24, 386-396 and 560-573, seem to be affected; peptide 15-24 locates to the tip of the Bro1-domain facing the V-domain and the peptides 386-396 and 560-573 locate to the inner surface of arm-1 of the V-domain facing arm-2. All of them seem to be more protected in the monomeric state. This thus suggests that the V-domain in the monomer adopts a closed conformation, possibly more pronounced than that observed in the crystal structures (Fisher, Chung *et al.* 2007; Lee, Joshi *et al.* 2007). The Bro1-domain presents also regions on its concave side that appear to be more exposed in the dimeric state. However, the labeling with deuterium may also reflect some of the intrinsic flexibility of the TPR (tetratricopeptide repeat) arrangement present in Bro1-domain. Importantly, exposing new regions upon dimerization may be of functional relevance as it may mediate new interactions (e.g. with other proteins) or modulate existing ones.

Figure 20. Kinetics of local H/D exchange for peptide fragments of Alix-ΔPRD monomer and dimer. Deuterium labeling was performed for different time intervals (from 10sec to 30min) using a final protein concentration of 1μM. After acidic quench, aliquots of deuterated protein were digested with pepsin and deuterium incorporation analysed for different peptide fragments by LC ESI-MS/MS. Each graph corresponds to the individual kinetics of the fragment identified on the top right corner. **(a)** Four examples of peptides belonging to the Bro1-domain (91-104 and 274-282) and to the V-domain (531-547 and 685-693) that present no remarkable difference in deuteration level between monomer and dimer. **(b)** Peptides showing significant differences, being more deuterated in the dimer than in the monomer (15-24, 338-354 and 386-396). Only one (637-648) out of 32 peptides analyzed (covering 57% of the protein sequence) presents a higher level of deuteration in the monomer than in the dimer, suggesting a potential dimer interface. Each point is the average of a duplicate analysis. *(Figure in the next page)*

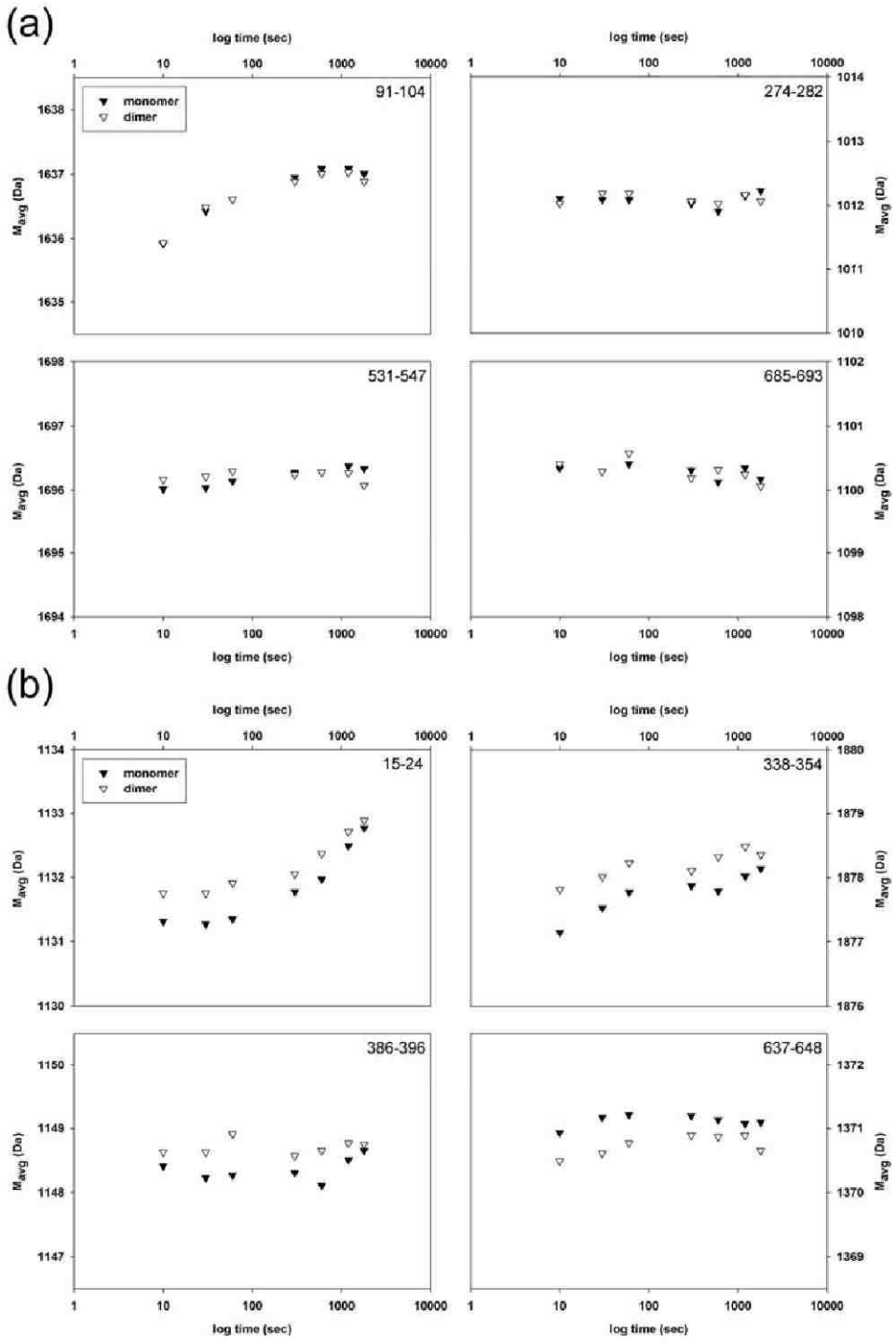

(Figure 20 – Legend in the previous page)

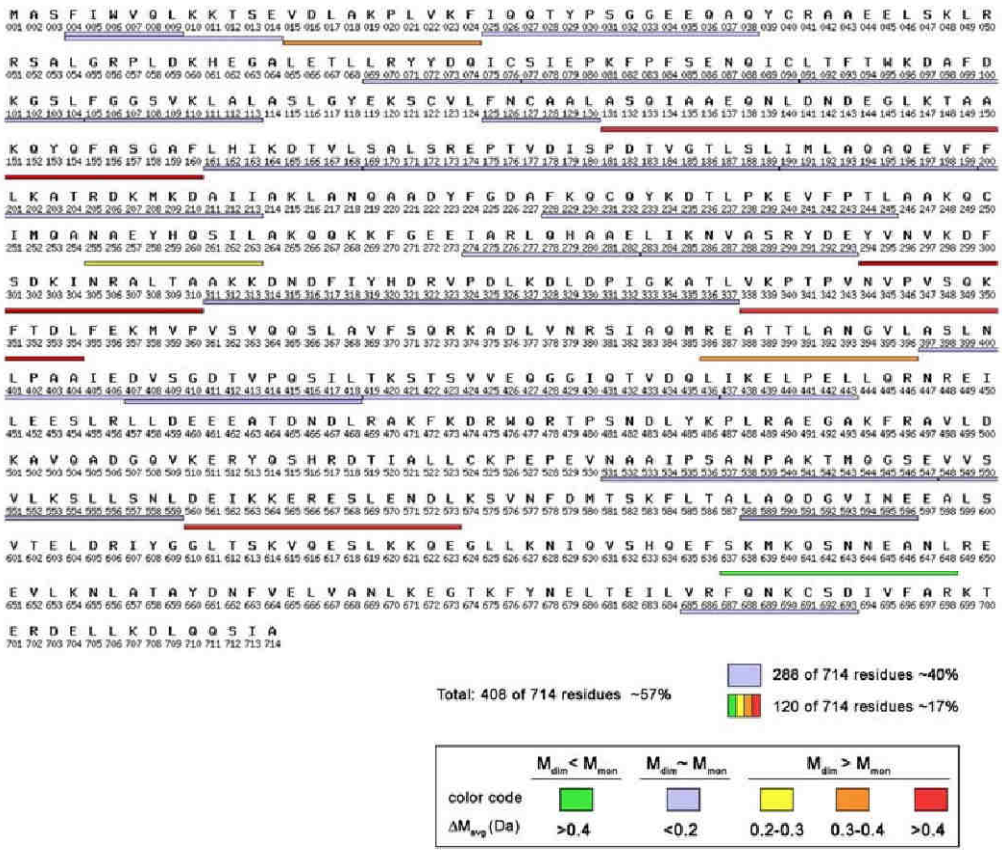

Figure 21. Map of Alix-ΔPRD peptides analyzed by H/D exchange. Deuterium incorporation kinetics was analyzed for 32 proteolytic fragments covering 57% of the protein sequence. Peptides are color-coded according to the average mass difference (ΔM_{avg}) between monomer (M_{mon}) and dimer (M_{dim}) calculated from individual local kinetics plots. Deuteration level obtained for each peptide can either be lower in the dimer when compared with the monomer ($M_{dim}<M_{mon}$) indicating protection upon dimerization, lower in the monomer ($M_{dim}>M_{mon}$) suggestion gain of accessibility in the dimer or similar between monomer and dimer ($M_{dim}\sim M_{mon}$).

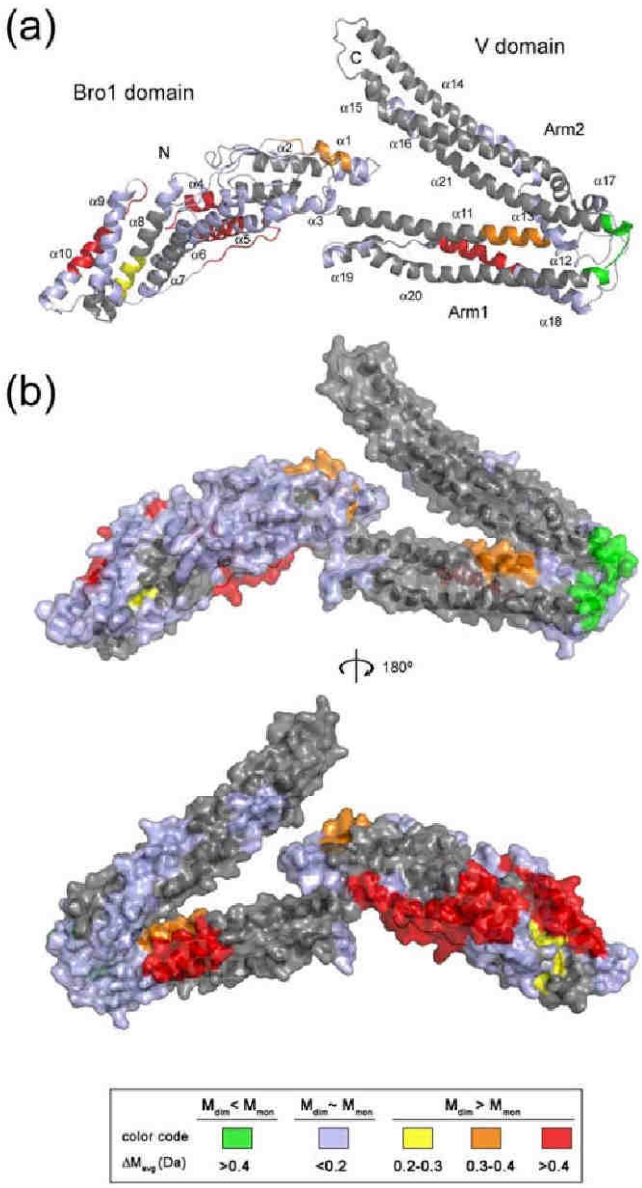

Figure 22. The regions of Alix-ΔPRD mapped by H/D exchange (a) Ribbon representation of the human Alix ortholog structure (Protein Data Bank code 2OEV) (Fisher, Chung *et al.* 2007) highlighting the position of the different peptides analized by H/D exchange. The color code represents average mass differences between monomer and dimer as described in Figure 21; non-mapped regions are colored in grey. Bro-1 and V domains as well as N- and C-terminal ends of the protein are indicated. **(b)** Surface representation shows the extension of the mapped region. The bottom molecule is the view from the "back" of the top one. Of note, the green region (peptide 637-648) is more protected on the dimer and red regions between the two arms of the V-domain and on the concave side of Bro1-domain, are more accessible upon dimerization.

Alix-V mutants impair dimerization and adopt elongated conformations

In order to analyze the role of the proposed V-domain hinge region in dimerization, solvent exposed residues within the loop region 637-SKMKQSNNEANL-648 were changed to generate two mutants: Alix-V_{Mut1} where 6 residues were substituted, 638-**EAA**QS**YKK**-645 and Alix-V_{Mut2} where only 3 residues were changed 638-KMKQS**YKK**-645 (Figure 23e,g). Gel filtration analyses performed on a Superdex 200 column revealed new elution profiles for both mutants when compared to the wild type Alix-V elution profile (Figure 23a). Alix-V_{Mut1} eluted as single peak at ~ 12 ml containing monomeric protein (Figure 23b) and Alix-V_{Mut2} eluted in two major peaks at ~11.2 and at ~12.6 ml (Figure 23a) corresponding to dimers and monomers respectively (Figure 23b). When compared to the wild type profile on S200, the elution volume shifted (~2ml for Alix-V_{Mut1} and ~1ml Alix-V_{Mut2}) indicating that both mutants adopted a larger hydrodynamic radius. Substitution of residues 638-KMK-640 impaired Alix-V dimerization, indicating that these residues are critical to the dimerization process and dimer stability and represent at least part of Alix dimerization interface.

Furthermore Alix-V was analyzed by limited proteolysis using trypsin and this revealed three major proteolytic fragments that helped to design three deletion mutants (Figure 23e). Gel filtration analysis of Alix-V deletions mutants resulted in similar observations as described for Alix-V_{Mut1} and Alix-V_{-Mut2}. An Alix-V mutant lacking the first half of helix α11 (Δ358-386; Figure 23f) showed a significant shift in the elution profile when compared to the wild protein; a monomeric peak and a smaller peak, which may represent a dimeric form (Figure 23c). A mutant lacking the entire α11, α12 and a portion of α13 (Δ358-420; Figure 23f) behaved in gel filtration similar to Alix-V_{Mut1}, eluting as a single peak approximately 2ml earlier than monomeric wild type. Finally a third Alix-V deletion mutant lacking the last helix α21 (Δ649-714; Figure 23f) eluted in two major

peaks (Figure 23c), the first one corresponding to dimers as confirmed by cross-linking analysis (Figure 23d). Overall, the results obtained with Alix-V deletion mutants also support the importance of the hinge region for the stability of a closed (less elongated) conformation and give a first indication that at least the last helix α21 might be dispensable for dimerization.

Figure 23. Analysis of Alix-V mutant forms. (a) Size exclusion chromatography profiles of two substitution mutants (Mut1and Mut2) compared with wild type Alix-V. **(b)** Molecular weight determination by MALLS performed with Mut1 peak eluted at 11.99ml and with Mut2 peaks eluted at 11.15ml and 12.63ml. This confirmed the monomeric or dimeric state of each peak. **(c)** Size exclusion chromatography profiles of three deletion mutants compared to that of the wild type Alix-V. **(d)** Chemical cross linking analysis performed with Alix derived from the first elution peak of Alix-V Δ649-714. D, dimer. **(e)** Sequence details for the different substitution mutants and comparison with the native protein and diagram for deletion mutants. **(f)** Crystal structure of Alix-V human ortholog (Protein Data Bank code 2OEX) (Fisher, Chung *et al.* 2007) depicting the different regions deleted as well as the 6 residues substituted in the hinge region (within the box). The same color code for deletion mutants is used in (c),(e) and (f). **(g)** Close-up views of the hinge region (bottom view), comparing the targeted residues (Native) with the corresponding substitutions (Mutant-1). *(Figure in the next page)*

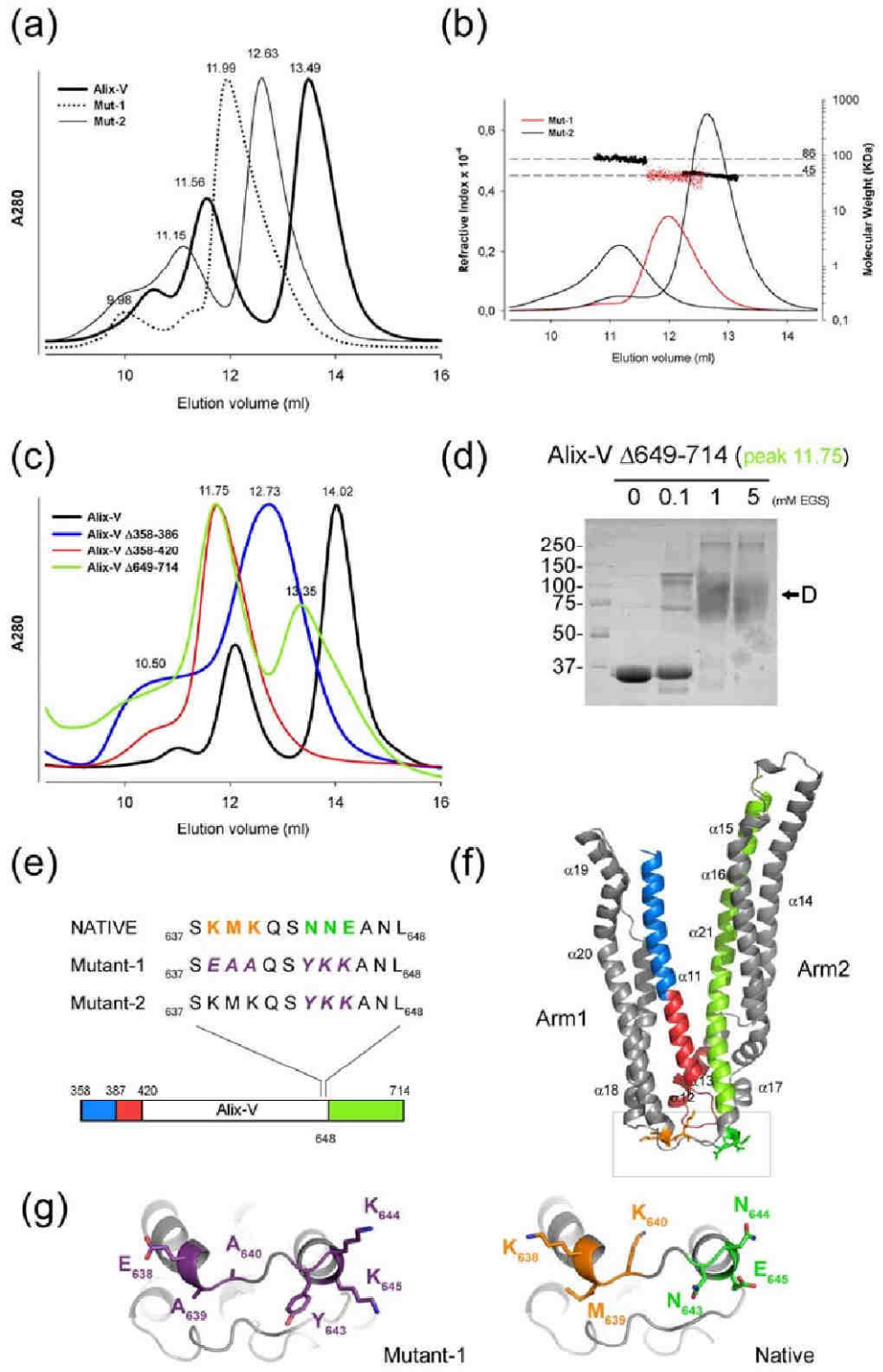
(a)
Alix-V
Mut-1
Mut-2
A280
9.98
11.15
11.56
11.99
12.63
13.49
Elution volume (ml)
(b)
Mut-1
Mut-2
Refractive Index x 10⁻⁴
Molecular Weight (KDa)
86
45
Elution volume (ml)
(c)
Alix-V
Alix-V Δ358-386
Alix-V Δ358-420
Alix-V Δ649-714
A280
10.50
11.75
12.73
13.35
14.02
Elution volume (ml)
(d)
Alix-V Δ649-714 (peak 11.75)
0 0.1 1 5 (mM EGS)
250-
150-
100-
75-
50-
37-
D
(e)
NATIVE 637 S K M K Q S N N E A N L 648
Mutant-1 637 S E A A Q S Y K K A N L 648
Mutant-2 637 S K M K Q S Y K K A N L 648
358 387 420 714
Alix-V
648
(f)
α15
α19
α16
α14
α21
α20
α11
Arm2
Arm1
α18
α12
α13
α17
(g)
K644
A640
E638
K645
A639
Y643
Mutant-1
K640
N644
K638
E645
N643
M639
Native

Solution structure of Alix by small angle X-ray scattering (SAXS)

Alix-ΔPRD folds into a crescent-shaped dimer

Alix-ΔPRD monomers and dimers were analyzed by small angle X-ray scattering. The scattering intensity patterns of these constructs are shown in Figure 24a and b. The Guinier analysis revealed a radius of gyration (Rg) of 40.6 ± 0.1 Å for the monomeric Alix-ΔPRD and 81.2 ± 0.8 Å for the dimer. Maximal protein dimensions (D_{max}) of approximately 300 Å for the dimeric and of 170 Å for the monomeric form were found by the distance distribution function p(r) computed by a Fourier transformation of the scattering intensity.

The shapes of the two constructs were determined *ab initio* from the scattering data using the program DAMMIN (Svergun 1999). The reconstructed models of Alix-ΔPRD monomer and dimer fitted the corresponding experimental data with the discrepancy χ of 1.9 and 1.2 respectively (Figure 24a,b). The *ab initio* modeling resulted for the Alix-ΔPRD monomer in an elongated shape with dimensions of ~ 45 x 60 x 145 Å (Figure 25a). The overall shape is consistent with the crystal structure of the human Alix ortholog (Protein Data Bank code 2OEV) (Fisher, Chung *et al.* 2007) fitted manually into the low resolution map calculated from the SAXS model (Figure 25b). The crystal structure comprises residues 1-702 of the human Alix ortholog, thus mainly corresponding to the Alix-ΔPRD construct experimentally used for SAXS analysis (residues 1-714, from *Mus Musculus*). A theoretical scattering curve calculated for the crystal structure using the program CRYSOL (Svergun, Barberato *et al.* 1995) fitted the experimental curve for Alix-ΔPRD in solution with a discrepancy χ of 2.7 (Figure 24e). Indeed, a certain difference is particularly clear at the level of the V-domain fit (Figure 25b). The molecular envelop obtained in solution suggests a more compact V-domain, potentially by keeping the two arms close together, in contrast with what is shown by the crystal structure. *Ab initio*

modeling of the Alix-ΔPRD dimer yielded a crescent-shaped structure with dimensions of ~ 45 x 100 x 270Å (Figure 26a). Two monomers seem to associate in a tail-to-tail fashion, potentially through their Alix-V domains (since they dimerize in solution), to span a concave surface of ~ 270 Å between the N-terminal ends (Bro1 domains) (Figure 26b).

Alix-V mutant adopts an extended conformation

Monomeric Alix-V and its dimer mutant version (Alix-V_{Mut1}) were also analyzed by small angle X-ray scattering. The scattering intensity patterns for both are shown in Figure 24c and d. The Guinier analysis revealed a radius of gyration (Rg) of 33.4 ± 0.1 Å for the native Alix-V and 56.3 ± 0.1 Å for the mutant. The D_{max} of Alix-V is approximately 125 Å, clearly shorter than the one observed for Alix-V_{Mut1} found to be around 170 Å. The *ab initio* model of Alix-V obtained from the scattering data reveals an L-shaped molecule with an approximate diameter of 20 x 20 Å and extensions of 40 and 100 Å each direction (Figure 27a). The model fitted the corresponding experimental data with a discrepancy χ of 1.4. Significant differences were however found when the Alix-V crystal structure of the human ortholog (residues 360-702, Protein Data Bank code 2OJQ) (Lee, Joshi *et al.* 2007) was manually fit into the molecular envelop calculated for Alix-V in solution (Figure 27b). In parallel a high discrepancy (χ > 5) was also obtained when the theoretical scattering curve calculated from the crystal structure was fit to the experimental scattering curve obtained for Alix-V (Figure 24f), suggesting that the crystal packing locks Alix-V in one specific conformation (Figure 27b). Dimeric Alix-V could not be analyzed by small angle X-ray scattering due to insufficient monodispersity of the preparations.

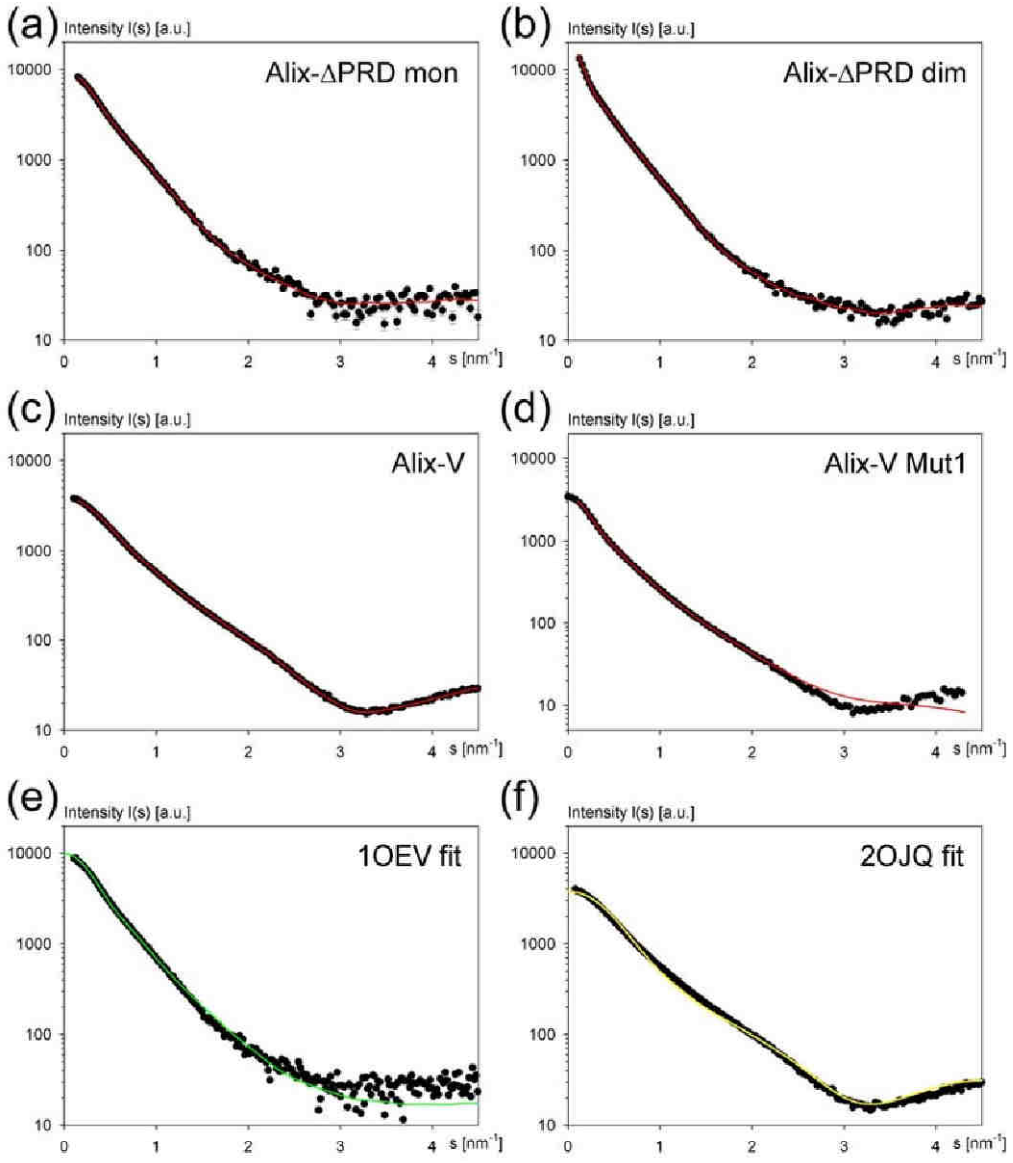

Figure 24. Small angle X-ray scattering profiles for Alix-ΔPRD. Experimental scattering intensities (black dots) measured for **(a)** Alix-ΔPRD monomer, **(b)** Alix-ΔPRD dimer, **(c)** Alix-V and **(d)** Alix-V_{Mut1} are plotted as a function of momentum transfer (s). The solid red line indicates the theoretical scattering curve calculated for the SAXS *ab initio* models of each Alix form. Theoretical scattering curves for **(e)** Alix-ΔPRD monomer (green solid line) and **(f)** Alix-V monomer (yellow solid line) calculated from the corresponding crystal structures (respective Protein Data Bank Codes, 1OEV and 2OJG) are fitted to the corresponding experimental scattering intensities.

The shape of Alix-V_{Mut1} was determined *ab initio* from the solution scattering data and resulted in an elongated structure spanning approximately 170 Å, with a diameter of about 20 x 20 Å (Figure 28a). The reconstructed model fit the corresponding experimental data with the discrepancy χ of 1.8 (Figure 24d) The model suggests an open conformation of Alix-V and indeed this becomes clear when the crystal structure of the human ortholog (Lee, Joshi *et al.* 2007) was manually fit into the elongated SAXS envelop: one arm must be rotated by ~140º to generate the extended conformation (Figure 28b). This mutation introduced into Alix-V_{Mut1} most likely stabilizes the open Alix-V conformation. Together these observations suggest a potential role for the conformational dynamics of the V-domain in the Alix dimerization process.

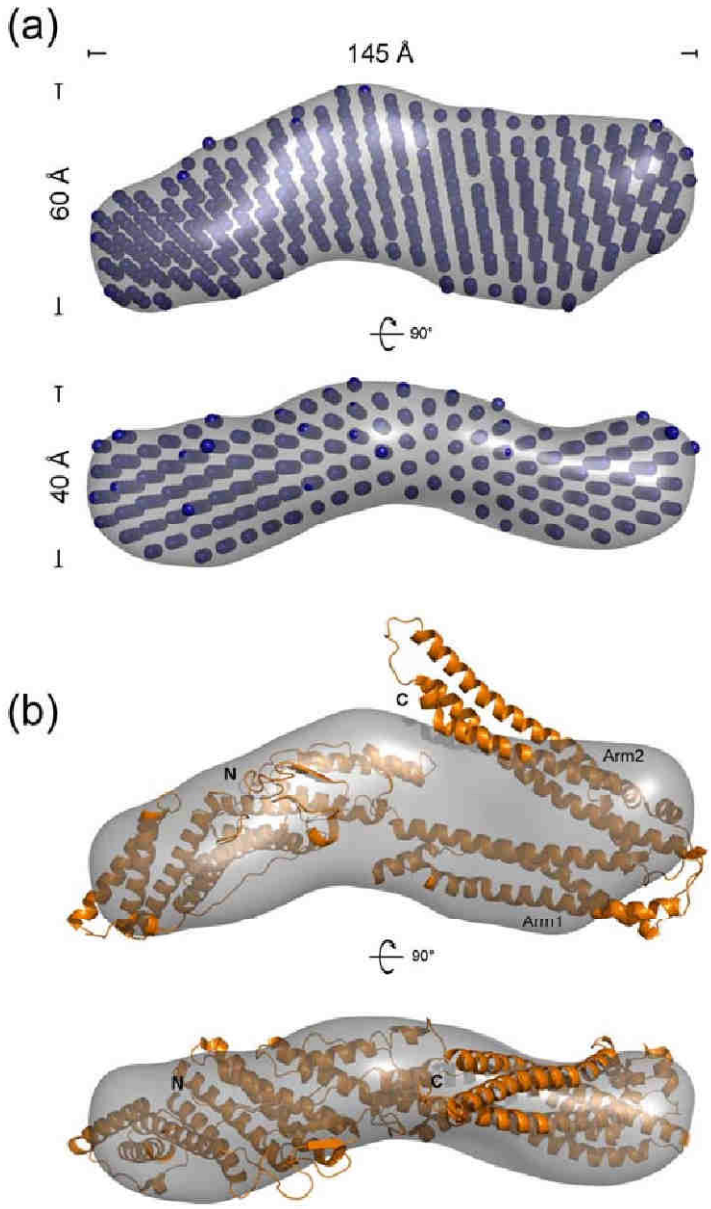

Figure 25. Small angle X-ray scattering model of the Alix-ΔPRD monomer. (a) *Ab initio* shape model of the Alix-ΔPRD monomer is shown in two perpendicular orientations. The bead model (blue spheres) was used to calculate the molecular envelop represented in grey. **(b)** Manual fit of the human Alix ortholog crystal structure (residues 1-702, in orange, Protein Data Bank code 2OEV) (Fisher, Chung *et al.* 2007) into the monomeric molecular envelop shown above. The N- and C- terminal ends of the crystal structure as well as the Arm1 and Arm2 of the V-domain are indicated.

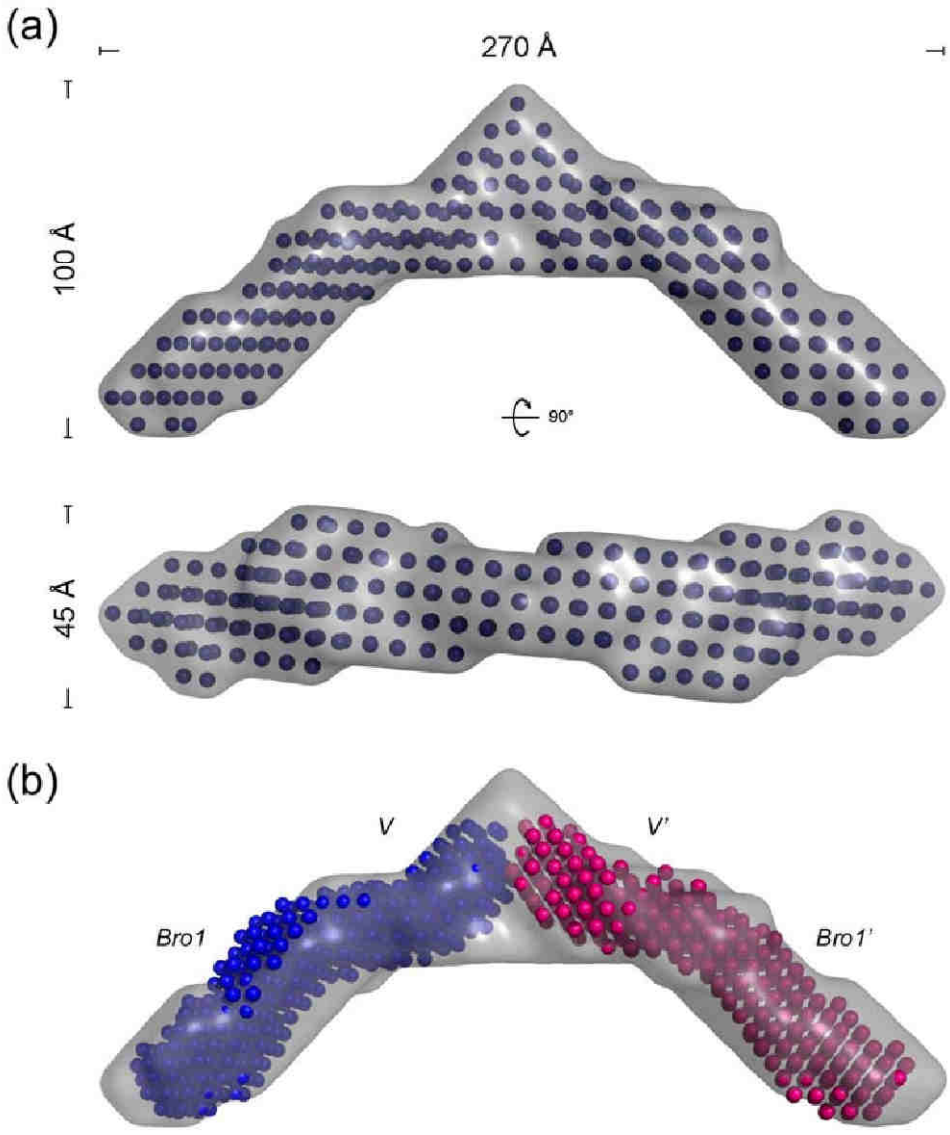

Figure 26. Small angle X-ray scattering model of Alix-ΔPRD dimer. (a) *Ab initio* shape model of dimeric Alix-ΔPRD reveals a crescent shape structure. Two perpendicular orientations show the molecular envelop (in grey) calculated from the bead model (blue spheres). **(b)** Manual fit of two monomeric bead models (blue and magenta) into the dimer envelop. The crescent shape suggests that two monomers associated in a tail-to-tail fashion. Putative Bro1- and V-domain positions are indicated.

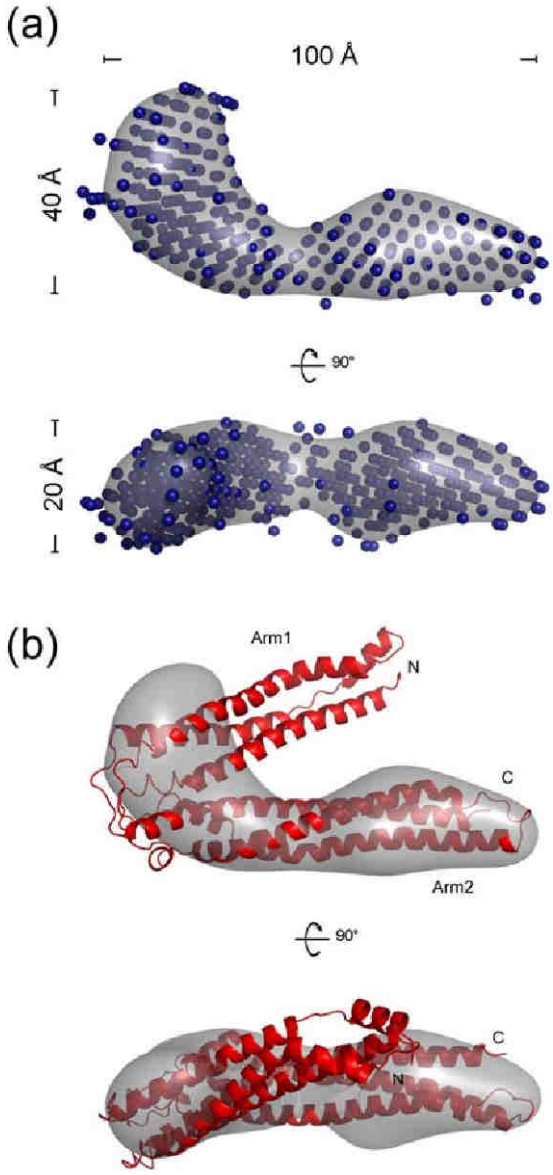

Figure 27. Small angle X-ray scattering model of the Alix-V monomer. (a) Ab initio shape model of monomeric Alix-V reveals an L-shaped form. Two perpendicular orientations show the molecular envelop (in grey) calculated from the obtained bead model (blue spheres). **(b)** Manual fit of the crystal structure of the human Alix-V ortholog (residues 360-702, in red, Protein Data Bank code 2OJQ) (Lee, Joshi *et al.* 2007) into the molecular envelop of Alix-V. The N- and C- terminal ends as well as the Arm1 and Arm2 of the crystal structure are indicated.

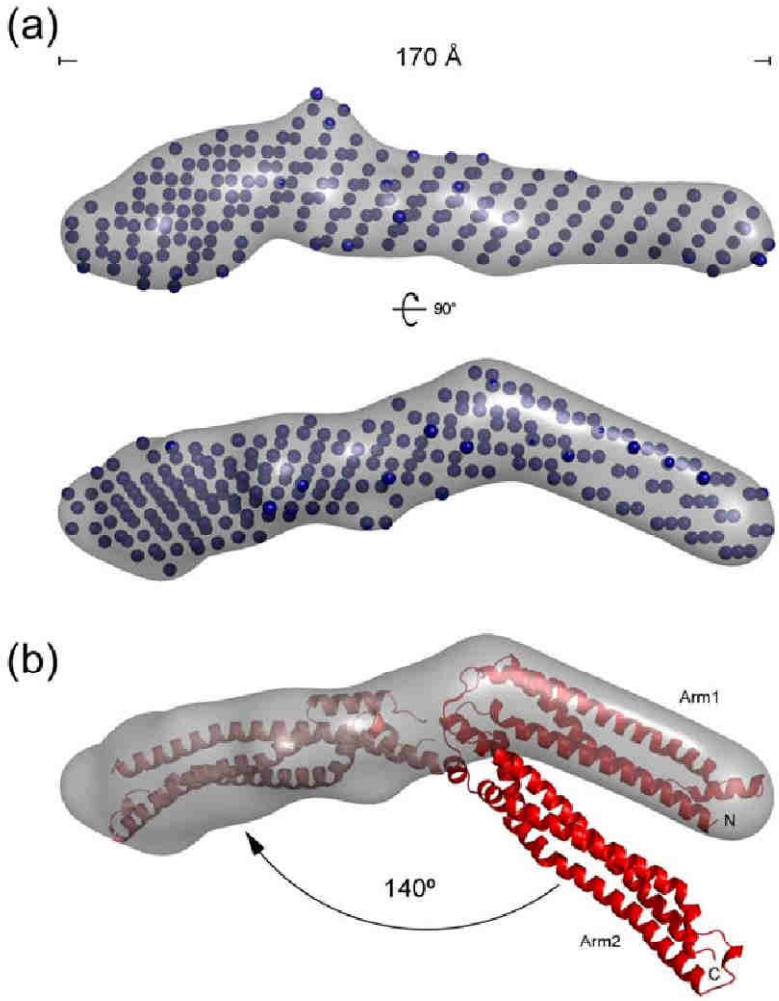

Figure 28. Small angle X-ray scattering model of the Alix-V_{Mut1}. (a) *Ab initio* shape model obtained for Alix-V_{Mut1} reveals an elongated conformation. Two perpendicular views show the molecular envelop (in grey) calculated from the bead model (blue spheres). **(b)** Manual fit of the crystal structure of the human Alix-V ortholog (residues 360-702, in red, Protein Data Bank code 2OJQ) (Lee, Joshi *et al.* 2007) into the molecular envelop of the mutant. The N- and C-terminal ends as well as the Arm1 and Arm2 of the crystal structure are indicated. The rotation of Arm2 (by ~140°; light red) has been simulated to fit the elongated model.

Crystallization and preliminary X-ray crystallographic analysis of Alix

As a result of biophysical studies on different Alix constructs, novel crystallization targets became priority in the project's context. Since the structures of an Alix-ΔPRD and monomeric Alix-V had been published (Fisher, Chung *et al.* 2007; Lee, Joshi *et al.* 2007), we focused our effort on the Alix-V dimer and the Alix-V_{Mut1}.

Crystallization of Alix-V dimer

Alix-V dimer crystals where first obtained by manual crystallization screening in the condition: 0.1 M bicine pH 9.0, 1M ammonium sulfate (Figure 29a). The size of crystals was improved by growing them in the same crystallization condition supplemented with 10-30% glycerol; crystals grew 5-10 times bigger, to about 200-400 μm (Figure 29c,d). Larger crystals grown in conditions containing glycerol diffracted X-rays only to approximately 10 Å (Figure 30) at the ESRF beam lines ID14-1 and ID29 as well as on the microfocus beamline ID23-1 (Grenoble, France). Preliminary determination of the space group and unit cell indicated that these crystals have a tetragonal lattice with cell dimensions of a=338, b=338 and c=164 Å. Different approaches were employed to improve the diffraction; this included dehydrating procedures based on gradients of ionic strength (with ammonium sulfate), screening of cryo-protectants and cryo procedures and optimization of the purification protocol to obtain single Alix-V dimeric species rather than a heterogeneous mixture of conformers (like showed in Figure 16). None of the procedures resulted however in better diffracting crystals.

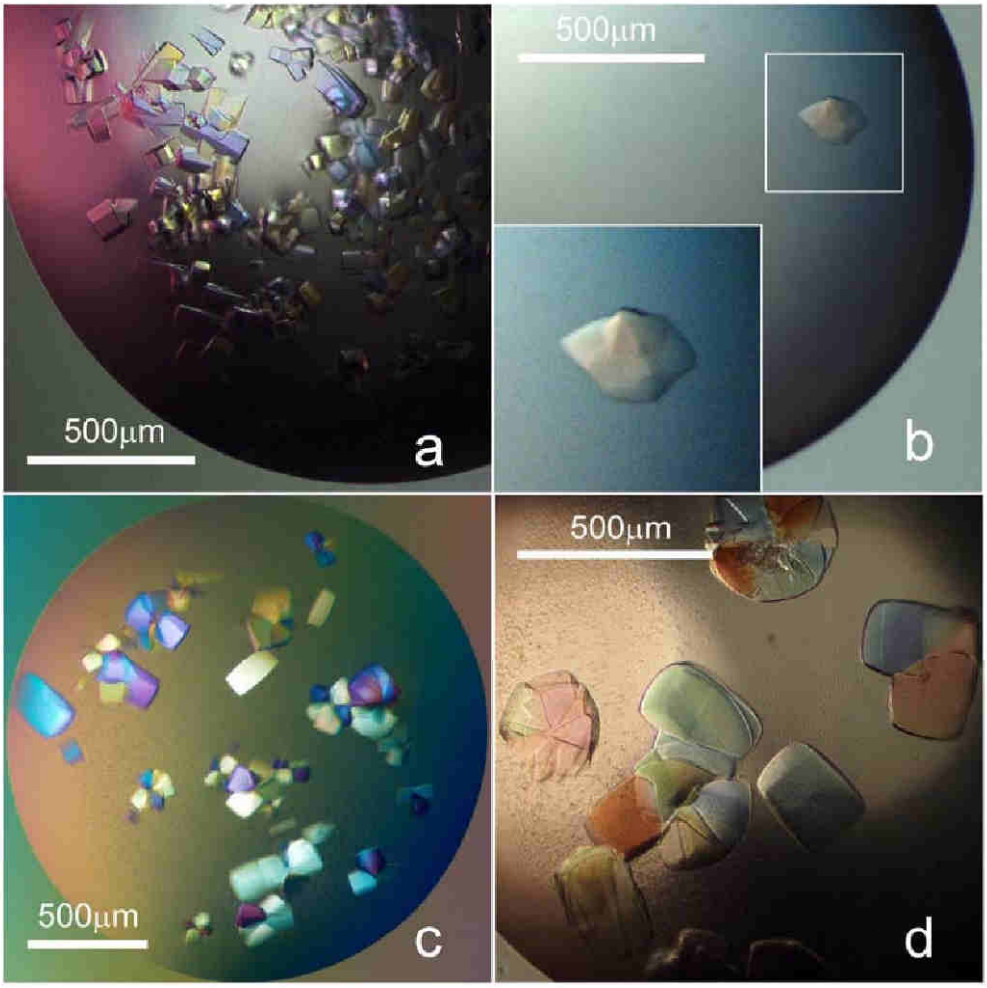

Figure 29. Alix-V dimer crystals. (a) Prismatic-shaped crystals grown in 0.1M bicine pH 9.0, 1M ammonium sulfate; **(b)** Single crystal obtained in 0.1M MES pH 5.6, 10% PEG 6K. **(c,d)** crystals grown in the same conditions as (a) supplemented respectively with 10% and 20% glycerol.

Noteworthy, a different crystal form grown in 0.1 M MES pH 5.6, 10% PEG 6K (Figure 29b) also diffracted only to ~10 Å resolution. Later experiments then showed that lower pHs (4-6) destabilize the Alix-V dimer and the condition was not further pursued. Interestingly, the single crystal obtained at pH 5.6 belongs to the space group $P2_1$ (or $P2_12_12_1$) with cell dimensions of 75x125x140 Å (both are preliminary parameters),

resembling the crystallographic parameters obtained for the open Alix-V mutant (described below). No crystals of selenomethionine-derivatized Alix-V dimer were formed in the same conditions selected for crystallization of the native form and neither a high-throughput screening resulted in new crystallization hits for the labeled protein.

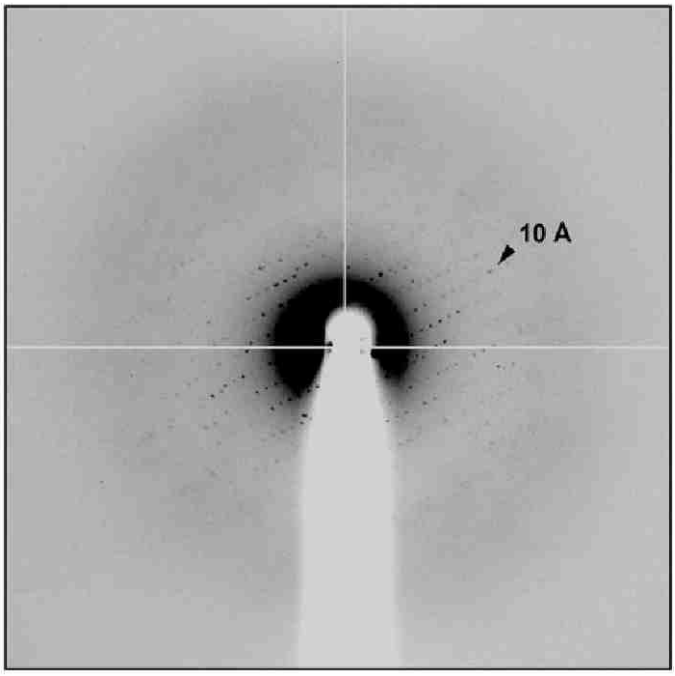

Figure 30. X-ray diffraction pattern of Alix-V dimer crystals.

Crystallization of Alix-V mutant

Alix-VMut1 crystallized in a broad range of conditions and two of them were selected for optimization as they presented crystals of relevant sizes and different morphologies. Using 0.1M Bicine pH 9.0, 15% PEG 5K, conical-shaped crystals were obtained (Figure 31a), clearly different from the sharp needles grown in 0.1M Tris-HCl pH 8.0, 10-12 % PEG 20K (Figure 31b). Nucleation problems were overcame by

lowering protein concentration below 15mg/ml or growing the crystals at 4ºC. Combining lower temperature and lower molarities of different buffers at pH8.0, in particular HEPES and Bicine (0.025-0.05M), blade-like crystals growing to rather remarkable sizes could be obtained (Figure 31c). Nevertheless large crystals under both conditions showed also diffraction limited to ~ 10 Å. All the dehydrating procedures tried for freezing or shrinkage purposes, indicated an abnormal high solvent content most likely responsible for a fragile crystalline order. The only exception came with additive screening where a condition with nickel chloride gave a few crystals diffracting X-ray better than 10 Å. Indeed the in presence of 10mM $NiCl_2$, crystals grow with a different morphology, more prismatic-shaped rather than needle-like crystals and even if not all were of better quality a few small $NiCl_2$ containing crystals diffracted X-rays to ~ 3 Å resolution (Figure 32). Complete data sets were collected at ESRF beam lines ID29 and ID14-1 (Grenoble, France). The crystals belong to space group P222 with cell parameters of a= 59.026, b= 123.27 and c= 131.02. The data was indexed and integrated with the *MOSFLM* (Leslie 1992) and *XDS* (Kabsch 1993) packages and scaled using *SCALA* (Collaborative Computational Project Number 4 1994). Data-collection statistics are listed in Table 3. Structure determination was attempted by molecular replacement using *MOLREP* (Collaborative Computational Project Number 4 1994) and two search models corresponding to each of the two arms of the V-domain (Protein Data Bank code 2OEX; (Fisher, Chung *et al.* 2007) where the loop regions were deleted. However, so far no solution has been found.

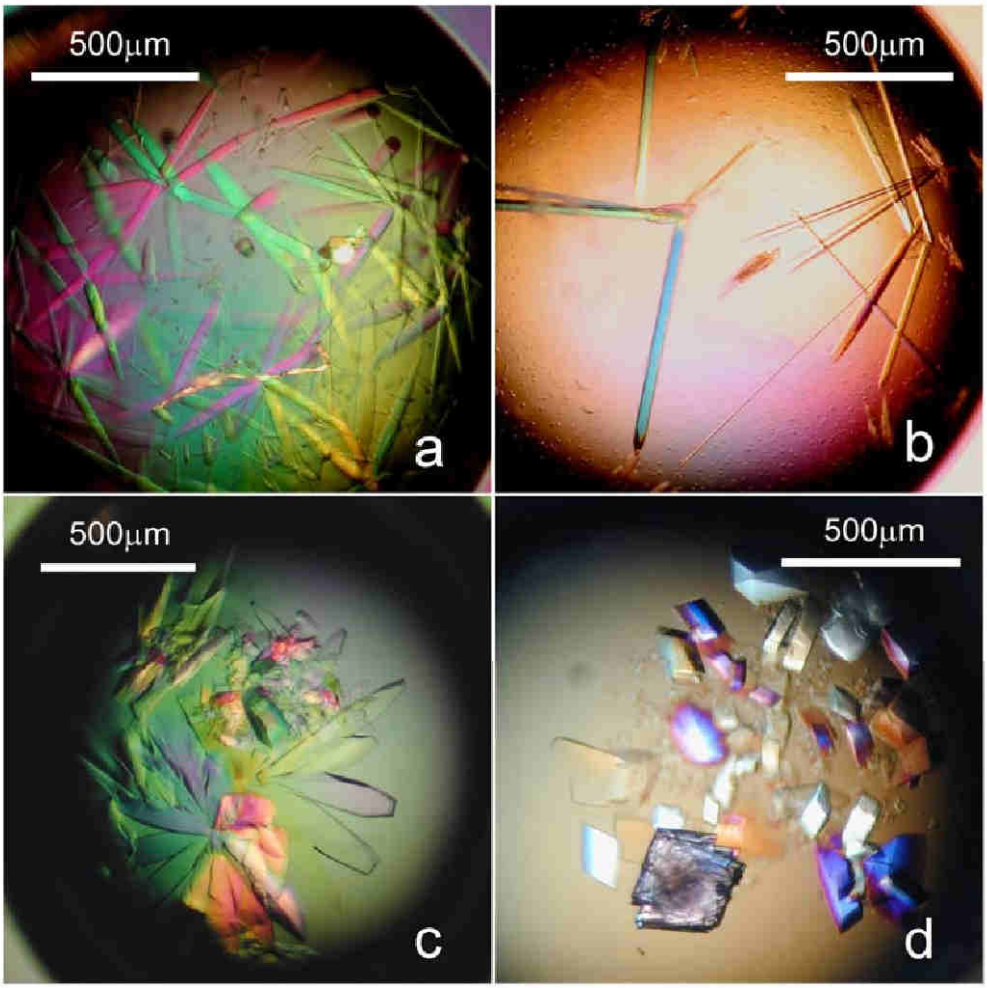

Figure 31. Alix-V_{Mut1} crystals. (a) Conical-shaped crystals obtained in 0.1M Bicine pH 9.0, 15% PEG 5K;**(b)** sharp needle-like crystals grown in 0.1M Tris-HCl pH 8.0, 10-12 % PEG 20K; **(c)** blade-like crystals grown at 4ºC with the same buffer conditions as (b); **(d)** crystals grown in the same condition as in (b) but in the presence of 10mM $NiCl_2$.

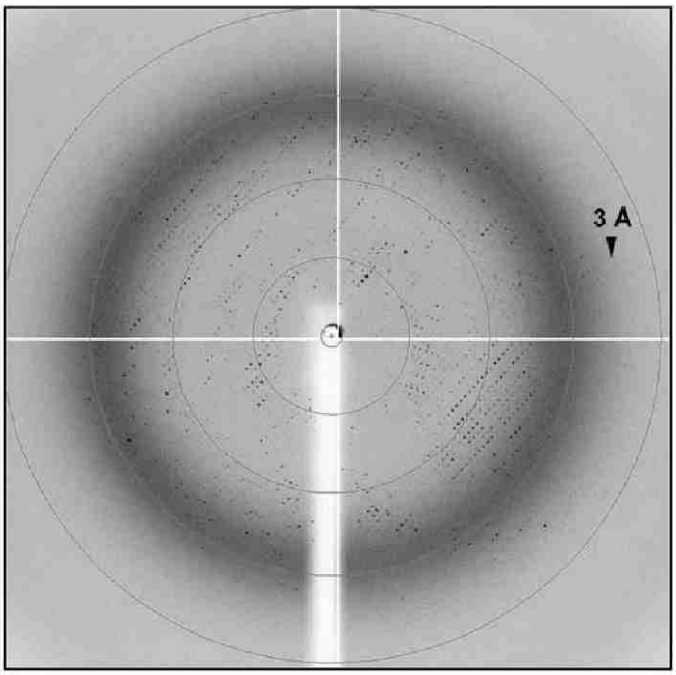

Figure 32. X-ray diffraction pattern of Alix-V_{Mut1} crystals.

Table 3. X-ray data collection statistics. Values in parentheses are for the highest resolution shell.

	Alix-V_{Mut1}
DATA COLLECTION [a]	
Resolution (Å)	49.30–3.30 (3.48-3.30)
Wavelength (Å)	0.933
Space group	P222
Unit-cell parameters	
a, b, c (Å)	59.03, 123.27, 131.02
No. of molecs per asymm unit [b]	2
Data-collection temperature (K)	110
No. of observed reflections	103382 (15228)
No. of unique reflections	14997 (2150)
Completeness (%)	99.82 (100.00)
Average multiplicity	6.89 (7.08)
$I/\sigma(I)$	3.33 (1.26)
R_{sym} (%) [c]	21(61)
Wilson B-factor ($Å_2$)	64.68

[a] Data were collected from single crystals at the beamline ID14-1 at the European Synchrotron Radiation Facility (ESRF), Grenoble, France.
[b] Estimated using Matthews coefficient probabilities (corresponding solvent content of 57.65 %).
[c] $R_{sym} = \Sigma|I-\langle I\rangle|/\Sigma^I$

Alix interaction with lipid bilayers

Monomeric and dimeric Alix interact with liposomes

In order to test whether Alix can interact with membranes *in vitro*, liposomes composed of a DOPE:DOPS:DOPC (5:3:2, w/w) were used as model bilayers. Alix-ΔPRD as well as Alix-V and Alix-Bro1 were incubated with liposomes and protein-lipid association analyzed by sucrose step gradient centrifugation or co-sedimentation assays.

Equimolar amounts of Alix-ΔPRD monomer and dimer (Figure 33a) incubated with liposomes revealed the binding ability of both conformers. On sucrose gradient centrifugation liposomes float to the top fractions of about 5-10% sucrose and carry associated proteins. Figure 33 shows that the amount of protein in the upper fractions 2 is dependent on the initial protein input for both Alix-ΔPRD monomer and dimer (compare lanes I, II and III). However, both conformers show a moderate binding efficiency with a small fraction (15-20%) of the protein interacting with liposomes as detected in the upper fraction 2, while most of it (~80%) remained unbound in the bottom fraction 5 (40% sucrose). Comparing equivalent mass inputs for monomer and dimer (e.g. Figure 33a, monomer lane II with dimer lane I, corresponding to a protein input of 10μg), one can observe no obvious difference in fraction 2 suggesting a similar binding efficiency between monomer and dimer.

For Alix-Bro1 incubated with liposomes, sucrose gradient centrifugation showed significant binding, with 50% of the protein input floating to upper the fractions 2 and 3 (Figure 33b). This indicates that the Bro1 domain represents a critical domain for lipid membrane binding.

The V-domain was also independently analyzed by incubating Alix-V monomer and dimer with liposomes. For both, a very weak association with lipid membranes was observed as only a minor amount floated with the liposomes in a sucrose gradient (Figure 33c). However, co-sedimentation assays showed that a higher amount of Alix-V dimers pelleted with the liposomes when analyzed in parallel with Alix-V monomers (Figure 33c). This suggested that the Alix-V binding efficiency is higher in the dimeric state compared to the monomeric one.

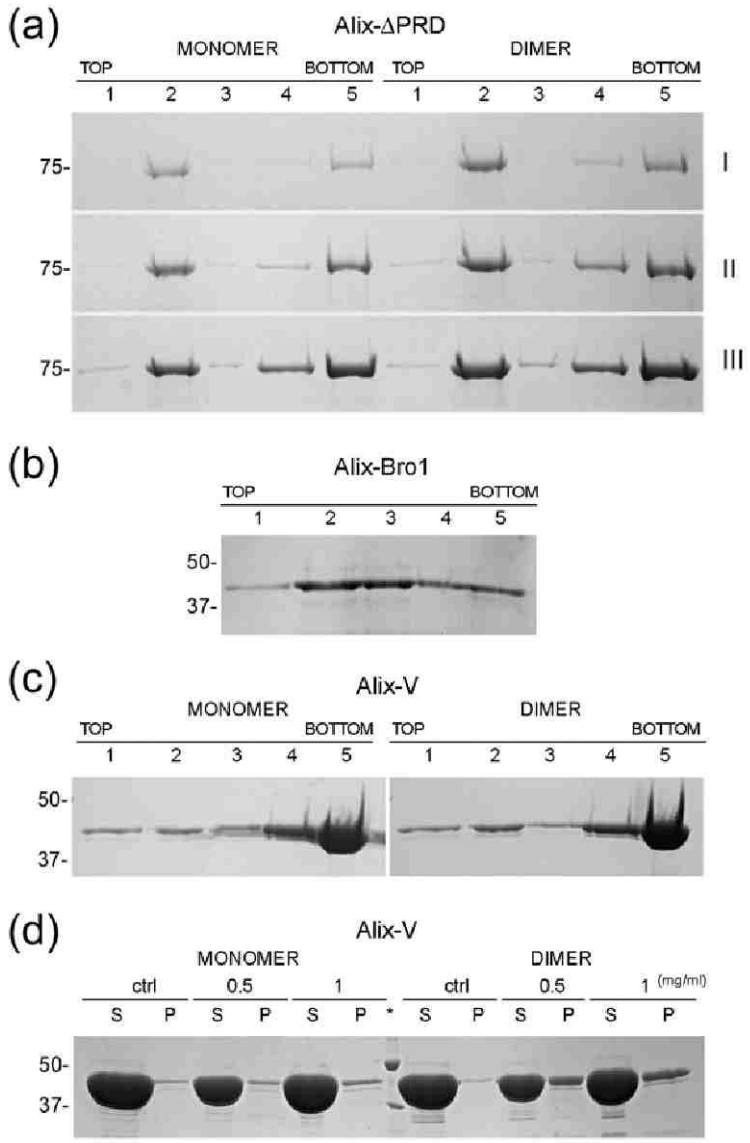

Figure 33. Monomeric and dimeric Alix interact with liposomes. (a) Sucrose gradient centrifugation of liposomes incubated with monomeric and dimeric Alix-ΔPRD. Samples from 5 fraction of the gradient were analyzed by SDS-PAGE and Alix-ΔPRD bands detected by Coomassie blue staining. Each lane corresponds to incubation with an equimolar amount of monomer and dimer: (I) 0.06 nmol, (II) 0.12 nmol and (III) 0.24 nmol. This represents respectively 5, 10 and 20μg of monomer and 10, 20 and 40μg of dimer. Only 20% of fractions 4-5 have been loaded on the gel. **(b)** Sucrose gradient centrifugation of liposomes incubated with 0.25 nmol (10μg) of Alix-Bro1. **(c)** Gradient centrifugation of liposomes incubated with 1.25 nmol (50μg) of Alix-V monomer and 0.63 nmol (50μg) of Alix-V dimer. Only 50% of fractions 4-5 have been loaded on the gel. **(d)** Co-sedimentation assays performed to liposomes incubated with Alix-V monomer and dimer at two different final protein concentrations: 0.5 and 1mg/ml. Supernatant (S) and pellet (P) are indicated for each assay. Control assays (ctrl) were done with the protein samples in the absence of liposomes. (*) Protein marker.

Alix-ΔPRD and Alix-V dimerize upon lipid bilayer binding

The oligomeric state of Alix bound to liposomes was analyzed by chemical cross-linking. Liposomes incubated with monomeric Alix-ΔPRD and monomeric Alix-V were purified by sucrose gradient centrifugation and the protein fraction associated resolubilized in a buffer containing 1% Triton X100. Chemical cross-linking of detergent solubilized Alix-ΔPRD produces a second band migrating close to the 250kDa protein marker (Figure 34a) similar to cross linked dimeric Alix-ΔPRD in the absence of liposomes (Figure 7a) and some minor higher molecular weight species. A similar result is obtained for solubilized Alix-V, with a cross linked product running above the 100kDa marker protein (Figure 34b), comparable to that observed for the Alix-V dimer in solution (Figure 7a). This suggests that lipid bilayer interaction might induce the conformational switch from Alix monomers to dimers as well as higher order oligomers.

To test whether Alix-ΔPRD associated with liposomes on the outside or inside of the liposomes, gradient purified liposomes were treated with trypsin. This revealed that Alix-ΔPRD bound to liposomes is sensitive to trypsin treatment in the absence and presence of Triton X100, suggesting that Alix is present on the surface of the liposomes (Figure 34C). Moreover Alix-ΔPRD containing liposomes were resistant to treatment with 1M NaCl, since no significant amount of Alix-ΔPRD was solubilized upon washing the liposomes in a buffer containing 1M NaCl (Figure 34D). This thus indicates that the Alix-ΔPRD lipid bilayer interaction was not significantly perturbed by high ionic strength.

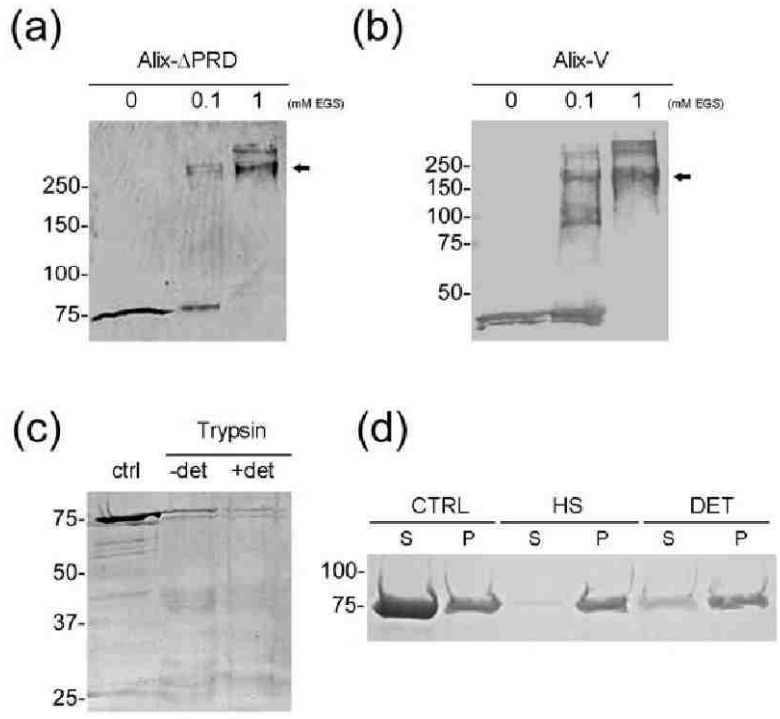

Figure 34. Oligomeric state of Alix bound to lipid bilayers. Chemical cross linking of **(a)** Alix-ΔPRD and **(b)** Alix-V isolated from proteoliposomes. Black arrows indicate the new high molecular weight band produced upon incubation with increasing amounts of EGS. Alix was detected by western blott. **(c)** Alix-ΔPRD proteoliposomes are sensitive to trypsin treatment. Control (ctrl) lane, purified proteoliposomes; Lane (-det), trypsin treatment; Lane (+det) trypsin treatment of proteoliposomes solubilized in 1% Triton X100. **(d)** Co-sedimentation of liposomes after incubation with Alix-ΔPRD (CTRL), supernatant (S) and pellet (P) fractions are indicated; Pellet fraction (lane 2) was washed with a buffer containing either 1M NaCl (HS, high salt) or 1% Triton X100 (DET). The treated samples were pelleted again and supernatant (S) and pellet (P) analyzed by SDS-PAGE.

Alix-ΔPRD liposome interaction does not depend on the vesicle curvature

Co-sedimentation assays were used to test preferential binding of Alix-ΔPRD to a specific lipid bilayer curvature. The incubation of both Alix-ΔPRD monomer and dimer with liposomes of different sizes ranging from 0.05μm to 0.8μm (thus of decreasing positive curvature; Figure 35a) showed no remarkable differences with rather equal amounts of protein being pelleted together with liposomes independently of their size (Figure 35b and c). In addition no particular membrane curvature seems to prefer one

protein state over the other, consistent with a similar binding behavior for Alix-ΔPRD monomer and dimer.

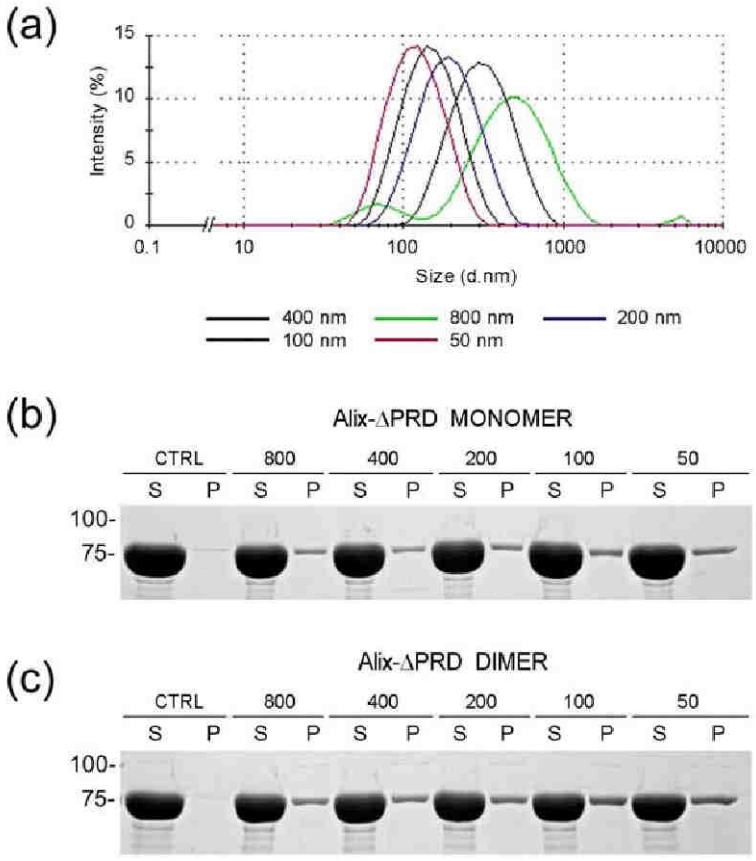

Figure 35. Membrane curvature dependent Alix binding. (a) Dynamic light scattering analysis of liposomes with different diameters (50, 100, 200, 400 and 800nm). The Gaussian distribution arrow one particular diameter (size, d.nm) indicates a mixed population and thus sample polydispersity. Liposome samples with polydispersities lower than 20-30% are selected for protein binding assays. Co-sedimentation assays were performed with liposomes of different sizes incubated either with **(b)** Alix-ΔPRD monomer or **(c)** with Alix-ΔPRD dimer. Supernatant (S) and pellet (P) fractions are indicated.

Alix-ΔPRD deforms lipid membranes *in vitro*

Cryo and negative staining electron microscopy analysis of liposomes showed round vesicles with average diameters of 200 to 400 nm (Figure 36a,f). Upon incubation

with Alix-ΔPRD they are deformed into tubular structures (Figure 36b,c,g,h). Tubular liposome structures were found in fractions 1, 2 and few in fraction 3 of the sucrose gradient, which contained mostly smaller liposomes. The tubules vary in diameter from 20 to 100 nm and were in most cases still connected to round structures (Figure 36g,h). The liposome structures observed appear to have a larger surface than just a single vesicle. Thus some of them must have undergone fusion as observed in other membrane deforming assays (Gallop, Jao *et al.* 2006). In the presence of Alix-V no major effects were observed on the liposomes' morphology (Figure 36d,e). This indicates that the ability of Alix to tubulate membranes requires the Bro1 domain even though its independent effects on liposomes were not analyzed by electron microscopy.

The effect of tubulation is not yet understood since it turned out to be difficult to reproduce. It was however observed in at least three independent experiments using monomeric Alix-ΔPRD (incubated with liposomes using a final protein concentration of 0.2-0.5mg/ml) and two independent experiments using dimeric Alix-ΔPRD with which very few and small tubules were observed. Although a number of parameter has been changed to reproduce this tubulation effect: i) fresh protein and liposome preparations; ii) different protein:lipid ratios (see surface saturation assays); iii) different liposome sizes (to test different starting curvature); iv) time and temperature of incubation, none of them seemed to influence the dynamics of the tubulation process.

Figure 36. Electron microscopy of proteoliposomes shows tubulation activity of Alix-ΔPRD. Negative staining electron microscopy to **(a)** liposomes before incubation, **(b,c)** after incubation with Alix-ΔPRD monomer and **(d,e)** with Alix-V monomer. Cryo electron microscopy to **(f)** liposomes before incubation and **(g,h)** after incubation with Alix-ΔPRD monomer.

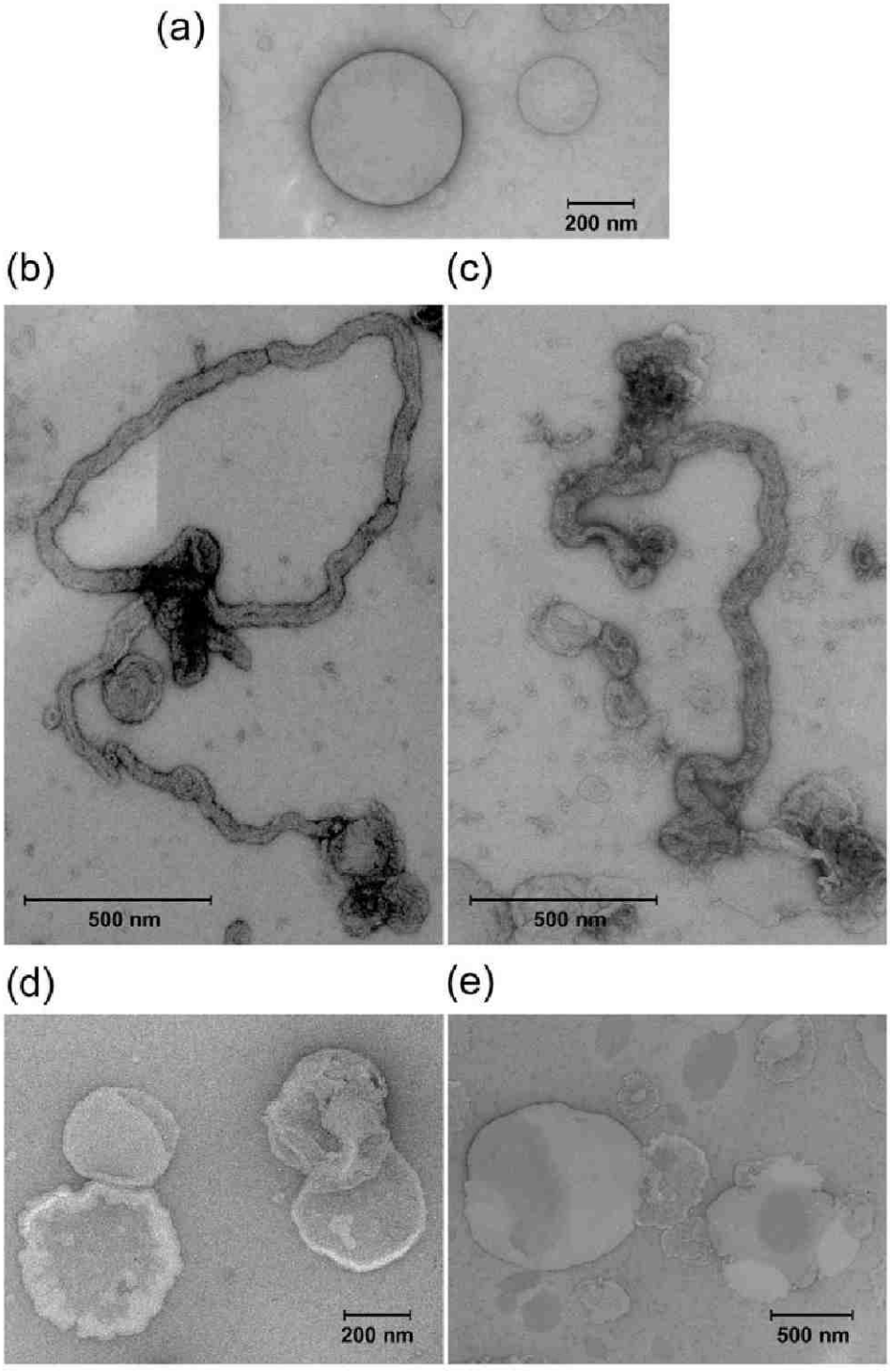

(Figure 36 – *Legend in the previous page***)**

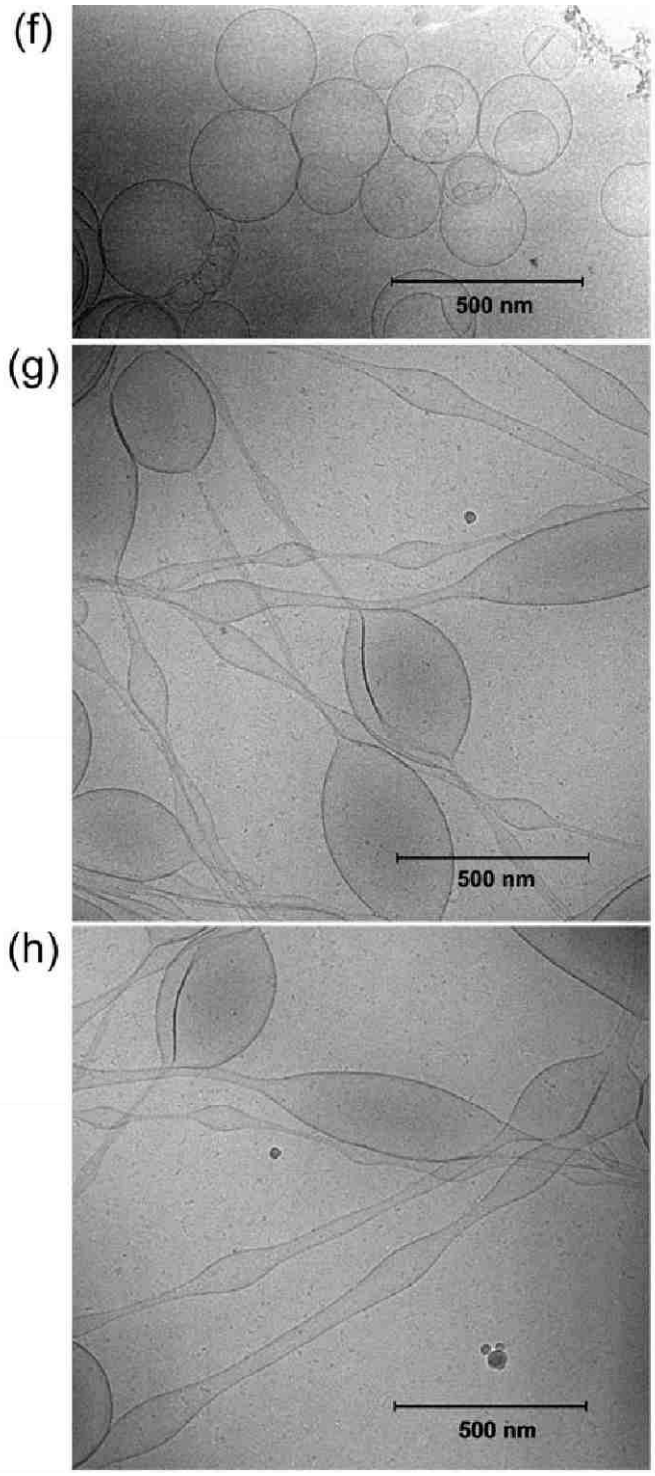

(Figure 36 – *Legend in the previous page***)**

Alix distribution on the lipid bilayer

The tubular liposomes analyzed by electron microscopy (Figure 36) exhibit no obvious Alix-ΔPRD protein coat-like structure on their surfaces. Theoretical protein amounts needed to saturate the surface of liposomes were calculated indicating that 0.8 nmol of Alix-ΔPRD monomer or 0.4 nmol of Alix-ΔPRD dimer (corresponding to about 64 μg of protein per standard binding experiment) are sufficient to cover the total solvent exposed liposome surface. Incubation of liposomes with more than theoretical amounts to saturate the surface resulted in significant protein binding (Figure 37), as observed by sucrose gradient centrifugation where upper fractions 2 and 3 are enriched in protein, indeed denoting in some cases higher densities of the proteoliposome fraction (Figure 37c). Electron microscopy analyses show that Alix saturation led to aggregated liposome structures, revealing no additional tubulation effects and no obvious protein coat-like structures in the tubules observed.

In order to study the protein distribution on the tubulated liposomes, both Alix-ΔPRD and liposomes were labeled with fluorescence markers purified by sucrose gradient and analyzed by fluorescence microscopy. The control liposomes labeled with rhodamine appear as round structures with sizes of ~ 300 to 800 nm (Figure 38a). In contrast, the liposomes containing Alix-ΔPRD appear as elongated structures, with average lengths of several microns (Figure 38b). Fluorescein-labeled Alix-ΔPRD shows the same staining pattern (Figure 38c) and both fluorescein and rhodamine labels co-localize (Figure 38d). While the liposome rhodamine label is evenly distributed (Figure 38e), the Alix-ΔPRD fluorescein label appears in stripes on the liposome structures (Figure 38f). Consistent with this, monomeric Alix-ΔPRD labeled with 1.8nm nanogold particles (Figure 39a and b), after incubation with liposomes and purification by sucrose gradient (Figure 39c), also exhibit linear distributions in several regions of the liposome's surface as analyzed by

negative staining electron microscopy (Figure 39d). Together, these results thus suggest that the tubular structures visualized by electron microscopy (Figure 39) contain Alix-ΔPRD potentially distributed along their surface.

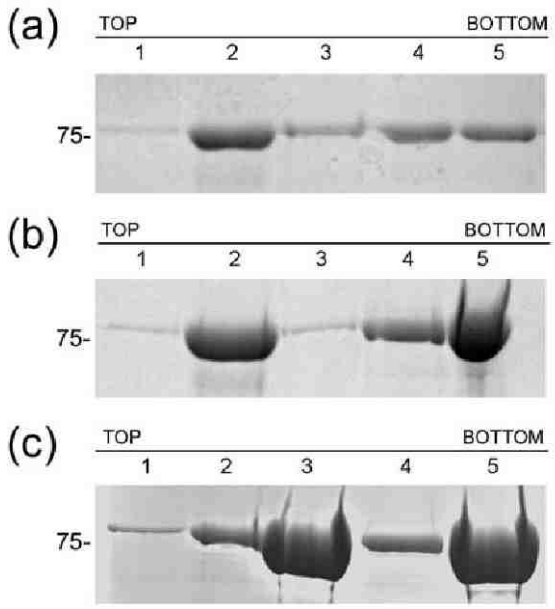

Figure 37. Saturation of the liposomes surface with Alix-ΔPRD. Sucrose gradient centrifugations to liposomes incubated with **(a)** 0.45nmol **(b)** 1nmol and **(c)** 2.4nmol of monomeric Alix-ΔPRD. Saturation induced higher density structures as suggested in (c) where the protein containing fraction floated less. The incubation with dimeric Alix-ΔPRD led to a parallel result (data not shown). In all gradients fraction 1-3 were fully loaded on the SDS-PAGE; in (a) and (b) only 50% of fractions 4-5 were loaded and in (c) only 20% of fraction 4-5 were loaded.

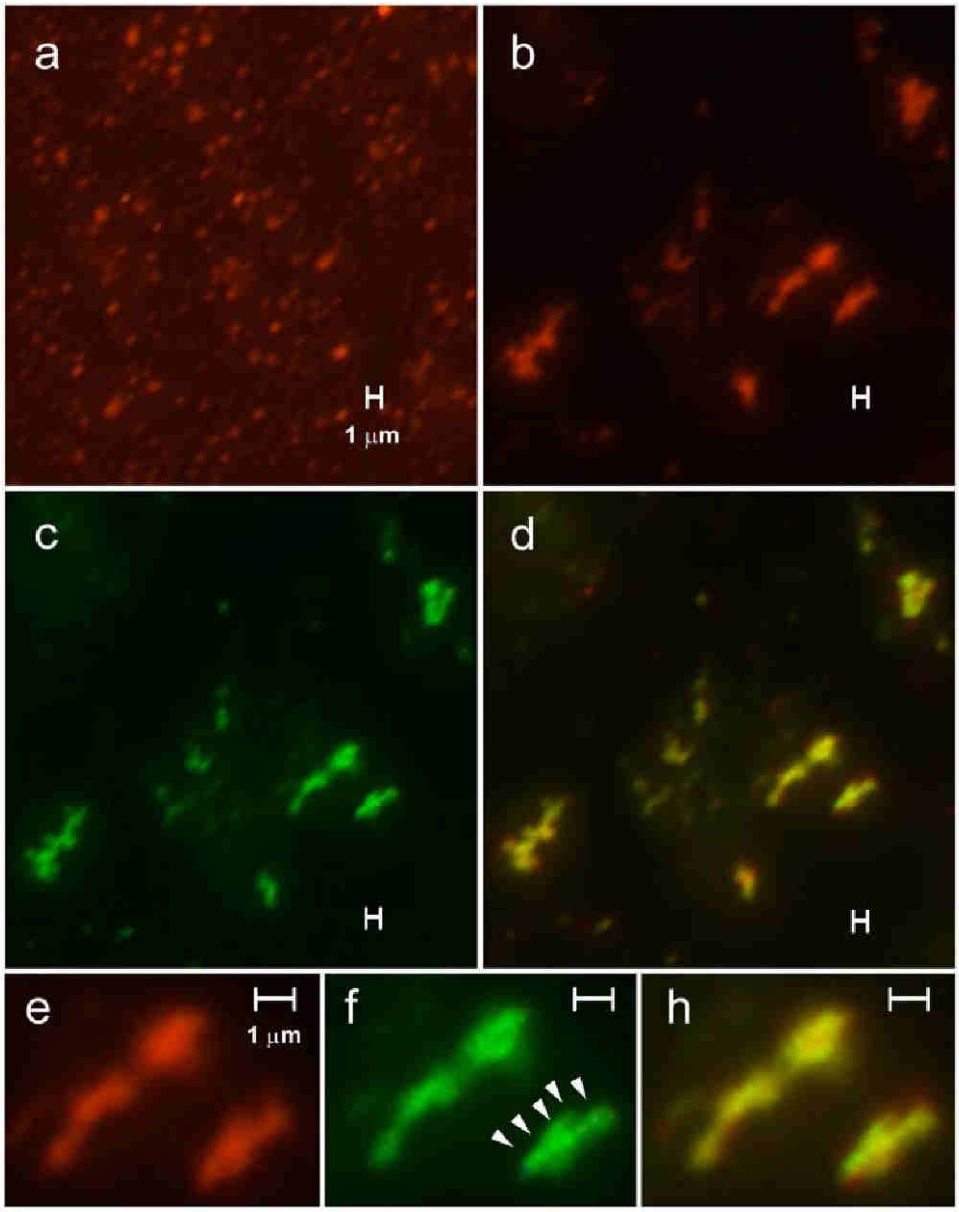

Figure 38. Fluorescence microscopy of liposomes incubated with Alix-ΔPRD. (a) Control sample of rhodamine labeled liposomes floated on a sucrose gradient. **(b)** Alix-ΔPRD containing liposomes visualized by rhodamine fluorescence and by **(c)** fluorescein fluorescence. **(d)** Overlay of both fluorescent markers. **(e)** Close up of an elongated structure shows an even distribution of rhodamine labeling and **(f)** a striped pattern (white arrows) for the fluorescein labeling, also clear in the **(h)** merged picture. All the samples were purified by sucrose gradient centrifugation. A control sample where liposomes were incubated in the presence of fluorescein reagent showed round single liposomes (like in (a)) and no green fluorescence was detected (data not shown).

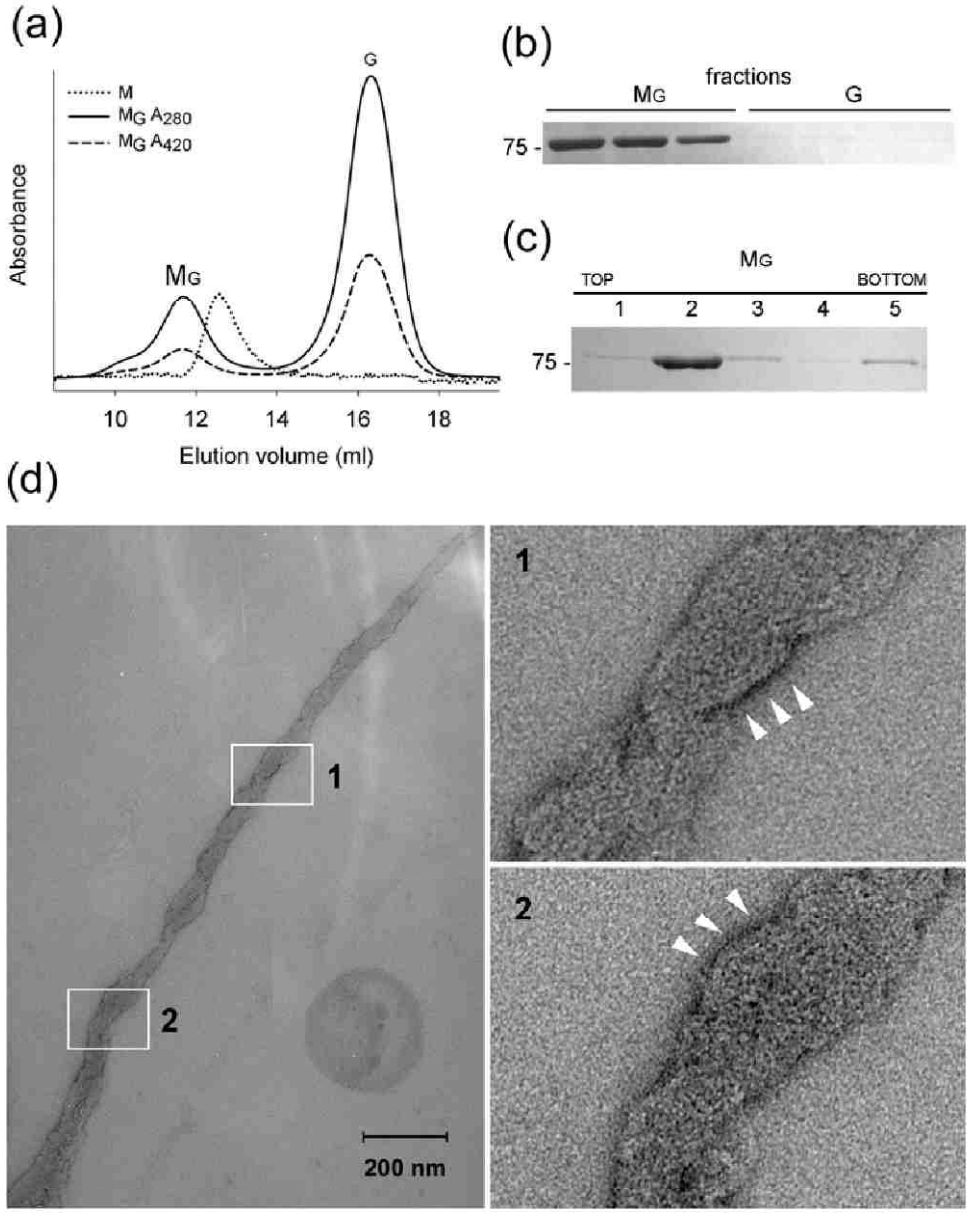

Figure 39. Nanogold labeling of Alix-ΔPRD. (a) Size exclusion chromatography profile of unlabeled (M) and nanogold labeled Alix-ΔPRD (M_G). Elution of the labeled protein was detected at two wavelength: 280nm (M_G A_{280}) and 420nm (M_G A_{420}). The peak labeled as "G" corresponds to the excess of nanogold particles; the ratio A_{280}/A_{420} is ~2.5 as expected for free gold. **(b)** SDS-PAGE of three fractions within the M_G a G elution peaks. The absence of protein in the second one, confirms that it corresponds to the excess of nanogold particles. **(c)** Sucrose gradient centrifugation performed to liposomes incubated with labeled Alix-ΔPRD; the protein co-floats with liposomes to the upper fraction 2. **(d)** Negative staining electron microscopy analysis performed to the fraction 2 of the sucrose gradient (c). Left panel shows a liposome tubular structure and right panels magnified views of the areas labeled as 1 and 2. White arrows indicate linear arrays of 1.8nm gold particles (black dots) corresponding to labeled Alix-ΔPRD.

Binding of monomeric and dimeric Alix-V to EIAV late domain

In order to determine the interaction of Alix-V with EIAV viral late domain as well as its conformational requirements, isothermal titration calorimetry (ITC) experiments were performed by using both Alix-V monomer and dimer. A peptide derived from EIAV Gag p9 (peptide sequence TQNLYPDLSEIKK) corresponding to the minimal Alix binding site in this late domain, was used for these experiments. Our results revealed an equilibrium dissociation constant (K_d) of 5 μM for monomeric Alix-V by fitting a 1:1 binding mode and a K_d of 8 μM for dimeric Alix-V by fitting a one binding site per dimer model (Figure 40). No substantial difference in enthalpy was observed since the ΔH of both reactions is -4.058 kcal/mol and -6.254 kcal/mol. This suggests that Alix dimerization implies a different interface than the one implicated in viral late domain binding, as both monomer and dimer states of Alix seem to interact with the viral peptide.

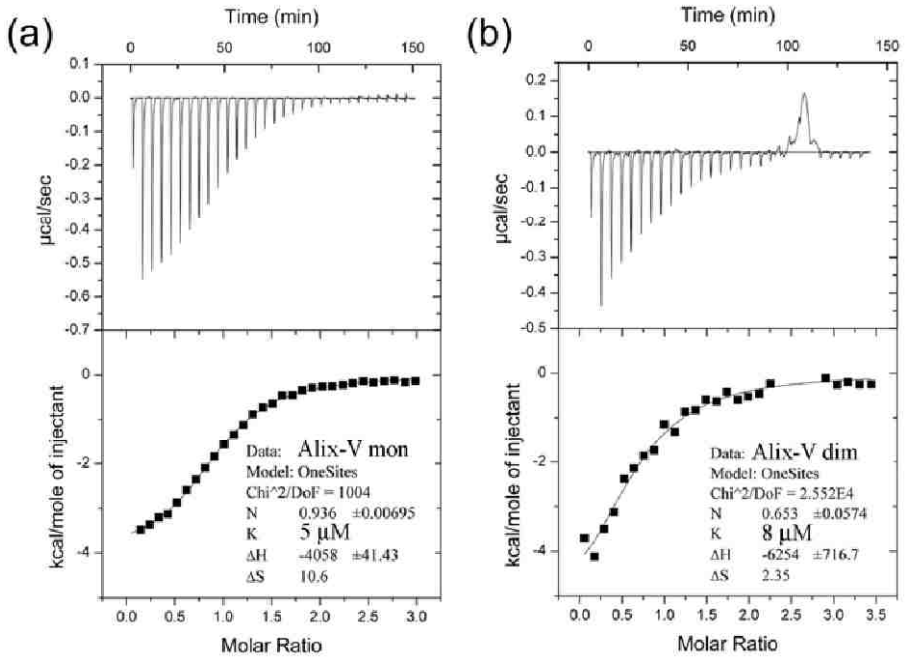

Figure 40. Isothermal titration calorimetry (ITC) binding curves for the interactions **(a)** Alix-V monomer-EIAV $p9^{Gag}$ and **(b)** Alix-V dimer/-EIAV $p9^{Gag}$.

Characterization of Alix-CHMP4B interaction

Alix binds a C-terminal region of CHMP4B

Alix-CHMP4B interaction was analyzed by co-purification assays. Full-length human CHMP4B (residues 1-225) purified as an MBP-fusion protein from a cell-lysate pool containing GST-fusion Alix-ΔPRD, revealed a new band corresponding to Alix (Figure 41a) thus indicating interaction between both proteins. Domains involved in the Alix-CHMP4B interaction were further mapped using CHMP4B deletion mutants designed for crystallization purposes on the basis of CHMP3 sequence alignment (Muziol, Pineda-Molina *et al.* 2006). Co-purification assays showed that an N-terminal deletion mutant, CHMP4B-ΔN (residues 9-225), preserves the ability to recruit Alix (Figure 41b); however a C-terminal deletion mutant, CHMP4B-ΔC (residues 1-194) is no longer able to interact with Alix (Figure 41d). This result indicates that the critical residues for Alix interaction are within the last 30 residues of CHMP4B. Moreover, using an N-terminal form of Alix (Alix-Bro1, residues 1-357) the co-purification profile suggested that CHMP4B interaction occurs mainly through the Bro1 domain of Alix, as confirmed by other works (Kim, Sitaraman *et al.* 2005; Fisher, Chung *et al.* 2007; Zhai, Fisher *et al.* 2008), since a clear Alix band is co-purified with CHMP4B-ΔN (Figure 41c). Overall the results point out an interaction between CHMP4B C-terminal and Alix N-terminal.

CHMP4B forms ring-like polymers *in vitro*

The full-length and C-terminal deletion mutant of CHMP4B were characterized by several methods, including size exclusion chromatography (Figure 43b,c), that revealed a concentration dependent aggregation of both CHMP4B forms. Typically, both forms are more stable in solution as MBP-fusions.

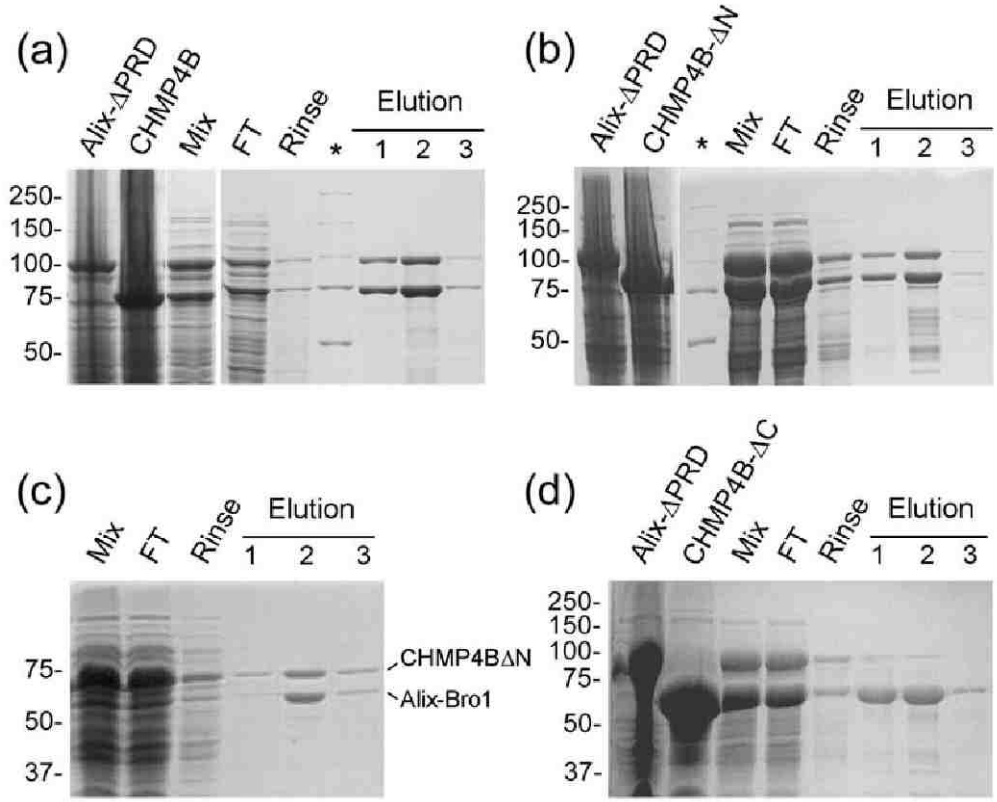

Figure 41. Co-purification of Alix with CHMP4B. Co-purification assays were performed on an amylose sepharose column using MBP-tagged CHMP4B (full-length or deletion mutants) as bait. Alix-ΔPRD is co-purified with **(a)** full-length CHMP4B (residues 1-225) and **(b)** CHMP4B-ΔN (residues 9-225). **(c)** Alix-Bro1 is also co-purified with CHMP4B-ΔN. **(d)** Alix-ΔPRD is poorly co-purified with CHMP4B-ΔC (residues 1-194), indicating the importance of CHMP4B's C-terminal end for Alix interaction. All Alix proteins used are GST-tagged.

Sucrose gradient centrifugation analysis performed to full-length CHMP4B and to CHMP4B-ΔC (Figure 42a) showed that a significant fraction of the purified proteins runs to the bottom of the gradient (~ 60% sucrose) thus corresponding to high molecular weight structures. Electron microscopy analysis showed CHMP4B-ΔC appeared to form ring-like structures with a diameter of about 50 nm (Figure 42c). Full-length CHMP4B polymers also presented ring-like arrangements, even though much less regular than CHMP4B-ΔC ones, which suggests a critical role for the C-terminal region in modulating

CHMP4B polymerization. Sucrose gradient centrifugation followed by electron microscopy analysis was also performed with full-length CHMP4B purified in the presence of Alix-ΔPRD. This showed Alix-ΔPRD running to the bottom of the sucrose gradient indicating its recruitment to CHMP4B polymers (Figure 42b). Electron microscopy images of Alix-CHMP4B ring-like polymers (Figure 42d) revealed extra electron dense structures; however the polymers were still quite irregular like the ones formed by CHMP4B alone.

In order to better characterize Alix-CHMP4B interaction and its potential implications in Alix dimerization, both monomeric and dimeric states of Alix-ΔPRD were analyzed in the presence and absence of CHMP4B. A native gel analysis revealed a minor band shift for Alix-ΔPRD monomer in the presence of CHMP4B (Figure 43a), suggesting the formation of a protein complex; on the other hand the Alix-ΔPRD dimer did no longer migrate into the gel in the presence of CHMP4B. The protein complexes were further analyzed by analytical size exclusion chromatography. Even though no evident Alix-CHMP4B complex peak was observed, the analysis showed that both monomeric and dimeric states of Alix are preserved in the presence of CHMP4B, since no monomer/dimer equilibrium was triggered by its presence. Neither Alix-ΔPRD monomer (Figure 43b) nor Alix-ΔPRD dimer (Figure 43c) seem to affect CHMP4B elution profile, but Alix-ΔPRD dimer elution peak was strongly reduced in the presence of CHMP4B (Figure 43c), a fact consistent with the native gel analysis where CHMP4B potentially promoted the formation of large Alix-ΔPRD structures that did not enter the gel.

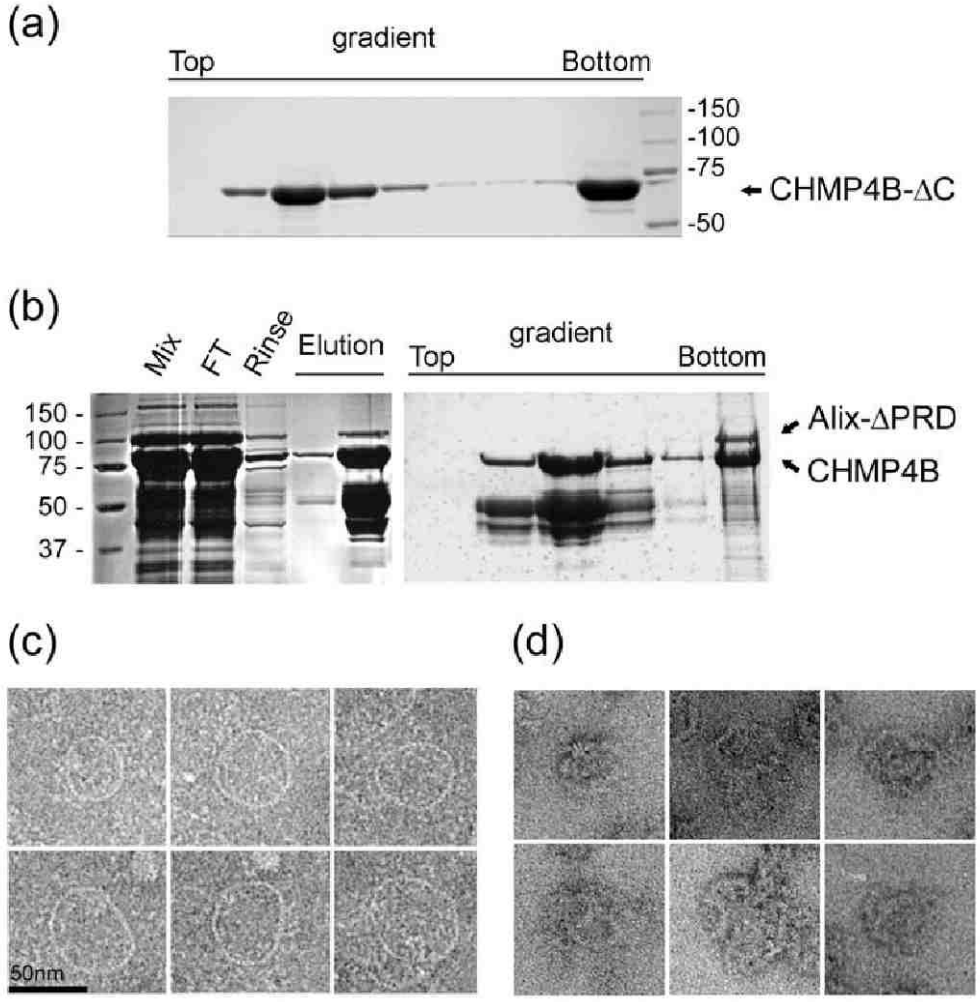

Figure 42. Purification and analysis of CHMP4B polymers. (a) Sucrose gradient analysis of purified MBP-tagged CHMP4B-ΔC (residues 1-194) **(b)** Co-purification and sucrose gradient analysis of full-length CHMP4B with Alix-ΔPRD **(c)** Cryo-electron microscopy images of ring-like polymers formed by CHMP4B-ΔC (bottom fraction in (a)). **(d)** Negative staining electron microscopy images of polymers formed by full-length CHMP4B and Alix-ΔPRD (bottom fraction in (b))

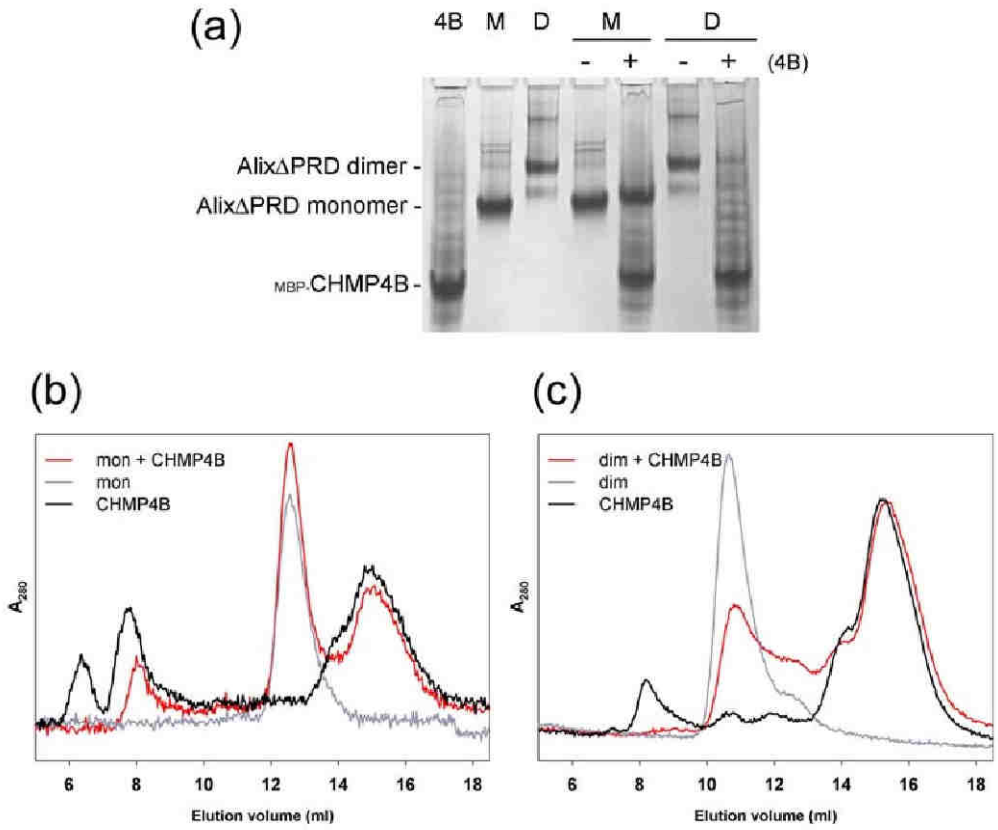

Figure 43. Analysis of Alix-CHMP4B complexes. (a) Native gel analysis of purified Alix-ΔPRD monomer (M), dimer (D) and MBP-tagged CHMP4B. **(b,c)** Analytical size exclusion chromatography performed to the single proteins and respective mixtures. 100μg of each protein were used per chromatographic run. Alix-CHMP4B mixtures were incubated for 1h at 4ºC prior to each experiment.

Localization of endogenous Alix in mammalian cells

In order to determine the cellular distribution of endogenous Alix and potentially localize dimeric Alix in cells, antiserum was produced in rabbits against dimeric Alix-V. The antiserum was affinity purified and tested for its specificity in pull down assays; these revealed that the antibodies were not specific for dimeric Alix-ΔPRD since both monomeric and dimeric form were efficiently copurified as shown in Figure 44. The Alix antiserum was then employed to localize endogenous Alix in Hela cells using confocal microscopy. Alix presented a homogeneous distribution throughout the cytoplasm showing specific punctuate staining on the periphery of the cells (Figure 45a). To determine whether this punctuate staining was consistent with endosomal markers, double labeling with anti-EEA1 antibodies (specific for early endosomes), anti-LBPA antibodies (specific for late endosomes) and anti-Rab11 antibodies (specific for recycling endosomes) was performed. No or very little co-localization was observed with the early endosomal marker EEA1 (Figure 45b) and the late endosomal marker LBPA (Figure 45c). In contrast substantial staining overlap was observed with the recycling endosomal marker Rab11, specific for recycling endosomes (Figure 45d). Double labeling was also performed using affinity purified IgGs against Alix and CHMP4B or CHMP3. Interestingly a “skeleton-like” distribution was observed for Alix and partial overlaps were found with CHMP4B and CHMP3 (Figure 45e,f).

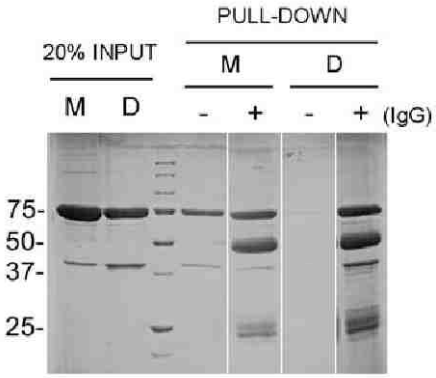

Figure 44. Specificity of the affinity purified Alix antibody. Monomeric (M) and dimeric (D) Alix-ΔPRD were incubated with Protein A sepharose beads saturated with affinity purified Alix antibodies. No relevant specificity was detected since both forms of Alix are equally binding to the antibodies (IgGs).

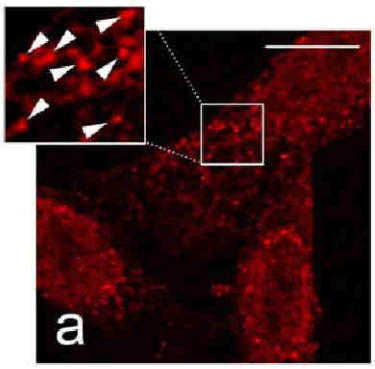

Figure 45. Localization of endogenous Alix in mammalian cells. (a) Alix is distributed thoughtout the cytoplasm of Hela cells and presents a punctated staining (white arrows) suggesting it co-localizes with membranar structures. **(b)** Early endosome marker (EAA1) shows no relevant overlap with Alix. **(c)** Similar observation was done using a late endosomal marker (LBPA) that also presented no obvious co-localization signal. **(d)** Recycling endosome marker, Rab11 shows a distribution pattern that correlates with Alix as shown by the overlap of the detected signals (white arrows). **(e)** CHMP4B and Alix reveal a skeletal-like distribution when detected with purified IgGs directly labeled with a fluorophore. **(f)** Same is observed for CHMP3. The scale bar represents 10μm. (*continues in the next page*)

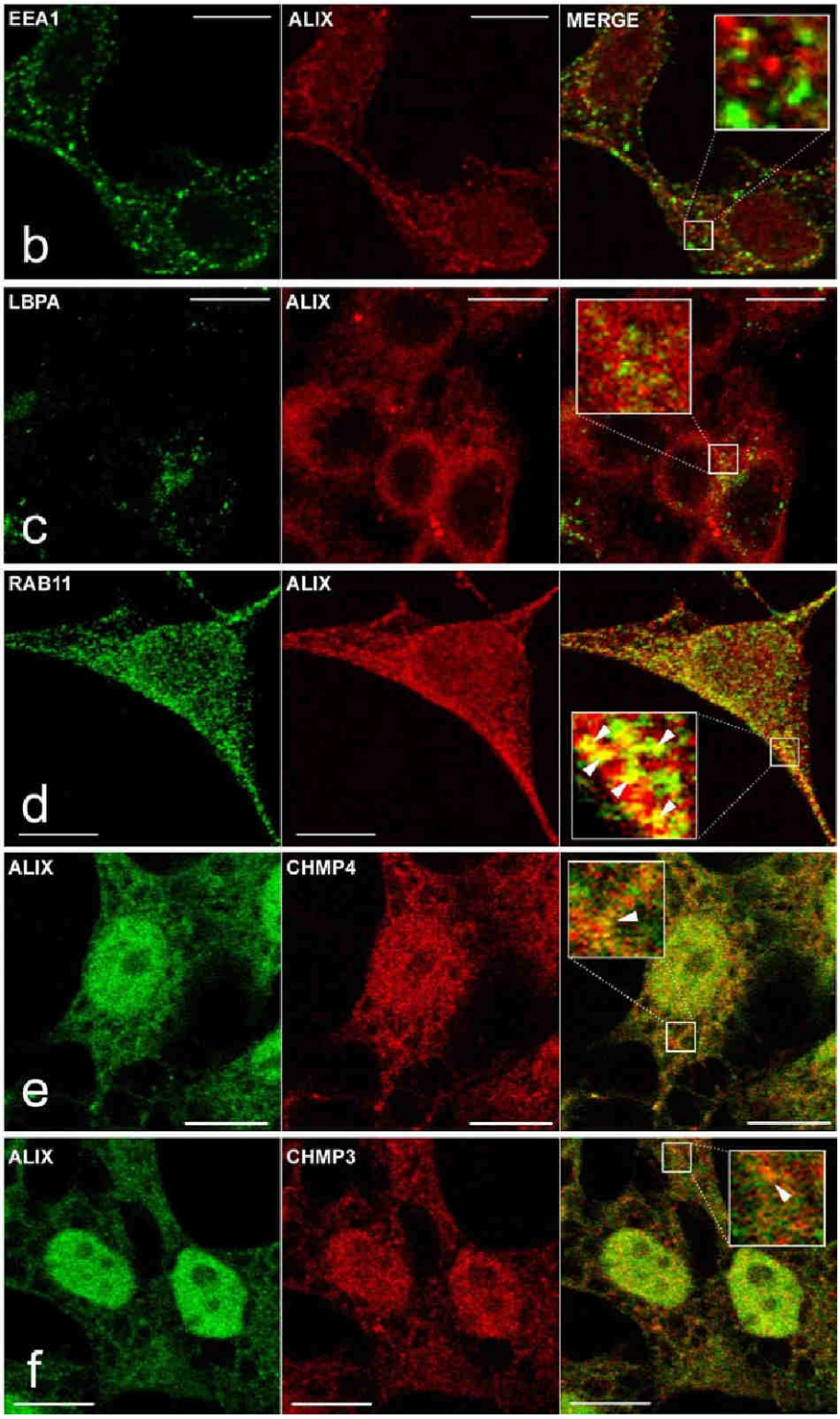
EEA1
ALIX
MERGE
b
LBPA
ALIX
c
RAB11
ALIX
d
ALIX
CHMP4
e
ALIX
CHMP3
f

Alix dimerization is involved in HIV-1 release

Previous studies showed that overexpression of the fusion protein RFP-Alix$_{\Delta BRO}$ in 293T cells expressing a full-length HIV-1 provirus (Accola, Strack *et al.* 2000), significantly inhibits HIV-1 virion production, as monitored by the release of particle-associate MA and CA into the medium (Figure 46). In order to analyze a potential involvement of Alix dimerization in viral budding, Mut1 and Mut2 versions of RFP-Alix$_{\Delta BRO}$ (see Alix-V mutants) were produced and the effects on HIV-1 release compared with the wild-type form. Cotransfection with Alix$_{\Delta BRO}$-Mut2 resulted in significant inhibition of HIV-1 virion production, similar to the one obtained with Alix$_{\Delta BRO}$ (Figure 46b). On the other hand, Alix$_{\Delta BRO}$-Mut1 efficiently rescued HIV-1 virion production, as monitored by the release of particle-associate CA into the medium (Figure 46a). Of note, neither of the mutants affected the overall levels of cell-associated Gag. In contrast, both seem to change the ratio of mature CA versus CAp2 processing intermediate, as well as to cause accumulation of p41 Gag processing intermediate, typical observations when late assembly steps are defective (Gottlinger, Dorfman *et al.* 1991; Garrus, von Schwedler *et al.* 2001). Interestingly, even though Alix$_{\Delta BRO}$-Mut1 rescues viral release, it seems that the maturation of CA is still compromised by the mutant overexpression. As described *in vitro* for recombinant Alix-V harboring the same mutations, both Mut1 and Mut2 target a putative dimerization interface, but only Mut1 impairs dimerization. Therefore, the present result is the first evidence that Alix dimerization is relevant *in vivo* and might play a critical role in HIV-1 release.

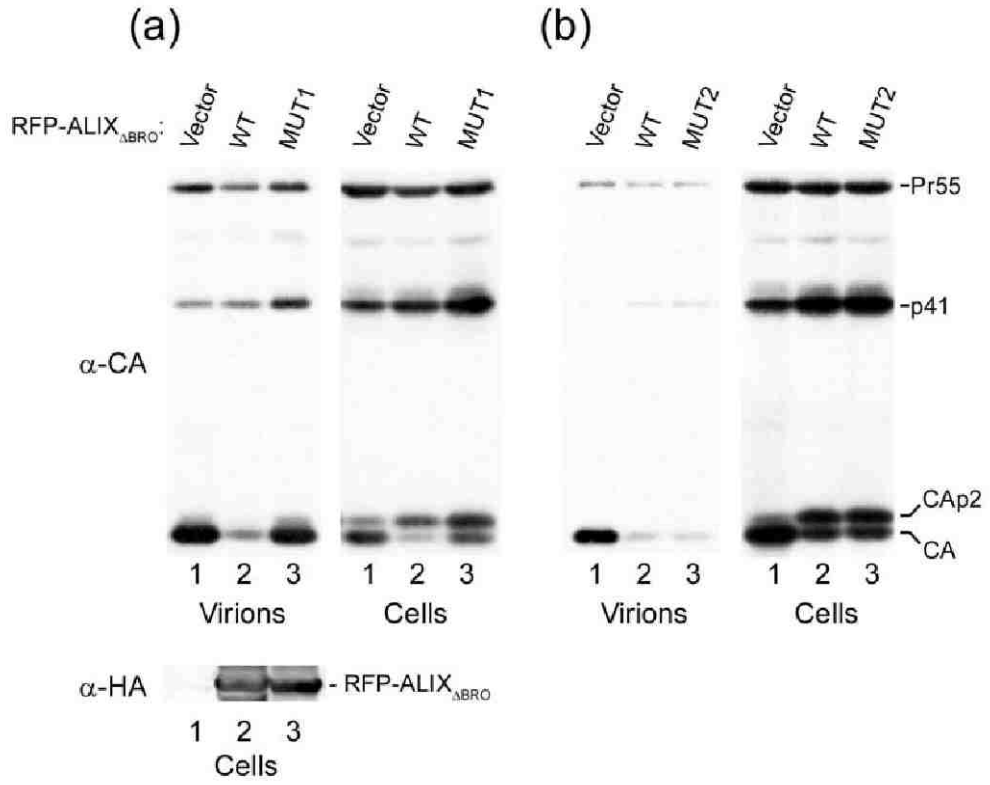

Figure 46. Alix dimerization mutant rescues HIV-1 release. Virion release assays performed with 293T cells, cotransfected with a proviral construct encoding full-length HIV-1 and the expression vector encoding the fusion protein RFP-Alix$_{\Delta BRO}$ (WT) that inhibits HIV-1 release. **(a)** RFP-Alix$_{\Delta BRO}$ Mut1 harbours a set of mutations that impair dimerization *in vitro*. Overexpression of this mutant *in vivo* rescues HIV-1 release (compare Virions' lane 2 and 3). **(b)** RFP-Alix$_{\Delta BRO}$ Mut2 still dimerizes *in vitro* and conserves the ability to inhibit HIV-1 production *in vivo*, like the WT RFP-Alix$_{\Delta BRO}$. Virion pellets and cells lysates are analyzed by Western blotting with anti-CA serum. Alix mutants revealed equivalent expression levels, as confirmed by Western blotting with anti-HA serum.

Chapter III

DISCUSSION

Cellular adaptor proteins are characterized by a versatile behavior engaging a large number of apparently unrelated cellular processes. Alix has been implicated in endocytic trafficking (Saksena, Sun *et al.* 2007), apoptosis (Vito, Pellegrini *et al.* 1999; Trioulier, Torch *et al.* 2004), cell-adhesion (Schmidt, Dikic *et al.* 2005), cell-surface receptors down-regulation (Schmidt, Hoeller *et al.* 2004), cytoskeleton reorganization (Cabezas, Bache *et al.* 2005; Pan, Wang *et al.* 2006) and retrovirus budding (von Schwedler, Stuchell *et al.* 2003), making it a clear example of an adaptor protein. The variety of functions engaged by Alix implies a tight regulation of its actions. The C-terminal proline-rich region (PRD) of Alix is a flexible tail harboring numerous protein-protein interacting motifs that appear to be important for function and regulation of Alix (Odorizzi 2006). Several observations indicate that the PRD folds back towards the Alix N-terminal Bro1-domain: i) Schmidt and coworkers showed that a cytoskeleton-associated tyrosine kinase that binds Alix Tyr319 (on its N-terminal Bro1 domain), phosphorylates tyrosine residues within the Alix C-terminal PRD region (Schmidt, Dikic *et al.* 2005); ii) the protein RabGAPLP was shown to bind *in vivo* to Alix lacking the PRD but not the full-length Alix, likely because the PRD partially masks the remaining domains (Ichioka, Horii *et al.* 2005); iii) Lazert and coworkers showed that the PRD has an active role in alleviating conformational constraints in HIV-1 p6 improving its binding to the V-domain of Alix (Lazert, Chazal *et al.* 2008). Together, these observations reflect the importance of PRD in the regulation of certain Alix functions. Unfortunately, besides its flexible behavior, recombinant expression of the PRD in bacterial systems leads to truncated protein products, a fact that has largely limited studies of its structural details. Thus much of the structural research on Alix has therefore focused on the other two domains.

Two recent reports provide structural details on both the Bro1-domain (Fisher, Chung *et al.* 2007) and the V-domain (Fisher, Chung *et al.* 2007; Lee, Joshi *et al.* 2007) from human ortholog. Similar to its yeast counterpart (Kim, Sitaraman *et al.* 2005), the

Bro1-domain of Alix has a banana-like shape containing a tetratricopeptide repeat (TPR) substructure and harbors a conserved hydrophobic surface that constitutes at least part of the CHMP4-binding site. The central domain of Alix adopts an unusual arrangement with two extended three-helix bundles forming a V-shaped structure. As a consequence, such intricate structure brings in close proximity Bro1 and PRD domains (which are at opposite ends of the sequence), a fact that is consistent with the PRD regulatory function discussed above. Importantly the V-shaped structure presents conformational flexibility, since the relative positions of the two arms were shown to vary in different crystal forms. Implications of this molecular hinge function for the V-domain are discussed later in the text. In addition, one of the arms harbors an hydrophobic pocket that has been shown to be crucial for binding YPX_nL type late domains and for the function of Alix in virus budding (Fisher, Chung *et al.* 2007; Lee, Joshi *et al.* 2007; Zhai, Fisher *et al.* 2008).

We used limited proteolysis to define Alix-Bro1 and Alix-V (residues 358-714) on mouse Alix-ΔPRD. For the Alix-Bro1 (residues 1-357), despite being essentially the same fragment as crystallized from the human ortholog ($Alix_{Bro}$, residues 1-359) (Fisher, Chung *et al.* 2007) we observed a tendency for aggregation. It is unlikely that this behavior comes from the fact that we worked with mouse Alix, since its sequence remains highly identical (94.2%) to the human one; on the other hand, it is neither related to the GST tag, as both cleaved an uncleaved forms seem to aggregate. Such behavior of Alix-Bro1 compromised several biophysical studies including crystallization.

The Alix-V crystallized (residues 360-702) (Fisher, Chung *et al.* 2007; Lee, Joshi *et al.* 2007) was 12 residues shorter at its C-terminal end than the mouse Alix-V (residues 358-714) used in our work. The extra residues most likely compromised the ability of the longer Alix-V to crystallize, as no crystal hits were ever obtained with the monomeric form of this construct.

Even though the defined mouse Alix-Bro1 and Alix-V appeared as poor crystallization targets, we successfully use them for mapping binding regions: Alix-Bro1 was mapped as the critical region for CHMP4B interaction and Alix-V was shown to contain the viral late domain binding site. As mentioned above, this has been confirmed by several works (Katoh, Shibata *et al.* 2003; Kim, Sitaraman *et al.* 2005; Fisher, Chung *et al.* 2007; Lee, Joshi *et al.* 2007) and the crystal structures obtained from the human ortholog have bee further used to map the specific residues involved in both CHMP4 and late domain binding by co-crystallization strategies (McCullough, Fisher *et al.* 2008; Zhai, Fisher *et al.* 2008).

We showed that recombinant Alix lacking the PRD region (Alix-ΔPRD) as well as Alix-V form dimers *in vitro* consistent with the report on Alix-V dimerization (Fisher, Chung *et al.* 2007; Munshi, Kim *et al.* 2007). Dimeric species produced *in vitro* by both recombinant forms revealed no equilibrium with their monomeric states as confirmed by size exclusion chromatography and SAXS analysis. Indeed, it seems that both monomers and dimers adopt stable conformations and behave like independent species. Noteworthy, the presence of the Bro1-domain in Alix-ΔPRD seems to compromise the dimerization ability, as showed by size exclusion chromatography where the relative amount of dimer produced by Alix-ΔPRD is significantly lower than the one obtained with Alix-V. Even though the recombinant Alix-Bro1 form used in this work showed a tendency to aggregate, no relevant double peak profile was observed on size exclusion chromatography and no such dimerization ability has ever been reported in previous structural studies on the Bro1-domain from yeast and human orthologs (Kim, Sitaraman *et al.* 2005; Fisher, Chung *et al.* 2007). Together these results indicate that the V-domain is the main region mediating *in vitro* Alix dimerization.

To date two other studies also report the production of dimeric species by recombinant expression of Alix-ΔPRD and Alix-V (Fisher, Chung *et al.* 2007; Munshi, Kim *et al.* 2007). However, none of them explores further this process and its potential functional implications. Therefore, we focused our research on the structural characterization of Alix dimers and went on to confirm the importance of Alix dimerization in a pre-established *in vivo* system and to deduce further implications of the process in a cellular context based on additional experimental results.

We used SAXS to explore the structural overall arrangement of the purified Alix-ΔPRD monomers and dimers and showed that two monomers seem to associate in a tail-to-tail fashion assembling a crescent-shaped dimer that spans 270 Å. As already mentioned both monomer and dimer are stable species and this implies the existence of a factor able to activate the monomers promoting dimerization into a novel locked conformation. The defined banana-shape of the dimer suggests a more intricate dimerization motif than a simple association of two monomers and supports the involvement of major conformational changes in the dimerization process. The structural organization of Alix-ΔPRD may contribute to the final conformation of the dimer. It has been suggested that the simple tripeptide segment that links Bro1- and V-domains most likely allows changes between their relative positions (Fisher, Chung *et al.* 2007). Our results show that the V-domain is the dimerization domain. Furthermore the structures published suggest that Alix-V consists of two flexible linked arms (Fisher, Chung *et al.* 2007), making it a potential region for conformational changes to occur promoting dimer formation and stabilization.

In order to characterize Alix dimers we used hydrogen/deuterium exchange combined with mass spectrometry (Zhang and Smith 1993) to map regions important for dimerization. The approach identified regions with different solvent accessibility when

comparing monomers and dimers of Alix-ΔPRD. The most striking result involved the loop connecting α20 and α21 of the V-domain (Fisher, Chung *et al.* 2007), in fact one of the three loops composing the hinge region between the two arms of this domain. The mapped loop becomes less accessible upon dimerization, strongly indicating that it belongs to the interface mediating this process. To confirm this hypothesis we have mutated several residues along this region in the recombinant Alix-V form and showed not only that V-domain dimerization is impaired but also that its conformation is drastically affected.

Comparison between size exclusion chromatography profiles of Alix-V wild-type and mutants revealed significant shifts of their equivalent elution peaks. The result indicated that both mutations were able to trigger and stabilize new V-domain conformations that might entail opening of the V-shaped structure. Supporting this hypothesis, SAXS analysis performed on Alix-V_{Mut1} confirmed a new extended conformation of the V-domain, where the two arms open up the V. The difference between the two mutants tested resides only in a tripeptide segment (638-KMK-640) additionally changed in Alix-V_{Mut1} and this resulted in an efficient blocking of the V-domain dimerization. From these results it is reasonable to assume that the crescent-shaped dimeric structure observed in solution may result from an antiparallel assembly of the two monomers through their opened V-domains (see dimerization model in Figure 47). Bioinformatic analyses using the MultiCoil program (Wolf, Kim *et al.* 1997) predict a high probability of both dimeric and trimeric coiled-coil for both α-14 (residues 442-470) and α-18 (residues 546-583). Even though these regions are already involved in trimeric coiled-coil structures (that form both arms of the V-domain) they may additionally contribute to such a dimeric arrangement. In addition the mutations (especially Mut1) seem to promote and stabilize the observed extended conformation. Curiously in the mammalian Alix structure the

K640 residue participates in a salt bridge interaction with E650 and N400 and this appears to be critical in stabilizing the closed conformation of the V-domain, as it brings together the two arms at the level of their hinge region. The specific role of these residues in the dimerization process will however need further studies at the atomic level resolution in order to be clarified.

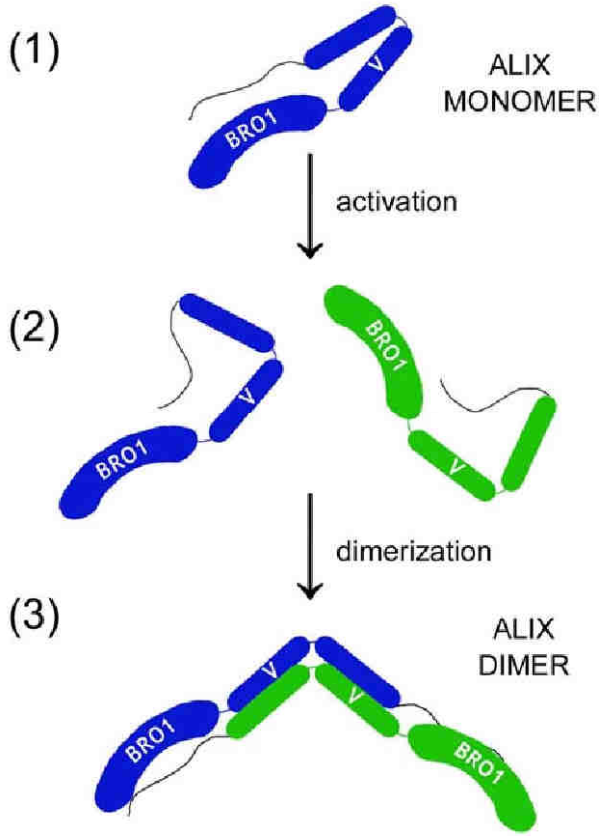

Figure 47. Model for Alix dimerization. Alix may hold a **(1)** monomeric metastable conformation that needs to be **(2)** activated potentially by interacting with different factors (e.g. proteins or lipids) that ultimately lead to **(3)** dimerization. This model is consistent with different observations reported in the present work: i) the V-domain is susceptible to major conformational changes and dimerizes on its own; ii) a putative dimerization interface sits on the hinge region between the two V-domain arms; iii) Alix-ΔPRD dimer folds into a crescent-shaped dimer in solution.

The crescent-shaped fold of the dimeric Alix-ΔPRD ressembles the one of membrane bending BAR and F-BAR domains (Peter, Kent *et al.* 2004; Weissenhorn 2005; Itoh and De Camilli 2006) (Figure 48), presenting though larger dimensions than the latter. The concave side of dimeric Alix-ΔPRD spans ~270 Å, compared to the average 130 Å of BAR domains. BAR domains are typically dimers formed by the antiparallel interaction of 2 three helical bundles, generating a stable elongated curved-shaped structure (Figure 48) somewhat similar to the models presented for dimeric Alix in Figure 47. The opening of the V-domain of an Alix monomer can generate stretches of three elongated α-helices that interact with the α-helices from another Alix monomer promoting a BAR-like fold in Alix dimers. Since BAR-domain containing proteins have largely been reported to sense, generate and/or stabilize membrane curvature (Habermann 2004; Peter, Kent *et al.* 2004; Dawson, Legg *et al.* 2006), we went on to explore potential membrane reorganizing properties of dimeric Alix.

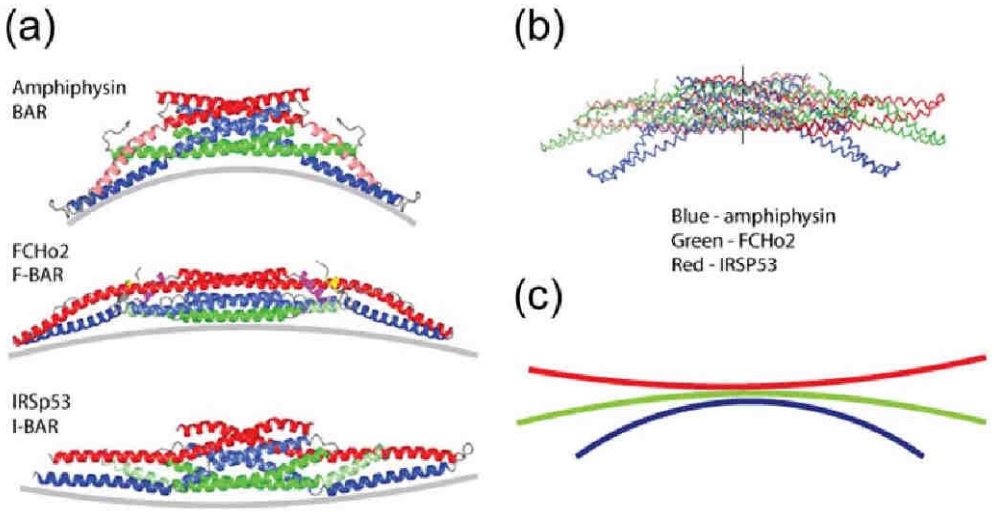

Figure 48. The BAR superfamily. (a) Structural similarities between the three subgroups within the BAR superfamily: BAR; F-BAR and I-BAR. **(b)** Superposition of the different structures reveals a similar central dimerization core attached to extended wings that provide different overall curvatures. **(c)** Different curvature binding preferences: highly positive (BAR, blue); moderately positive (F-BAR, green) and negative (I-BAR, red). *Adapted from (Henne, Kent et al. 2007)*.

The role of Alix in membrane biology is indirectly supported by the preferential localization of Alix at the plasma membrane and endosomes (Welsch, Habermann *et al.* 2006) and its role in regulating lysobisphosphatidic acid (LBPA)-induced membrane vesiculation (Matsuo, Chevallier *et al.* 2004). Moreover the yeast Bro1 has been suggested to bind membranes via a charged Bro1-domain patch (Kim, Sitaraman *et al.* 2005) though no further studies explored this hypothesis. Using liposome binding assays we showed that both monomeric and dimeric Alix-ΔPRD bound to synthetic membranes *in vitro*. The binding activity was equivalent for both Alix-ΔPRD conformations with a low efficiency, 15-20% of the Alix protein was generally found on membranes. We observed that dimeric Alix-V binds more efficiently to membranes than its monomeric state. Furthermore, dimerization of monomeric Alix-ΔPRD and monomeric Alix-V seems to be triggered upon membrane binding.

We analyzed Alix-containing proteoliposomes using electron microscopy. This revealed the ability of monomeric Alix-ΔPRD to deform round liposomes into tubular structures. Dimeric Alix-ΔPRD was however less efficient in producing such structures (fewer tubules were observed when compared with the monomer in equivalent conditions). One can speculate that the driving force for membrane deformation is the on-membrane dimerization process, meaning that preassembled dimers are no longer active to perform such task. This would however contrast with a BAR-like activity of Alix. Importantly, we observed that Bro1-domain has the ability to bind membranes on its own and thus it is possible that this domain mediates an initial step of membrane association that somehow triggers dimerization with subsequent membrane deformation.

Negative staining and cryo-EM analysis performed to AlixΔPRD-containing proteoliposomes revealed no clear protein coat as observed for BAR domain and F-BAR domain liposome interaction (Takei, Slepnev *et al.* 1999; Frost, Perera *et al.* 2008).

Although Alix labeling with a fluorescent marker or with nano-gold particles suggested that the protein seems to be present on the surface of tubular structures using fluorescence microscopy and negative staining EM respectively, no systematic pattern of protein distribution was observed. Thus the observed membrane deformation processes are difficult to interpret.

Liposome tubulation was observed in several independent experiments, but the dynamics of this process turned out to be difficult to control. In fact, increasing protein concentration on the membranes did not promote additional tubulation and rather caused liposome aggregation. Curiously, some of the tubulated structures were larger than the initial liposomes, indicating that fusion was promoted between proteoliposomes. This process is not uncommon in liposome binding assays and it has been observed in tubulated structures induced by BAR-domain containing proteins (Gallop, Jao *et al.* 2006). Thus fusion might allow Alix internalization and association with the inner surface of the liposomes. Dimeric Alix could therefore act like an inverted BAR-domain (Figure 48), present in proteins that induce and stabilize negative curvature (McMahon and Gallop 2005; Mattila, Pykalainen *et al.* 2007). In summary, the results suggest that Alix binds synthetic lipid membranes, but further studies are needed in order to validate Alix membrane remodeling activities. The ability of Alix to induce or stabilize membrane curvature could be of critical importance in processes of membrane vesiculation and budding in which Alix participates.

The V-domain of Alix binds the YPX_nL late domains of HIV $p6^{Gag}$ and EIAV $p9^{Gag}$ and this interaction is required for Alix-dependent viral budding (Martin-Serrano, Yarovoy *et al.* 2003; Strack, Calistri *et al.* 2003; Fisher, Chung *et al.* 2007; Lee, Joshi *et al.* 2007; Munshi, Kim *et al.* 2007). Full-length HIV $p6^{Gag}$ protein (52 residues) binds to Alix 60-fold less tightly than EIAV $p9^{Gag}$ protein (51 residues), however peptides spanning the HIV-1 (16-mer) and EIAV (15-mer) YPX_nL motifs bind Alix with similar affinities (Kd ~7 μM), as

shown by solution-phase isothermal titration calorimetry (Lee, Joshi *et al.* 2007; Munshi, Kim *et al.* 2007). This result suggests that the late-domain YPX$_n$L sequences indeed provide the primary recognition interface, but the binding affinity is tuned by context dependent effects. Recent co-crystal structures revealed the details of Alix-V late-domain interaction (Zhai, Fisher *et al.* 2008).

In order to elucidate potential effects of Alix dimerization in viral late domain binding, we carried out isothermal titration calorimetry (ITC) measurements to quantify the affinity of a 14-mer peptide harbouring the YPX$_n$L of EIAV p9^{Gag} to Alix-V monomer and Alix-V dimer. This revealed a binding affinity of ~5μM for the Alix-V monomer by fitting a one-site binding model, consistent with previously reported K_d of ~7 μM also obtained by ITC (Lee, Joshi *et al.* 2007; Munshi, Kim *et al.* 2007). Interestingly, no significant difference was observed for the binding affinity of the peptide to the Alix-V dimer, since a K_d of ~8 μM was also determined by fitting a one binding site model. Indeed, one would expect a 2:1 stoichiometry in the case of Alix-V dimer binding; one potential explanation is that the different conformational states of the Alix-V dimer in solution reflect structural fluctuations that compromise heat measurements. Such an unstable folding makes Alix-V dimer a difficult target to study by ITC. Nevertheless, in the context of the full-length Alix dimer this structural flexibility could determine an important modulation of Alix-YPX$_n$L interaction.

Our ITC results show that both Alix-V monomer and dimer bind the late-domain of EIAV p9^{Gag}. Thus the region mediating Alix dimerization is distinct from the one implicated in viral late domain binding, a hypothesis also supported by dimer interface mapping obtained by H/D MS. This implies that dimeric Alix is still functional to bind the viral late domain, even though, for the moment, it is not clear if one or two binding sites are available in the dimer. Interestingly a recent report by Zhou *et al.* (Zhou, Pan *et al.*

2008) shows that in HEK293 cell lysates, active $p6^{Gag}$/$p9^{Gag}$ docking sites are specifically available in Alix associated with the membrane fraction. In this context, it would be important to confirm that the p9-derived peptide binds to the elongated Alix-V Mut1.

We investigated the importance of Alix dimerization in HIV-1 release using an $Alix_{\Delta BRO}$ fusion (where the N-terminal Bro1-domain is replaced by RFP) previously shown to inhibit HIV-1 release in 293T cells (Strack, Calistri *et al.* 2003). Mutant versions of $Alix_{\Delta BRO}$ were produced based on Alix-V dimerization mutants (Mut1 and Mut2) tested *in vitro*. Mut2, that conserves the ability to dimerize *in vitro*, was able to inhibit HIV-1 virion release as efficiently as the wild-type $Alix_{\Delta BRO}$. In contrast, Mut1 that impairs dimerization *in vitro*, has no or little effect on HIV-1 virion production (H. Göttlinger and colleagues, unpublished data) as monitored by the release of particle-associated CA into the medium, thus suggesting that Alix dimerization plays an important role in HIV-1 budding.

Wild-type RFP-$Alix_{\Delta BRO}$ used in the present assay localized exclusively to a few large vesicular structures in the cytoplasm (Strack, Calistri *et al.* 2003). A parallel observation was reported by Chatellard-Causse *et al.* (Chatellard-Causse, Blot *et al.* 2002) that showed abnormal cytoplasmic vacuolization in HEK293 cells upon overexpression of an equivalent mouse Alix mutant lacking the Bro1-domain. One hypothesis for the inhibition of viral release when $Alix_{\Delta BRO}$ is over-expressed can be the abnormal recruitment of endogenous Alix to such cytoplasmic vacuoles. The critical mechanism mediating this recruitment might be hetero-dimerization of $Alix_{\Delta BRO}$ and endogenous full-length Alix, thus compromising the pool of native Alix, either by mislocalizing it (in cytoplasmic vacuoles) or by producing aberrant heterodimers that are no longer able to perform the function of native Alix homodimers. This hypothesis is strongly supported by our results showing that Mut1 rescues HIV-1 release because it is

no longer able to dimerize and therefore does not compromise the normal activity of endogenous Alix.

We went on to investigate the potential implications of dimeric Alix in viral release based on the current understanding of the process. Retroviral late assembly (L) domains represent central docking sites for host proteins that regulate and promote viral release. As we showed for EIAV, it seems that dimeric Alix conserves the ability to bind viral late domains. Recent studies reported however that Alix late-domain interaction only functions in viral release when its ability to recruit CHMP4 is intact (Fisher, Chung *et al.* 2007). CHMP4 is a subfamily of ESCRT-III proteins which appears to be the core of the apparatus that drives MVB vesicle formation in yeast (Babst, Katzmann *et al.* 2002). The recruitment of Alix by viruses containing YPX_nL late domains suggests that the Alix-CHMP4 interaction may control ESCRT-III assembly at viral budding sites.

Current understanding of how membrane deformation and fission is driven by ESCRT-III proteins (CHMPs) is still limited. Different studies have shown that CHMPs exist in an auto-inhibited state in the cytosol (Zamborlini, Usami *et al.* 2006; Lata, Roessle *et al.* 2008) and removal of autoinhibition leads to membrane targeting (Lin, Kimpler *et al.* 2005; Muziol, Pineda-Molina *et al.* 2006; Shim, Kimpler *et al.* 2007) and presumably to the formation of the ESCRT-III complex, a putative protein lattice assembled on membranes that directs the budding process (Saksena, Sun *et al.* 2007; Williams and Urbe 2007). The late recruitment of the AAA-type ATPase VPS4 is essential for the termination of this process by disassembly and recycling of the different ESCRT-III components (Babst, Wendland *et al.* 1998; Bishop and Woodman 2000; Saksena, Sun *et al.* 2007). Consistent with this scenario, over-expression of CHMP4 in mammalian cells produced regular filaments that self-associate in circular arrays on the membranes. Moreover co-expression of a catalytically inactive VPS4 drew these filaments into tight circular scaffolds that bend the plasma membrane away from the

cytoplasm, inducing outward buds (Hanson, Roth *et al.* 2008). Recent work in our lab brought new insights into the polymerization mode of CHMP proteins and unveiled a putative organization of the ESCRT-III complex (Lata, Schoehn *et al.* 2008).

In the present work we showed that Alix can be co-purified with full-length CHMP4B but not with its C-terminal truncated form, CHMP4B-ΔC, indicating that the last 30 residues of CHMP4B harbor an essential motif for interaction with Alix. This is indeed confirmed by the co-crystal structure (McCullough, Fisher *et al.* 2008) showing that CHMP4 uses a C-terminal amphipathic helix (motif M/L/I*xx*L*xx*W) to bind the conserved concave surface of Alix-Bro1 (Kim, Sitaraman *et al.* 2005; Fisher, Chung *et al.* 2007). Interestingly, sequence alignment of different CHMPs' subfamilies, it appears that different patterns of hydrophobic residues displayed on such amphipathic helices, provide a "code" to bind specific ESCRT-III partners (McCullough, Fisher *et al.* 2008). These interacting partners most likely modulate the activity of CHMPs namely by promoting the switch between activated (open) and inactivated (close) conformation (Lata, Roessle *et al.* 2008).

We showed that CHMP4B-ΔC formed ring-like polymers in solution with a diameter ~50 nm. Circular structures of CHMP4B-ΔC are consistent with the observed ability of CHMP4 to form circular arrays when over-expressed *in vivo* (Hanson, Roth *et al.* 2008). We also tested the ability of full-length CHMP4B to produce ring-like polymers; the presence of the C-terminal changed the polymerization behavior of CHMP4B and did not produce single ring structures. On the other hand, the Alix-ΔPRD fraction co-purified with CHMP4B was exclusively found associated with CHMP4B polymers, as confirmed by sucrose gradient centrifugation. In addition both analytical gel filtration and native gel analysis suggest that dimeric Alix is selectively recruited to higher molecular weight structures in the presence of CHMP4B. This was reflected by the reduction of the

soluble fraction of dimeric Alix in the presence of CHMP4B, contrasting with the soluble fraction of monomeric Alix, that remained constant in the same conditions.

Several observations along the present work can be integrated to support the hypothesis that dimeric Alix plays a critical scaffolding role, promoting and stabilizing ring structures composed of CHMP4: i) H/D MS analysis revealed that Alix dimers undergo a structural rearrangement along the concave surface of Bro1-domain (where CHMP4 binds) and this could determine a preferential binding of full-length CHMP4 to dimeric Alix; ii) viral release assays demonstrated that Alix dimers appear to be involved in HIV-1 viral budding, process that has been shown to be strictly dependent on the conserved Alix-CHMP4 interaction (Fisher, Chung *et al.* 2007); iii) the average inner diameter of CHMP4B-ΔC ring-like polymers (~50 nm) could accommodate 4 molecules of dimeric Alix on the inside (Figure 49a) and 8 on the outside and the dimer curvature is consistent with such narrow-diameter structures. Therefore, Alix dimers could serve as a scaffold at the inner surface of CHMP4-containing rings, or alternatively on the top of them (Figure 49b), by binding the C-terminal CHMP4 motifs. These might be exclusively available on the inside as shown for CHMP2A/CHMP3 tubes binding VPS4B (Lata, Schoehn *et al.* 2008). Even though quite speculative, the model fits the putative scaffolding properties of Alix, suggested by the liposome tubulation assays. To date we have been unable to demonstrate such organization *in vitro* with purified Alix-CHMP4B polymers, which tend to be irregular fiber-like rings like the ones obtained with CHMP4B alone.

Alix seems to participate in protein assemblies that promote membrane deformation (Hanson, Roth *et al.* 2008), but its scaffolding activities may not exclusively engage CHMP4 protein complexes. It has been recently shown that Alix, in addition to bind the late domain of HIV-1 Gag through its C-terminal V-domain, is also able to bind the nucleocapsid (NC) domain of HIV-1 Gag through its N-terminal Bro1-domain (Popov, Popova *et al.* 2008). Such multi-domain interactions suggest that during viral assembly

at the plasma membrane, Gag domains might also engage Alix in a similar way as proposed for CHMP4 tubes (Figure 49), in order to support their intrinsic membrane budding activities.

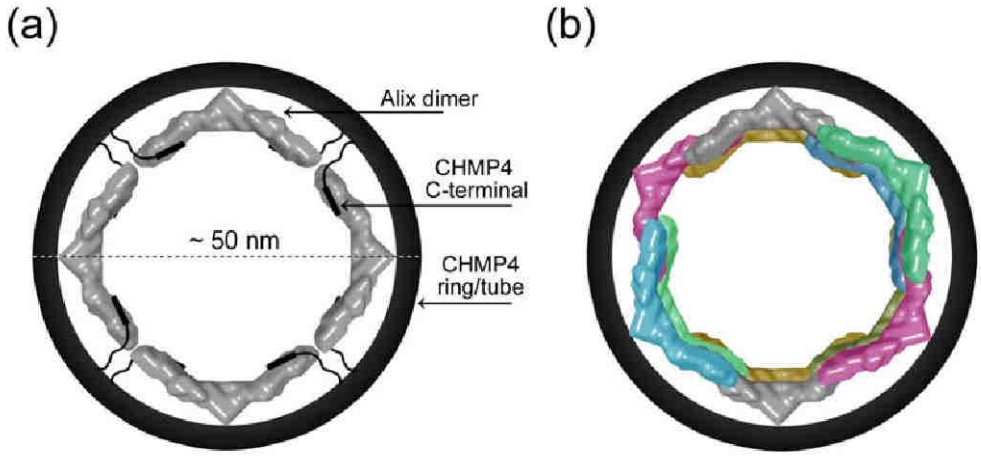

Figure 49. Models for the putative arrangement of Alix dimers inside and outside CHMP4 rings. **(a)** Alix dimers could stabilize CHMP4 rings/tubes by binding along their inner surface. This model assumes that the C-terminal tails of CHMP4 are available inside the ring/tube as shown for CHMP2/3 tubes (Lata, Schoehn *et al.* 2008). In Alix dimers, the concave surface of Bro1-domain most likely will face the concave surface of the dimer. Nevertheless, a slight rotation of Bro1-domain towards one of the sides will be sufficient to accommodate an interaction with the flexible C-terminal tail of CHMP4 that faces the convex surface of the dimer. Both curvature and dimentions observed *in vitro* for Alix dimer (spanning ~27 nm) and CHMP4-ΔC rings have a diameter ~50 nm) are consistent with this model. **(b)** Alix dimers might stabilize CHMP4 rings by forming a polymeric network.

Another role for Alix might be to couple cytoskeleton dynamics and membrane budding processes. In this context, Alix depletion has been shown to cause an accumulation of unusual actin structures containing clathrin and cortactin, a phenotype additionally characterized by a dramatic redistribution of early endosomes from peripheral to perinuclear location (Cabezas, Bache *et al.* 2005). In fact, Alix was shown to directly interact *in vitro* with filamentous actin (F-actin) using both its N-terminal Bro1-domain and the C-terminal PRD. Moreover, in WI38 cells, the N-terminal half of the Alix V-domain binds cortactin, while its C-terminal half binds α-actinin. These interactions are

critical for WI38 cells to maintain their typical fibroblast morphology and reveal a central role for Alix in cytoskeleton regulation (Pan, Wang *et al.* 2006). In fact, cortactin is an activator of the ARP2/3 complex-mediated initiation of actin polymerization (Goley and Welch 2006) and α-actinin is a key factor that bundles F-actin in stress fibers. Therefore, Alix might assist in membrane deformation processes, by acting as a scaffold that permits linkage to cytoskeleton during budding. Interestingly, the scaffolding protein IRSp53 (insulin receptor tyrosine substrate p53) is an actin regulator shown to assemble a novel actin-bundling domain, that is actually an inverted BAR-domain (Millard, Bompard *et al.* 2005; Mattila, Pykalainen *et al.* 2007).

The involvement of Alix in the degradative branch of the mammalian endocytic pathway, in a concerted action with the ESCRT machinery, is a hypothesis that has remained elusive. Indeed, only indirect observations and especially the fact that Alix physically interacts with both early (TSG101) and late components (CHMP4) of the ESCRT machinery have supported this putative role of the protein. A recent study however suggested that HD-PTP, another Bro-domain-containing protein, is responsible for endosomal sorting and MVB biogenesis in mammalian cells (Doyotte, Mironov *et al.* 2008). HD-PTP harbours similar domains as Alix, including the Bro- and V-domains as well as the PRD region. In addition it contains a C-terminal PTPase domain responsible for a phosphotyrosine phosphatase activity. The loss of HD-PTP dramatically affected the structural organization of endosomes and caused ubiquitinated proteins to accumulate on aberrant endosomes (Doyotte, Mironov *et al.* 2008). Curiously, it was observed that the Bro1-V domain constitutes the minimal functional unit within HD-PTP essential for these activities.

On the other hand, another study brought up new evidence for the involvement of the *C.elegans* Alix ortholog, ALX-1, in the recycling branch of the endocytic pathway (Shi, Pant *et al.* 2007). ALX-1 was shown to directly interact with RME-1 a key regulator

of receptor recycling from endosomes to the plasma membrane. RME-1 associated with the endosomes independently of ALX-1; however depletion of the latter led to phenotypic defects similar to those triggered by loss of RME-1. These defects were observed both in *C.elegans* and in mammalian cells indicating conservation of an Alix role in regulating RME-1 function.

In the present work we used an anti-Alix polyclonal antibody to analyze the distribution of endogenous Alix in Hela cells. This revealed a broad cytoplasmic distribution of Alix consistent with previous studies using overexpression of full-length mouse Alix in HEK293 cells (Chatellard-Causse, Blot *et al.* 2002). Notably, some punctuated staining across the cytoplasm and particularly concentrated on the periphery of the cells, suggested co-localization of Alix with vesicular structures. Co-localization assays performed with markers for three distinct endocytic compartments revealed litte co-localization of Alix with either EEA1 (early endosomes) or LBPA (late endosomes; MVBs) markers and good co-localization with Rab11-positive structures. Because the small-GTPase Rab11 is the most prominent recycling endosome marker (Maxfield and McGraw 2004; van Ijzendoorn 2006), our result is in agreement with the proposed role of Alix in the endocytic recycling in Hela cells (Shi, Pant *et al.* 2007). Moreover it is consistent with the observation that endogenous Alix is also enriched on tubular vesicular endosomal membranes (recycling endosomes) in other mammalian cells, including human T cells and macrophages (Welsch, Habermann *et al.* 2006).

Rab-family GTPases are conserved regulators of membrane trafficking (Zerial and McBride 2001) and their functions are tightly controlled by GAPs (GTP-hydrolysis-activating-proteins). Alix was shown to bind the GAP-like protein, RabGAPLP (Ichioka, Horii *et al.* 2005). This association turned out to be specific for Alix within the family of mammalian Bro-domain-containing proteins, as neither Brox nor HD-PTP were able to bind RabGAPLP (Ichioka, Kobayashi *et al.* 2008). Since RabGAPLP is identical to Rab5-

specific GAP (RabGAP5), that as been shown to participate in endocytic trafficking (Haas, Fuchs *et al.* 2005), this raised a new hypothesis for the involvement of Alix in regulating trafficking through endosomes by acting in concert with GAPs. A conservation of this putative function is indeed supported by the fact that *C.elegans* ALX-1 (ortholog of Alix) partially co-localizes with Rab5 structures (Shi, Pant *et al.* 2007).

Rab5 is specifically enriched in early endosomes (Zerial and McBride 2001) and the presence of Alix in such compartments is consistent with its regulatory role in EGFR internalization. Although Alix has been shown to prevent EGFR internalization (Schmidt, Hoeller *et al.* 2004), it is susceptible to accompain internalized vesicles while interacting with other effector or regulatory factors. Since we showed that Alix co-localizes with Rab11-positive structures (recycling endosomes, RE) in HeLa cells, it is reasonable to assume that membrane associated Alix could recycle back to the plasma membrane by incorporating endocytic recycling compartments. Alix could thus be a bifunctional Rab regulator and, as proposed for Rab5, play an important modulating role in the function of Rab11.

Studies of the activities of Rab11 and the proteins with which it interacts suggest that cells use REs for the delivery of membranes to regions of their surface that are subjected to dynamic reorganization (Maxfield and McGraw 2004; van Ijzendoorn 2006). The implications of Alix as a regulator of Rab11 hence of the endocytic recycling pathway, are consistent with the critical role of Alix in different cellular processes. In receptor downregulation, it may represent an advantage the fact that Alix can antagonize receptor degradation by promoting recycling of the internalized receptors back to the plasma membrane, instead of impairing receptor internalization (Schmidt, Hoeller *et al.* 2004). Such activity would be particularly important in signaling processes that depend on the presence of an active receptor at the plasma membrane and its misregulation could correlate with the developmental defects observed in Alix-depleted *Dictyostelium*

strains (Mattei, Ryves *et al.* 2005; Mattei, Klein *et al.* 2006). In the process of viral budding, it might be advantageous for enveloped virus to recruit the activity of recycling endosomes in order to maintain the total plasma membrane surface intact. In cytokinesis, the recruitment of RE seems to be essential for the abscission step since the latter involves the formation of internal membrane networks that help in the constriction of the midbody ultimately leading to membrane fission (Fielding, Schonteich *et al.* 2005; Gromley, Yeaman *et al.* 2005; Wilson, Fielding *et al.* 2005).

During cell cycle progression Rab11 remains associated with RE which is thought to provide a means for rapid redistribution of cell surface components following mitosis (Hobdy-Henderson, Hales *et al.* 2003). The delivery of recycling endosomes to the cleavage furrow is essential for completion of abscission. The family of Rab11-interacting proteins FIP3 and FIP4 serve to couple Rab11-positive vesicle traffic from recycling endosomes to the cleavage furrow/midbody (Wilson, Fielding *et al.* 2005). FIP3 and FIP4 are localized to midbodies during cytokinesis by the action of Arf6, which interacts with Exo70p, a component of the exocyst complex (a multiprotein complex containing Sec5, Sec6, Sec8, Sec10, Sec15 and Exo70 proteins, that is thought to recruit material to areas of membrane growth) (Fielding, Schonteich *et al.* 2005). In this complex membrane trafficking to the furrow during abscission, the dynamic of Rab11-FIP3/FIP4 interactions is thought to control the delivery, targeting and fusion of RE with furrow. One can speculate that Alix will play a role in some of these events by modulating or acting in concert with Rab11-effector complexes. Alix could for instance support actin remodelling during initial stages of furrow formation, since it seems to act in cytoskeleton remodelling activities as described before. Indeed this has been shown for the Rab11-effector protein Nuf in *Drosophila*, that is mutually required with Rab11 to promote vesicle mediated membrane delivery and actin organization at the invaginating furrow (Riggs, Rothwell *et al.* 2003; Riggs, Fasulo *et al.* 2007).

Exosomes are derived from the fusion of multivesicular bodies with the plasma membrane and extracellular release of the intraluminal vesicles. A systematic proteomic approach revealed that the majority of the proteins present in exosomes are related to endocytic compartments (Thery, Boussac *et al.* 2001). Alix, TSG101 and other components of the MVB machinery were particularly enriched in exosomal fractions, a fact that contrasts with the current hypothesis that Alix does not act at the level of MVB biogenesis (Doyotte, Mironov *et al.* 2008). On the other hand the same proteins were also found in virions (Pelchen-Matthews, Raposo *et al.* 2004), reinforcing their importance in promoting a common mechanism in the exosomal (MVB) pathway and viral budding. Of note, Rab11 was also enriched in the exosomal fraction supporting again the correlation of the recycling endocytic pathway with the activities of Alix in membrane vesiculation and fission events (Thery, Boussac *et al.* 2001). An interesting example concerning alternative exosomal sorting comes from reticulocytes, which loss their transferrin receptors (TfRs), during their maturation in erythrocytes, by secreting them via exosomes. Curiously in this process TfR sorting into exosomes has been proposed to occur without TfR ubiquitination (Geminard, De Gassart *et al.* 2004) but instead to involve a YTRF motif present on the TfR cytosolic domain that is thought to directly interact with Alix (since it interacts with its homolog PalA). This might link TfR to the ESCRT machinery to promote exosomal sorting, just like in the case of p9 Gag during EIAV budding, that is also sorted independently of ubiquitination (Patnaik, Chau *et al.* 2002).

.

Chapter IV

CONCLUSIONS AND PERSPECTIVES

Conclusions and Perspectives

From the results presented in this work one can conclude that:

- Alix is able to dimerize *in vitro* independently of the C-terminal PRD region. Its middle V-domain is sufficient to mediate such dimerization and the presence of the N-terminal Bro domain negatively influences this process. Isolated Alix monomers and dimers are stable species in solution and are not in equilibrium with each other.

- The dimerization interface of Alix comprises at least a loop belonging to the hinge region connecting the two arms that form the V-domain of Alix. Mutations along this loop impair the dimerization ability of the isolated V-domain (Alix-V) and in addition trigger a dramatic conformational change from an initial closed V-shaped conformation to an open extended one.

- The C-terminal truncated form of Alix lacking the PRD (Alix-ΔPRD) dimerizes *in vitro* into an elongated curved structure (revealed by SAXS) that resembles membrane bending BAR domains. This dimeric fold most likely results from an antiparallel association of two monomers through their opened V-domains. The stability of Alix monomers and dimers implies that an efficient trigger is required to promote dimerization in a physiological context.

- Dimeric Alix-V binds to a peptide derived from EIAV Gag p9 with similar affinity as the monomeric form (~ 7 μM). Thus the Alix dimeric arrangement conserves the ability to bind viral late domains.

- Overexpression of a mutant Alix-ΔBro that is no longer able to dimerize, abolished the dominant negative phenotype of the native Alix-ΔBro, characterized by a strong inhibition of HIV-1 virus-like particles release. This is the first evidence that Alix dimerization plays a relevant role *in vivo*, namely in viral release.

- Endogenous Alix co-localizes with Rab11-positive structures (recycling endosomes) in HeLa cells, suggesting a role for Alix in the recycling branch of the endocytic pathway. In contrast, poor or no co-localization was observed with early endosome (EEA1) and late endosome/MVB markers (LBPA).

- A C-terminal truncated form of CHMP4B lacking the last 30 residues (CHMP4B-ΔC), self-assembles *in vitro* in regular ring-like polymers with a diameter of ~50 nm. Full-length CHMP4B also forms polymers though less well-ordered than the ones obtained with the truncated form.

- Alix uses its N-terminal Bro1 domain to bind the C-terminal region of CHMP4B (last 30 residues). In sucrose gradient sedimentation assays Alix co-purifies with CHMP4B polymers. The Alix-CHMP4B cooperative function may implicate that dimeric Alix acts like a scaffold for CHMP4B ring-like structures.

Overall, the results gathered in the present Work reveal and characterize a novel conformation of Alix that seems to result from a structural rearrangement of the middle V domain of the protein. In addition to the previously described viral late-domain binding activity, the V domain presents a dynamic conformation that we propose to be correlated with its dimerization ability. *In vivo* Alix may hold a monomeric metastable conformation

that needs to be activated by interaction with other factors (e.g. proteins, lipids) in order to dimerize. Alix dimerization may represent a molecular mechanism for coordination of multiple processes via interaction with partners such as viral late domain containing proteins and other cellular factors that function on membranes to promote budding.

There is a fundamental interest on the atomic-resolution structural information of dimeric Alix and therefore we focused on two promising targets for crystallization and structure determination: dimeric Alix-V and monomeric Alix-V Mut1. Although the structure solution of dimeric Alix-V could ultimately reveal the arrangement of the minimal dimerization module of Alix, to date, we were unable to obtain dimeric Alix-V crystals diffracting better than 10 Å resolution. On the other hand, we were able to collect a full data set to 3 Å resolution on monomeric Alix-V Mut1 crystals, and structure determination is ongoing. Although not dimeric, Alix-V Mut1 represents a stable opened (extended) conformation of the V domain in solution and might bring new insights to support our dimer model where we propose that two opened V domains associate in an antiparallel fashion.

Alix dimerization is physiologically relevant. This has been shown in the process of HIV-1 release representing an important contribution for the clarification of Alix function in HIV-1 infection. Nevertheless, further studies will be needed to explore other *in vivo* implications of Alix dimerization and especially to identify the actual presence of endogenous Alix dimers in cells. This will probably be a hard task given the fact that Alix has inumerous interacting partners and complex formation with other proteins could mislead the conclusions.

Finally, two promising functional implications of Alix dimers have been approached in this work and will deserve further attention in order to by clarified. The first one concerns the resemblance of Alix dimers to BAR-like modules and respective membrane deformation and/or stabilization capability. The second relates to the close relationship

between Alix and CHMP4B ring-like polymers that underscores a potential cooperative action of these proteins in the processes of membrane fusion and fission.

This work brings important insights into the conformational flexibility of Alix and provides the framework for further functional analyses on the role of dimeric Alix in the cell machinery requested for distinct membrane vesiculation processes.

Conclusions et Perspectives

A partir de l'ensemble des résultats présentés, il peut être conclu que:

- La protéine Alix, dépourvue de sa région C-terminale PRD, est capable de dimériser *in vitro*. Son domaine central « en V » est suffisant pour permettre cette dimérisation. A l'inverse, la présence du domaine Bro N-terminal l'influence négativement. Les formes monomériques et dimériques isolées d'Alix forment des espèces stables en solution et ne sont pas en équilibre l'une avec l'autre.

- L'interface de dimérisation d'Alix se compose au minimum d'une boucle de la région charnière reliant les deux bras formant le domaine « en V ». Des mutations dans cette boucle affectent la capacité du domaine « en V » (Alix-V) isolé à dimériser et induisent un changement conformationnel drastique du domaine, passant ainsi d'une conformation fermée en forme de V à une conformation ouverte étendue.

- La forme d'Alix tronquée de son domaine C-terminal PRD (Alix-ΔPRD) dimérise *in vitro,* formant une structure allongée incurvée (observée en SAXS) identique à celle des domaines BAR impliqués dans les phénomènes d'incurvation de membrane. L'organisation dimérique résulte vraisemblablement de l'association antiparallèle de deux monomères par l'intermédiaire de leurs domaines « en V » dans la conformation ouverte. La stabilité des formes monomériques et dimériques implique un réarrangement important pour promouvoir la dimérisation dans un contexte physiologique.

- La forme dimérique d'Alix-V interagit avec un peptide provenant de la protéine EIAV Gag p9 avec une affinité comparable à celle de la forme monomérique (~ 7 μM). Ainsi, la forme dimérique d'Alix conserve sa capacité à interagir avec les domaines viraux tardifs.

- La surrexpression d'un mutant Alix-ΔBro incapable de dimériser, abolît le phénotype dominant négatif de la forme native, correspondant à une forte inhibition de la libération des particules virales de type HIV-1. Ces résultats montrent pour la première fois l'implication *in vivo* du processus de dimérisation d'Alix, notamment dans le relargage des particules virales.

- La forme endogène d'Alix a été co-localisée avec les structures Rab11-positive (endosomes de recyclage) dans des cellules HeLa, suggérant l'implication d'Alix dans le recyclage de la voie d'endocytose. A l'inverse, une faible, voir aucune, co-localisation n'ont été observées avec les marqueurs des endosomes précoces (EEA1) et des endosomes tardifs/MVB (LBPA).

- Le mutant de CHMP4B, tronqué en C-terminal des 30 derniers résidus (CHMP4B-ΔC), s'organise *in vitro* en anneaux réguliers de diamètre d'environ 50 nm. Les polymères obtenus à partir de la forme native de CHMP4B forment quant à eux des structures nettement non régulières.

- L'interaction entre la région C-terminale de CHMP4B (30 derniers résidus) et Alix se fait par l'intermédiaire du domaine Bro1 N-terminal de celle-ci. Des expériences de sédimentation en gradient de saccharose montrent qu'Alix peut être co-purifiée

avec les polymères de CHMP4B. Cette coopération semble indiquer un rôle de soutient des structures en anneau de CHMP4B joué par la forme dimérique d'Alix.

Plus généralement, les résultats obtenus au cours de cette thèse ont permis de mettre à jour et de caractériser une nouvelle conformation d'Alix qui semble provenir du réarrangement du domaine central « en V » de la protéine. En plus de son implication dans l'interaction avec les domaines viraux tardifs, le domaine « en V » possèderait une conformation dynamique que nous pensons, reliée à sa capacité à dimériser. *In vivo* Alix pourrait exister dans une conformation monomérique métastable nécessitant d'être activée par l'intermédiaire d'autres facteurs (protéines, lipides) afin de dimériser. De part son interaction avec différents partenaires (protéines contenant des domaines viraux tardifs et autres facteurs cellulaires impliqués dans le bourgeonnement de la membrane), le processus de dimérisation d'Alix pourrait alors représenter un mécanisme moléculaire important de la cellule.

L'importance fondamentale de l'obtention de données structurales à haute résolution de la forme dimérique d'Alix nous a poussée à nous focaliser sur deux cibles prometteuses lors d'essais de cristallisation : la forme dimérique Alix-V et son mutant monomérique Alix-V Mut1. Bien que la structure tridimensionnelle aurait pu permettre de répondre à la question de l'arrangement du module minimal de dimérisation d'Alix, nous n'avons pu obtenir que des cristaux de la forme dimérique Alix-V diffractant à 10 Å de résolution. Nous avons par contre réussi à collecter un jeu de données de diffraction à 3 Å de résolution à partir de cristaux de la forme monomérique Alix-V Mut1, la résolution de la structure étant encore en cours. Malgré le fait qu'elle ne soit pas dimérique, Alix-V Mut1 représente une conformation stable ouverte (étendue) du domaine « en V » en solution et pourrait soutenir notre modèle pour la forme dimérique dans lequel nous proposons que deux domaines « en V » ouverts soient associés de façon antiparallèle.

Le processus de dimérisation d'Alix apparaît comme physiologiquement pertinent. Cela a été démontré lors de la libération de HIV-I, constituant une contribution importante à la compréhension du rôle d'Alix lors de l'infection par HIV-I. Cependant, des études complémentaires seront nécessaires pour déterminer *in vivo* d'autres effets de la dimérisation d'Alix et notamment pour identifier la présence effective de dimères endogènes d'Alix dans les cellules. Cette tache sera vraisemblablement ardue du fait du nombre important de partenaires formant ainsi de nombreux complexes qui pourraient fausser les conclusions.

Enfin, au cours de cette thèse, deux implications fonctionnelles prometteuses de la forme dimérique d'Alix ont été observées et méritent de plus amples investigations. La première concerne la similarité des dimères d'Alix avec les modules de type BAR et son implication dans sa capacité à déformer ou à consolider les membranes. La seconde est à rattacher à la relation étroite qui lie Alix et les polymères de CHMP4B en anneau ainsi que l'action coopérative de ces deux partenaires dans le processus de fusion des membranes.

Ce travail apporte un éclairage important sur la flexibilité de la protéine Alix et fournit le cadre pour de futures analyses fonctionnelles visant à détailler le rôle de la forme dimérique d'Alix dans la machinerie cellulaire, notamment les processus de vésiculation de la membrane.

Chapter V

MATERIALS AND METHODS

Expression and purification of Alix-ΔPRD

Plasmids containing the DNA sequence encoding for *Mus musculus* (mouse) Alix protein (UniProtKB/Swiss-Prot Q9WU78) were provided by R. Sadoul (Chatellard-Causse, Blot *et al.* 2002): two clones were supplied in a pGEX-6P-2 plasmid (Amersham Biosciences), one encoding full-length mouse Alix (residues 1-869) and the other encoding a C-terminal truncated form Alix-ΔPRD (residues 1-714).

Escherichia coli BL21(DE3) competent cells (Invitrogen) were transformed with pGEX-6P-2/Alix-ΔPRD plasmid and incubated overnight at 37ºC in LB-Agar(Miller) plates containing Ampicillin (100μg/ml). A single colony was used to inoculate 5ml of LB-medium(Miller) containing Ampicillin to produce an overnight starter culture. 1L of the same medium was inoculated with the starter culture and cells were further grown at 37ºC and 250 rpm agitation. Expression of the fusion protein $_{GST}$Alix-ΔPRD was induced with 0.2mM of isopropyl-β-D-thiogalactopyranoside (IPTG) at OD_{600}= 0.6 for 4h in the same incubation conditions.

Cells were harvested by centrifugation at 7500g in a JLA-8100 rotor (Beckman) for 15min and each litre pellet ressuspended in 50ml of buffer A (50mM Tris-HCl pH 8.0; 80mM NaCl and 2mM β-mercaptoethanol). Cells were lysed by sonication (using 10 seconds bursts at 8A, Sonicator XL-202, Misonix Inc., on ice) in the presence of protease inhibitors (1 tablet of complete EDTA-free, Pierce). Lysates were cleared by centrifugation at 15000rpm in a JA-25.50 rotor (Beckman) and the supernatant loaded onto a Glutathione Sepharose 4 Fast Flow (Amersham Biosciences) pre-equilibrated in buffer A. The protein was purified according to the manufacturer's instructions with additional washing steps of 1M NaCl and 1M KCl in buffer A. Protein elution was monitored using Bradford solution (Biorad) and the eluted fraction adjusted to 1mM DTT and 1mM EDTA for GST-tag cleavage with PreScission Protease (1:200 w/w, overnight

at 4ºC) (EMBL, Protein Expression and Purification Facility). The cleaved sample was filtered (0.2 μm filter, Millipore) and loaded on a Q-sepharose Fast Flow (Amersham Biosciences) pre-equilibrated in buffer A for GST-tag removal. The flow-through containing untagged Alix-ΔPRD protein was concentrated in an Amicon Ultra-4 10K MWCO (Millipore) and further purified on an AKTA Purifier system (Amersham Biosciences) with a Superdex S-200 size exclusion column (Pharmacia) pre-equilibrated in buffer B (20mM Hepes pH 8.0; 100mM NaCl).

Cloning Alix-Bro1 and Alix-V

The DNA fragments encoding Alix-Bro1 (residues 1-357) and Alix-V (residues 358-714) were generated by standard PCR amplification using pGEX6P-2/Alix-ΔPRD plasmid as template and the following pairs of primers: Alix-Bro1 5'-CATGCCATGGCGTCGTTCATCTGGGTG-3'/ 5'-CGGGGTAACTTACTTCTCAAACAAATCCGT-3' Alix-V-5'-CATGCCATGGTCCCTGTGTCTGTGCAG-3'/ 5'-CGGGGTACCTTAACTGGCAATGCTCTGCTG-3'. The fragments were cloned into pETM30 expression vector (EMBL, Protein Expression Facility) using NcoI/Acc65I cloning sites, leading to N-terminal His_6-GST-tagged constructs. All sequences were confirmed by DNA sequencing.

Expression and purification of Alix-Bro1 and Alix-V

Expression of Alix-Bro1 and Alix-V proteins followed the same procedures described for Alix-ΔPRD. Final bacterial culture pellets were ressuspended in buffer C (50mM Tris-HCl pH 8.0; 100mM NaCl and 2mM β-mercaptoethanol) and cleared lysates were loaded onto a Nickel (Ni^{2+}) Chelating Sepharose Fast Flow column (Amersham Biosciences) pre-equilibrated in the same buffer. The protein was purified according to the manufacturer's instructions with additional washing steps of 1M NaCl and 1M KCl in buffer C. Protein elution was monitored using Bradford solution (Biorad) and the eluted

fraction adjusted to 1mM DTT and 1mM EDTA for His_6GST-tag cleavage with TEV protease (1:200 w/w, overnight at 4ºC) (EMBL, Protein Expression Facility). The cleaved sample was dialysed for 4h against 5L of buffer C for EDTA and Imidazol removal, using a dialysis membrane with a 12/14KDa MW cut-off (Spectra/Por 2). The sample was reloaded onto a Nickel (Ni^{2+}) Chelating Sepharose column and the flow-through containing untagged protein further purified on size exclusion column as described for Alix-ΔPRD. In the case of Alix-Bro1 the dialysis and second Nickel column steps were skipped as the His_6GST-tag appeared not to be cleaved off. For this reason, a pETM11 construct of Alix-Bro1 (encoding a His-tag fusion protein) was also generated for further characterization of the protein.

Mutagenesis of Alix-V

Two Alix mutants were generated by residue changes along the Alix middle segment 638-KMKQSNNE-645: mutant-1 (638-*EAA*QS*YKK*-645) and mutant-2 (638-KMKQS*YKK*-645). Alix mutant constructions for bacterial expression were obtained by PCR-based site-specific mutagenesis using pGEX-6P-2/Alix-V (coding for residues 355-714 of mouse Alix) as template for generating: Alix-V_{Mut1} with the primers 5'-CCAAGAATTCTCCGAGGCGGCGCAATCTTATAAAAAAGCTAACTTGAGAGAAGAAGTTCTGAAGAACC-3'/ 5'-GGTTCTTCAGAACTTCTTCTCTCAAGTTAGCTTTTTTATAAGATTGCGCCGCCTCGGAGAATTCTTGG-3', and Alix-V_{Mut2} with the primers 5'-CCAAGAATTCTCCAAAATGAAGCAATCTTATAAAAAAGCTAACTTGAGAGAAGAAGTTCTGAAGAACC-3'/ 5'-GGTTCTTCAGAACTTCTTCTCTCAAGTTAGCTTTTTTATAAGATTGCTTCATTTTGGAGAATTCTTGG-3'. All constructs were sequenced over the entire gene to confirm the mutations.

DNA fragments encoding Alix-V deletion mutants were generated by standard PCR methods using pGEX6P-2/Alix-ΔPRD as a template and the following pairs of primers: Alix-VΔ358-386, 5'-CATGCCATGGAAGCTACGACTTTGGCA-3'/ 5'-CGGGGTACCTTAACTG

GCAATGCTCTGCTG -3'; Alix-VΔ358-420, 5'-CATGCCATGGGTTCTACATCTGTAGTTGAA-3'/ 5'-CGGGGTACCTTAACTGGCAATGCTCTGCTG -3'; Alix-VΔ649-714 5'-CATGCCATGGTCCCTGTGTCTGTGCAG-3'/ 5'-CGGGGTACCTTACAAGTTAGCCTCGTT-3'. The fragments were cloned into pETM30 and pETM11 expression vectors (EMBL, Protein Expression Facility) using NcoI/Acc65I cloning sites, leading respectively to N-terminal His6-GST-tagged and His6-tagged constructs. All sequences were confirmed by DNA sequencing.

Expression and purification of Alix-V mutants

Alix-VΔ358-386 and Alix-VΔ358-420 were expressed as His_6GST-fusion proteins and Alix-VΔ649-714 was expressed as His_6-fusion protein. Purification followed the procedure described for native Alix-V (residues 358-714; described above) except that for mutant Alix-VΔ649-714, the intact fusion protein was used directly for size exclusion chromatography after the Nickel (Ni^{2+}) Chelating Sepharose purification. Alix-V_{Mut1} and Alix-V_{Mut2} were expressed as GST-fusion proteins and purified as described for Alix-ΔPRD. Different Alix-V versions were used as native control of the size exclusion chromatography profiles of the mutants. For deletion mutants the control was Alix-V - residues 358-714, encoded on a pETM30 construct and for the substitution mutants was Alix-V - residues 355-714, encoded on a pGEX-6P-2 construct.

Cloning CHMP4B deletions mutants

Bacterial expression constructs encoding full-length and truncated forms of human CHMP4B were cloned by standard PCR techniques into a pBADM41+ (EMBL, Protein Expression and Purification Facility) using NcoI/HindIII cloning sites. DNA fragments were generated using pMALc2x/CHMP4B as template (clone supplied by R.Sadoul; vector from New England BioLabs) and the following primers: CHMP-4B full-length (residues 1-225), 5'-CATGCCATGGGTTCGGTGTTCGGGAAG-3'/ 5'-CCCAAGCTTGCCTGCAGGTC

GACTTAC-3'; CHMP4B-ΔN (residues 9-225) 5'-CATGCCATGGGGGCTGGAGGGGGT-3'/ 5'-CCCAAGCTTGCCTGCAGGTCGACTTAC-3' CHMP4B-ΔC (residues 1-194), 5'-CATGCCATGGGTT CGGTGTTCGGGAAG-3'/ 5'-CCCAAGCTTAATTTGG TAGAGGGACTGTTTCGG-3'. All sequences were confirmed by DNA sequencing.

Expression and purification of CHMP4B forms

CHMP4B expression followed the same steps described for Alix-ΔPRD except that 0.2% arabinose was used for induction of protein production. Purification was performed on Amylose sepharose column (Amersham Biosciences) according to the manufacturer's instructions using buffer F (50mM Tris-HCl pH 8,0; 150mM NaCl and 2mM β-mercaptoethanol). Co-purifications of CHMP4B with Alix-ΔPRD and Alix-Bro1 were done by mixing cell pellets of 1L cultures from each one and following the same purification procedure as described for CHMP4B alone.

Oligomeric structures of CHMP4B in the presence or absence of Alix-ΔPRD were purified using sucrose step gradient centrifugation as described below in the liposome's section, except that the gradients were generated in buffer F and the protein samples loaded on the top of the gradient rather than the bottom.

Limited proteolysis

Alix-ΔPRD protein was purified as described above and used for limited proteolysis experiments. Protein concentration was determined by absorbance at 280 nm in a denaturating buffer (6M guanidium hydrochloride, 0.02M phosphate buffer pH 6.5) using the protein's theoretical extinction coefficient ($\varepsilon_{Alix\Delta PRD}$ =39910 $M^{-1}cm^{-1}$). Proteolysis was performed at room temperature (25ºC) in buffer B (20mM Hepes pH 8.0; 100mM NaCl) by incubation of 80μg of Alix-ΔPRD monomer with trypsin (Sigma) in 1:200 enzyme/protein (w/w) ratio. Sample aliquots (20μg) were taken at different reaction time

points: 1, 5, 15, 60 min and immediately boiled after the addition of SDS-loading buffer (final concentration: 50mM Tris-HCl pH 6.8, 2% sodiumdodecyl sulfate, 0.02% bromophenol blue, 1% β-mercaptoethanol 12.5mM EDTA and 10% glycerol). Proteolytic fragments were analyzed on a 12% SDS-PAGE (Maniatis, Fritsch *et al.* 1982) and bands detected with Coomassie Blue staining.

The proteolysis reaction was scaled-up (using trypsin 1:200 ratio for 60 min) to obtain major Alix-ΔPRD proteolytic fragments. A final step of purification performed on a Superdex S-75 size exclusion column (Pharmacia) pre-equilibrated in buffer B with 1mM of phenylmethylsulfonyl fluoride (PMSF) allowed fragments isolation. The samples were loaded on a 12% SDS-PAGE and transferred to a polyvinylidene difluoride (PVDF) membrane using a semi-dry blotting system. Selected Coomassie Blue stained bands (0.1% Coomassie Blue R-250, 40% methanol, 10% acetic acid) were cut from the PVDF membrane and sent for N-terminal sequencing analysis (Institut de Biologie Structurale, Laboratory of Molecular Enzymology).

Chemical cross-linking

Monomeric and oligomeric fractions of Alix-ΔPRD and Alix-V were equilibrated by size exclusion chromatography in buffer D (50mM Hepes pH 8.0, 100mM NaCl). Protein samples of 10-20 μg were cross-linked with 0, 0.1, 1 and 5mM ethyleneglycol bis(-succinimidylsuccinate) (EGS, Pierce) using a 50mM stock solution prepared in dimethyl sulfoxide (DMSO). The reactions were incubated for 20 minutes at room temperature and quenched with 50mM Tris-HCl (pH 8). Cross-linked material was analysed on 10% SDS-PAGE and bands detected with Coomassie Blue staining.

Size exclusion chromatography and multi-angle laser light scattering

Size exclusion chromatography was performed with a Shodex Protein KW-804 HPLC column (300mm x 8.0mm). The column was equilibrated in buffer E (20mM Tris-HCl pH 7.5, 150mM NaCl) and the runs were perform at 20°C with a flow rate of 0.8 ml/min. Stokes' radii were determined by calibrating the column with globular proteins of known Stokes' radius. On-line detection was performed by multi-angle laser light scattering (MALLS) using a DAWN-EOS detector (Wyatt Technology Corp., Santa Barbara, CA) equipped with a laser emitting at 690 nm and by refractive index measurement using a RI2000 detector (Schambeck SFD). Light scattering intensities were measured at different angles relative to the incident beam, and analysis of the data was performed with the ASTRA software (Wyatt Technology Corp., Santa Barbara, CA). The excess light scattering intensity at angle θ (R_θ) is related to molecular mass of solute particle according to Zimm's formalism of the Rayleigh–Debye–Gans model for a diluted polymer solution (Wyatt 1998). For small (gyration radius smaller than 100 nm), non-interacting particles R_θ is given by:

$$\frac{R_\theta}{K^* C} = M \qquad \text{(Equation 1)}$$

where R_θ is the measured excess Rayleigh ratio, C is the protein concentration (g/ml) as measured by on-line refractive index detector, M is the molar mass (g/mol), and K^* is an optical constant given by the following equation:

$$K^* = \frac{1}{N_A}\left(\frac{2\pi n_0}{\lambda^2}\right)^2\left(\frac{dn}{dC}\right)^2 \qquad \text{(Equation 2)}$$

where N_A is Avogadro's number, n_0 is the refractive index of the solvent at the incident radiation wavelength (1.33 for a diluted aqueous buffer), dn/dc (ml/g) is the specific refractive index increment of the solute (0.185 ml/g), and λ is the wavelength of the incident light in void (690 nm). Within the elution peak, the chromatogram is divided in

slices, and for each slice, MALLS and refractive index measurements are used to calculate the molecular weight. Weight-averaged (M_w) molecular weights are obtained from the molecular weight distribution across the elution peak.

Small angle X-ray scattering data collection and analysis

The synchrotron radiation X-ray scattering data were collected following standard procedures on the X33 SAXS camera (Koch and Bordas 1983; Roessle, Klaering *et al.* 2007) of the EMBL Hamburg located on a bending magnet (fan D) on the storage ring DORIS III of the Deutsches Elektronen Synchrotron (DESY). An image plate with online readout (MAR345, MarResearch, Norderstedt, Germany) was used at a sample - detector distance of 2.4 m covering the range of momentum transfer $0.1 < s < 4.5$ nm^{-1} ($s = 4\pi \sin(\theta)/\lambda$, where θ is the scattering angle and $\lambda = 0.15$ nm is the X-ray wavelength). The s-axis was calibrated by the scattering pattern of Silver-behenate salt (d-spacing 5.84 nm). The scattering patterns from Alix-ΔPRD in the monomeric and dimeric phase were measured at protein concentrations of 10.0, 7.4, 5.0 and 2 mg/ml and 2.9, 1.4 and 1.2 mg/ml, respectively. Alix-V monomer was measured at concentrations of 20.0, 14.25 and 4.25 mg/ml. Protein samples were prepared in 20 mM Hepes pH 8.0, 100 mM NaCl. Repetitive measurements of 180 sec at 15 °C of the same protein solution were performed in order to check for radiation damage. Stable intensities especially at low angles indicated that no protein aggregation took place during the exposure times. The data were normalized to the intensity of the incident beam; the scattering of the buffer was subtracted and the difference curves were scaled for concentration. All the data processing steps were performed using the program package PRIMUS (Konarev, Volkov *et al.* 2003). The forward scattering *I(0)* and the radius of gyration *Rg* were evaluated using the Guinier approximation (Guinier 1939) assuming that at very small angles ($s < 1.3/R_g$) the intensity is represented by $I(s) = I(0)$

exp(-(sR$_g$)^2/3). These parameters were also computed from the entire scattering patterns using the indirect transform package GNOM (Svergun, Semenyuk *et al.* 1988; Svergun 1992), which also provide the distance distribution function *p(r)* of the particle as defined:

$$p(r)=2\pi \int I(s)sr\sin(sr)ds \qquad \text{(Equation 3)}$$

The molecular mass of Alix-ΔPRD and Alix-V were calculated by comparison with the forward scattering from the reference solution of bovine serum albumin (BSA). From this procedure a relative calibration factor for the molecular mass (MM) can be calculated using the known molecular mass of BSA (66kDa) and the concentration of the reference solution.

Small-angle X-ray scattering data for Alix-V Mut1 were collected on the Beamline ID02 at the European Synchrotron Radiation Facility (ESRF), Grenoble, France (Narayanan, Diat *et al.* 2001). The data were collected with sample-to-detector distances of 1.0 and 5.0 m, covering the range of momentum transfer $0.06 < s < 4.7$ nm^{-1}. The sample at a protein concentration of 7 mg/mL was delivered through a 19mm wide capillary using a motorized syringe and maintained at 20°C. The exposure time was optimized to minimizing radiation damage and each sample was measured in 10 to 20 time frames of 0.2 or 0.4 s each.

Ab inito shape modeling of Alix-ΔPRD and Alix-V

Low-resolution models of Alix-ΔPRD and Alix-V were built by the program DAMMIN (Svergun 1999), which represents the protein as an assembly of dummy atoms inside a search volume defined by a sphere of the diameter D_{max}. Starting from a random model, DAMMIN employs simulated annealing to build a scattering equivalent model fitting the experimental data $I_{exp}(s)$ to minimize discrepancy:

$$\chi^2 = \frac{1}{N-1}\sum_j \left[\frac{I_{\exp}(s_j) - cI_{calc}(s_j)}{\sigma(s_j)}\right]^2 \qquad \text{(Equation 4)}$$

where N is the number of experimental points, c a scaling factor and $I_{calc}(s_j)$ and $\sigma(s_j)$ are the calculated intensity and the experimental error at the momentum transfer s_j, respectively. Ten independent DAMMIN bead models for Alix-ΔPRD in the monomeric and dimeric phase and for Alix-V were calculated. Final models of these proteins were obtained by superposition of the ten independent shape reconstructions for each protein by using the program packages DAMAVER (Volkov and Svergun 2003) and SUBCOMP (Kozin and Svergun 2001). For Alix-ΔPRD in the dimeric conformation *ab initio* shape models were calculated either without symmetry constrains or assuming a 2-fold symmetry axis. For the symmetric models, ten DAMMIN models were obtained, superimposed and averaged as explained before. The overall envelope, especially the crescent-shape of the Alix-ΔPRD dimer was the same for both unconstrained and constrained models. Molecular envelops were generated using Situs Program Package (Wriggers, Ronald A. Milligan *et al.* 1999) and all figures of structures and molecular envelops were generated in PyMol (DeLano 2002).

Hydrogen/deuterium (H/D) exchange mass spectrometry (MS)

Monomers and dimers of Alix-ΔPRD protein were purified as described in above and stored at 4ºC in buffer B (20mM Hepes pH8.0 and 100mM NaCl) until use. Deuterium labeling of intact proteins was carried out by 20- or 80-fold dilution of the protein samples in deuterated buffer (5mM Hepes, 100mM NaCl in D_2O, pD 7.6) followed by incubation at ice-bath temperature for different time intervals (from 10 sec to 30 min). The solution was then quenched by lowering the pD to 2.1 with cold 0.1 M HCl. Pepsin digestion was performed at ice-bath temperature and pH 2.5 for 2 min using an enzyme stock solution at 1.7mg/ml pepsin (Sigma-Aldrich) in 0.1M HCl. Native

monomers/dimers and deuterated monomers/dimers were digested separately with a protein:protease ratio of 1:1 (w/w). The native sample digestion was used for peptide mapping and deuterated samples for local kinetics of H/D exchange. Peptides obtained by protease digestions were loaded on a peptide MacroTrap column (Michrom Bioresources) and desalted using mobile phase A (0.03% (v/v) trifluoroacetic acid in water) for 1 min at 300 µl/min. Peptide separation was performed on a reverse phase C18 column (1mm x 100mm, IDxL; Interchrom) pre-equilibrated at 15% (v/v) CH_3CN-0.03% (v/v) trifluoroacetic acid in water) with a linear gradient in mobile phase B (15-40%B in 45min for LC-MS and in 80 min for LC-MS/MS experiments; flow rate 50 µl/min). All experiments were carried out with valves, trap cartridge and column cooled to ice-bath temperature to minimize deuterium back-exchange during separation. Global kinetics of H/D exchange on the whole protein and local kinetics of H/D exchange on peptide fragments were analysed on a 6210 TOF LC-MS system (Agilent Technologies). Peptide mapping (MS/MS) were performed on an ion trap mass spectrometer (Esquire 3000+, Bruker Daltonics) connected to a two-pump HPLC system (Shimadzu). The data was processed using DataAnalysis 3.2 (Bruker Daltonics) and Analyst QS 1.1 (Applied Biosystems) softwares.

Isothermal titration calorimetry (ITC)

Analysis of the Alix-V/EIAV late domain interaction was investigated by ITC (Wiseman, Williston *et al.* 1989) using a VP-ITC (MicroCal Inc., USA). The peptide TQNLYPDLSEIKK, corresponding to the minimal Alix binding site in EIAV $p9^{Gag}$ late domain (Strack et al 2003), was purchased from Peptide Specialty Laboratories GmbH (Germany). Monomeric and dimeric Alix-V purified samples were extensively dialyzed against buffer B (20mM Hepes pH 8.0, 100mM NaCl) and the synthetic peptide was ressuspended in 0.1M ammonium bicarbonate, re-lyophilized overnight in a speed-

vacuum system for removal of residual trifluoroacetic acid (TFA) and finally solubilized in the buffer D. Protein and peptide concentrations were determined by measuring the OD_{280}. The sample solutions were degassed by vacuum aspiration for 5min prior to loading. Calorimetric assays were performed at 25°C with a stirring speed of 286rpm and consisted in 30 injections of 9 μl of peptide every 300 sec. into the reaction cell containing the protein solution (cell volume: 1.4569 ml). The following concentrations were used for the different experiments: 600μM of peptide in the syringe injected into 40μM Alix-V monomer solution and 500μM of peptide into 30μM Alix-V dimer solution. Titration curves were fitted to the data using the Origin 5.0 package supplied with the instrument.

Liposome preparation

Liposomes were prepared using a blend of synthetic lipid (DOPE:DOPS:DOPC; 5:3:2, w/w) purchased from Avanti Polar Lipids, Inc. in chloroform. A dried lipid film was prepared in a 50ml volumetric flask by evaporation of 5μg of lipids in chloroform using a rotating evaporator and a room temperature water bath. The lipid film was re-suspended in 2ml of buffer D (50mM Hepes pH 8.0, 100mM NaCl) at a final lipid concentration of 2.5mg/ml and the suspension was extruded through a polycarbonate filter with a pore size of 0.4μm using a hand extruder (Avanti Polar Lipids, Inc). The polydispersity of the extruded suspension was analyzed by dynamic light scattering (DLS) using a Zetasizer Nano S (ZEN1600 – Malvern Instruments). The extruded sample was stored at 4°C with sodium azide (0.02%) and used within 4-5 days after preparation.

For the curvature dependence binding assays, liposomes prepared with the same lipid blend composition as described above were extruded using polycarbonate filters with different pore sizes (0.05, 0.1, 0.2, 0.4 and 0.8μm) generating liposomes of different diameters as confirmed by DLS analysis.

Liposome binding, floatation and co-sedimentation experiments

Different amounts of Alix-ΔPRD monomer and dimer (0.06nmol, 0.12nmol and 0.24nmol) were incubated with 50μl of liposomes in a final volume of 65μl at 37°C for 1h. After incubation, sucrose gradients were generated in buffer D, first by adjusting the incubated preparation to 40% sucrose (by 1:1 dilution using 80% sucrose) and subsequently by overlaying sucrose solutions of 20%, 15%, 7% and 3%. Centrifugation was performed in a Beckman SW55 rotor at 40000 r.p.m. for 4-6h at 4°C. Fractions of 100μl were recovered from the gradient, concentrated in a heat block and analyzed by 12% SDS-PAGE and bands detected with Coomassie Blue staining.

Alix-V monomer and dimer binding to liposomes was also analyzed by sucrose gradient centrifugation as described above, using 1.25 nmol and 0.625 nmol of protein respectively; 0.25 nmol of Alix-Bro1 were used in this assay.

Co-sedimentation assays were performed with Alix-V monomers and dimers using 1.25 nmol and 0.625 nmol of protein. After incubation with 50μl of liposomes in a final volume of 60μl, for 30min at room temperature, samples were pelleted by centrifugation in a Beckman Airfuge (20 min, 30 psi). The supernatant was thoroughly removed, the sedimented liposomes resuspended in 60μl of buffer D and aliquots of both supernatant and pellet were analysed by 12% SDS-PAGE and bands detected with Coomassie Blue staining.

Characterization of Alix associated with liposomes

The upper fractions 2 of monomeric Alix-ΔPRD and monomeric Alix-V sucrose gradients were solubilized by adding Triton X100 to a final concentration of 1%. After removal of aggregates by centrifugation (Beckman Airfuge; 20 min, 30 psi) chemical cross-linking was performed with EGS to determine the oligomeric state of Alix-ΔPRD

and Alix-V. Cross-linked samples were separated on SDS-PAGE, blotted in a nitrocellulose membrane and bands were analyzed using a rabbit anti-Alix antibody. Of note, a different Alix-V construct with the N-terminal end extended by three residues (starting residue 355 instead of 358) was used for this experiment. Liposomes incubated with Alix-ΔPRD were pelleted by centrifugation in a Beckman Airfuge (20 min, 30 psi), the supernatant was thoroughly removed and the sedimented liposomes resuspended in buffer D (final volume as during incubation) or further solubilized in the same buffer containing 1M sodium chloride or 1% Triton X100 and subjected to a second centrifugation step. Aliquots of both supernatant and pellet were analysed by 12% SDS-PAGE and bands detected with Coomassie Blue staining. In order to test whether Alix-ΔPRD is on the outside or the inside of the liposomes, samples containing Alix-ΔPRD recovered from the sucrose gradient were treated with trypsin (1:200) for 20min at room temperature, either after solubilization in 1% Triton X100 or untreated with detergent and analyzed by SDS-PAGE.

Electron microscopy

Liposomes containing Alix were either purified by sucrose gradient centrifugation or directly pelleted by centrifugation. Samples were analyzed by electron microscopy using either negative staining with uranyl acetate or cryo-electron microscopy as described (Dubochet, Adrian *et al.* 1988). Briefly, quantifoil R2/1 grids (Quantifoil Micro Tools GmbH, Germany) were loaded with 4 µl of sample at 0.5-1.0 mg/ml, blotted and rapidly frozen in liquid ethane within a liquid nitrogen bath using a Zeiss cryo-plunger. Grids were imaged on Kodak SO163 films with low dose techniques using an FEI CM200 microscope equipped with a Gatan 626 cryoholder operated at 200 kV and 38,000x nominal magnification. Negatives were developed in full strength D19 for 12 minutes,

and digitized at a 14 µm sampling step on a Z/I Imaging PhotoScan (previously the Zeiss SCAI).

Microscopy of fluorescence labeled Alix-ΔPRD and liposomes

Liposomes were prepared with the same composition plus rhodamine labeled 1,2-dihexadecanoyl-*/sn/*-glycero-3-phosphoethanolamine triethylammonium salt (rhodamine DHPE; Molecular Probes). Alix-ΔPRD was labeled with 5-Iodoacetamidofluorescein (5-IAF) (PIERCE). 70 µg Alix-ΔPRD were incubated with a 10-fold molar excess of 5-IAF for 2 hours at room temperature and the reaction was quenched with 5mM β-mercaptoethanol. Labeled Alix-ΔPRD was incubated with labeled liposomes and purified over a sucrose gradient as described above. Proteoliposomes were analyzed using an Axio Imager Z1 fluorescence microscope (Zeiss, Germany) and a 100x Plan-APOCHROMAT oil immersion objective magnification.

Saturation of liposomes surface

The theoretical amount of protein needed to saturate the total lipid surface exposed to the solvent in a standard liposome binding experiment was calculated based on the following parameters: surface area per lipid molecule, 0.6nm^2; average molecular weight of a lipid molecule, 750 Da. In a standard experiment 50µl of extruded liposomes at a final concentration of 2,5mg/ml are used; this corresponds to an amount of 160 nmol of lipids or 80 nmol of per leaflet. Considering the dimensions of the molecular envelop obtained for the Alix-ΔPRD dimer in solution, 270Å x 100Å x 45Å, a theoretical surface area of 122nm^2 has been estimated for the concave side of the molecule. The result is a protein:lipid ratio of 1:200 with one molecule of Alix-ΔPRD dimer potentially covering approximately 200 lipid molecules. Finally a theoretical amount of 0.4 nmol of Alix-ΔPRD dimer or 0.8 nmol of monomer is needed to cover an exposed lipid surface generated by

80 nmol of lipids. Protein-liposome incubations for testing surface saturation effects were performed with the following amounts: 0.225 nmol (36μg, 56%), 0.5 nmol (80μg, 125%) and 1.2 nmol (200μg, 330%) of Alix-ΔPRD dimer and 0.45 nmol (36μg, 56%), 1 nmol (80μg, 125%) and 2.4 nmol (200μg, 330%) of Alix-ΔPRD monomer.

Nanogold-labeling of Alix-ΔPRD

Alix-ΔPRD (residues 1-714) was subcloned into a pETM11 expression vector (EMBL, Protein Expression Facility) using NcoI/XhoI cloning sites, leading to a N-terminal His_6-tagged construct. The protein was expressed and purified as described above for Alix-Bro1 and Alix-V, except that the size exclusion chromatography was done immediately after the Nickel (Ni^{2+}) Chelating Sepharose column without a tag cleavage step. Purified Alix-ΔPRD monomer (1.25nmol) was incubated with 4-fold molar excess of nickel-nitrilotriacetic acid (Ni2+-NTA) Nanogold (Nanoprobes Inc.) for 2h at 4ºC. The excess of labelling reagent was removed by size exclusion chromatography using a Superdex S-200 (Pharmacia) column pre-equilibrated in buffer B (20mM Hepes pH 8.0; 100mM NaCl). Labeled protein (0.125nmol) was incubated with liposomes (50μl at 2.5mg/ml) with the same composition as described above for 1h at 37ºC and finally proteoliposomes were purified by sucrose gradient. Samples were analyzed by electron microscopy using negative staining.

Cloning and purification of Alix-ΔPRD and Alix-V new constructs used for crystallization

Alix-V clone (residues 355-714) was generated by amplification of the initial pGEX6P-2/Alix-ΔPRD plasmid using the following oligonucleotide primers: 5'-GGGCCCC TGGAACAGAACTTCCA-3'/ 5'-CTGGATCCTATCGGCAAAGCCACACT-3' according to the method described in (Imai, Matsushima *et al.* 1991). Prior to the PCR reaction both primers are

phosphorilated using a polynucleotide kinase enzyme (PNK, New England Biolabs) to allow PCR product ligation. The strategy produced a pGEX6P-2 derived $_{GST}$Alix-V version with three additional residues in the N-terminal end (residues 355-357) when compared to the pETM-30 version (described above). Expression and purification procedures followed the same steps as described for Alix-ΔPRD.

The same cloning strategy was employed to remove the extra 19 residues linker present in the initial Alix-ΔPRD fusion protein, between the PreScission cleavage site and the beginning of the protein sequence. The following primers were used: 5'-GGGCCCGGATCCCTCACCATGGCGTCG-3'/ 5'-CTGGAACAGAACTTCCAGATCCGATTTTGG-3'. This resulted in an Alix-ΔPRD protein version free of 17 extra residues at its N-teminal end, thus a potential better candidate for crystallization. Both new constructs were purified as described for Alix-ΔPRD.

Alix-V dimer and Alix-V_{Mut1} crystallization and data collection

High-throughput screening crystallization trials were performed in the High-Throughput Crystallization Laboratory at EMBL-Grenoble. Alix-V dimer crystals were grown in hanging drops using protein purified by size exclusion chromatography in buffer B (20mM Hepes pH 8.0; 100mM NaCl) and concentrated to 10-30 mg/ml. Crystals grew at room temperature using reservoir buffer containing 0.1 M bicine pH 9.0 and 0.8-1 M ammonium sulfate by mixing 1-3 μl of protein solution with 1-2 μl of reservoir. Best crystals were obtained in drops made up of 2+1 μl and 3+1 μl of protein+reservoir mixtures. The size of the crystals was improved by growing them using the same reservoir solution supplemented with 10-30% of glycerol.

Alix-V_{Mut1} crystals grew a room temperature and at 4ºC using the same set-up described for Alix-V dimer and protein concentrated to 15 mg/ml. Best crystallization conditions were 1) 0.1 M Bicine pH 9.0, 15% PEG 5K and 2) 0.1 M Tris-HCl pH 8.0, 10-

12 % PEG 20K. The condition 2) gave better crystal in the presence of 10 mM $NiCl_2$ added to the protein:precipitant drops using a 10x concentrated stock solution from Additive Screen HR2-428 (Hampton Research).

Alix-V dimer crystals were either directly frozen or cryo-protected in reservoir solution containing 30% glycerol (achieved in 10% increments steps). Alix-V_{Mut1} crystals were frozen in the reservoir solution containing 30% glycerol or a 15%glycerol/15%ethyleneglycol mixture. Crystals were harvested in nylon loops and plunged into liquid nitrogen (for storage until collection) or directly frozen in the beam line cryo-stream. Complete data sets were collected at ESRF beam lines ID29 and ID14-1.

Selenomethionine labelling

Selenium-derivatized proteins were produced by growing bacterial cultures and inducing protein expression in minimal media containing selenomethionine. 1L of media was produced by mixing: 200ml of 5x M9 minimal media (5x solution contents, g/L: 33.9g Na_2HPO_4, 15g KH_2PO_4, 2.5g NaCl, 5g NH_4Cl) (Maniatis, Fritsch *et al.* 1982), 2ml $MgSO_4$ 1M, 0.1ml $CaCl_2$, 20ml glucose 20%, 1ml ampicillin (100mg/ml) and 1ml chloramphenicol (12.5mg/ml). A 50ml starter culture of *Escherichia coli* BL21(DE3) Codon Plus (Invitrogen) transformed with pGEX-6P-2/Alix-V was produced overnight in LB-medium(Miller) containing ampicillin (100μg/ml) and chloramphenicol (12.5μg/ml). The culture was spun at 3000g, 10min and the pellet ressuspended in minimal media and used to inoculate 1L of the same medium. Cultures were grown at 37ºC and 250 rpm for about 6-8h till OD_{600}= 0.5-0.6. An amino acid mix was prepared with 100mg of lysine, phenylalanine, threonine, 50 mg of isoleucine, leucine, valine and 60 mg of L-selenomethione, by solubilizing all the aminoacids in 40ml of HCl 5%, neutralizing with NaOH (pH~7) and finally filtering (0.2 μm filter, Millipore). The aminoacid mix was added to each litre culture and after 15min (at 37ºC, 250 rpm) protein expression was induced

with 0.2mM of isopropyl-β-D-thiogalactopyranoside (IPTG). Expression occurred for 4h and Alix-V protein was purified as described for Alix-ΔPRD.

Alix antibodies

Dimeric Alix-V purified as described above, CHMP4B and CHMP3 (purified as MBP-fusion proteins by standard Amylose affinity procedure) were used to generate rabbit antisera (Covalab, Lyon, France). Cleared Alix antiserum was loaded on an Alix-affinity column prepared by coupling purified monomeric Alix-ΔPRD to CNBr-activated Sepharose 4B (Amersham Biosciences) according to the manufacturer's instructions. Affinity purified antibodies were obtained in buffer G (50mM Tris-HCl pH 8,0; 150mM NaCl) according to same instructions. Pull-down assays were done by incubating 50μl of flow-through or elution fractions from the affinity column with 50μg of Alix-ΔPRD monomer or dimer and 20μl of Protein A sepharose beads (Amersham Biosciences) pre-equilibrated in buffer G, for 2h at 4ºC. The beads were extensively washed with buffer G and bound proteins were eluted by boiling in SDS-PAGE sample buffer, separated on SDS-PAGE and bands detected with Coomassie Blue staining.

Purification of total IgGs from Alix, CHMP4b and CHMP3 antisera was performed using a Protein A sepharose column (Amersham Biosciences) according to the supplier's instructions.

Immunofluorescence studies

For indirect immunofluorescence (IIF) HeLa cells cultured on coverslips were fixed with 4% PFA for 20 min at 4°C. Blocking was made with 3% Goat pre-immune serum (GPI)/ 0.1% Triton X-100 in PBS for 30 min, at RT, followed by the primary antibody incubation in 1% GPI/ 0.1% Triton X-100 in PBS for 1h, at RT. Slides were then washed three times with PBS, followed by the secondary antibody incubation at RT for 1h

(Alexa488 or 594 coupled anti-mouse or anti-rabbit goat antibodies in 1% GPI/ 0.1% Triton X-100 in PBS). After three washes with PBS, slides were mounted in Mowiol and studied using confocal microscopy (Confocal Axioplan2 LSM510, Zeiss; Institut Albert Bonniot - Grenoble, France). Mouse monoclonal antibodies against early endosome antigen-1 (EEA-1) and LAMP1 were purchased from Abcam (Cambridge, UK). Mouse anti-lysobisphosphatidic acid (anti-LBPA) was kindly provided by Jean Gruenberg (Geneva, Switzerland) and used as published (Kobayashi, Stang *et al.* 1998). For Alix and CHMP proteins co-localization the Zenon Tricolor Rabbit IgG Labeling Kit (Invitrogen) was used according to the manufacturer's instructions.

Mammalian expression constructs and viral release assays

The mammalian expression vector pDSRed2-C1/AIP1$_{\Delta BRO}$ (supplied by H. Göttlinger, (Strack, Calistri *et al.* 2003)), encoding an Alix$_{\Delta BRO}$ fusion where the N-terminal Bro1-domain is replaced by RFP (Red Fluorescent Protein), was mutated to produce equivalent dimerization mutants as the ones described for Alix-V. Mutant-2 construct was generated using pDSRed2-C1/AIP1$_{\Delta BRO}$ as template and the primers 5'-CACATCAGGAATTTTCAAAAATGAAACAATCTTATAAGAAAGCTAACTTAAGAGAAGAAG TTTTGAAG-3'/ 5'-CTTCAAAACTTCTTCTCTTAAGTTAGCTTTCTTATAAGATTGTTTCATTTTTGAAAATTC CTGATGTG-3'. This was then used as template for generating Mutant-1 construct using the primers 5'-CAGGTCTCACATCAGGAATTTTCAGAAGCAGCACAATCTTATAAGAAAGCTAACT TAAGAGAAG -3' / 5'-CTTCTCTTAAGTTAGCTTTCTTATAAGATTGTGCTGCTTCTGAAAATTCCTGATGT GAGACCTG -3'. Both mutagenic constructs were sequenced over the entire gene to confirm mutations introduced and to discard unwanted mutations. Virion release assays were performed in collaboration with H. Göttlinger (UMass Medical School, Worcester, USA) and followed the procedure described in (Strack, Calistri *et al.* 2003).

Supplementary figures

Figure S1. Sequence alignments of Bro1-domain containing proteins presented in Figure 7. *H. sapiens* Alix (hAlix; Q8WUM4), *M. Musculus* Alix (mAlix ; Q9WU78), *H. sapiens* PTN23 (HD-PTP; Q9H3S7), *H. sapiens* BROX (Q5VW32), *S. cerevisiae* palA (RIM20; Q12033), *S. cerevisiae* Bro1 (P48582). The extra sequence of HD-PTP has been omitted for simplification. Identical residues are shown on red background, similar residues are drawn in red and sequence similarity is underlined by blue boxes. Secondary structure elements seen in human $Alix_{Bro1\text{-}V}$ crystal structure (PDB code 2OEV)(Fisher, Chung *et al.* 2007) are indicated above the sequence. UniProtKB/Swiss-Prot protein accession numbers are indicated. Sequence alignments were performed using the Clustal server www.ebi.ac.uk/clustalw (Thompson, Higgins *et al.* 1994) and formatted using ESPript http://espript.ibcp.fr/ESPript/ (Gouet, Courcelle *et al.* 1999).

Figure S2. Sequence alignments of Alix homologs. Seven representative species were chosen: *H. sapiens* (Q8WUM4), *M. Musculus* (Q9WU78), *Drosophila melanogaster* (Q9VB05), *C. elegans* (P34552), *D. discoideum* (Q8T7K0), *A. thaliana* (Q8H1H8) and *S. cerevisiae* (P48582). Secondary structure elements seen in human $Alix_{Bro1\text{-}V}$ crystal structure are indicated above the sequence. UniProtKB/Swiss-Prot protein accession numbers are shown. Multiple sequence alignment was produced and formatted as described in Figure S1.

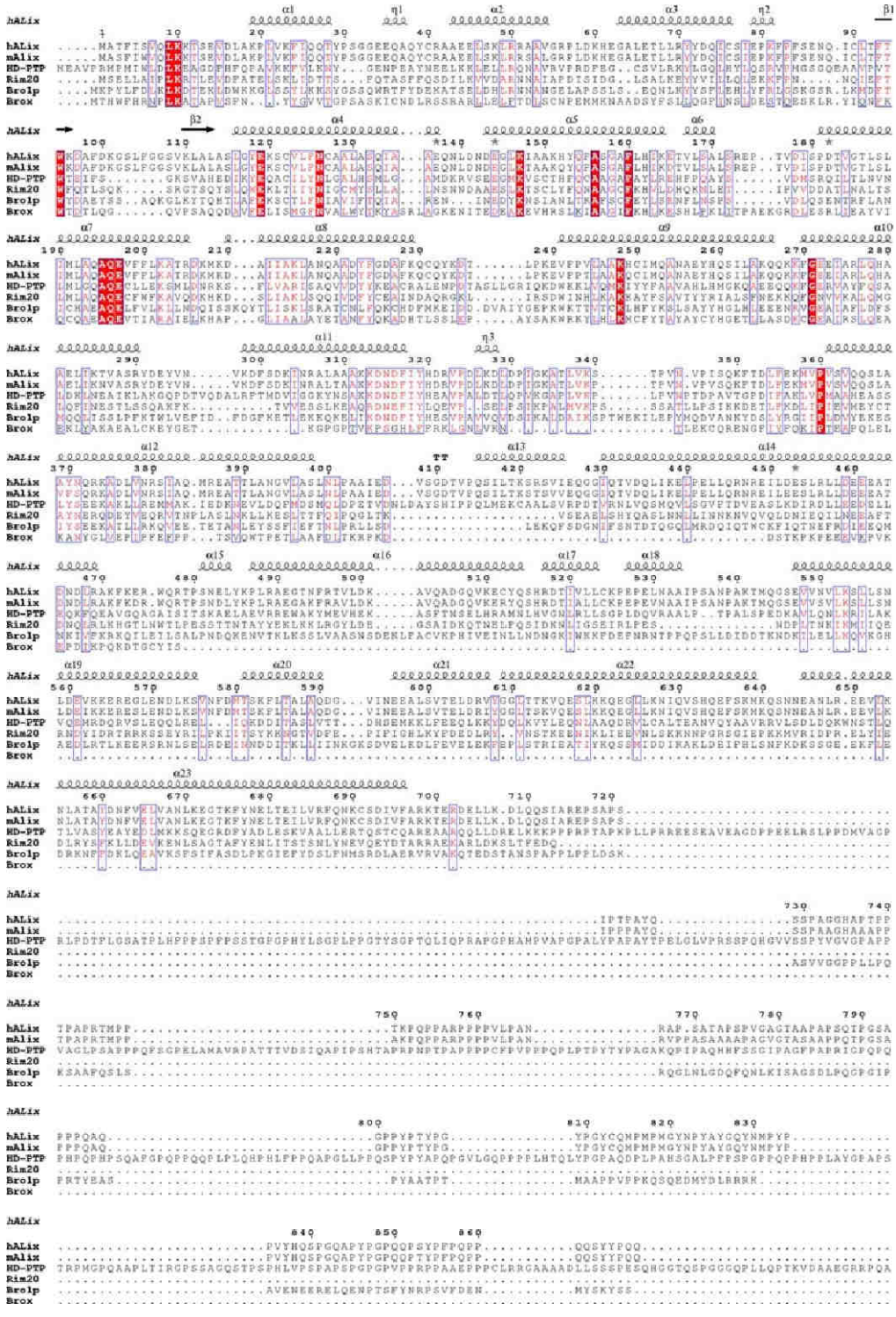

Figure S1

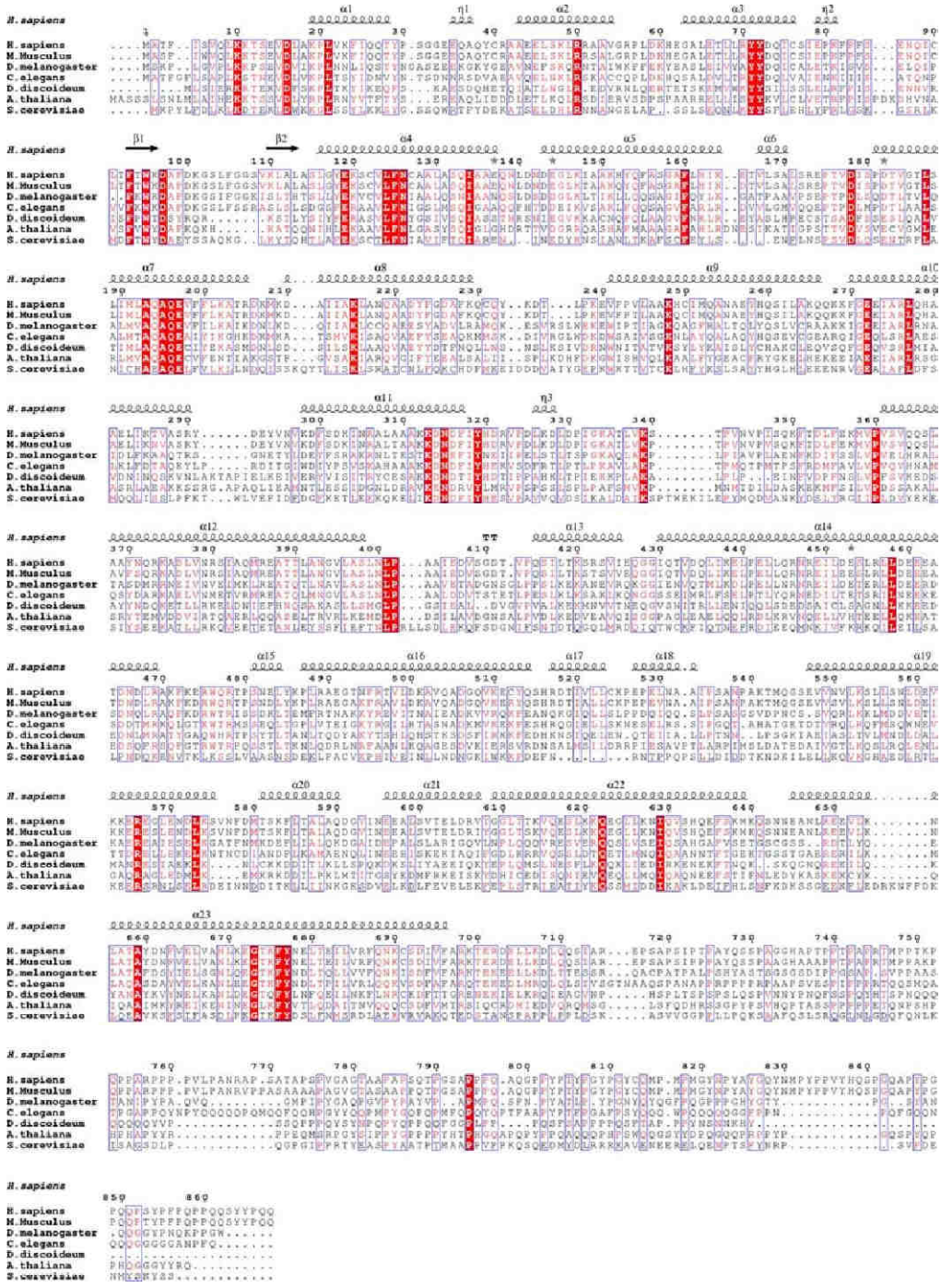

Figure S2

References

Accola, M. A., B. Strack and H. G. Gottlinger (2000). "Efficient particle production by minimal Gag constructs which retain the carboxy-terminal domain of human immunodeficiency virus type 1 capsid-p2 and a late assembly domain." J Virol **74**(12): 5395-402.

Agromayor, M. and J. Martin-Serrano (2006). "Interaction of AMSH with ESCRT-III and deubiquitination of endosomal cargo." J Biol Chem **281**(32): 23083-91.

Alam, S. L., C. Langelier, F. G. Whitby, S. Koirala, H. Robinson, C. P. Hill and W. I. Sundquist (2006). "Structural basis for ubiquitin recognition by the human ESCRT-II EAP45 GLUE domain." Nat Struct Mol Biol **13**(11): 1029-30.

Amerik, A. Y. and M. Hochstrasser (2004). "Mechanism and function of deubiquitinating enzymes." Biochim Biophys Acta **1695**(1-3): 189-207.

Arst, H. N. and M. A. Penalva (2003). "pH regulation in Aspergillus and parallels with higher eukaryotic regulatory systems." Trends Genet **19**(4): 224-31.

Aubry, L., S. Mattei, B. Blot, R. Sadoul, M. Satre and G. Klein (2002). "Biochemical characterization of two analogues of the apoptosis-linked gene 2 protein in Dictyostelium discoideum and interaction with a physiological partner in mammals, murine Alix." J Biol Chem **277**(24): 21947-54.

Azmi, I., B. Davies, C. Dimaano, J. Payne, D. Eckert, M. Babst and D. J. Katzmann (2006). "Recycling of ESCRTs by the AAA-ATPase Vps4 is regulated by a conserved VSL region in Vta1." J Cell Biol **172**(5): 705-17.

Babst, M., D. J. Katzmann, E. J. Estepa-Sabal, T. Meerloo and S. D. Emr (2002). "Escrt-III: an endosome-associated heterooligomeric protein complex required for mvb sorting." Dev Cell **3**(2): 271-82.

Babst, M., D. J. Katzmann, W. B. Snyder, B. Wendland and S. D. Emr (2002). "Endosome-associated complex, ESCRT-II, recruits transport machinery for protein sorting at the multivesicular body." Dev Cell **3**(2): 283-9.

Babst, M., G. Odorizzi, E. J. Estepa and S. D. Emr (2000). "Mammalian tumor susceptibility gene 101 (TSG101) and the yeast homologue, Vps23p, both function in late endosomal trafficking." Traffic **1**(3): 248-58.

Babst, M., B. Wendland, E. J. Estepa and S. D. Emr (1998). "The Vps4p AAA ATPase regulates membrane association of a Vps protein complex required for normal endosome function." Embo J **17**(11): 2982-93.

Bache, K. G., A. Brech, A. Mehlum and H. Stenmark (2003). "Hrs regulates multivesicular body formation via ESCRT recruitment to endosomes." J Cell Biol **162**(3): 435-42.

Bishop, N. and P. Woodman (2000). "ATPase-defective mammalian VPS4 localizes to aberrant endosomes and impairs cholesterol trafficking." Mol Biol Cell **11**(1): 227-39.

Blum, D., F. J. Hemming, M. C. Galas, S. Torch, L. Cuvelier, S. N. Schiffmann and R. Sadoul (2004). "Increased Alix (apoptosis-linked gene-2 interacting protein X) immunoreactivity in the degenerating striatum of rats chronically treated by 3-nitropropionic acid." Neurosci Lett **368**(3): 309-13.

Bowers, K., J. Lottridge, S. B. Helliwell, L. M. Goldthwaite, J. P. Luzio and T. H. Stevens (2004). "Protein-protein interactions of ESCRT complexes in the yeast Saccharomyces cerevisiae." Traffic **5**(3): 194-210.

Brown, F. D., A. L. Rozelle, H. L. Yin, T. Balla and J. G. Donaldson (2001). "Phosphatidylinositol 4,5-bisphosphate and Arf6-regulated membrane traffic." J Cell Biol **154**(5): 1007-17.

Cabezas, A., K. G. Bache, A. Brech and H. Stenmark (2005). "Alix regulates cortical actin and the spatial distribution of endosomes." J Cell Sci **118**(Pt 12): 2625-35.

Carlton, J. G. and J. Martin-Serrano (2007). "Parallels between cytokinesis and retroviral budding: a role for the ESCRT machinery." Science **316**(5833): 1908-12.

Chatellard-Causse, C., B. Blot, N. Cristina, S. Torch, M. Missotten and R. Sadoul (2002). "Alix (ALG-2-interacting protein X), a protein involved in apoptosis, binds to endophilins and induces cytoplasmic vacuolization." J Biol Chem **277**(32): 29108-15.

Chen, B., S. C. Borinstein, J. Gillis, V. W. Sykes and O. Bogler (2000). "The glioma-associated protein SETA interacts with AIP1/Alix and ALG-2 and modulates apoptosis in astrocytes." J Biol Chem **275**(25): 19275-81.

Chen, C. and A. J. Sytkowski (2005). "Apoptosis-linked gene-2 connects the Raf-1 and ASK1 signalings." Biochem Biophys Res Commun **333**(1): 51-7.

Chu, T., J. Sun, S. Saksena and S. D. Emr (2006). "New component of ESCRT-I regulates endosomal sorting complex assembly." J Cell Biol **175**(5): 815-23.

Clarke, S. (1992). "Protein isoprenylation and methylation at carboxyl-terminal cysteine residues." Annu Rev Biochem **61**: 355-86.

Collaborative Computational Project Number 4 (1994). "The CCP4 suite: programs for protein crystallography." Acta Crystallogr D Biol Crystallogr **50**(Pt 5): 760-3.

Dawson, J. C., J. A. Legg and L. M. Machesky (2006). "Bar domain proteins: a role in tubulation, scission and actin assembly in clathrin-mediated endocytosis." Trends Cell Biol **16**(10): 493-8.

DeLano, W. L. (2002). "The PyMOL Molecular Graphics System." DeLano Scientific, Palo Alto, CA, USA.

Denzer, K., M. J. Kleijmeer, H. F. Heijnen, W. Stoorvogel and H. J. Geuze (2000). "Exosome: from internal vesicle of the multivesicular body to intercellular signaling device." J Cell Sci **113 Pt 19**: 3365-74.

Doyotte, A., A. Mironov, E. McKenzie and P. Woodman (2008). "The Bro1-related protein HD-PTP/PTPN23 is required for endosomal cargo sorting and multivesicular body morphogenesis." Proc Natl Acad Sci U S A **105**(17): 6308-13.

Dubochet, J., M. Adrian, J. J. Chang, J. C. Homo, J. Lepault, A. W. McDowall and P. Schultz (1988). "Cryo-electron microscopy of vitrified specimens." Q Rev Biophys **21**(2): 129-228.

Farsad, K., N. Ringstad, K. Takei, S. R. Floyd, K. Rose and P. De Camilli (2001). "Generation of high curvature membranes mediated by direct endophilin bilayer interactions." J Cell Biol **155**(2): 193-200.

Fielding, A. B., E. Schonteich, J. Matheson, G. Wilson, X. Yu, G. R. Hickson, S. Srivastava, S. A. Baldwin, R. Prekeris and G. W. Gould (2005). "Rab11-FIP3 and FIP4 interact with Arf6 and the exocyst to control membrane traffic in cytokinesis." Embo J **24**(19): 3389-99.

Filimonenko, M., S. Stuffers, C. Raiborg, A. Yamamoto, L. Malerod, E. M. Fisher, A. Isaacs, A. Brech, H. Stenmark and A. Simonsen (2007). "Functional multivesicular bodies are required for autophagic clearance of protein aggregates associated with neurodegenerative disease." J Cell Biol **179**(3): 485-500.

Fisher, R. D., H. Y. Chung, Q. Zhai, H. Robinson, W. I. Sundquist and C. P. Hill (2007). "Structural and biochemical studies of ALIX/AIP1 and its role in retrovirus budding." Cell **128**(5): 841-52.

Forsberg, H., M. Hammar, C. Andreasson, A. Moliner and P. O. Ljungdahl (2001). "Suppressors of ssy1 and ptr3 null mutations define novel amino acid sensor-independent genes in Saccharomyces cerevisiae." Genetics **158**(3): 973-88.

Fotin, A., Y. Cheng, P. Sliz, N. Grigorieff, S. C. Harrison, T. Kirchhausen and T. Walz (2004). "Molecular model for a complete clathrin lattice from electron cryomicroscopy." Nature **432**(7017): 573-9.

Frost, A., R. Perera, A. Roux, K. Spasov, O. Destaing, E. H. Egelman, P. De Camilli and V. M. Unger (2008). "Structural basis of membrane invagination by F-BAR domains." Cell **132**(5): 807-17.

Fujita, H., M. Yamanaka, K. Imamura, Y. Tanaka, A. Nara, T. Yoshimori, S. Yokota and M. Himeno (2003). "A dominant negative form of the AAA ATPase SKD1/VPS4 impairs membrane trafficking out of endosomal/lysosomal compartments: class E vps phenotype in mammalian cells." J Cell Sci **116**(Pt 2): 401-14.

Gad, H., N. Ringstad, P. Low, O. Kjaerulff, J. Gustafsson, M. Wenk, G. Di Paolo, Y. Nemoto, J. Crun, M. H. Ellisman, P. De Camilli, O. Shupliakov and L. Brodin (2000). "Fission and uncoating of synaptic clathrin-coated vesicles are perturbed by disruption of interactions with the SH3 domain of endophilin." Neuron **27**(2): 301-12.

Gallop, J. L., C. C. Jao, H. M. Kent, P. J. Butler, P. R. Evans, R. Langen and H. T. McMahon (2006). "Mechanism of endophilin N-BAR domain-mediated membrane curvature." Embo J **25**(12): 2898-910.

Garrus, J. E., U. K. von Schwedler, O. W. Pornillos, S. G. Morham, K. H. Zavitz, H. E. Wang, D. A. Wettstein, K. M. Stray, M. Cote, R. L. Rich, D. G. Myszka and W. I. Sundquist (2001). "Tsg101 and the vacuolar protein sorting pathway are essential for HIV-1 budding." Cell **107**(1): 55-65.

Geminard, C., A. De Gassart, L. Blanc and M. Vidal (2004). "Degradation of AP2 during reticulocyte maturation enhances binding of hsc70 and Alix to a common site on TFR for sorting into exosomes." Traffic **5**(3): 181-93.

Gill, D. J., H. Teo, J. Sun, O. Perisic, D. B. Veprintsev, S. D. Emr and R. L. Williams (2007). "Structural insight into the ESCRT-I/-II link and its role in MVB trafficking." Embo J **26**(2): 600-12.

Goley, E. D. and M. D. Welch (2006). "The ARP2/3 complex: an actin nucleator comes of age." Nat Rev Mol Cell Biol **7**(10): 713-26.

Gottlinger, H. G., T. Dorfman, J. G. Sodroski and W. A. Haseltine (1991). "Effect of mutations affecting the p6 gag protein on human immunodeficiency virus particle release." Proc Natl Acad Sci U S A **88**(8): 3195-9.

Gouet, P., E. Courcelle, D. I. Stuart and F. Metoz (1999). "ESPript: analysis of multiple sequence alignments in PostScript." Bioinformatics **15**(4): 305-8.

Gromley, A., C. Yeaman, J. Rosa, S. Redick, C. T. Chen, S. Mirabelle, M. Guha, J. Sillibourne and S. J. Doxsey (2005). "Centriolin anchoring of exocyst and SNARE complexes at the midbody is required for secretory-vesicle-mediated abscission." Cell **123**(1): 75-87.

Guinier, A. (1939). "La diffraction des rayons X aux tres petits angles; application a l'etude de phenomenes ultramicroscopiques." Ann Phys (Paris) **12**: 161-237.

Haas, A. K., E. Fuchs, R. Kopajtich and F. A. Barr (2005). "A GTPase-activating protein controls Rab5 function in endocytic trafficking." Nat Cell Biol **7**(9): 887-93.

Habermann, B. (2004). "The BAR-domain family of proteins: a case of bending and binding?" EMBO Rep **5**(3): 250-5.

Hanson, P. I., R. Roth, Y. Lin and J. E. Heuser (2008). "Plasma membrane deformation by circular arrays of ESCRT-III protein filaments." J Cell Biol **180**(2): 389-402.

Hemming, F. J., S. Fraboulet, B. Blot and R. Sadoul (2004). "Early increase of apoptosis-linked gene-2 interacting protein X in areas of kainate-induced neurodegeneration." Neuroscience **123**(4): 887-95.

Henne, W. M., H. M. Kent, M. G. Ford, B. G. Hegde, O. Daumke, P. J. Butler, R. Mittal, R. Langen, P. R. Evans and H. T. McMahon (2007). "Structure and analysis of FCHo2 F-BAR domain: a dimerizing and membrane recruitment module that effects membrane curvature." Structure **15**(7): 839-52.

Hierro, A., J. Sun, A. S. Rusnak, J. Kim, G. Prag, S. D. Emr and J. H. Hurley (2004). "Structure of the ESCRT-II endosomal trafficking complex." Nature **431**(7005): 221-5.

Hirano, S., N. Suzuki, T. Slagsvold, M. Kawasaki, D. Trambaiolo, R. Kato, H. Stenmark and S. Wakatsuki (2006). "Structural basis of ubiquitin recognition by mammalian Eap45 GLUE domain." Nat Struct Mol Biol **13**(11): 1031-2.

Hobdy-Henderson, K. C., C. M. Hales, L. A. Lapierre, R. E. Cheney and J. R. Goldenring (2003). "Dynamics of the apical plasma membrane recycling system during cell division." Traffic **4**(10): 681-93.

Hwang, I. S., Y. S. Jung and E. Kim (2002). "Interaction of ALG-2 with ASK1 influences ASK1 localization and subsequent JNK activation." FEBS Lett **529**(2-3): 183-7.

Ichioka, F., M. Horii, K. Katoh, Y. Terasawa, H. Shibata and M. Maki (2005). "Identification of Rab GTPase-activating protein-like protein (RabGAPLP) as a novel Alix/AIP1-interacting protein." Biosci Biotechnol Biochem **69**(4): 861-5.

Ichioka, F., R. Kobayashi, K. Katoh, H. Shibata and M. Maki (2008). "Brox, a novel farnesylated Bro1 domain-containing protein that associates with charged multivesicular body protein 4 (CHMP4)." Febs J **275**(4): 682-92.

Ichioka, F., E. Takaya, H. Suzuki, S. Kajigaya, V. L. Buchman, H. Shibata and M. Maki (2007). "HD-PTP and Alix share some membrane-traffic related proteins that interact with their Bro1 domains or proline-rich regions." Arch Biochem Biophys **457**(2): 142-9.

Im, Y. J. and J. H. Hurley (2008). "Integrated structural model and membrane targeting mechanism of the human ESCRT-II complex." Dev Cell **14**(6): 902-13.

Imai, Y., Y. Matsushima, T. Sugimura and M. Terada (1991). "A simple and rapid method for generating a deletion by PCR." Nucleic Acids Res **19**(10): 2785.

Irie, T., N. Nagata, T. Yoshida and T. Sakaguchi (2008). "Recruitment of Alix/AIP1 to the plasma membrane by Sendai virus C protein facilitates budding of virus-like particles." Virology **371**(1): 108-20.

Itoh, T. and P. De Camilli (2006). "BAR, F-BAR (EFC) and ENTH/ANTH domains in the regulation of membrane-cytosol interfaces and membrane curvature." Biochim Biophys Acta **1761**(8): 897-912.

Jia, J., S. Tarabykina, C. Hansen, M. Berchtold and M. Cygler (2001). "Structure of apoptosis-linked protein ALG-2: insights into Ca2+-induced changes in penta-EF-hand proteins." Structure **9**(4): 267-75.

Kabsch, W. (1993). J. Appl. Cryst. **26**: 795-800.

Kaneko, T., T. Kumasaka, T. Ganbe, T. Sato, K. Miyazawa, N. Kitamura and N. Tanaka (2003). "Structural insight into modest binding of a non-PXXP ligand to the signal transducing adaptor molecule-2 Src homology 3 domain." J Biol Chem **278**(48): 48162-8.

Karbowski, M., S. Y. Jeong and R. J. Youle (2004). "Endophilin B1 is required for the maintenance of mitochondrial morphology." J Cell Biol **166**(7): 1027-39.

Kato, M., K. Miyazawa and N. Kitamura (2000). "A deubiquitinating enzyme UBPY interacts with the Src homology 3 domain of Hrs-binding protein via a novel binding motif PX(V/I)(D/N)RXXKP." J Biol Chem **275**(48): 37481-7.

Katoh, K., H. Shibata, K. Hatta and M. Maki (2004). "CHMP4b is a major binding partner of the ALG-2-interacting protein Alix among the three CHMP4 isoforms." Arch Biochem Biophys **421**(1): 159-65.

Katoh, K., H. Shibata, H. Suzuki, A. Nara, K. Ishidoh, E. Kominami, T. Yoshimori and M. Maki (2003). "The ALG-2-interacting protein Alix associates with CHMP4b, a human homologue of yeast Snf7 that is involved in multivesicular body sorting." J Biol Chem **278**(40): 39104-13.

Katzmann, D. J. (2006). "No ESCRT to the melanosome: MVB sorting without ubiquitin." Dev Cell **10**(3): 278-80.

Katzmann, D. J., M. Babst and S. D. Emr (2001). "Ubiquitin-dependent sorting into the multivesicular body pathway requires the function of a conserved endosomal protein sorting complex, ESCRT-I." Cell **106**(2): 145-55.

Katzmann, D. J., S. Sarkar, T. Chu, A. Audhya and S. D. Emr (2004). "Multivesicular body sorting: ubiquitin ligase Rsp5 is required for the modification and sorting of carboxypeptidase S." Mol Biol Cell **15**(2): 468-80.

Katzmann, D. J., C. J. Stefan, M. Babst and S. D. Emr (2003). "Vps27 recruits ESCRT machinery to endosomes during MVB sorting." J Cell Biol **162**(3): 413-23.

Kessels, M. M. and B. Qualmann (2004). "The syndapin protein family: linking membrane trafficking with the cytoskeleton." J Cell Sci **117**(Pt 15): 3077-86.

Kieffer, C., J. J. Skalicky, E. Morita, I. De Domenico, D. M. Ward, J. Kaplan and W. I. Sundquist (2008). "Two distinct modes of ESCRT-III recognition are required for VPS4 functions in lysosomal protein targeting and HIV-1 budding." Dev Cell **15**(1): 62-73.

Kim, J., S. Sitaraman, A. Hierro, B. M. Beach, G. Odorizzi and J. H. Hurley (2005). "Structural basis for endosomal targeting by the Bro1 domain." Dev Cell **8**(6): 937-47.

Kleijmeer, M., G. Ramm, D. Schuurhuis, J. Griffith, M. Rescigno, P. Ricciardi-Castagnoli, A. Y. Rudensky, F. Ossendorp, C. J. Melief, W. Stoorvogel and H. J. Geuze (2001). "Reorganization of multivesicular bodies regulates MHC class II antigen presentation by dendritic cells." J Cell Biol **155**(1): 53-63.

Kobayashi, T., M. H. Beuchat, J. Chevallier, A. Makino, N. Mayran, J. M. Escola, C. Lebrand, P. Cosson, T. Kobayashi and J. Gruenberg (2002). "Separation and characterization of late endosomal membrane domains." J Biol Chem **277**(35): 32157-64.

Kobayashi, T., E. Stang, K. S. Fang, P. de Moerloose, R. G. Parton and J. Gruenberg (1998). "A lipid associated with the antiphospholipid syndrome regulates endosome structure and function." Nature **392**(6672): 193-7.

Koch, M. H. J. and J. X. Bordas (1983). "X-ray diffraction and scattering on disordered systems using synchrotron radiation." Nucl. Instrum. Methods **208**: 461-469.

Konarev, P. V., V. V. Volkov, A. V. Sokolova, M. H. J. Koch and D. I. Svergun (2003). "PRIMUS- a Windows-PC based system for small-angle scattering data analysis." J. Appl. Crystallogr. **36**: 1277-1282.

Kostelansky, M. S., C. Schluter, Y. Y. Tam, S. Lee, R. Ghirlando, B. Beach, E. Conibear and J. H. Hurley (2007). "Molecular architecture and functional model of the complete yeast ESCRT-I heterotetramer." Cell **129**(3): 485-98.

Kostelansky, M. S., J. Sun, S. Lee, J. Kim, R. Ghirlando, A. Hierro, S. D. Emr and J. H. Hurley (2006). "Structural and functional organization of the ESCRT-I trafficking complex." Cell **125**(1): 113-26.

Kozin, M. B. and D. I. Svergun (2001). "Automated matching of high- and low-resolution structural models." J. Appl. Crystallogr. **34**: 33-41.

Kyuuma, M., K. Kikuchi, K. Kojima, Y. Sugawara, M. Sato, N. Mano, J. Goto, T. Takeshita, A. Yamamoto, K. Sugamura and N. Tanaka (2007). "AMSH, an ESCRT-III associated enzyme, deubiquitinates cargo on MVB/late endosomes." Cell Struct Funct **31**(2): 159-72.

Langelier, C., U. K. von Schwedler, R. D. Fisher, I. De Domenico, P. L. White, C. P. Hill, J. Kaplan, D. Ward and W. I. Sundquist (2006). "Human ESCRT-II complex and its role in human immunodeficiency virus type 1 release." J Virol **80**(19): 9465-80.

Lata, S., M. Roessle, J. Solomons, M. Jamin, H. G. Gottlinger, D. I. Svergun and W. Weissenhorn (2008). "Structural basis for autoinhibition of ESCRT-III CHMP3." J Mol Biol **378**(4): 816-25.

Lata, S., G. Schoehn, A. Jain, R. Pires, J. Piehler, H. G. Gottlinger and W. Weissenhorn (2008). "Helical structures of ESCRT-III are disassembled by VPS4." Science.

Lazert, C., N. Chazal, L. Briant, D. Gerlier and J. C. Cortay (2008). "Refined study of the interaction between HIV-1 p6 late domain and ALIX." Retrovirology **5**: 39.

Lee, J. A., A. Beigneux, S. T. Ahmad, S. G. Young and F. B. Gao (2007). "ESCRT-III dysfunction causes autophagosome accumulation and neurodegeneration." Curr Biol **17**(18): 1561-7.

Lee, J. A. and F. B. Gao (2008). "Roles of ESCRT in autophagy-associated neurodegeneration." Autophagy **4**(2): 230-2.

Lee, S., A. Joshi, K. Nagashima, E. O. Freed and J. H. Hurley (2007). "Structural basis for viral late-domain binding to Alix." Nat Struct Mol Biol **14**(3): 194-9.

Leslie, A. G. W. (1992). Jnt CCP4/EACBM Newsl. Protein Crystallogr. **26**.

Lin, Y., L. A. Kimpler, T. V. Naismith, J. M. Lauer and P. I. Hanson (2005). "Interaction of the mammalian endosomal sorting complex required for transport (ESCRT) III protein hSnf7-1 with itself, membranes, and the AAA+ ATPase SKD1." J Biol Chem **280**(13): 12799-809.

Lu, Q., L. W. Hope, M. Brasch, C. Reinhard and S. N. Cohen (2003). "TSG101 interaction with HRS mediates endosomal trafficking and receptor down-regulation." Proc Natl Acad Sci U S A **100**(13): 7626-31.

Luhtala, N. and G. Odorizzi (2004). "Bro1 coordinates deubiquitination in the multivesicular body pathway by recruiting Doa4 to endosomes." J Cell Biol **166**(5): 717-29.

Mahul-Mellier, A. L., F. J. Hemming, B. Blot, S. Fraboulet and R. Sadoul (2006). "Alix, making a link between apoptosis-linked gene-2, the endosomal sorting complexes required for transport, and neuronal death in vivo." J Neurosci **26**(2): 542-9.

Maki, M., Y. Kitaura, H. Satoh, S. Ohkouchi and H. Shibata (2002). "Structures, functions and molecular evolution of the penta-EF-hand Ca2+-binding proteins." Biochim Biophys Acta **1600**(1-2): 51-60.

Maniatis, T., E. F. Fritsch and J. Sambrook (1982). Molecular cloning : a laboratory manual. Cold Spring Harbor, N.Y., Cold Spring Harbor Laboratory.

Mao, Y., A. Nickitenko, X. Duan, T. E. Lloyd, M. N. Wu, H. Bellen and F. A. Quiocho (2000). "Crystal structure of the VHS and FYVE tandem domains of Hrs, a protein involved in membrane trafficking and signal transduction." Cell **100**(4): 447-56.

Martin-Serrano, J., A. Yarovoy, D. Perez-Caballero and P. D. Bieniasz (2003). "Divergent retroviral late-budding domains recruit vacuolar protein sorting factors by using alternative adaptor proteins." Proc Natl Acad Sci U S A **100**(21): 12414-9.

Matsuo, H., J. Chevallier, N. Mayran, I. Le Blanc, C. Ferguson, J. Faure, N. S. Blanc, S. Matile, J. Dubochet, R. Sadoul, R. G. Parton, F. Vilbois and J. Gruenberg (2004). "Role of LBPA and Alix in multivesicular liposome formation and endosome organization." Science **303**(5657): 531-4.

Mattei, S., G. Klein, M. Satre and L. Aubry (2006). "Trafficking and developmental signaling: Alix at the crossroads." Eur J Cell Biol **85**(9-10): 925-36.

Mattei, S., W. J. Ryves, B. Blot, R. Sadoul, A. J. Harwood, M. Satre, G. Klein and L. Aubry (2005). "Dd-Alix, a conserved endosome-associated protein, controls Dictyostelium development." Dev Biol **279**(1): 99-113.

Mattila, P. K., A. Pykalainen, J. Saarikangas, V. O. Paavilainen, H. Vihinen, E. Jokitalo and P. Lappalainen (2007). "Missing-in-metastasis and IRSp53 deform PI(4,5)P2-rich membranes by an inverse BAR domain-like mechanism." J Cell Biol **176**(7): 953-64.

Maxfield, F. R. and T. E. McGraw (2004). "Endocytic recycling." Nat Rev Mol Cell Biol **5**(2): 121-32.

McCullough, J., M. J. Clague and S. Urbe (2004). "AMSH is an endosome-associated ubiquitin isopeptidase." J Cell Biol **166**(4): 487-92.

McCullough, J., R. D. Fisher, F. G. Whitby, W. I. Sundquist and C. P. Hill (2008). "ALIX-CHMP4 interactions in the human ESCRT pathway." Proc Natl Acad Sci U S A **105**(22): 7687-91.

McCullough, J., P. E. Row, O. Lorenzo, M. Doherty, R. Beynon, M. J. Clague and S. Urbe (2006). "Activation of the endosome-associated ubiquitin isopeptidase AMSH by STAM, a component of the multivesicular body-sorting machinery." Curr Biol **16**(2): 160-5.

McMahon, H. T. and J. L. Gallop (2005). "Membrane curvature and mechanisms of dynamic cell membrane remodelling." Nature **438**(7068): 590-6.

Millard, T. H., G. Bompard, M. Y. Heung, T. R. Dafforn, D. J. Scott, L. M. Machesky and K. Futterer (2005). "Structural basis of filopodia formation induced by the IRSp53/MIM homology domain of human IRSp53." Embo J **24**(2): 240-50.

Missotten, M., A. Nichols, K. Rieger and R. Sadoul (1999). "Alix, a novel mouse protein undergoing calcium-dependent interaction with the apoptosis-linked-gene 2 (ALG-2) protein." Cell Death Differ **6**(2): 124-9.

Moberg, K. H., S. Schelble, S. K. Burdick and I. K. Hariharan (2005). "Mutations in erupted, the Drosophila ortholog of mammalian tumor susceptibility gene 101, elicit non-cell-autonomous overgrowth." Dev Cell **9**(5): 699-710.

Morita, E., V. Sandrin, S. L. Alam, D. M. Eckert, S. P. Gygi and W. I. Sundquist (2007). "Identification of human MVB12 proteins as ESCRT-I subunits that function in HIV budding." Cell Host Microbe **2**(1): 41-53.

Morita, E., V. Sandrin, H. Y. Chung, S. G. Morham, S. P. Gygi, C. K. Rodesch and W. I. Sundquist (2007). "Human ESCRT and ALIX proteins interact with proteins of the midbody and function in cytokinesis." Embo J **26**(19): 4215-27.

Morita, E. and W. I. Sundquist (2004). "Retrovirus budding." Annu Rev Cell Dev Biol **20**: 395-425.

Munshi, U. M., J. Kim, K. Nagashima, J. H. Hurley and E. O. Freed (2007). "An Alix fragment potently inhibits HIV-1 budding: characterization of binding to retroviral YPXL late domains." J Biol Chem **282**(6): 3847-55.

Muziol, T., E. Pineda-Molina, R. B. Ravelli, A. Zamborlini, Y. Usami, H. Gottlinger and W. Weissenhorn (2006). "Structural basis for budding by the ESCRT-III factor CHMP3." Dev Cell **10**(6): 821-30.

Narayanan, T., O. Diat and P. Bösecke (2001). "SAXS and USAXS on the high brillance beamline at the ESRF." Nucl. Instrum. Methods. Phys. Res. ser. A **467-468**: 1005-1009.

Nikko, E. and B. Andre (2007). "Split-ubiquitin two-hybrid assay to analyze protein-protein interactions at the endosome: application to Saccharomyces cerevisiae Bro1 interacting with ESCRT complexes, the Doa4 ubiquitin hydrolase, and the Rsp5 ubiquitin ligase." Eukaryot Cell **6**(8): 1266-77.

Nikko, E., A. M. Marini and B. Andre (2003). "Permease recycling and ubiquitination status reveal a particular role for Bro1 in the multivesicular body pathway." J Biol Chem **278**(50): 50732-43.

Obita, T., S. Saksena, S. Ghazi-Tabatabai, D. J. Gill, O. Perisic, S. D. Emr and R. L. Williams (2007). "Structural basis for selective recognition of ESCRT-III by the AAA ATPase Vps4." Nature **449**(7163): 735-9.

Odorizzi, G. (2006). "The multiple personalities of Alix." J Cell Sci **119**(Pt 15): 3025-32.

Odorizzi, G., D. J. Katzmann, M. Babst, A. Audhya and S. D. Emr (2003). "Bro1 is an endosome-associated protein that functions in the MVB pathway in Saccharomyces cerevisiae." J Cell Sci **116**(Pt 10): 1893-903.

Ohkouchi, S., M. S. El-Halawany, F. Aruga, H. Shibata, K. Hitomi and M. Maki (2004). "DdAlix, an Alix/AIP1 homolog in Dictyostelium discoideum, is required for multicellular development under low Ca2+ conditions." Gene **337**: 131-9.

Ohkouchi, S., H. Saito, F. Aruga, T. Maeda, H. Shibata and M. Maki (2005). "Dictyostelium discoideum requires an Alix/AIP1 homolog, DdAlix, for morphogenesis in alkaline environments." FEBS Lett **579**(7): 1745-50.

Pan, S., R. Wang, X. Zhou, G. He, J. Koomen, R. Kobayashi, L. Sun, J. Corvera, G. E. Gallick and J. Kuang (2006). "Involvement of the conserved adaptor protein Alix in actin cytoskeleton assembly." J Biol Chem **281**(45): 34640-50.

Patnaik, A., V. Chau, F. Li, R. C. Montelaro and J. W. Wills (2002). "Budding of equine infectious anemia virus is insensitive to proteasome inhibitors." J Virol **76**(6): 2641-7.

Peck, J. W., E. T. Bowden and P. D. Burbelo (2004). "Structure and function of human Vps20 and Snf7 proteins." Biochem J **377**(Pt 3): 693-700.

Pelchen-Matthews, A., G. Raposo and M. Marsh (2004). "Endosomes, exosomes and Trojan viruses." Trends Microbiol **12**(7): 310-6.

Persechini, P. M., C. C. Liu, P. A. Detmers and J. D. Young (1989). "Heterogeneity of granules of murine cytolytic T lymphocytes. Isolation of a homogeneous population of dense granules." J Immunol Methods **124**(1): 7-15.

Peter, B. J., H. M. Kent, I. G. Mills, Y. Vallis, P. J. Butler, P. R. Evans and H. T. McMahon (2004). "BAR domains as sensors of membrane curvature: the amphiphysin BAR structure." Science **303**(5657): 495-9.

Pineda-Molina, E., H. Belrhali, A. J. Piefer, I. Akula, P. Bates and W. Weissenhorn (2006). "The crystal structure of the C-terminal domain of Vps28 reveals a conserved surface required for Vps20 recruitment." Traffic **7**(8): 1007-16.

Pisitkun, T., R. F. Shen and M. A. Knepper (2004). "Identification and proteomic profiling of exosomes in human urine." Proc Natl Acad Sci U S A **101**(36): 13368-73.

Popov, S., E. Popova, M. Inoue and H. G. Gottlinger (2008). "Human immunodeficiency virus type 1 Gag engages the Bro1 domain of ALIX/AIP1 through the nucleocapsid." J Virol **82**(3): 1389-98.

Qualmann, B. and R. B. Kelly (2000). "Syndapin isoforms participate in receptor-mediated endocytosis and actin organization." J Cell Biol **148**(5): 1047-62.

Radhakrishna, H. and J. G. Donaldson (1997). "ADP-ribosylation factor 6 regulates a novel plasma membrane recycling pathway." J Cell Biol **139**(1): 49-61.

Raiborg, C., K. G. Bache, A. Mehlum, E. Stang and H. Stenmark (2001). "Hrs recruits clathrin to early endosomes." Embo J **20**(17): 5008-21.

Raiborg, C., B. Bremnes, A. Mehlum, D. J. Gillooly, A. D'Arrigo, E. Stang and H. Stenmark (2001). "FYVE and coiled-coil domains determine the specific localisation of Hrs to early endosomes." J Cell Sci **114**(Pt 12): 2255-63.

Raiborg, C., T. E. Rusten and H. Stenmark (2003). "Protein sorting into multivesicular endosomes." Curr Opin Cell Biol **15**(4): 446-55.

Rao, R. V., K. S. Poksay, S. Castro-Obregon, B. Schilling, R. H. Row, G. del Rio, B. W. Gibson, H. M. Ellerby and D. E. Bredesen (2004). "Molecular components of a cell death pathway activated by endoplasmic reticulum stress." J Biol Chem **279**(1): 177-87.

Raymond, C. K., I. Howald-Stevenson, C. A. Vater and T. H. Stevens (1992). "Morphological classification of the yeast vacuolar protein sorting mutants: evidence for a prevacuolar compartment in class E vps mutants." Mol Biol Cell **3**(12): 1389-402.

Reggiori, F. and H. R. Pelham (2001). "Sorting of proteins into multivesicular bodies: ubiquitin-dependent and -independent targeting." Embo J **20**(18): 5176-86.

Richter, C., M. West and G. Odorizzi (2007). "Dual mechanisms specify Doa4-mediated deubiquitination at multivesicular bodies." Embo J **26**(10): 2454-64.

Riggs, B., B. Fasulo, A. Royou, S. Mische, J. Cao, T. S. Hays and W. Sullivan (2007). "The concentration of Nuf, a Rab11 effector, at the microtubule-organizing center is cell cycle regulated, dynein-dependent, and coincides with furrow formation." Mol Biol Cell **18**(9): 3313-22.

Riggs, B., W. Rothwell, S. Mische, G. R. Hickson, J. Matheson, T. S. Hays, G. W. Gould and W. Sullivan (2003). "Actin cytoskeleton remodeling during early Drosophila furrow formation requires recycling endosomal components Nuclear-fallout and Rab11." J Cell Biol **163**(1): 143-54.

Roessle, M. W., R. Klaering, U. Ristau, B. Robrahn, D. Jahn, T. Gehrmann, P. Konarev, A. Round, S. Fiedler, C. Hermes and D. I. Svergun (2007). "Upgrade of the Small Angle X-ray scattering Beamline X33 at the EMBL Hamburg. ." J. Appl. Crystallogr. **40**: 190-S194.

Rusten, T. E., T. Vaccari, K. Lindmo, L. M. Rodahl, I. P. Nezis, C. Sem-Jacobsen, F. Wendler, J. P. Vincent, A. Brech, D. Bilder and H. Stenmark (2007). "ESCRTs and Fab1 regulate distinct steps of autophagy." Curr Biol **17**(20): 1817-25.

Sachse, M., G. J. Strous and J. Klumperman (2004). "ATPase-deficient hVPS4 impairs formation of internal endosomal vesicles and stabilizes bilayered clathrin coats on endosomal vacuoles." J Cell Sci **117**(Pt 9): 1699-708.

Sadoul, R. (2006). "Do Alix and ALG-2 really control endosomes for better or for worse?" Biol Cell **98**(1): 69-77.

Sakaguchi, T., A. Kato, F. Sugahara, Y. Shimazu, M. Inoue, K. Kiyotani, Y. Nagai and T. Yoshida (2005). "AIP1/Alix is a binding partner of Sendai virus C protein and facilitates virus budding." J Virol **79**(14): 8933-41.

Saksena, S., J. Sun, T. Chu and S. D. Emr (2007). "ESCRTing proteins in the endocytic pathway." Trends Biochem Sci **32**(12): 561-73.

Schmidt, M. H., B. Chen, L. M. Randazzo and O. Bogler (2003). "SETA/CIN85/Ruk and its binding partner AIP1 associate with diverse cytoskeletal elements, including FAKs, and modulate cell adhesion." J Cell Sci **116**(Pt 14): 2845-55.

Schmidt, M. H., I. Dikic and O. Bogler (2005). "Src phosphorylation of Alix/AIP1 modulates its interaction with binding partners and antagonizes its activities." J Biol Chem **280**(5): 3414-25.

Schmidt, M. H., D. Hoeller, J. Yu, F. B. Furnari, W. K. Cavenee, I. Dikic and O. Bogler (2004). "Alix/AIP1 antagonizes epidermal growth factor receptor downregulation by the Cbl-SETA/CIN85 complex." Mol Cell Biol **24**(20): 8981-93.

Scott, A., H. Y. Chung, M. Gonciarz-Swiatek, G. C. Hill, F. G. Whitby, J. Gaspar, J. M. Holton, R. Viswanathan, S. Ghaffarian, C. P. Hill and W. I. Sundquist (2005). "Structural and mechanistic studies of VPS4 proteins." Embo J **24**(20): 3658-69.

Scott, A., J. Gaspar, M. D. Stuchell-Brereton, S. L. Alam, J. J. Skalicky and W. I. Sundquist (2005). "Structure and ESCRT-III protein interactions of the MIT domain of human VPS4A." Proc Natl Acad Sci U S A **102**(39): 13813-8.

Sevrioukov, E. A., N. Moghrabi, M. Kuhn and H. Kramer (2005). "A mutation in dVps28 reveals a link between a subunit of the endosomal sorting complex required for transport-I complex and the actin cytoskeleton in Drosophila." Mol Biol Cell **16**(5): 2301-12.

Shi, A., S. Pant, Z. Balklava, C. C. Chen, V. Figueroa and B. D. Grant (2007). "A novel requirement for C. elegans Alix/ALX-1 in RME-1-mediated membrane transport." Curr Biol **17**(22): 1913-24.

Shibata, H., K. Yamada, T. Mizuno, C. Yorikawa, H. Takahashi, H. Satoh, Y. Kitaura and M. Maki (2004). "The penta-EF-hand protein ALG-2 interacts with a region containing PxY repeats in Alix/AIP1, which is required for the subcellular punctate distribution of the amino-terminal truncation form of Alix/AIP1." J Biochem **135**(1): 117-28.

Shiflett, S. L., D. M. Ward, D. Huynh, M. B. Vaughn, J. C. Simmons and J. Kaplan (2004). "Characterization of Vta1p, a class E Vps protein in Saccharomyces cerevisiae." J Biol Chem **279**(12): 10982-90.

Shim, S., L. A. Kimpler and P. I. Hanson (2007). "Structure/function analysis of four core ESCRT-III proteins reveals common regulatory role for extreme C-terminal domain." Traffic **8**(8): 1068-79.

Skibinski, G., N. J. Parkinson, J. M. Brown, L. Chakrabarti, S. L. Lloyd, H. Hummerich, J. E. Nielsen, J. R. Hodges, M. G. Spillantini, T. Thusgaard, S. Brandner, A. Brun, M. N. Rossor, A. Gade, P. Johannsen, S. A. Sorensen, S. Gydesen, E. M. Fisher and J. Collinge (2005). "Mutations in the endosomal ESCRTIII-complex subunit CHMP2B in frontotemporal dementia." Nat Genet **37**(8): 806-8.

Slagsvold, T., R. Aasland, S. Hirano, K. G. Bache, C. Raiborg, D. Trambaiolo, S. Wakatsuki and H. Stenmark (2005). "Eap45 in mammalian ESCRT-II binds ubiquitin via a phosphoinositide-interacting GLUE domain." J Biol Chem **280**(20): 19600-6.

Soubeyran, P., K. Kowanetz, I. Szymkiewicz, W. Y. Langdon and I. Dikic (2002). "Cbl-CIN85-endophilin complex mediates ligand-induced downregulation of EGF receptors." Nature **416**(6877): 183-7.

Springael, J. Y., E. Nikko, B. Andre and A. M. Marini (2002). "Yeast Npi3/Bro1 is involved in ubiquitin-dependent control of permease trafficking." FEBS Lett **517**(1-3): 103-9.

Strack, B., A. Calistri, S. Craig, E. Popova and H. G. Gottlinger (2003). "AIP1/ALIX is a binding partner for HIV-1 p6 and EIAV p9 functioning in virus budding." Cell **114**(6): 689-99.

Stuchell-Brereton, M. D., J. J. Skalicky, C. Kieffer, M. A. Karren, S. Ghaffarian and W. I. Sundquist (2007). "ESCRT-III recognition by VPS4 ATPases." Nature **449**(7163): 740-4.

Sugiura, H., K. Iwata, M. Matsuoka, H. Hayashi, T. Takemiya, S. Yasuda, M. Ichikawa, T. Yamauchi, P. Mehlen, T. Haga and K. Yamagata (2004). "Inhibitory role of endophilin 3 in receptor-mediated endocytosis." J Biol Chem **279**(22): 23343-8.

Sundquist, W. I., H. L. Schubert, B. N. Kelly, G. C. Hill, J. M. Holton and C. P. Hill (2004). "Ubiquitin recognition by the human TSG101 protein." Mol Cell **13**(6): 783-9.

Svergun, D. I. (1992). "Determination of the Regularization Parameter in Indirect-Transform Methods Using Perceptual Criteria." J. Appl. Cryst. **25**: 495-503.

Svergun, D. I. (1999). "Restoring low resolution structure of biological macromolecules from solution scattering using simulated annealing." Biophys J **76**(6): 2879-86.

Svergun, D. I., C. Barberato and M. H. J. Koch (1995). "CRYSOL - a program to evaluate X-ray solution scattering of biological macromolecules from atomic coordinates." J. Appl. Cryst. **28**: 768-773.

Svergun, D. I., A. V. Semenyuk and L. A. Feigin (1988). Acta Cryst. **A44**: 244-250.

Sweeney, N. T., J. E. Brenman, Y. N. Jan and F. B. Gao (2006). "The coiled-coil protein shrub controls neuronal morphogenesis in Drosophila." Curr Biol **16**(10): 1006-11.

Takei, K., V. I. Slepnev, V. Haucke and P. De Camilli (1999). "Functional partnership between amphiphysin and dynamin in clathrin-mediated endocytosis." Nat Cell Biol **1**(1): 33-9.

Teo, H., D. J. Gill, J. Sun, O. Perisic, D. B. Veprintsev, Y. Vallis, S. D. Emr and R. L. Williams (2006). "ESCRT-I core and ESCRT-II GLUE domain structures reveal role for GLUE in linking to ESCRT-I and membranes." Cell **125**(1): 99-111.

Teo, H., O. Perisic, B. Gonzalez and R. L. Williams (2004). "ESCRT-II, an endosome-associated complex required for protein sorting: crystal structure and interactions with ESCRT-III and membranes." Dev Cell **7**(4): 559-69.

Teo, H., D. B. Veprintsev and R. L. Williams (2004). "Structural insights into endosomal sorting complex required for transport (ESCRT-I) recognition of ubiquitinated proteins." J Biol Chem **279**(27): 28689-96.

Thery, C., M. Boussac, P. Veron, P. Ricciardi-Castagnoli, G. Raposo, J. Garin and S. Amigorena (2001). "Proteomic analysis of dendritic cell-derived exosomes: a secreted subcellular compartment distinct from apoptotic vesicles." J Immunol **166**(12): 7309-18.

Thompson, B. J., J. Mathieu, H. H. Sung, E. Loeser, P. Rorth and S. M. Cohen (2005). "Tumor suppressor properties of the ESCRT-II complex component Vps25 in Drosophila." Dev Cell **9**(5): 711-20.

Thompson, J. D., D. G. Higgins and T. J. Gibson (1994). "CLUSTAL W: improving the sensitivity of progressive multiple sequence alignment through sequence weighting, position-specific gap penalties and weight matrix choice." Nucleic Acids Res **22**(22): 4673-80.

Toyooka, S., M. Ouchida, Y. Jitsumori, K. Tsukuda, A. Sakai, A. Nakamura, N. Shimizu and K. Shimizu (2000). "HD-PTP: A novel protein tyrosine phosphatase gene on human chromosome 3p21.3." Biochem Biophys Res Commun **278**(3): 671-8.

Trioulier, Y., S. Torch, B. Blot, N. Cristina, C. Chatellard-Causse, J. M. Verna and R. Sadoul (2004). "Alix, a protein regulating endosomal trafficking, is involved in neuronal death." J Biol Chem **279**(3): 2046-52.

Tsang, H. T., J. W. Connell, S. E. Brown, A. Thompson, E. Reid and C. M. Sanderson (2006). "A systematic analysis of human CHMP protein interactions: additional MIT domain-containing proteins bind to multiple components of the human ESCRT III complex." Genomics **88**(3): 333-46.

Urbanowski, J. L. and R. C. Piper (2001). "Ubiquitin sorts proteins into the intralumenal degradative compartment of the late-endosome/vacuole." Traffic **2**(9): 622-30.

Urbe, S., M. Sachse, P. E. Row, C. Preisinger, F. A. Barr, G. Strous, J. Klumperman and M. J. Clague (2003). "The UIM domain of Hrs couples receptor sorting to vesicle formation." J Cell Sci **116**(Pt 20): 4169-79.

Usami, Y., S. Popov, E. Popova and H. G. Gottlinger (2008). "Efficient and specific rescue of human immunodeficiency virus type 1 budding defects by a Nedd4-like ubiquitin ligase." J Virol **82**(10): 4898-907.

van Ijzendoorn, S. C. (2006). "Recycling endosomes." J Cell Sci **119**(Pt 9): 1679-81.

Vida, T. A., G. Huyer and S. D. Emr (1993). "Yeast vacuolar proenzymes are sorted in the late Golgi complex and transported to the vacuole via a prevacuolar endosome-like compartment." J Cell Biol **121**(6): 1245-56.

Vincent, O., L. Rainbow, J. Tilburn, H. N. Arst, Jr. and M. A. Penalva (2003). "YPXL/I is a protein interaction motif recognized by aspergillus PalA and its human homologue, AIP1/Alix." Mol Cell Biol **23**(5): 1647-55.

Vito, P., E. Lacana and L. D'Adamio (1996). "Interfering with apoptosis: Ca(2+)-binding protein ALG-2 and Alzheimer's disease gene ALG-3." Science **271**(5248): 521-5.

Vito, P., L. Pellegrini, C. Guiet and L. D'Adamio (1999). "Cloning of AIP1, a novel protein that associates with the apoptosis-linked gene ALG-2 in a Ca2+-dependent reaction." J Biol Chem **274**(3): 1533-40.

Volkov, V. V. and D. I. Svergun (2003). "Uniqueness of ab initio shape determination in small-angle scattering." J. Appl. Crystallogr. **36**: 860-864.

von Schwedler, U. K., M. Stuchell, B. Muller, D. M. Ward, H. Y. Chung, E. Morita, H. E. Wang, T. Davis, G. P. He, D. M. Cimbora, A. Scott, H. G. Krausslich, J. Kaplan, S. G. Morham and W. I. Sundquist (2003). "The protein network of HIV budding." Cell **114**(6): 701-13.

Wang, M. Q., W. Kim, G. Gao, T. A. Torrey, H. C. Morse, 3rd, P. De Camilli and S. P. Goff (2003). "Endophilins interact with Moloney murine leukemia virus Gag and modulate virion production." J Biol **3**(1): 4.

Ward, D. M., M. B. Vaughn, S. L. Shiflett, P. L. White, A. L. Pollock, J. Hill, R. Schnegelberger, W. I. Sundquist and J. Kaplan (2005). "The role of LIP5 and CHMP5 in multivesicular body formation and HIV-1 budding in mammalian cells." J Biol Chem **280**(11): 10548-55.

Weissenhorn, W. (2005). "Crystal structure of the endophilin-A1 BAR domain." J Mol Biol **351**(3): 653-61.

Welsch, S., A. Habermann, S. Jager, B. Muller, J. Krijnse-Locker and H. G. Krausslich (2006). "Ultrastructural analysis of ESCRT proteins suggests a role for endosome-associated tubular-vesicular membranes in ESCRT function." Traffic **7**(11): 1551-66.

Wernimont, A. K. and W. Weissenhorn (2004). "Crystal structure of subunit VPS25 of the endosomal trafficking complex ESCRT-II." BMC Struct Biol **4**(1): 10.

Whitley, P., B. J. Reaves, M. Hashimoto, A. M. Riley, B. V. Potter and G. D. Holman (2003). "Identification of mammalian Vps24p as an effector of phosphatidylinositol 3,5-bisphosphate-dependent endosome compartmentalization." J Biol Chem **278**(40): 38786-95.

Williams, R. L. and S. Urbe (2007). "The emerging shape of the ESCRT machinery." Nat Rev Mol Cell Biol **8**(5): 355-68.

Wilson, G. M., A. B. Fielding, G. C. Simon, X. Yu, P. D. Andrews, R. S. Hames, A. M. Frey, A. A. Peden, G. W. Gould and R. Prekeris (2005). "The FIP3-Rab11 protein complex regulates recycling endosome targeting to the cleavage furrow during late cytokinesis." Mol Biol Cell **16**(2): 849-60.

Wiseman, T., S. Williston, J. F. Brandts and L. N. Lin (1989). "Rapid measurement of binding constants and heats of binding using a new titration calorimeter." Anal Biochem **179**(1): 131-7.

Wolf, E., P. S. Kim and B. Berger (1997). "MultiCoil: a program for predicting two- and three-stranded coiled coils." Protein Sci **6**(6): 1179-89.

Wriggers, W., R. A. Ronald A. Milligan and J. A. McCammon (1999). "Situs: A Package for Docking Crystal Structures into Low-Resolution Maps from Electron Microscopy." J. Structural Biology **125**: 185-195.

Wyatt, P. J. (1998). "Submicrometer Particle Sizing by Multiangle Light Scattering following Fractionation." J Colloid Interface Sci **197**(1): 9-20.

Xu, W. and A. P. Mitchell (2001). "Yeast PalA/AIP1/Alix homolog Rim20p associates with a PEST-like region and is required for its proteolytic cleavage." J Bacteriol **183**(23): 6917-23.

Xu, W., F. J. Smith, Jr., R. Subaran and A. P. Mitchell (2004). "Multivesicular body-ESCRT components function in pH response regulation in Saccharomyces cerevisiae and Candida albicans." Mol Biol Cell **15**(12): 5528-37.

Yeo, S. C., L. Xu, J. Ren, V. J. Boulton, M. D. Wagle, C. Liu, G. Ren, P. Wong, R. Zahn, P. Sasajala, H. Yang, R. C. Piper and A. L. Munn (2003). "Vps20p and Vta1p interact with Vps4p and function in multivesicular body sorting and endosomal transport in Saccharomyces cerevisiae." J Cell Sci **116**(Pt 19): 3957-70.

Yorikawa, C., H. Shibata, S. Waguri, K. Hatta, M. Horii, K. Katoh, T. Kobayashi, Y. Uchiyama and M. Maki (2005). "Human CHMP6, a myristoylated ESCRT-III protein, interacts directly with an ESCRT-II component EAP20 and regulates endosomal cargo sorting." Biochem J **387**(Pt 1): 17-26.

Zamborlini, A., Y. Usami, S. R. Radoshitzky, E. Popova, G. Palu and H. Gottlinger (2006). "Release of autoinhibition converts ESCRT-III components into potent inhibitors of HIV-1 budding." Proc Natl Acad Sci U S A **103**(50): 19140-5.

Zerial, M. and H. McBride (2001). "Rab proteins as membrane organizers." Nat Rev Mol Cell Biol **2**(2): 107-17.

Zhai, Q., R. D. Fisher, H. Y. Chung, D. G. Myszka, W. I. Sundquist and C. P. Hill (2008). "Structural and functional studies of ALIX interactions with YPX(n)L late domains of HIV-1 and EIAV." Nat Struct Mol Biol **15**(1): 43-9.

Zhang, Z. and D. L. Smith (1993). "Determination of amide hydrogen exchange by mass spectrometry: a new tool for protein structure elucidation." Protein Sci **2**(4): 522-31.

Zhou, X., S. Pan, L. Sun, J. Corvera, S. H. Lin and J. Kuang (2008). "The HIV-1 p6/EIAV p9 docking site in Alix is autoinhibited as revealed by a conformation-sensitive anti-Alix monoclonal antibody." Biochem J.

Zimmerberg, J. and S. McLaughlin (2004). "Membrane curvature: how BAR domains bend bilayers." Curr Biol **14**(6): R250-2.